Recent Central American and low latitude climate variability revealed using speleothem-based rainfall proxy records from southern Belize

RIDLEY, HARRIET,ELIZABETH

Durham University

Recent Central American and low latitude climate variability revealed using speleothem-based rainfall proxy records from southern Belize

Harriet Elizabeth Ridley

A thesis submitted in partial fulfilment of the requirements for the degree of Doctor of Philosophy at Durham University

Department of Earth Sciences, Durham University

2014

I declare that this thesis, which I submit for the degree of Doctor of Philosophy at Durham University, is my own work and not substantially the same as any which has previously been submitted at this or any other university.

Harriet E. Ridley

Durham University

April 2014

-x-

This thesis is dedicated to the memory of Alex Cicchino.

-x-

Acknowledgments

One of the features of thesis writing I have been most looking forward to is writing these acknowledgements. There are so many people to whom I am unwaveringly grateful for helping me reach this stage.

Before I launch into a flood of effusive gratitude for all who have helped me during my PhD, I must acknowledge the sources of funding which have made this research possible. My PhD is funded through a grant awarded to my supervisor, James Baldini, by the European Research Council (ERC). I gratefully acknowledge the ERC for financially supporting my PhD and James for masterminding the research and then offering me the opportunity to contribute to it.

I would like to further thank James for his incredible patience, good-will and enthusiasm as my PhD supervisor; I could not have done this without your invaluable guidance and your friendship. Thank you so much for putting up with me, for not laughing when I ask stupid questions, for never being too stern with me and for *always* having the time to talk. I could not be more grateful. My thanks also extend to my second supervisor, Colin MacPherson, for his help with all my isotope data, Sebastian Breitenbach for his unrivalled enthusiasm for science and to all the other members of my research group: Bakey, Iza, Lisa, Bob, Franzi, and Sam. It's been a pleasure working with you all. Thank you to Bakes, Iza and Franzi for fun and rum in the field; wish we could do it again! Thank you Iza for always wanting to drink beer (regardless of time of day) and thank you Bakey for never refusing breakfast for dinner.

I owe a substantial chunk of both my sanity and my isotope data to Jo Peterkin. Jo made running 10,000 carbonate samples almost seem like fun (she must be magical). Thank you, Jo, for all your support in the lab and keeping Michael in good working order. I would like to thank the gorgeous office ladies; particularly Paula who has been so brilliant in organising my numerous fieldwork trips. I will give a special high-five acknowledgment to Gaz purely because he is awesome.

I also greatly appreciate having had the opportunity to collaborate with such enthusiastic and motivated people outside Durham; particularly Keith Prufer, Douglas

Kennett, Yemane Asmerom and their respective research groups. I would like to thank Keith Prufer especially for his support in the field and for knowing that no fieldwork is complete without a trip to Placencia! My thanks also extend to all the people in Belize who made my fieldwork such a joy and helped it always run so smoothly: Bruno and the pups, Francisca and Don, Raymundo Sho, Jose Mess and their families and all the villagers at Santa Cruz. Meeting you all will forever be one of my most treasured experiences.

In the department I would like to extend thanks to everyone I've interacted with during my time here. The friendships I've made at Durham I will value forever. I must mention Alice pickle, for being the most gentle, fun and kind of people, Izzy Yeo for being hilarious, SPorter for having such a big heart, Kathy for being an inspirational crafter and friend, Leo for being a cublet, Richie Brown for simply being a dude and BJ for showing me that laughter is the key to happiness. Everybody else, please forgive me for not naming you all personally; you know that your friendship is greatly valued.

Outside work I would like to thank everyone I've met climbing in the North-East who kept me active and social. I've loved being a part of your community and I will miss you all. Thank you to Alison for being a kick-ass female climbing inspiration and thank you to Kev for your devoted friendship and big heart. Wherever life takes me next there *will be* rocks, so you'd better all be coming to visit!

Perhaps the most important thanks must be given to my wonderful family and to David. I am sure that I have reached this position only because of the love, encouragement and belief you have always offered. Thank you for helping me through these last few years, for being proud of me and for supporting me in everything I do. I love you all more than anything.

Finally, I would like to acknowledge how highly I value the times I shared with Alex Cicchino while here in Durham. He was a beautiful person whom I am privileged to have known. Alex was so close to finishing his own thesis and so, in honour of his efforts, I dedicate this to him.

-x-

Abstract

Comprehensive assessment of recent tropical climate variability is essential in order to understand the full spatial expression of climate change in the context of long term climate variability. This requires highly resolved and precisely dated tropical proxy records which include the critical transition from the pre-industrial to industrial eras. Speleothem provide highly-resolved and well preserved climate signals and are particularly valuable in tropics where few alternative high resolution records are available. This thesis presents a comprehensive study of recent Central American and low latitude climate variability through assessment of two highly resolved speleothem stable isotope based rainfall proxy records from Yok Balum Cave, southern Belize.

The YOK-G stalagmite $\delta^{13}C$ record has a bi-monthly resolution and robust chronology permitting the inference of palaeo-seasonality as well as intra annual rainfall variations over the last 453 years. The record strongly suggests that volcanic aerosol injections into the Northern Hemisphere atmosphere result in southward Intertropical Convergence Zone (ITCZ) repositioning, and firmly implicate anthropogenic aerosol emissions as having caused 20th Century rainfall reductions in the northern tropics.

The YOK-I stalagmite $\delta^{13}C$ record provides a bi-annually resolved correlate records of North Atlantic Oscillation for the last 2000 years. Links between high latitude explosive volcanism and repositioning of the ITCZ are further investigated with emphasis on the subsequent impact of observed North Atlantic Oscillation (NAO) phases. High latitude eruptions are compellingly linked to negative NAO circulatory patterns in the North Atlantic thereby providing new insight into atmospheric mechanics of the North Atlantic.

Cave monitoring data provides essential background information on cave environmental variables which could modify climate signals preserved within speleothem carbonate, precluding or complicating interpretations. Using remote monitoring techniques the cave ventilation dynamics and hydrology at Yok Balum are characterised, thereby helping to put the speleothem geochemical data discussed into correct environmental context.

Contents

List of Figures

List of Tables

Stable isotope ratio notation

Throughout this thesis, stable isotope ratios, as measured by mass-spectrometric methods, are expressed in the conventional delta (δ) notation, in units of ‰ relative to a material standard (Sharp, 2007) such that:

$$\delta_{Sample} = \left(\frac{R_{sample}}{R_{standard}} - 1\right) \times 1000 \qquad \text{(Equation 1.1)}$$

where material standards expressed as Vienna Pee Dee Belemnite (VPDB) are used for carbonate samples and R is the isotope ratio:

$$R = \frac{\text{rare isotope}}{\text{common isotope}} \qquad \textit{e.g.,} = \frac{^{13}C}{^{12}C} \qquad \text{(Equation 1.2)}$$

General notation

Frequently used notation terms are detailed in Table 1.1. Specific terms in equations are defined in the text immediately after the equation is given.

Table 1.1 Notation used frequently throughout this thesis.

Notation	Unit	Description
$\delta^{18}O$	‰	$^{18}O/^{16}O$ of speleothem carbonate relative to VPDB standard
$\delta^{13}C$	‰	$^{13}O/^{12}O$ of speleothem carbonate relative to VPDB standard
pCO_2	ppm, ppmv, atm or %atm	Partial pressure of carbon dioxide
T	^{o}C	Temperature
ENSO		El Niño Southern Oscillation
NAO		North Atlantic Oscillation
ITCZ		Intertropical Convergence Zone
NH / SH		Northern Hemisphere / Southern Hemisphere
VEI		Volcanic Explosivity Index

Chapter 1

Introduction

Introduction

1.1 Thesis rationale

Climate varies on all timescales, from decades to hundreds of millions of years. This variability is caused by a variety of factors, both internal and external to the climate system and subsequent complex interactions and feedbacks (Bradley, 1999; Jones and Mann, 2004; Ruddiman, 2001). Our ability to predict future climate changes is dependent on our understanding of the interaction of climate system components obtained through characterisation of past variability (Jones and Mann, 2004). Extensive instrumental meteorological records extend back only to the mid-19th century. Climate science is therefore heavily dependent on palaeoclimate proxy data derived from natural archives such as tree rings, ice cores, corals, and ocean and lake sediments to extend our knowledge of weather and climate information beyond the short instrumental record. Palaeoclimate proxy data has provided important qualitative data for discerning climate variability and associated forcing mechanisms and feedbacks and is essential for informing climate models.

1.1.1 Recent climate variability

Characterising climate evolution over the last 2000 years is essential for isolating natural variability from anthropogenically forced climate change. Principal boundary conditions on the climate (e.g., Earth orbital geometry and global ice mass) have not changed appreciably over the last two millennia and therefore climate variability over this time is most applicable to our current climate state (Jones and Mann, 2004). As well as being the most analogous period to the current climate, the last 2000 years experienced marked regional and global scale climate fluctuations such as the Medieval Climate Anomaly (MCA; ~950-1250AD) and Little Ice Age (LIA; ~1550-1850) (Mann et al., 2009) and includes the transition into the late twentieth-century

anthropogenically forced climate state. It is generally considered that the last two millennia (prior to industrialisation) are representative of natural climate variability and characterisation of climate variability during this period is essential to contextualise the recent modern warming (Jones and Mann, 2004).

Climate variability on multi-millennial timescales is clearly dominated by changes in the distribution of insolation controlled by the Earth's orbit (Ruddimann 2001). Over the last two millennia however, it is natural changes in solar irradiance and explosive volcanism combined with recent anthropogenic influences which are considered to dominate (Crowley, 2000; Jones and Mann, 2004; Mann, 2007; Robertson et al., 2001; Shindell et al., 2003). Fortunately, the last 2000 years is characterised by particularly well-resolved palaeoclimate records which facilitates assessment of high-frequency variability induced by changes in radiative forcing associated with natural solar and volcanic variations and anthropogenically induced greenhouse gases (Alley et al., 2007; Hegerl et al., 2011; Mann, 2007; Mann et al., 2005; Neukom and Gergis, 2012).

In the last millennium explosive volcanism has contributed significantly to decadal and centennial scale variability in reconstructed Northern Hemisphere surface temperature and is known to be a leading natural driver of climate change on a range of timescales (Ammann et al., 2007; Briffa et al., 1998; Crowley, 2000; Mann et al., 2005). Explosive volcanism alters the climate primarily through the injection of large amounts of sulphate aerosols into the stratosphere which affect the radiative balance of the planet through interaction with incoming and outgoing radiation (Robock, 2000). The most recent large eruption, Pinatubo in 1991, injected approximately 20 mega tonnes of SO_2 into the atmosphere, which subsequently led to a temporary reversal of the late twentieth-century global warming trend (Robock, 2000). Indeed, throughout the historical record, volcanic events are associated with droughts and famine thus illustrating how volcanically forced atmospheric reorganisation has severe societal consequences (Ludlow et al., 2013; Oman et al., 2006).

Records of volcanic radiative forcing, developed from sulphate deposition in polar ice-cores (Zielinski et al., 1994), provide a record of global and hemispheric explosive volcanism over the last two millennia (Crowley and Unterman, 2012; Gao et al., 2008; Gao et al., 2012) (Fig. 1.1a). These estimates are based on several assumptions

regarding the relationship between sulphate aerosol deposition and the extent and duration of its climatically significant residence in the stratosphere (Gao et al., 2008; Robock, 2000). Observations and reconstructions of volcanic eruptions suggest that large aerosol injections result in a strong but short-lived change in radiative forcing and are therefore relevant on annual to decadal timescales. Short-lived volcanic events therefore are only identifiable in sub-annually resolved proxy records which clearly allow inter-annual changes to be observed. Production of such records will enable further characterising the specific climate response of volcanic radiative forcing events.

Variation in solar activity, often measured as total solar irradiance (IPCC, 2013), has a direct effect on the global energy budget and subsequently atmospheric and oceanic energy transport mechanisms. Due to land mass distribution between the hemispheres and the variable specific heat capacity of land and sea, the Northern Hemisphere (NH) experiences greater warming than the Southern Hemisphere (SH) when solar activity increases. Observations of sunspots calibrated against modern satellite measurements provide an estimate of solar irradiance back to 1610AD (Lean et al., 1995). This record is extended back millennia using isotopic information recorded in tree rings (^{14}C) and ice-cores (^{10}Be), the production of which are known to be affected by solar interaction with the upper atmosphere (Bard et al., 1997; Bard et al., 2000; Crowley, 2000). Reconstructions of solar activity are characterised by multi-decadal periods of low activity known as grand solar minima (e.g the Maunder Minimum, ~1645-1715) that are superimposed on longer term trends (Fig. 1.1).

Although variability in solar activity is clearly influential in the global energy budget its radiative forcing is relatively small when compared to volcanic forcing events. Therefore variability in solar irradiance is more pertinent at multi-decadal timescales or longer (Crowley and Kwang-Yul, 1996; Weber, 2005) and it's observed climate signal may be 'overprinted' by stronger, short-term forcings.

The anthropogenic contribution of the late twentieth century must not be underestimated when considering climate variability over the last 2000 years. Since the dawn of industrialisation around 1850, rapidly increasing greenhouse gas concentrations have contributed to unprecedented to rates of global surface warming

(Crowley, 2000; IPCC, 2013). Among the plethora of worrying information presented in the Intergovernmental Panel on Climate Change (IPCC) 2013 summary for policy makers, it is stated with confidence that anthropogenically forced changes in North Atlantic climate are linked to low-latitude precipitation (IPCC, 2013). Considerable evidence also exists that anthropogenic activity in the NH has led to modification of the monsoons and low-latitude rain belts (Bollasina et al., 2011; Chung and Ramanathan, 2006; Hwang et al., 2013; Kawase et al., 2010; Zhang et al., 2008). Billions of people rely on seasonal rains in the low latitudes; discerning past drought and seasonal precipitation patterns is clearly important from a societal as well as a scientific perspective. Moreover, understanding past precipitation patterns can help develop our understanding of past changes in atmospheric circulation (Luterbacher et al., 2002) and climate modes such as the North Atlantic Oscillation (NAO) and El Niño Southern Oscillation (ENSO).

Characterising variability over the last 2000 years is exceptionally important for fully evaluating anthropogencially forced climate changes and making accurate predictions for the coming centuries. Such aims can be achieved only if suitably high-resolution and precisely dated palaeo-proxies are developed from regions which capture pertinent signals of climate change.

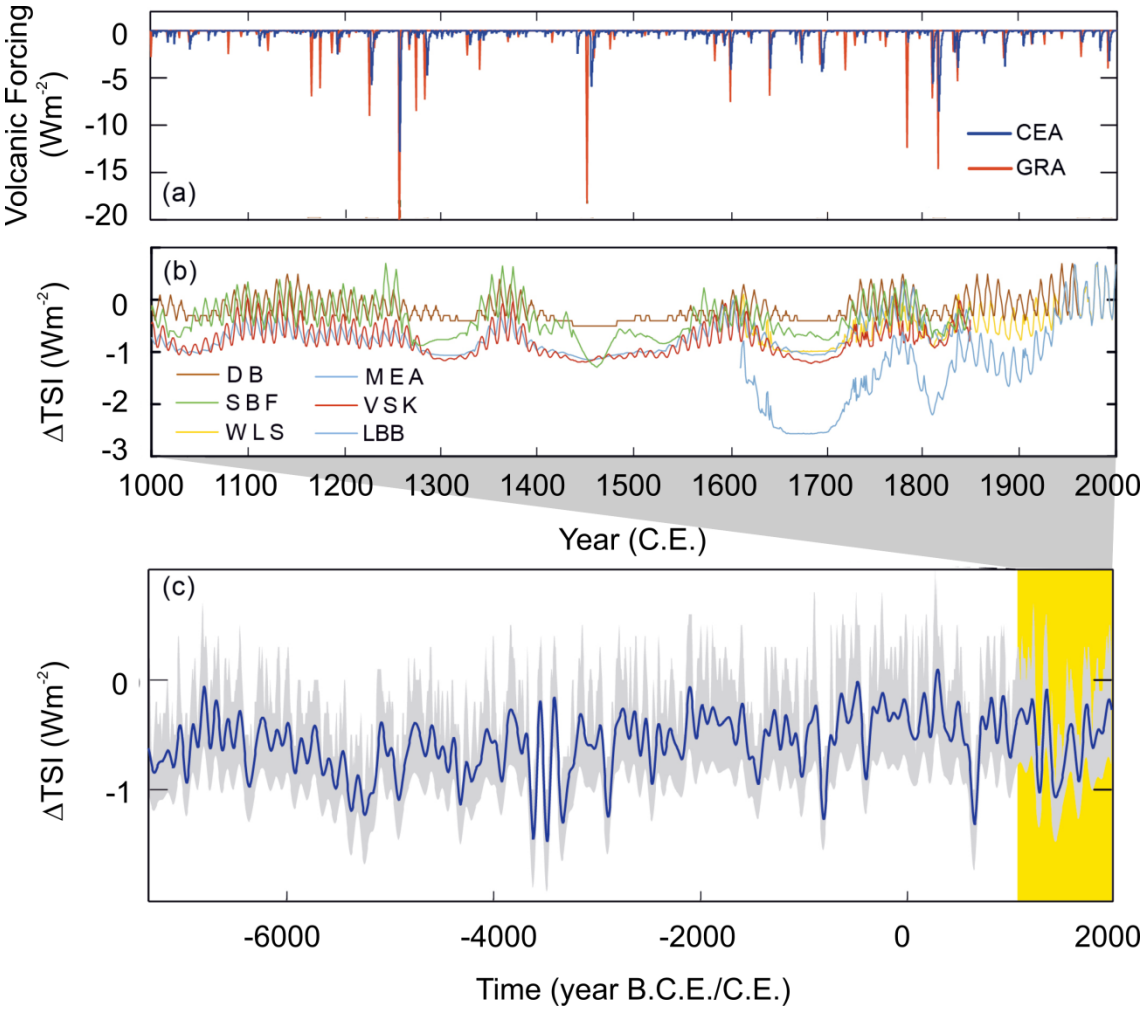

Figure 1.1 a) Two reconstructions of volcanic forcing over the past 1000 years derived from ice core sulphate GRA: Gao et al. (2012); CEA: Crowley and Unterman (2012). **b)** Reconstructed total solar irradiance (TSI) anomalies back to the year 1000; DB: Delaygue and Bard (2011); MEA: Muscheler et al. (2007); SBF: Steinhilber et al. (2009): VSK: Vierira et al. (2011); WLS; Wang et al. (2005b); LBB: Lean et al. (1995). Prior to 1600 the 11-year sunspot cycles have been added artificially to the original data with an amplitude proportional to the mean level of TSI (IPCC, 2013) **c)** Reconstructed TSI anomalies, based on ^{10}Be nuclides, with 100-year low pass filter applied (blue line) and 1σ uncertainty range (grey shading) for the last 9300 years (Steinhilber et al., 2009). Yellow panel highlights period expanded in panels **a)** and **b)**.

1.1.2 Tropical palaeoclimatology

During the last decade there has been a growing interest in tropical palaeoclimate (Chiang, 2009). In a 1998 *Science* paper entitled 'Climate Change - A role for the Tropical Pacific' Cane argued that the tropics plays an important part in climate change. He noted that the tropics had been largely neglected as focus fell on climate change in the higher latitudes (CLIMAP, 1976). This influential paper was part of a larger movement working towards the tropical hypothesis, which posits a significant, if not dominant, role for the tropics in determining palaeoclimatic change (Chiang, 2009). This hypothesis was stimulated both by outstanding questions in palaeoclimate which hinted at the involvement of the tropics in global and hemispheric processes and advances in the understanding and application of climate dynamics regarding tropical systems such as the monsoons and ENSO.

Before the 1980s palaeoclimate research focused primarily on the high northern latitudes due, in part, to the success of the GISP ice cores as NH climate proxies and the lack of a sizeable Sea Surface Temperature (SST) change in the tropics observed during the Last Glacial Maximum (LGM) in the CLIMAP reconstruction (1976). In the 1990's however temperature proxy records from Pacific corals (Beck et al., 1992; Guilderson et al., 1994) and continental boreholes in Brazil (Stute et al., 1995) suggested a greater cooling during the LGM, of up to 5^{o}K. Development in the understanding of the palaeomonsoons and their link to ~19,000 to 23,000-year precessional orbital cycles (Pokras and Mix, 1987; Prell and Kutzbach, 1987; Rossignol-Strick, 1985) also provided considerable evidence of the distinct nature of the tropics from that of the northern extra-tropics which are dominated by 100,000 year eccentricity cycles. At approximately the same time advances in the understanding of equatorial climate dynamics (Cane and Sarachik, 1981; Gill, 1980; Philander, 1981; Zebiak and Cane, 1987) was developing a picture of the powerful climate modes, such as ENSO, with important global impacts. These early developments highlighted the unique nature of the tropics and prompted a surge of interest in tropical paleoclimatology.

Tropical climate is dominated by mesoscale convective processes which drive global heat transport mechanisms. It is clear, both from observations, modelling and reconstructions that the tropical climate has a remarkable ability to reorganize in response to external forcing and can effectively project these perturbations both zonally and latitudinally (Chiang, 2009). This is summarised by Chaing (2009) in two examples: i) reorganisations in response to ENSO perturbations in the Equatorial Pacific and ii) in response to inter-hemispheric thermal gradients. The quasi-periodic warming and cooling of the tropical Pacific associated with ENSO leads to considerable convective reorganisation across the tropics. During El Niño events enhanced convection occurs in the central equatorial Pacific due to increased SST and reduced convection occurs in the western sector and Indonesian subcontinent. These changes influence convection over South America, the tropical Atlantic, Africa and the Indian Ocean (Alexander et al., 2002; Giannini et al., 2001; Lau and Nath, 2003; Su et al., 2001) through tropospheric temperature increase and related feedbacks which alter the nature of remote tropical convection via atmospheric teleconnections (Lintner and Chiang, 2007; Su et al., 2004). The second example given by Chaing relates to the response of the ITCZ to inter-hemispheric temperature gradients driven by extra-tropical cooling (Broccoli et al., 2006; Chiang and Bitz, 2005; Friedman et al., 2013; Frierson and Hwang, 2011; Frierson and Hwang, 2012; Kang et al., 2009; Kang et al., 2008). Variations in the thermal contrast between the Northern and Southern Hemispheres act to reposition the ITCZ by drawing the rising limb of the Hadley cell towards the warmer hemisphere (Broccoli et al., 2006). Mechanistically, this displacement is associated with cross-equatorial atmospheric heat transports acting to compensate for increased loss of radiative flux in the colder hemisphere (Chiang and Bitz, 2005) and therefore to maintain cross-equatorial heat equilibrium. Due to the non-uniform distribution of landmasses across the tropics, and hence non-uniform heating, ITCZ displacement is unlikely to be homogenous across the globe, but will take on regional characteristics.

Despite the numerous outstanding questions regarding tropical – extra-tropical climate interaction, the IPCC Fourth Assessment Report concluded that climate variability in the tropics is ‘severely limited by the lack of palaeoclimate records’ (Jansen et al.,

2007). This is in comparison to the rich network of NH extra-tropical palaeoclimate data. The spatial disparity is partially due to the limited spatial distribution of suitable high-resolution climate archives such as tree-rings and ice cores in the low-latitudes. In recent years, geochemical studies of tropical corals have been extremely informative in characterising climate in tropical and sub-tropical marine regions (Dunbar and Cole, 1999; Felis and Patzold, 2004; Gagan et al., 2000; Grottoli and Eakin, 2007; Lough, 2004; Lough, 2010) and have been valuable for reconstructing ENSO variability (Suzuki et al., 2006; Wilson et al., 2010) tropical Sea Surface Temperatures (SST) (Hetzinger et al., 2010; Pfeiffer and Dullo, 2006) and as evidence of hydrological changes induced by ITCZ migration (Pfeiffer et al., 2004). Although often sub-annually resolved, modern corals are temporally restrictive as they tend not to extend beyond the 17th century. Sediment records can provide longer term palaeo-proxy records at annual resolution (Jones and Mann, 2004) but not ubiquitously. These limitations have all contributed to the spatial inequality of high resolution palaeoclimate across the latitudes.

1.1.3 Speleothems as palaeoclimate proxy archives

Speleothems, secondary cave carbonate deposits, provide important information of terrestrial palaeoclimate in the tropics, where other palaeo-proxies, such as tree-rings and ice cores, are rare. As well as being common at almost all latitudes, speleothems have several additional advantages which make them powerful palaeo-proxies. Firstly, speleothem regularly provide several potentially sub-annually resolved climate proxies in their carbonate and petrography which can be used in combination to deconvolve past climate variability. Most commonly utilised proxies include stable isotope ratios of oxygen ($\delta^{18}O$) and carbon ($\delta^{13}C$), major trace elements and annual luminescence or petrographical laminae which are all found to contain regional and global climate signals (Fairchild and Treble, 2009; Genty et al., 2003; Henderson, 2006). Secondly, caves are highly stable environments in which these geochemical signals can be preserved, protected from climate induced erosion and bioturbation which potentially mar other palaeoclimate repositories over long timescales (Fairchild et al., 2006). Speleothem up to 600kyrs old can also be precisely dated using U-series dating

methods which are analytically more precise than radiocarbon (Richards and Dorale, 2003; Scholz and Hoffman, 2008; Wackerbarth et al., 2010). Recent advancement of microanalytical techniques (Spötl and Mattey, 2006) and achievements in U-series dating (Cheng et al., 2009) permit accurate sub-annual records to be constructed. These attributes make speleothems invaluable for reconstructing the climate of the tropics where other archives are lacking.

Speleothem records have provided important multi-proxy records of past low-latitude climate and led to significant advances in the understanding of tropical climate on a range of timescales including valuable insights into global climate teleconnections and large scale climate patterns, (Cheng et al., 2009; Frisia et al., 2003; Wang et al., 2004; Wang et al., 2005a), provided critical information for reconstructing large scale climate modes, such as the North Atlantic Oscillation and El Niño Southern Oscillation (Brook et al., 1999; Lachniet et al., 2004; Proctor et al., 2002; Trouet et al., 2009; Wassenburg et al., 2013) and local synoptic-scale climate events such as palaeo-hurricane activity (Frappier et al., 2007; Haig et al., 2014). Speleothem records have also been included in multi-proxy reconstruction of hemispheric temperature in conjunction with sediment and tree-ring records, due, in part, to their ability to capture low-frequency climate variability which can be lost in tree-ring records (Moberg et al., 2005).

An important caveat of palaeoclimate reconstruction from speleothems lies in the unique nature of proxy variables for each record. There is abundant literature describing the palaeoclimatic interpretation of speleothems (Fairchild et al., 2006; Genty et al., 2003; Lachniet, 2009; McDermott, 2004) yet the unique nature of each speleothem and cave system demands an understanding of the relationships between modern carbonate deposition and the cave environment, local hydrology and regional atmospheric dynamics for accurate geochemical interpretation (Baldini et al., 2008; Banner et al., 2007; Johnson et al., 2006; Kowalczk, 2009; Kowalczk and Froelich, 2010; Spötl et al., 2005). Palaeoclimate studies regularly assume that speleothem isotopic chemistry reflects local precipitation (Lachniet, 2009), however through cave monitoring it has become increasingly apparent that the epikarst and vadose zone above the cave creates a complex heterogenous system of water mixing, storage and transport (Bradley et al., 2010). Research indicates that dripwater hydrochemistry

within the same cave, even in adjacent drips, is distinct due to different mixing pathways (Baldini et al., 2006b; Fairchild and Baker, 2012). Upon entering the cave, further geochemical modification of the dripwater can occur through variations in drip rate, which affect the degree of prior carbonate precipitation (Wong et al., 2011) and due to environmentally controlled fractionation associated with evaporation and degassing rate (Fairchild et al., 2006; Lachniet, 2009; Mickler et al., 2004; Spötl et al., 2005). Cave air pCO_2 exerts a first order control on drip water degassing and hence carbonate precipitation (Baldini, 2010; Mattey et al., 2010). Cave air pCO_2 is controlled by ventilation dynamics which are unique to each cave system (Sanchez-Canete et al., 2013). Hence ventilation dynamics and atmospheric compositions should be characterised in order to correctly understand speleothem growth (Baldini, 2010; Banner et al., 2007; Kowalczk and Froelich, 2010).

Due to the individuality of every cave, and indeed each speleothem, monitoring is an essential precursor of paleo-speleological reconstruction as it can help to discern relationships between carbonate geochemistry and local precipitation (Cobb et al., 2007; Cruz et al., 2005; Lachniet, 2009; Mattey et al., 2008; McDonald et al., 2007; Treble et al., 2005), karst hydrology (McDermott, 2004; Bradley et al., 2010), cave micro-climate (Fairchild et al., 2006; Mattey et al., 2010) and soil productivity, cave ventilation and CO_2 outgassing (Baldini et al., 2006a; Kowalczk, 2009).

1.2 Overview of thesis

This thesis presents a holistic study of Central American climate variability over the last 2000 years using cave monitoring information (Chapter 3) and two highly-resolved speleothem stable isotope records from Belize (Chapter 4 and 5). Although related, the original contributions in Chapters 3, 4 and 5 are presented as stand-alone studies as they are intended for publication. Author contributions and information is provided at the start of each chapter.

The primary motivation for this work stems from the need to develop high resolution climate records from tropical regions as a means of both understanding tropical climate variability and its connection with the mid to high latitudes. This is coupled with the appreciation that correct speleothem proxy interpretation requires a composite understanding of *in-situ* conditions which affect proxy signal emplacement. With this in mind three principal topics are presented and discussed in this thesis:

1) High resolution monitoring: Results from a monitoring programme at a remote tropical cave site discussed as a means of understanding cave environmental parameters and links to local climate. Quantitative assessment of cave atmosphere and hydrology will facilitate palaeoclimate interpretation of speleothem geochemical signals from the cave and help guide the identification of new speleothem samples for analysis.

2) Production of a highly resolved stable carbon and oxygen isotope record from a Belizean stalagmite to reconstruct rainfall over the last 450 years, thus covering the pre- post-anthropogenic era (post AD 1850) of climate history in detail.

3) Investigation of the relationships between local rainfall, derived from speleothem records from Yok Balum, and large scale Atlantic climate variability with particular reference to external forcing mechanisms.

Southern Belize is an excellent field site for this study for several reasons: firstly, it is within the tropics and therefore, as previously discussed, work from this area will help

to fill the gap in the understanding of tropical hydrology and palaeoclimate. Secondly, southern Belize is at the northernmost extent of the ITCZ and therefore is extremely sensitive to latitudinal changes in ITCZ position over time. Thirdly, Central America is influenced by both Pacific and Atlantic large scale climate modes and therefore Belize is well placed to capture contributions from both, although discerning the result of interaction between these two centres of action may initially be challenging. Finally, southern Belize receives more than three meters of rain a year, thereby facilitating fast speleothem growth rates which are essential when creating sub-annually resolved records. As an aside, southern Belize is also interesting from an archaeological perspective. This area was in the heart of the Maya Lowlands during the height of the Maya Classic Period (2500-900AD) and yet is one of the least well understood regions of the Maya Lowlands. Climate study from this area therefore provides an interesting environmental perspective on the growth and demise of the Maya Civilisation in the area (Kennett et al. 2012; see Appendix A).

Understanding cave ventilation dynamics and speleothem drip hydrology is crucial for the correct interpretation of speleothem geochemical records. In light of this, Chapter 3 presents data from an ongoing remote monitoring effort at Yok Balum Cave, initiated in 2011, which provides supporting information for speleothem based palaeoclimate studies from the site and to identify one or more suitable samples for high resolution analysis. Cave atmosphere and hydrology are the focus of this chapter as these parameters have important consequences for geochemical climate signal emplacement in speleothem carbonate. The study focusses on seasonal ventilation regimes to determine whether cave air pCO_2 displays variability sufficient to cause significant seasonal bias in carbonate deposition. Hydrological links between the local climate and speleothem drip rates are also investigated to help discern climate signals contained within the palaeoclimate records discussed in Chapter 4 and 5 and to identify other samples for high resolution study. Active monitoring during a large (M7.4) earthquake in November 2012 provides a unique opportunity to assess the response of cave atmosphere and hydrology to substantial seismic activity. This is important for speleothem palaeo-proxy records in seismically

active regions. Chapter 3 therefore addresses aim 1) and supports the work presented in Chapters 4 and 5.

Development of a highly resolved (monthly scale) stable carbon and oxygen isotope record from stalagmite YOK-G, from Yok Balum Cave is presented in Chapter 4. This is one of the longest high resolution palaeoclimate records ever produced and helps to illustrate the impressive potential speleothems hold as palaeoclimate archives. The carbon stable isotope ($\delta^{13}C$) data is used to reconstruct wet and dry season rainfall variability over the last 430 years (1553 – 1983AD) and to identify relationships between rainfall and increasing anthropogenic aerosol emission rates since 1850AD. The resolution of the record, with approximately nine stable isotope measurements per year, is sufficient to permit investigation of short lived exogenous climate forcings, and consequently this chapter characterises the regional impact of these forcing events and links them to 20th century climate.

The ideas presented in Chapter 4, regarding the influence of volcanic forcing on North Atlantic climate variability and ITCZ migration, are extended in Chapter 5 using a 2000 year, highly resolved and precisely dated stable carbon isotope record from stalagmite YOK-I, from Yok Balum Cave (Kennett et al, 2012). Agreement with existing North Atlantic Oscillation (NAO) reconstructions confirms the validity of the record as an outstanding NAO correlate record. Results suggest that solar variability and explosive volcanism modify inter-hemispheric temperature contrasts resulting in meridional relocation of the ITCZ and subsequent atmospheric restructuring in the mid-latitude Atlantic region, creating NAO type circulatory signals. Comparison to rainfall proxies from other northerly low-latitude locations suggest that this is a global phenomenon and therefore has extensive implications for the low latitudes.

A summary of the major conclusions reached in each chapter is provided in the concluding chapter (6) and acts to draw together the implications of the three studies. Suggestions are made regarding future work and methods for advancing the data and arguments synthesised in this thesis.

Chapter 2

Yok Balum Cave

Yok Balum Cave

2.1 Introduction

This thesis presents research based on Yok Balum Cave, southern Belize. The cave was officially 'discovered' in 2005 but evidence exists that the ancient Maya visited the cave at various times during their population of the region (approximately 600-1100 AD) although very little disturbance is observed. Since 2005 small groups of tourists and scientists have visited the cave on an infrequent basis. In 2006 a number of speleothems were removed from the cave, including YOK-I (Kennett et al., 2012) and YOK-G, both of which feature in this thesis. The remote and undisturbed nature of Yok Balum cave makes it an ideal site for cave monitoring and speleological studies. Furthermore, the tropical location of the cave is significant for low-latitude climate reconstruction which has already been identified as a necessary field of development for the palaeoclimate community.

2.2 Geologic and tectonic setting

Nearly 3000km^2 of Belize is characterised by well-developed karst and more than 150km of surveyed cave passages (Miller, 1996). Actun Yok Balum (Jaguar Paw Cave in Mopan Mayan) is located in the Toledo District of southern Belize, ~3km south of the modern Mopan Maya village of Santa Cruz (16^o 12' 30.7" N, 89^o 4' 24.4" W; 366 meters above sea level) (Fig. 2.1). The cave, named after the large paw shaped flowstone at its main entrance (Fig. 2.2), is developed within the tectonically uplifted Cretaceous Campur limestone formation (Kennett et al., 2012; Miller, 1996) which originates from massive limestone deposition around the granite intrusions of the Maya Mountains to the north (Fig. 2.3). The cave is one of several which occur in a SW-to-NE trending

limestone karst ridge whose formation is likely associated with the vertical flow of chemically aggressive allogenic water originating on the highlands of the Maya Mountains (Miller, 1996). For a comprehensive explanation of geologic and karstic processes in southern Belize please see Miller (1996) and Bateson (1972) and references therein.

Yok Balum extends as a main trunk passage 540m from a small opening in the east to a larger, more elevated opening to the southwest – a result of more recent cave roof collapse (Fig. 2.4). Uranium-series dating of the base of a stalagmite growing on a breakdown block associated with the collapse dates the collapse at a minimum of 44,000 ± 3300 years BP (D. Richards, 2013 P.C). There is also considerable evidence of seismic activity within the cave including large faulted flowstones and displaced speleothems. Uranium-series dating of carbonate precipitated within a faulted flowstone provided a date of 26,400 ± 170 years BP (D. Richards, 2013 P.C).

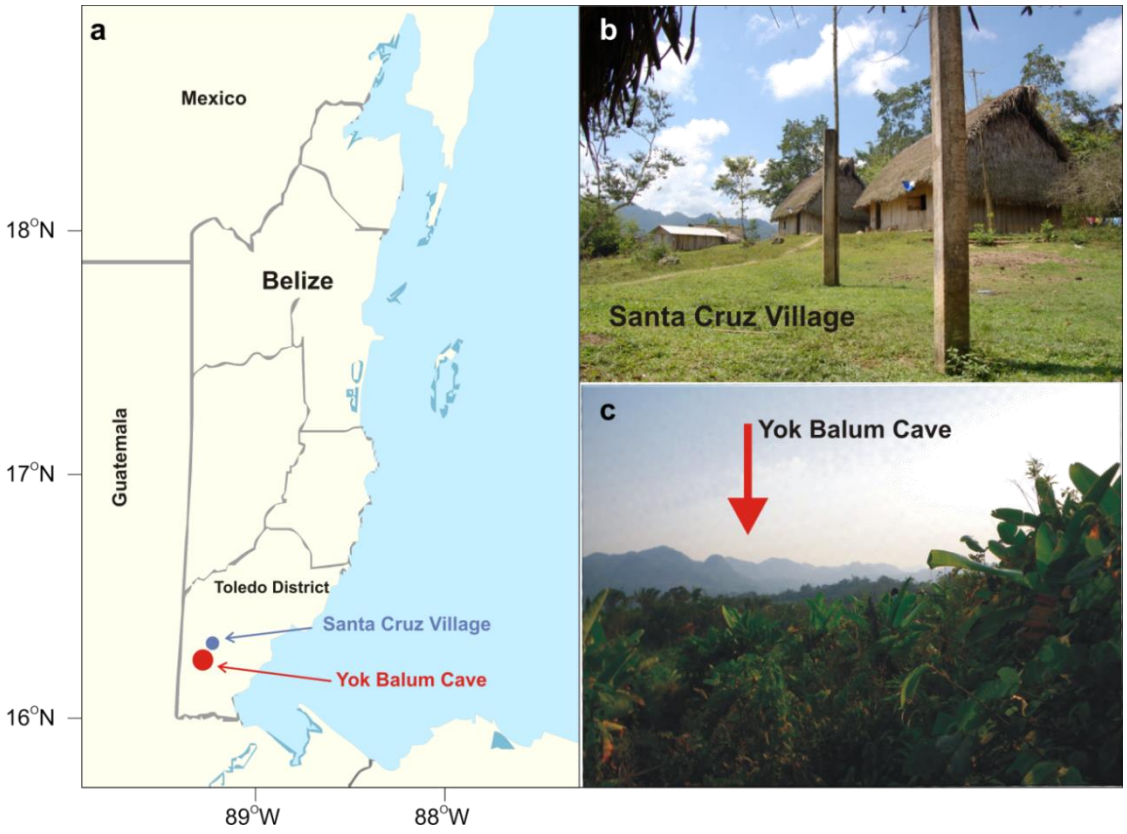

Figure 2.1 a) Map of Belize identifying the Toledo District, Santa Cruz Village and Yok Balum Cave **b)** Photograph of Santa Cruz Village and **c)** Photograph looking south-west from Santa Cruz towards the limestone ridge of Yok Balum Cave.

Figure 2.2 'Jaguar Paw' flowstone at the entrance to Yok Balum Cave

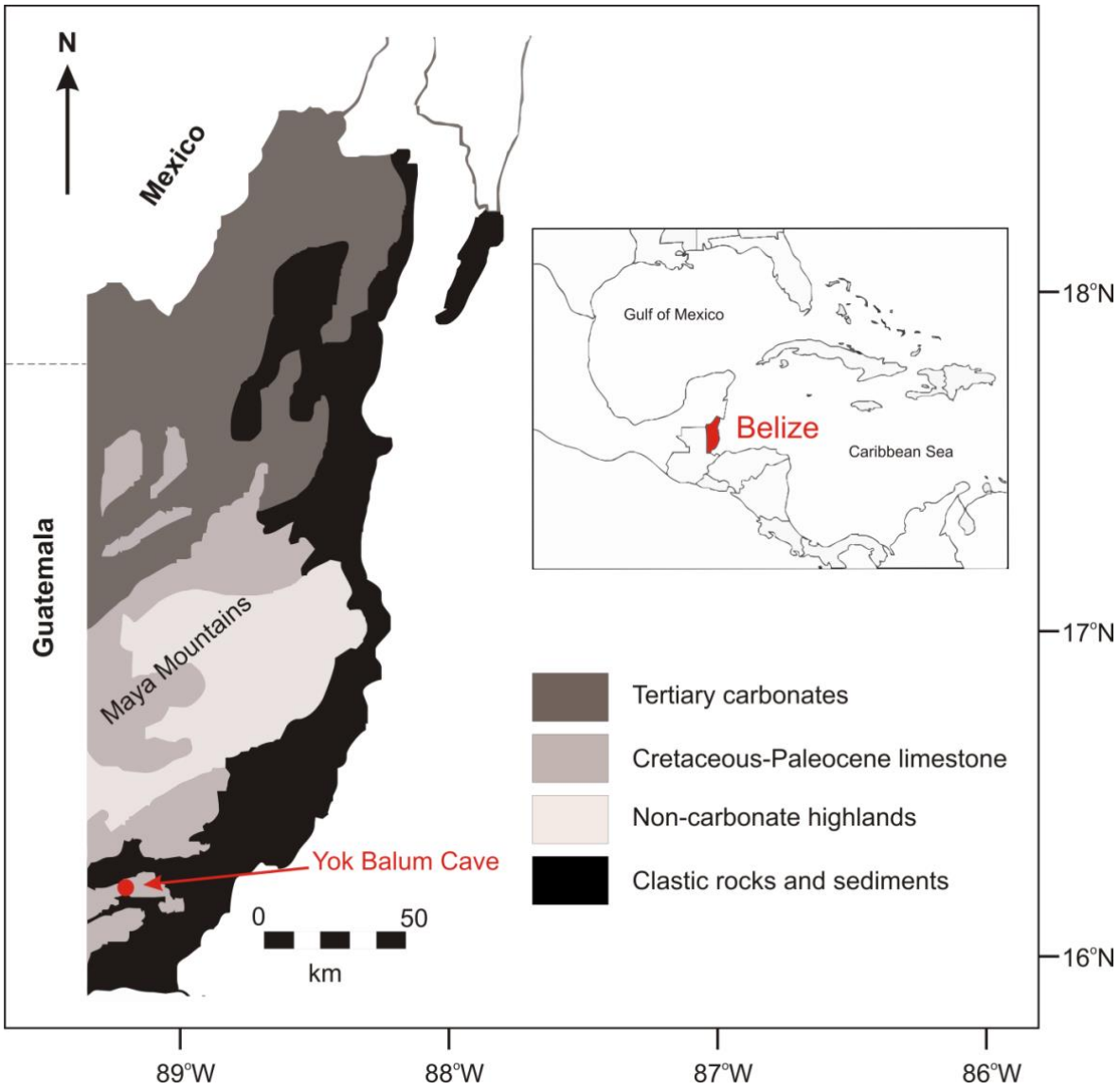

Figure 2.3 Geological map of Belize (adapted from Miller 1996) and the location of Yok Balum Cave. Wider geographic location of Belize shown in insert.

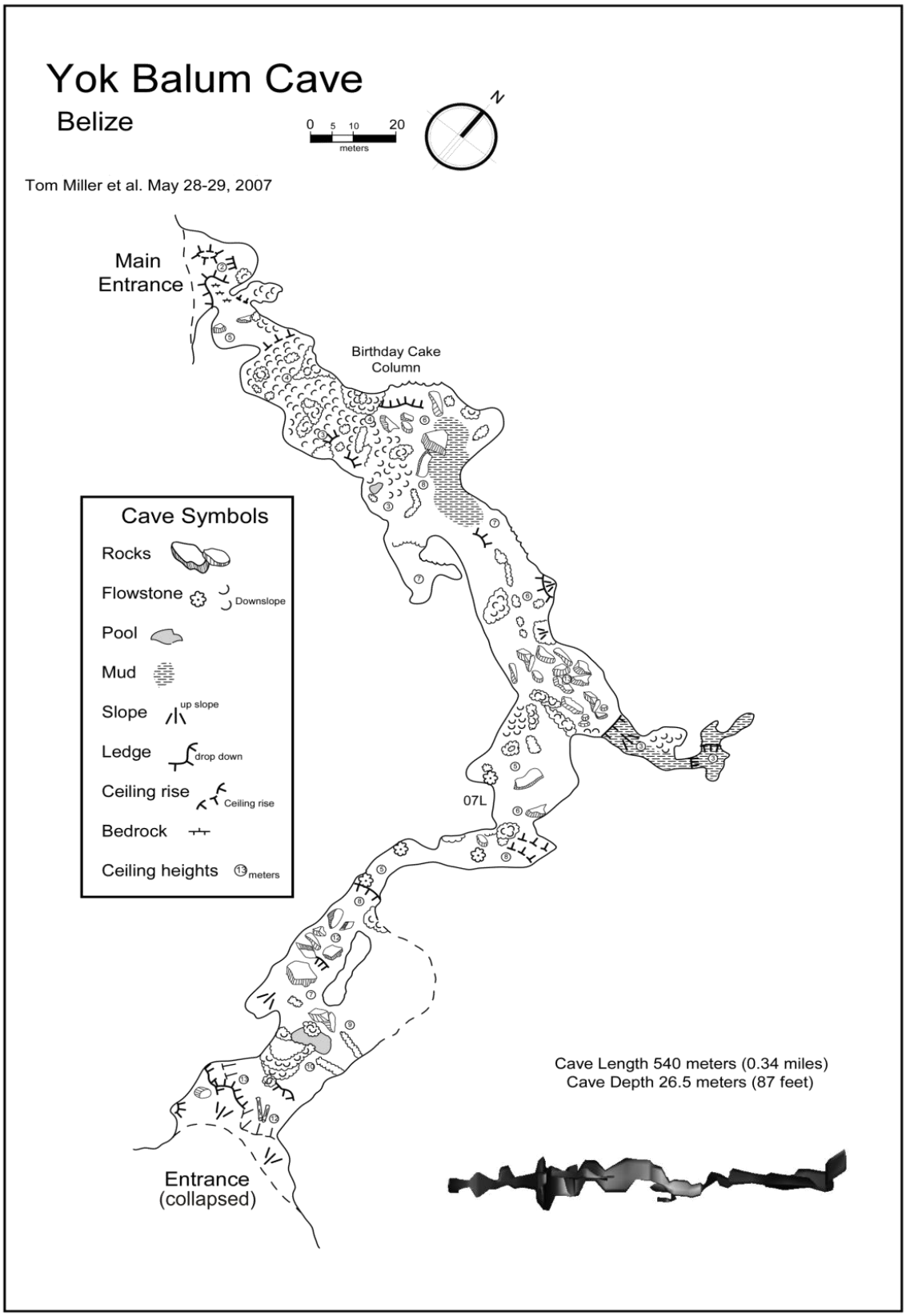

Figure 2.4 Yok Balum cave map (Mapped by Miller et al, 2007)

The cave is extremely active in terms of speleothem development, particularly in the north-eastern portion of the cave around the large 'Birthday Cake' stalagmite feature. In this area of the cave the overhead karst roof was calculated to be ~14m thick from cave cavity to the surface. Many drips feeding stalagmites in this area are active all year round but with considerably more water through flow during the summer wet season. Aside from the very infrequent visits by tourists and scientists since its discovery in 2005, the cave is undisturbed. The area surrounding the cave has been logged selectively using hand tools by indigenous subsistence farmers on and off since the 1950s, but the vegetation directly above the cave is thought to be undisturbed due to the steep and precarious slopes leading to the area above the cave.

Central America is a diverse tectonic region. Much of the structural geology in the region results from up-thrust features associated with tectonic activity and large igneous intrusions (Miller, 1996). Along the western coast of Central America the Cocos Plate is subducting beneath the North American and Caribbean Plates (Fig. 2.5). The result of this subduction is the Central America Volcanic Arc, a belt of volcanic and seismic activity which extends parallel to the Pacific coast from Costa Rica to Mexico. A divergent boundary exists between the North American and Caribbean Plates approximately 100km south of the southern Belize border. The dominant source of seismic activity felt in southern Belize however will be intermediate depth earthquakes occurring within the subducted Cocos Plate.

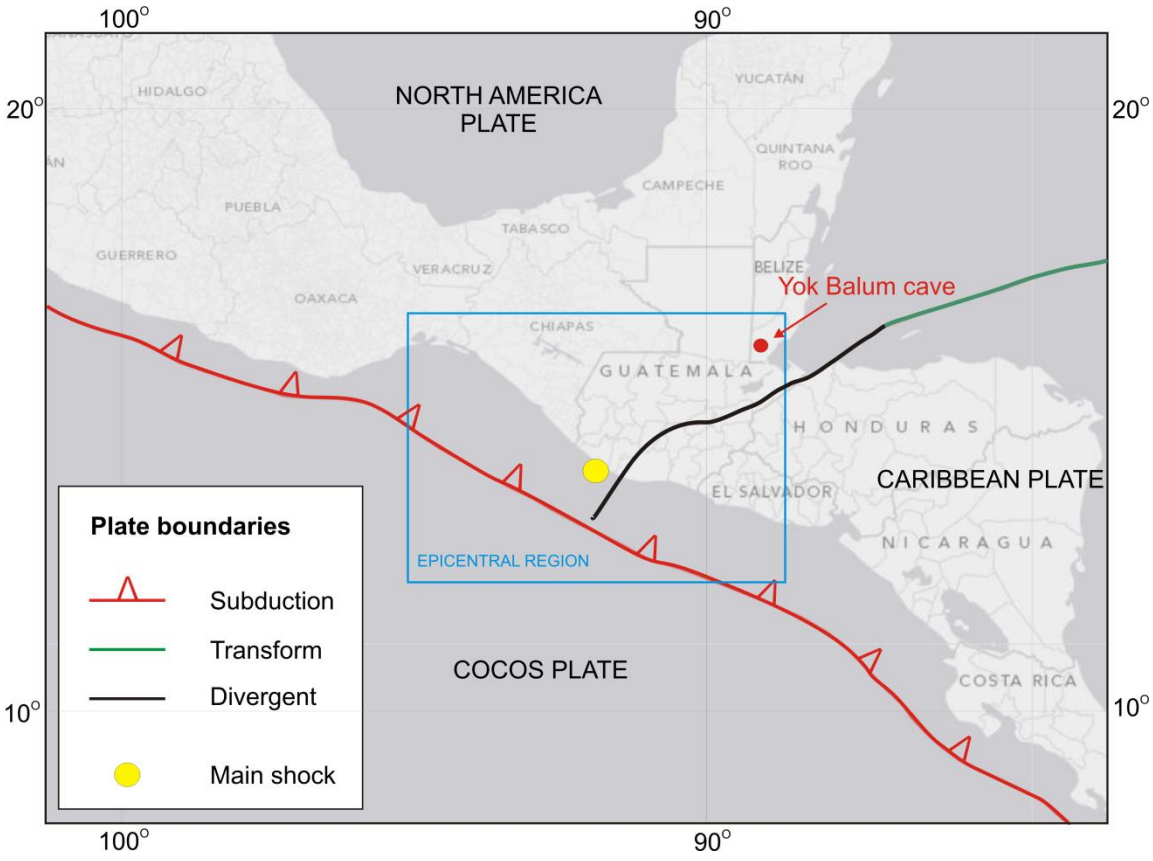

Figure 2.5 Tectonic setting of Belize region, including tectonics boundaries (adapted from the United States Geological Survey). Estimated epicentre (yellow dot) and epicentral region (blue rectangle) of 7th November 2012 earthquake.

2.3 Climate and hydrology

Belize undergoes a climate transition from tropical savannah in the north to tropical forest in the south. In southern Belize monthly temperatures remain fairly constant, ranging ~4^{o}C around the annual mean of 22.8^{o}C. The coolest months are December through to February. Daily temperatures are controlled predominately by cloud cover, with extensive cloud cover limiting solar insolation reaching the surface. Rainfall distribution in Belize is controlled predominantly by elevation and latitude. Total annual rainfall is ~1300mm in the north and west and as high as 4500mm in the south (Fig. 2.5). The topographic bulk of the Maya Mountains contribute to this latitudinal discrepancy (Miller, 1996) as does southern Belize's proximity to the current most northerly extent of the ITCZ. Distinct wet (May through January) and dry (February through April) seasons exist, with >80% of total annual rainfall occurring between June and September as a direct result of seasonal ITCZ migration (Kennett et al., 2012). Evaporation surpasses precipitation during the dry season, greatly reducing the amount of water infiltrating soil and karst zone (Kennett et al., 2012; Miller, 1996). However, intense rainfall on daily timescales provides recharge to the karst year round. Modelling studies have identified the Caribbean Sea as the principal moisture source, with a far smaller contribution coming from the Pacific Ocean (Kennett et al., 2012). The Caribbean Sea climate and hydrology varies seasonally, predominantly with the patterns of trade wind convergence and the seasonal migration of the ITCZ in accordance with the shift in the thermal equator between boreal summer and winter. In the boreal summer the ITCZ will be in a more northerly position, between 6^{o} and 10^{o}N, over the Caribbean. During this time the Caribbean climate is characterised by enhanced precipitation. Additionally, hurricanes and large-scale convective systems can bring heavy localised rain to southern Belize. Since 1900 42 storms, ranging from tropical depression to Category H5 (Saffir-Simpson scale), have passed within 200km of the cave site.

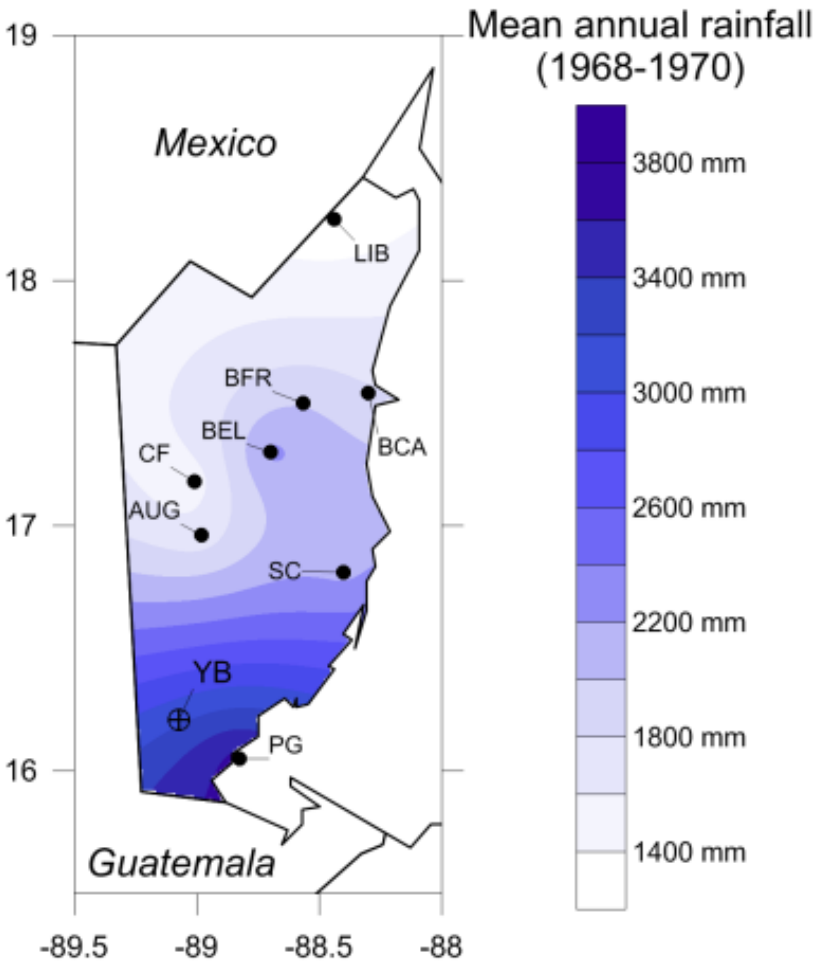

Figure 2.6 Mean annual rainfall in Belize based on records from 1968-1970. These are the only years where full rainfall records were complete for all sites. (LIB = Libertad, BCA = Belize City Airport, AUG = Augustine, CF = Central Farm, BEL = Belmopan, BFR= Big Falls ranch, SC = Stann Creek, PG = Punta Gorda, YB = Yok Balum Cave).

Chapter 3

High resolution monitoring of a tropical cave system reveals dynamic ventilation and hydrologic resilience to seismic activity

A version of this chapter has been submitted to the Journal of Cave and Karst Studies co-authored by
Harriet E. Ridley[1], James U.L. Baldini[1], Keith M. Prufer[2], Izabela W. Walczak[1] and Sebastian F.M. Breitenbach[3].

[1] Department of Each Sciences, Durham University, Durham, UK.
[2] Department of Archaeology, University of New Mexico, Albuquerque, New Mexico, USA.
[3] Department of Earth Science, Eidgenössische Technische Hochschule (ETH), Zürich, Switzerland.

A version of this chapter has been submitted to *The Journal of Cave and Karst Studies* with the following author contributions:

Harriet Ridley conducted fieldwork, performed data analysis and wrote the manuscript thereby contributing to over 95% of the work presented in this Chapter.

James Baldini, **Keith Prufer**, **Izabella Walczak** and **Sebastian Breitenbach** assisted with fieldwork, provided comment on and approved the manuscript.

High resolution monitoring of a tropical cave system reveals dynamic ventilation and hydrologic resilience to seismic activity

3.1 Abstract

The nature of cave ventilation is of interest to cavers, speleologists and palaeoclimatologists working with stalagmites. Because cave ventilation systematics may change over the growth span of a stalagmite, understanding what factors affect them is critical for determining events that may have potentially affected climate proxies contained within the carbonate. Similarly, understanding how the hydrology of the drip feeding a stalagmite evolves through time and responds to surface climate is key to building robust records of palaeoclimate. Here we present data from an extensive, ongoing monitoring effort at Yok Balum Cave, Belize, initiated in 2011, that characterises high resolution ventilation and hydrology dynamics at this site. Seven characteristically diverse drip regimes were studied to facilitate the selection of speleothem samples which display good hydrological connectivity with the surface. Clear seasonal ventilation regimes exist, driven by thermally induced inside-outside air density differences. The winter regime is dominated by air inflow and lower karstic drawdown into the cave and a limited diurnal signal, while summer is dominated by air outflow, high karstic CO_2 drawdown and drip water degassing and a strong diurnal signal. Active monitoring during a large (M7.4) earthquake in November 2012 provides a unique opportunity to assess the response of cave atmosphere and hydrology to substantial seismic activity. Cave atmosphere and hydrology is found to be highly resilient to seismic activity, with no observable disturbance occurring around the earthquake, despite there being considerable evidence of physical disruption in the cave. Monitoring included a complete cross-section of different drip hydrologies, and no drip type was affected by the earthquake. This suggests that stalagmite-derived palaeoclimate records are not affected by seismic activity, except in extreme cases where the stalagmite or conjugate stalactite are damaged or reoriented.

3.2 Introduction

Long-term cave monitoring studies provide site-specific information on cave dynamics which is of use to cavers and speleologists; particularly speleo-climatologists who utilise monitoring information to correctly interpret proxy information derived from speleothems.

Characterising caves in terms of their unique ventilation processes is important as it has a first order control on atmosphere composition, can potentially lead to seasonal bias in speleothem growth and consequently has significant implications when interpreting palaeoclimate proxy signals from speleothems (Baldini, 2010; Kowalczk and Froelich, 2010; Sanchez-Canete et al., 2013). Real-time cave atmosphere data is also useful when characterising cave ecosystems (De Freitas et al., 1982; Oh and Kim, 2011) and assessing cave suitability for industry and tourism (De Freitas et al., 1982; Dueñas et al., 1999; Dueñas et al., 2011; Smithson, 1991; Virk et al., 1997). Estimation of cave ventilation is possible directly, via anemometers (Sanchez-Canete et al., 2013), indirectly via measurement of radon gas (^{222}Rn) levels (Faimon et al., 2006; Hakl et al., 1997; Kowalczk and Froelich, 2010; Oh and Kim, 2011) and other tracer gases (De Freitas et al., 1982) or by studies of air density contrasts and thermal patterns within the cave (Faimon et al., 2012; Sanchez-Canete et al., 2013; Smithson, 1991). The importance of understanding unique cave ventilation mechanisms has been highlighted in recent studies (Baker et al., 2014; Cowan et al., 2013; Kowalczk and Froelich, 2010; Mattey et al., 2010) as the unique nature of ventilation in individual caves can negate general assumptions regarding the seasonality of carbonate precipitation. For example, Mattey et al. (2010) identified unusual seasonal ventilation regimes in New St Michaels Cave, Gibraltar where the summer season was typified by low cave air pCO_2. This proved important when linking seasonal regimes to calcite fabric, paired annual laminae and stable isotope and trace element variability and highlighted the importance of understanding unique cave environments to aid speleothem proxy interpretation. Monitoring studies like this become increasingly paramount as speleothem based palaeoclimate studies continue to develop higher resolution records which are resolved to a seasonal or sub-seasonal level.

Karst hydrology and flow routing pathways specific to each speleothem control how directly geochemical climate signals are transferred from the surface to speleothem carbonate. Changes in karst hydrology can be caused via changes in seasonal rainfall patterns (Baldini et al., 2006b; Treble et al., 2003) and result in considerable modification of drip water chemistry and carbonate precipitation rates (Banner et al., 2007; Mickler et al., 2006; Spötl et al., 2005). These factors are unlikely to be static through time and extensive monitoring can reveal variability on daily to multi-annual timescales. Cave monitoring therefore provides insight into how a cave responds to above ground climatic forcing events and is an essential pre-requisite to speleothem sample selection and palaeoclimate proxy interpretation.

Caves in seismically active regions can display considerable evidence of past seismic activity, such as: broken speleothems, speleothem growth anomalies and deformation, and displacement and rock fall events (Becker et al., 2006; Gilli, 1999; Gilli and Delange, 2001; Gilli and Serface, 1999). A limited number of studies have attempted to quantify the possible effect of seismic activity on the karst cave atmosphere (Sebela et al., 2010), particularly with regarding CO_2 variability and seismic disruption to hydrology. Seismic activity affects cave ^{222}Rn and CO_2 levels through increased rock permeability leading to higher within cave concentrations (Menichetti, 2013; Sebela et al., 2010; Virk et al., 1997; Wu et al., 2003). Because cave air pCO_2 levels exert a strong control on carbonate precipitation rates (Baldini, 2010; Banner et al., 2007; Kowalczk et al., 2008; Palmer, 2007) this is particularly significant when interpreting palaeoclimate proxy evidence from speleothems in caves which may have been subject to substantial tectonic activity as substantial crustal degassing has the potential to stagnate speleothem growth; particularly in deep, poorly ventilated passages. This can complicate palaeoclimate proxy interpretations from speleothems for weeks to years depending on site specific ventilation regimes. ^{222}Rn is a radioactive yet inert tracer gas frequently used to assess cave ventilation (Kowalczk and Froelich, 2010; Oh and Kim, 2011). It also poses a health risk in confined, poorly ventilated caves (Field, 2007; Virk et al., 1997) and therefore its relation to seismic activity warrants assessment, particularly in commercial or tourist caves.

It is also largely unknown how seismic activity may affect karst hydrology and stalagmite drip regimes. Changes in the hydrological regime feeding a stalagmite can also affect speleothem growth rates and the transmission of geochemical signals from overlying climate to the speleothem carbonate and consequently, seismic disruption to hydrology can have important implications when interpreting palaeoclimate proxy data in speleothems.

This study presents high resolution cave monitoring data from Yok Balum Cave, Belize. These data provide detailed information regarding seasonal cave ventilation mechanisms through investigation of cave pCO_2 and air density relationships and via examination of thermal gradients as evidence of internal-external air exchange. An understanding of the subtle seasonally variable fluxes of cave air CO_2 allows improved interpretations from not only Yok Balum, but other tropical sites as well. Additionally, active monitoring during a large (M7.4) earthquake in November 2012 provides a unique opportunity to assess the response of cave atmosphere and hydrology to substantial seismic activity.

3.3 Monitoring equipment

Tropical environments provide a challenging environment for electrical monitoring equipment, especially for long term monitoring studies in remote areas. The threat of high humidity and water was minimised by storing non-waterproofed equipment in airtight boxes and sealed plastic bags with a silica desiccant where appropriate. Above cave soil temperature was recorded hourly using a Tinytag temperature logger buried at 0.4m depth. Cave air CO_2 was monitored every three hours between April 2011 and January 2013 (with a four month break from June 2012 to October 2012 due to equipment failure) using a Vaisala CARBOCAP Carbon Dioxide GMP343 Probe (± 3 ppm + 1% of reading) linked to a Vaisala MI70 Indicator and powered by two parallel Duracell MN918 Lantern batteries. A Radon Scout Plus, powered by two D-cell batteries and a four D-cell external battery pack was set up next to the within cave CO_2 logger to detect radon fluctuations every three hours for the same time period. The

Radon Scout, being extremely sensitive to moisture, was kept in a water tight box. This resulted in a muted radon measurement as α particle passage to the logger was somewhat restricted. For qualitative assessment of ^{222}Rn fluctuations this was not considered an issue, however, ^{222}Rn values peaked during data download when the logger was removed from the box. To account for this, ten days of data were removed after data was download to allow ^{222}Rn values to return to 'normal' levels. A Barotroll pressure and temperature logger was installed to measure hourly barometric pressure and temperature (precision ±0.1% and ±0.1^{o}C) both inside and above the cave. Tintytag temperature loggers were placed in transect along the cave, measuring hourly temperature and relative humidity. Stalagmate automated drip loggers were chosen to record hourly drip rates of drips feeding stalagmites of interest. A total of seven Stalagmates were installed, five on actively dripping stalagmites with promising morphologies and two on scars of previously removed stalagmites (YOK-G, Chapter 4 and YOK-I, Chapter 5). Cleaned Iceland calcite spars were placed on top of the Stalagmates to allow effective calcite farming. Calcite spar is considered more appropriate than eye glass plates for calcite collection as initiation of new calcite growth is eased by an already present calcite lattice. Each Stalagmate was tested during installation to ensure that drips were registering correctly.

Data was downloaded and the equipment maintained every four months. The location of all equipment and monitored drip sites is shown in Figure 3.1.

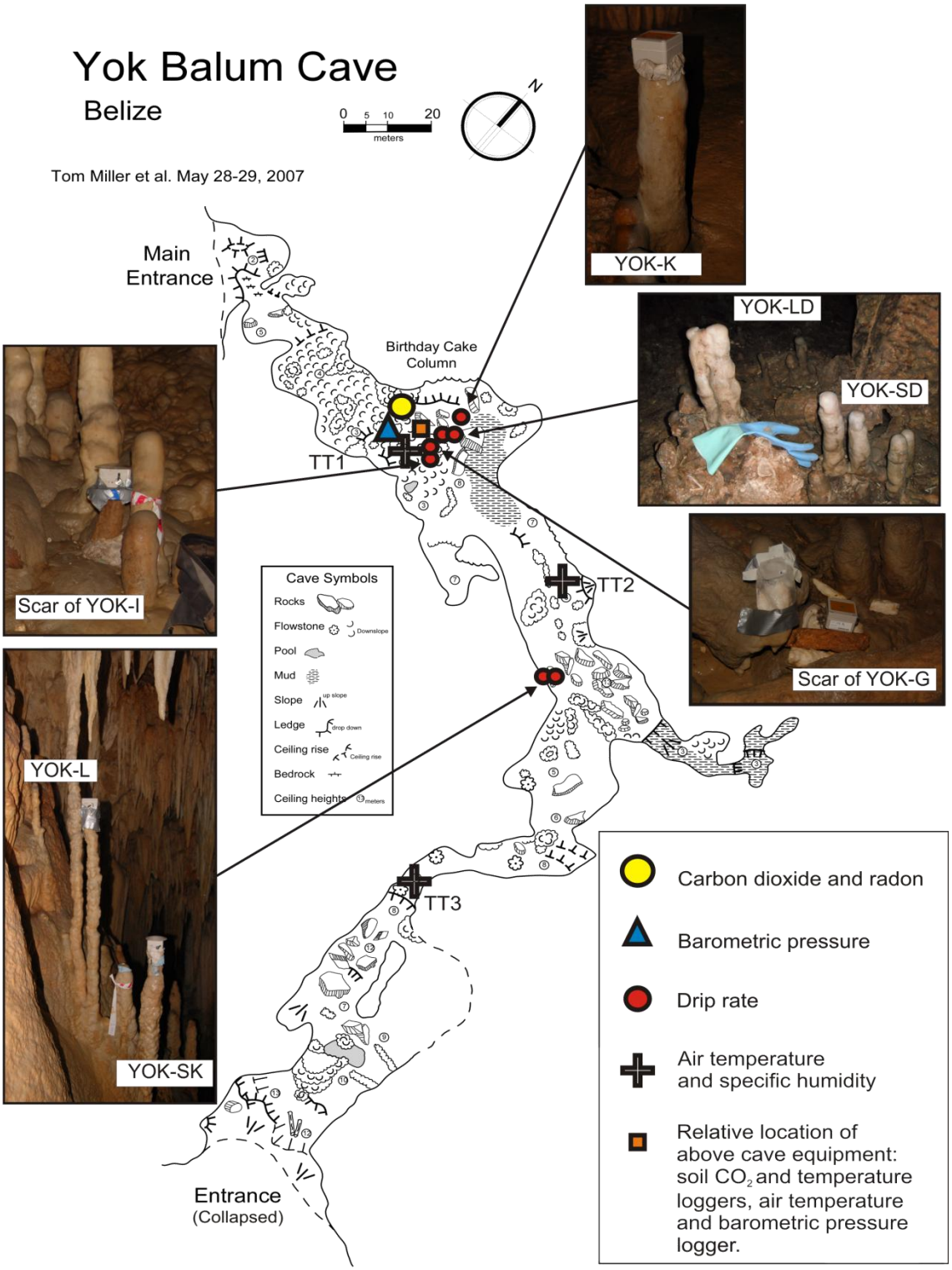

Figure 3.1 Location of all monitoring equipment in Yok Balum Cave. Adapted from map by Miller et al. (2007).

3.4 Recent seismic activity

On November 7th 2012 at 16:35 (UTC) (10.35AM local time) a 7.4 magnitude earthquake was recorded off the coast of Guatemala, 35km south of Champerico (13.963°N 91.854°W). The epicentre was estimated to be at a depth of 24.0km and occurred as a result of thrust faulting on, or near, the subduction zone of the Cocos plate and the overlying Caribbean and North American plates (Chapter 2, Fig. 2.2) (United States Geological Survey). Tremors were felt in parts of Mexico, El Salvador, Belize, Honduras, Nicaragua and Costa Rica and villagers from Santa Cruz reported experiencing the tremors. According to United States Geological Survey estimates this magnitude quake would result in a seismic hazard at the cave site of 1.6 – 2.4 m/sec^2 (measured in peak ground acceleration). A field crew returned to the cave in January 2013 to find large fallen blocks at the cave main entrance and numerous displaced and freshly broken stalagmites and stalactites within the cave. Reasonable evidence therefore suggests that the cave was subject to seismic activity on or around November 7th 2012. There are only a handful of published studies reporting earthquake damage to caves (Gilli, 1999; Gilli and Delange, 2001; Renault, 1970) and so these observations of the effect of seismic activity on cave environmental variables are pertinent to the science of speleology.

3.5 Study of Yok Balum Cave Ventilation

3.5.1 Cave Ventilation

Cave ventilation (air exchange with the outside atmosphere) has a first order control on cave atmosphere composition and is dependent on a number of factors including fluctuations in temperature and pressure, cave geometry and susceptibility to external winds (Baldini et al., 2006a; Bourges et al., 2001; Cowan et al., 2013; Denis et al., 2005; Kowalczk and Froelich, 2010; Spötl et al., 2005). Pfitsch and Piasecki (2003) classify cave passages in terms of air movement as being dynamic, transitional or static,

however the static state is very rarely observed, aside from in deep passages (Pflitsch and Piaseki, 2003; Przylibski and Ciezkowski, 1999). Convective air circulation, driven by internal versus external air density differences, is a dominant ventilation mechanism in caves with more than one entrance at different elevations (Badino, 2010; Gregoric et al., 2013; Kowalczk and Froelich, 2010; Wigley, 1967). In tropical caves, where cave air temperatures do not vary significantly on seasonal timescales, air density difference will be predominantly controlled by surface temperature and barometric pressure variations (Fairchild et al., 2006). Air density responds primarily to temperature (Faimon et al., 2012; Gregoric et al., 2013; Gregoric et al., 2011) and to a lesser extent pressure and humidity as expressed in equation (1) below (after Kowalczk (2009)):

$$\rho_{air} = \frac{P}{R_d \bullet T_v}$$

(Equation 1)

Where T_v is virtual temperature calculated via equation (2), R_d is the universal gas constant and P is barometric pressure.

$$T_v = (T + 273.15)/(1 - (0.379 \bullet \frac{6.11 \bullet 10^{\frac{7.5 \bullet T_d}{237.7 + T_d}}}{P}))$$

(Equation 2)

Failure to account for cave CO_2 can lead to errors of up to 9°C between internal vs external T_v when CO_2 of the cave air is an order of magnitude or greater than that of the free atmosphere (Sanchez-Canete et al., 2013). At Yok Balum maximum recorded CO_2 is 770ppm and the summertime mean is ~500ppm and therefore insufficient to warrant this correction.

Typically, during the winter months, external air temperature will be cooler than that of the cave and a positive air density difference will dominate. Alternatively, during the summer, warmer external temperatures will result in typically negative air density

difference. Local weather may result in short lived reversals in cave-atmosphere air density differences. The particular ventilation influence of seasonal air density differences between cave and free atmosphere is governed by the specific cave geometry (e.g passage orientation and size), the distance from cave entrances and total cave volume (Batiot-Guilhe et al., 2007; Cowan et al., 2013).

3.5.2 Results and Discussion

The diurnal and seasonal patterns of airflow at Yok Balum are a direct response to a thermally induced disequilibrium in air density between the cave and outside air. This has been identified as the primary driver of cave ventilation at other caves (De Freitas et al., 1982; Kowalczk and Froelich, 2010). Within cave temperature is nearly constant at 22.4^{o}C ($^{+}$/$_{-}$ 0.5^{o}C) year round, although a low amplitude diurnal signal is present. Within cave temperature is equivalent to the average yearly external temperature (Fig. 3.2) and is likely the result of moderation of outside temperatures by the epikarst. External air temperature can affect cave air pCO_2 by both inducing density driven ventilation associated with inside-outside air density differences (De Freitas et al., 1982) (Fig. 3.3) and by promoting higher soil pCO_2 stimulating biological activity in the soil zone (Baldini et al., 2008; Bond-Lamberty and Thomson, 2010; Hess and White, 1993; Murthy et al., 2003; Sherwin and Baldini, 2011).

The simple structure of Yok Balum cave, with two entrances, one at either end of a single main trunk passage, results in a well-ventilated dynamic cave system, evidenced by the low annual mean CO_2 values (461ppm) (Fig. 3.3b). However, CO_2 displays clear seasonal trends in both mean concentration and variability. Summer (April - October) is characterised by higher mean pCO_2 (~500ppm) and high temporal variability (standard deviation of 72.5ppmv) whereas winter (November – March) has lower pCO_2 (~420ppm) and displays lower temporal variability (standard deviation 24.3ppmv). This is evidenced by the respective summer and winter pCO_2 entropy values (E) (Fig. 3.3). Entropy isthe mean cumulative sum of absolute first differences of a time or spatial derivative and is therefore a measure of the variability of a time series (Denis and Crémoux, 2002; Denis et al., 2005). CO_2 displays entropy of approximately 430 during

the summer and 150 during the winter, indicating that the variance is nearly three times greater during the summer months. These trends in pCO_2 mean values and variance are controlled by seasonal CO_2 flux into the cave and ventilation, most likely controlled by rainfall and temperature respectively. The following sections will use high resolution monitoring data to describe the seasonal ventilation regimes occurring in Yok Balum. It should be noted that the summer and winter seasons are not synonymous with the wet and dry seasons, but are classified here by relative external to cave temperatures. During the summer months external temperature is greater than within cave temperature and vice versa for winter.

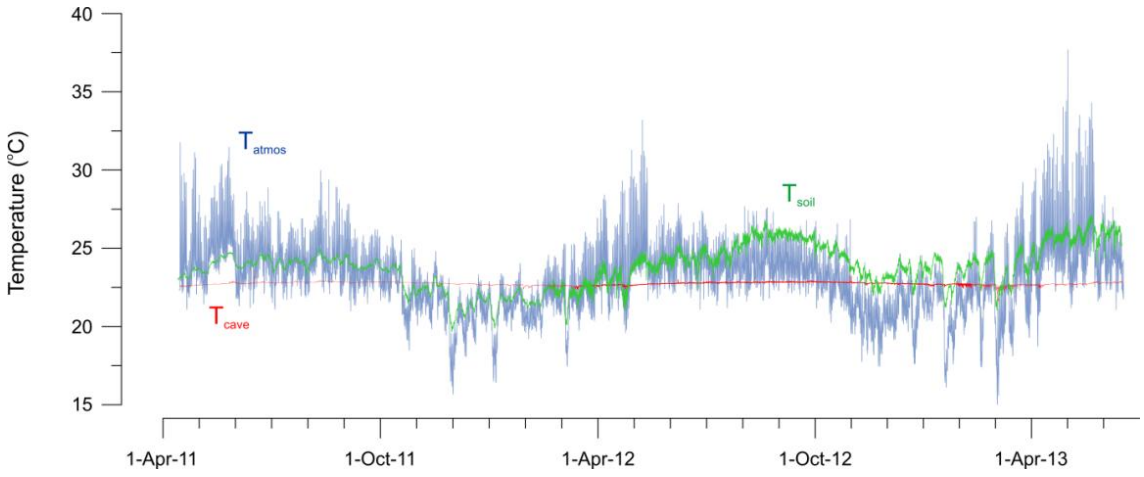

Figure 3.2 26.5 month time series of hourly within cave (T_{cave}), soil (T_{soil}) and external air (T_{atmos}) temperature.

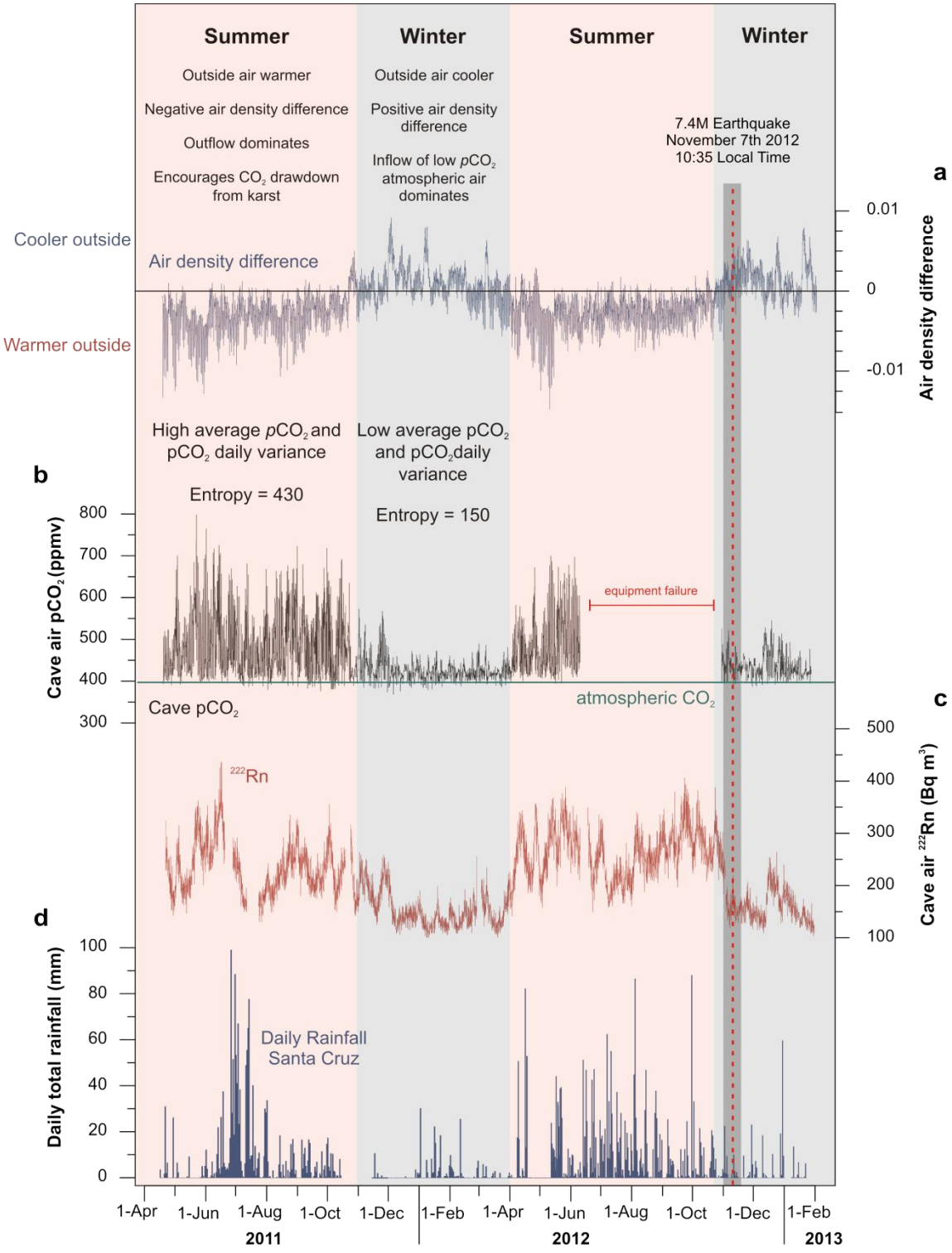

Figure 3.3 Seasonal regimes and dominant characteristics of a) hourly inside vs outside cave air density difference b) Three hourly cave pCO_2 and summer (April through October) and winter (December through March) pCO_2 Entropy values (E) c) Three hourly ^{222}Rn and d) daily rainfall at Santa Cruz. November 7th earthquake (red dashed line) and surrounding two week period (grey shaded section, shown in Figure 3.10).

3.5.2.1 Summer regime

Air density differences between the cave and the free atmosphere, controlled predominantly by external temperature, drives the summer season diurnal ventilation regime. Outside air temperature (T_{atmos}) is higher on average than that inside the cave (T_{cave}), producing an almost constant negative air density difference (Fig. 3.3a). In a typical one entrance cave system this could cause severe season long stagnation, and subsequently very high pCO_2, as the cooler denser cave air becomes trapped at the lowest point of elevation in the cave (Cowan et al., 2013; Spötl et al., 2005). At Yok Balum complete stagnation does not occur because the dual entrance system provides a means of outflow for density driven flow from the more elevated south-western (second) entrance to the lower north-eastern (main) entrance.

Outside air temperature begins to rise around 06:00am and reaches a maximum in the early afternoon. At this point cave-atmosphere air density difference is greatest and air outflow is at a maximum (Fig. 3.4a). As the air density difference increases during this period, outflow occurs at both entrances; CO_2 concentrations will simultaneously increase as high pCO_2 air is drawn out of the overlying karst and soil zones. During the day biological activity in the soil will also be at a diurnal maximum producing higher soil pCO_2. By late afternoon the cave-atmosphere air density difference begins to decrease and the volume of outflowing air decreases, reducing CO_2 drawdown from the karst. Outflow at the lower, main entrance weakens or ceases completely. As the cave-atmosphere air density difference reaches a minimum, around 01:00am, cave air pCO_2 reaches minimal values. This is most likely due to minimised CO_2 drawdown and inflow of low pCO_2 atmospheric air from the second entrance (if T_{cave} reaches or surpasses T_{atmos}) flushing through the cave from the second entrance to the lower main entrance. If the outside air density remains considerably higher than that of the cave then pCO_2 may remain elevated, but will decrease somewhat due to decreased karst drawdown, lower soil activity and some air movement driven by the venturi effect (Fig. 3.5). Areas closest to the entrances can be expected to undergo the most ventilation, particularly at the second entrance which is larger. Increased water through-flow during the wet season is undoubtedly an additional driver of higher

average summer pCO_2 as it increases dissolved CO_2 transport to the cave, increasing degassing and consequently producing higher cave pCO_2.

3.5.2.2 Winter regime

During the winter season outside air temperatures are generally cooler than those inside the cave, producing a positive air density difference and a ventilation regime dominated by inflow. Ventilation is therefore more continuous than during the summer.

Maximum air density difference occurs at night (around 03:00am) when T_{atmos} is at a minimum (Fig. 3.4b). Cooler outside air flushes into the cave, predominantly through the more elevated, second entrance but also at the main entrance. Cave air pCO_2 will therefore approximate that of the external atmosphere. Outside air temperatures begin to rise at ~06:00am and reach a maximum at ~14:00pm, as in the summer season. However, as the outside temperature increases it approaches that of the cave air, reducing the air density difference to near zero (or to negative values if T_{cave} surpasses T_{atmos}). This reduces air inflow to the cave and if a negative air density difference occurs then outflow may occur during this time. This variation of air density difference over a threshold value results in a daily ventilation regime whereby the cave 'inhales' during the day and 'exhales' at night. The 'inhalation' during the day draws low pCO_2 air into the cave, flushing the cave and keeping pCO_2 values similar to atmospheric levels. Any weak 'exhalation' at night continues effective air turnover and maintains low pCO_2 concentrations. Again, it is the areas close to the entrances that will undergo the most rigorous air turnover (Fig. 3.6). A combination of inflow dominated ventilation and less CO_2 from drip water degassing keeps winter cave air pCO_2 at near atmospheric levels. A less distinct diurnal regime is observed in CO_2 and air density difference variability. During the summer, increased water through flow, strong air outflow and large CO_2 drawdown, increase average pCO_2 and daily variability.

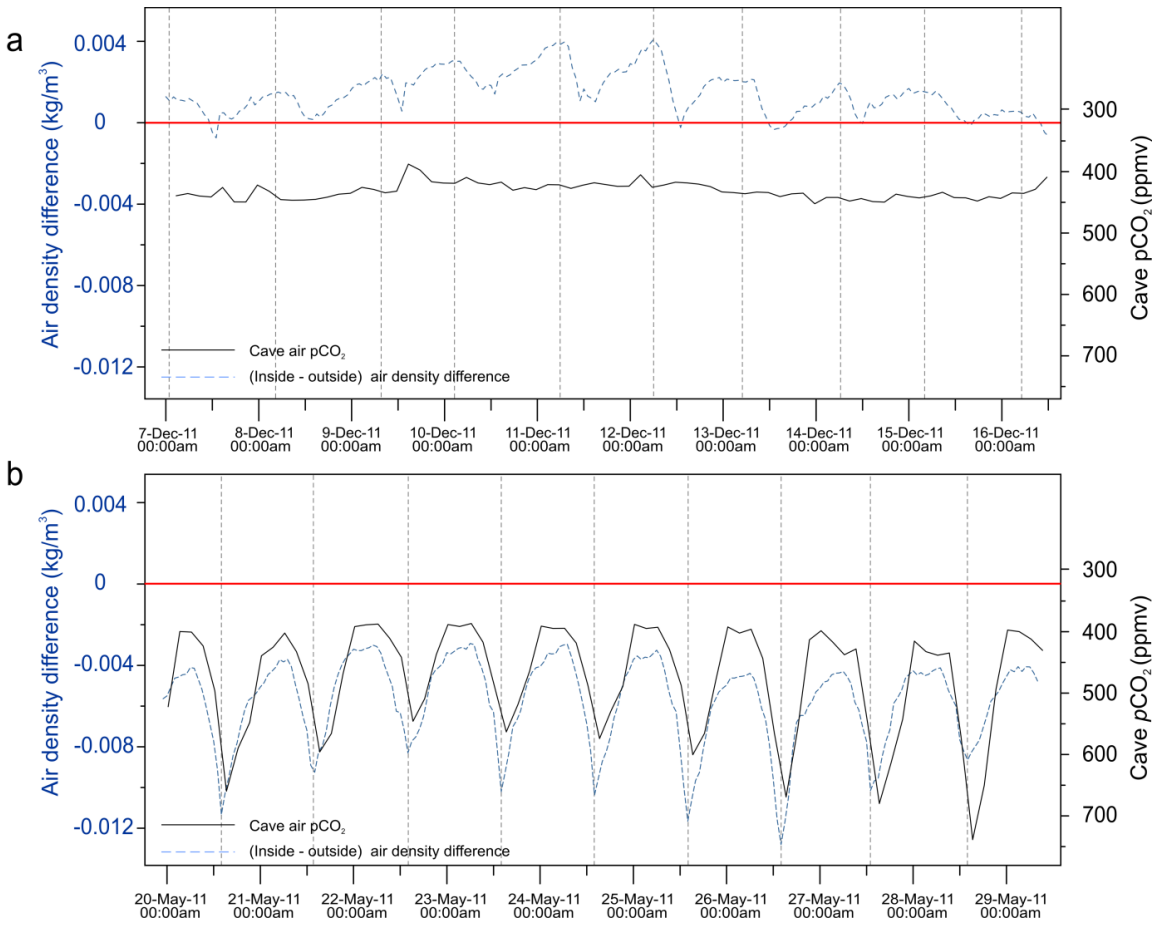

Figure 3.4 Hourly cave air density difference and cave pCO_2 over **a)** 7th – 16th December 2011 (winter) and **b)** 20th – 29th May 2011 (summer).

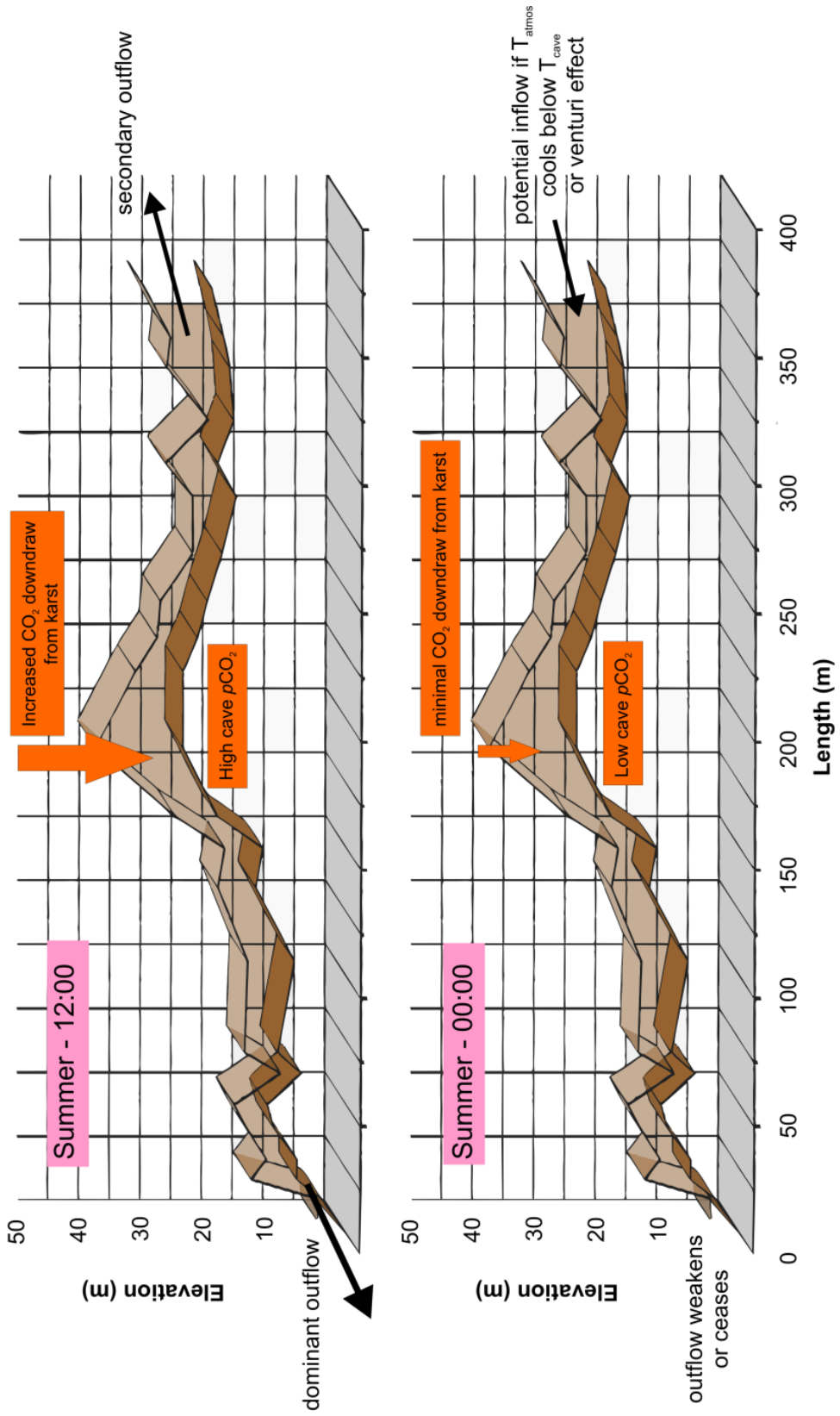

Figure 3.5 Yok Balum long profile with schematic of theorised primary air flows and CO_2 flux during the summer at 12:00pm (top panel) and 00:00am (bottom panel).

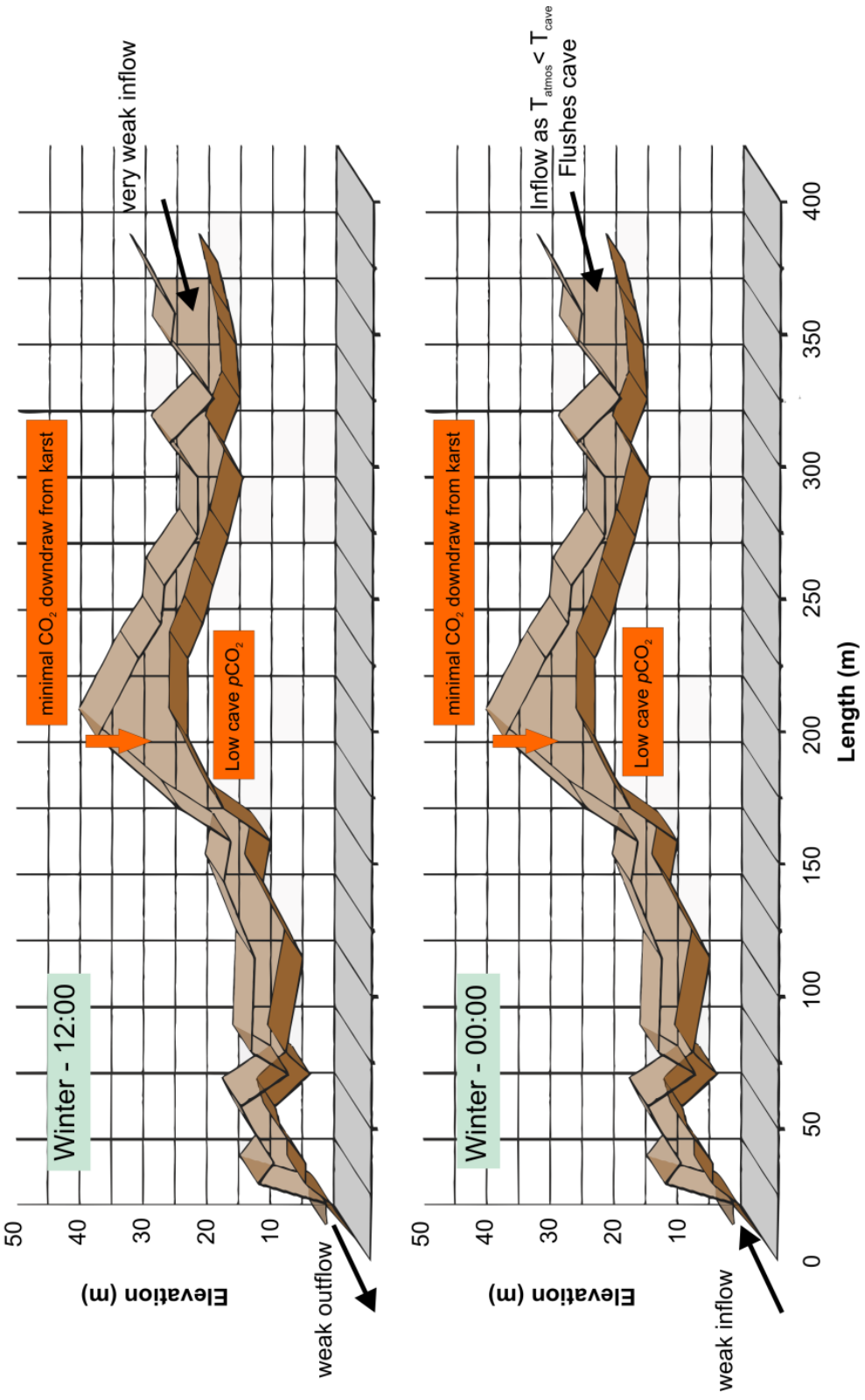

Figure 3.6 Yok Balum long profile with schematic of theorised primary air flows and CO_2 flux during the winter at 12:00pm (top panel) and 00:00am (bottom panel).

3.5.2.3 Temperature observations

Hourly temperature data is used as an indicator of air movement in order to determine seasonal modes of ventilation and to understand exactly how air moves through the cave. We use Tinytag (TT) temperature loggers at different sites to assess thermal variability. TT3, a temperature logger located ~50m from the second entrance shows more variance than TTI, located ~50m from the main entrance and TT2, located in the midsection of the cave ~100m from the main entrance and ~140m from the second entrance (Fig 3.7). TT2 displays the least variance and most moderated temperature. Figure 3.7b displays entropy curves for the three loggers, facilitating comparison of their variance with time. TT3 shows the greatest variability over the whole time series, suggesting that this region of the cave is most strongly coupled with external air temperatures via air exchange. During the summer months TT3 increases by 0.4^{o}C, as air in this region responds to warmer external temperatures. TT2 is stable through the same period and TT1 displays an increase similar to that of TT3 but of only 0.3^{o}C. This thermal variability decreasing with distance from a cave entrance is in accordance with traditional cave temperature models (Wigley, 1967) and previous thermal profile studies of caves (De Freitas et al., 1982; Sanchez-Canete et al., 2013).

During the winter, TT3 displays greater variance than the other two loggers, again indicating that this section of the cave is more closely coupled to the outside air during winter than summer. This is consistent with the ventilation mechanism described in the previous section where inflow of cooler atmospheric air dominates the winter ventilation regime, simultaneously lowering long term cave air temperature in this area of the cave and mimicking the diurnal external temperature cycle in the cave. TT2 remains the least variable, due to its location in the midsection of the cave. TT1 decreases, suggesting that cooler atmospheric air flows in, but that ventilation at this entrance is less rigorous than at the second entrance. Furthermore, short lived decreases in temperature recorded by TT1 (and to a lesser extent in TT2) are in anti-phase with TT3. This could be an indication of air entering at the main entrance and flushing through the cave, forcing warmer air from the less dynamic mid-section of the cave through to the second entrance, where it is recorded as a small increase in

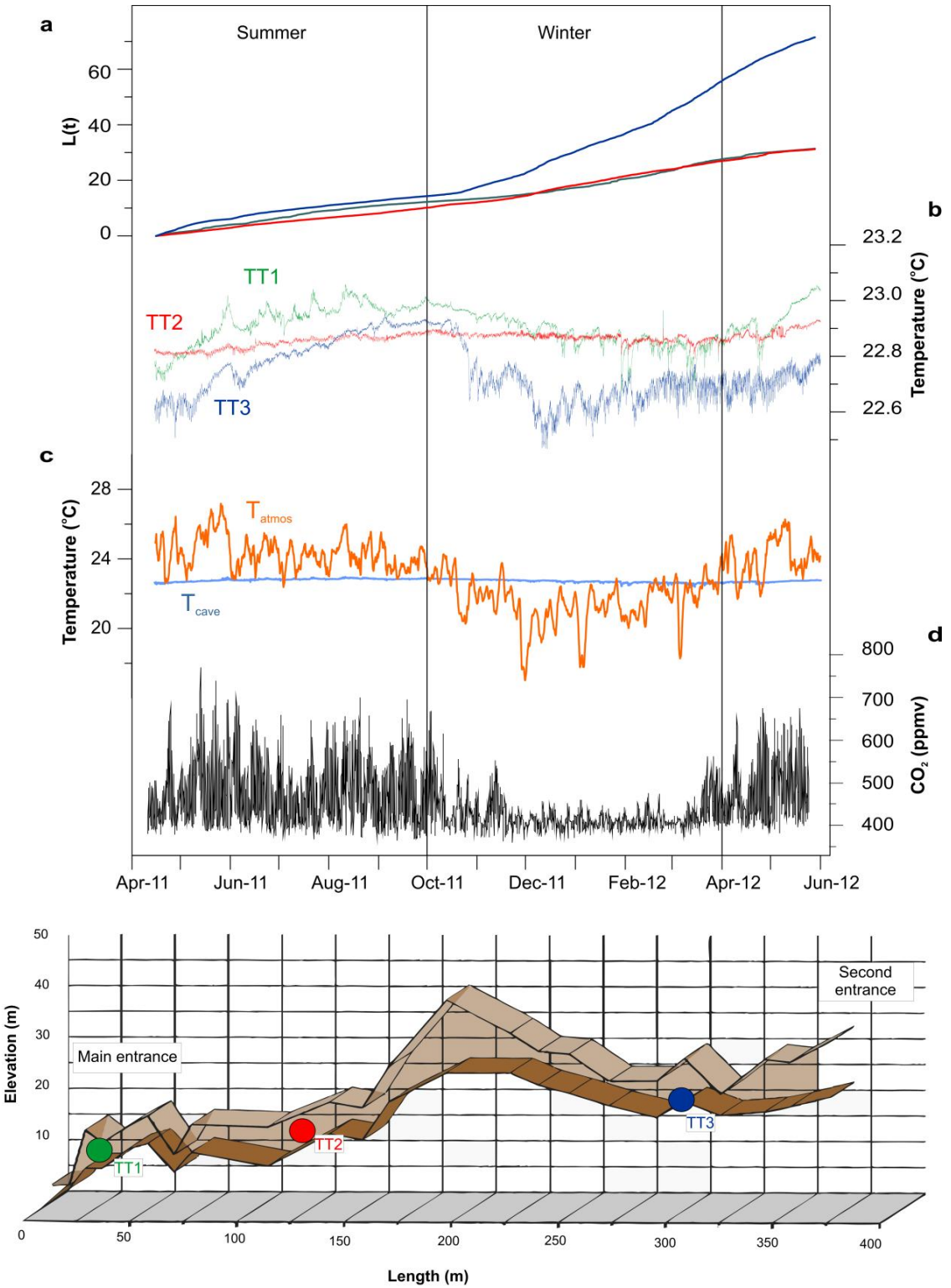

Figure 3.7 14-month time series of **a)** hourly temperature from three temperature loggers in the cave **b)** variability of three time series loggers expressed as entropy (cumulative sum of the absolute first differences) against time (L(t)) **c)** hourly inside and outside cave temperature **d)** three hourly cave air pCO_2. **e)** Location of temperature loggers within the cave.

temperature at TT3. This thermal 'pulse' process would also operate in reverse, with cooler air entering at the second entrance and forcing air through the cave to the main entrance.

Two high resolution temperature experiments were conducted over two 14 hour intervals in June and late October 2012, in an attempt to characterise ventilation on short time scales. A transect of three temperature loggers were placed through the cave, set to record temperature every 10 seconds to capture very short term thermal fluctuations. Both experiments were conducted overnight, from 18:00pm to 08:00am, as this fitted with possible visits to the cave. Failure of one of the loggers during the summer experiment limited the number of loggers to two, but this does not affect data interpretation for this project. During the June experiment (Fig. 3.8) the two loggers, TT5 and TT7 are essentially static, supporting the idea that air density driven outflow dominates during this season. During the logging interval, the cave – atmosphere air density difference does not drop below zero and so inflow did not occur. During the late October experiment thermal variance at all three sites is much greater (Fig. 3.9). TT5 and TT8 display more variability than TT7 suggesting that air inflow close to the main entrance is less persistent. TT8 and TT7 both record cooler temperatures than TT5, presumably due to their proximity to a cave entrance. TT8 and TT5 track each other, roughly in accordance with cave – atmosphere air density difference and are weakly in anti-phase with TT7. This is similar to what we see in the longer term record (Fig. 3.7) where cooler external air enters the main entrance and forces air along the main passage, which is recorded as a pulse of warmer deep cave air at the second entrance. It would appear from this high resolution time series that this occurs in both directions. The limited timeframe of these two experiments hinders making firm conclusions about the diurnal movement of air at Yok Balum cave, although it is encouraging that the results acquired are in agreement with the longer, hourly resolution time series.

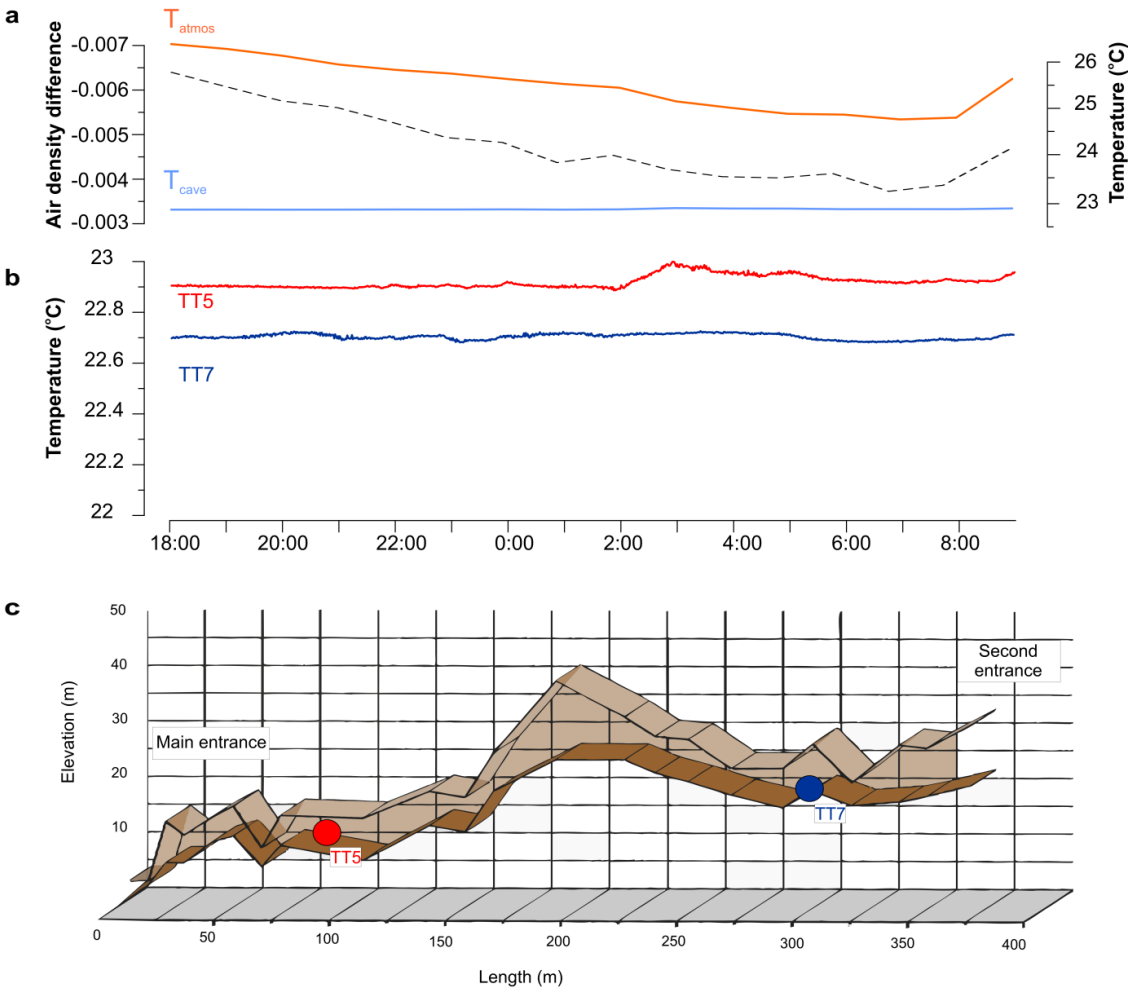

Figure 3.8 Summer high resolution experiment. 14 hour time series of **a)** hourly cave temperature, external air temperature and internal - external air density difference and **b)** 10 second temperature measurements of TT5 and TT7. **c)** location of TT5 and TT7 in the cave.

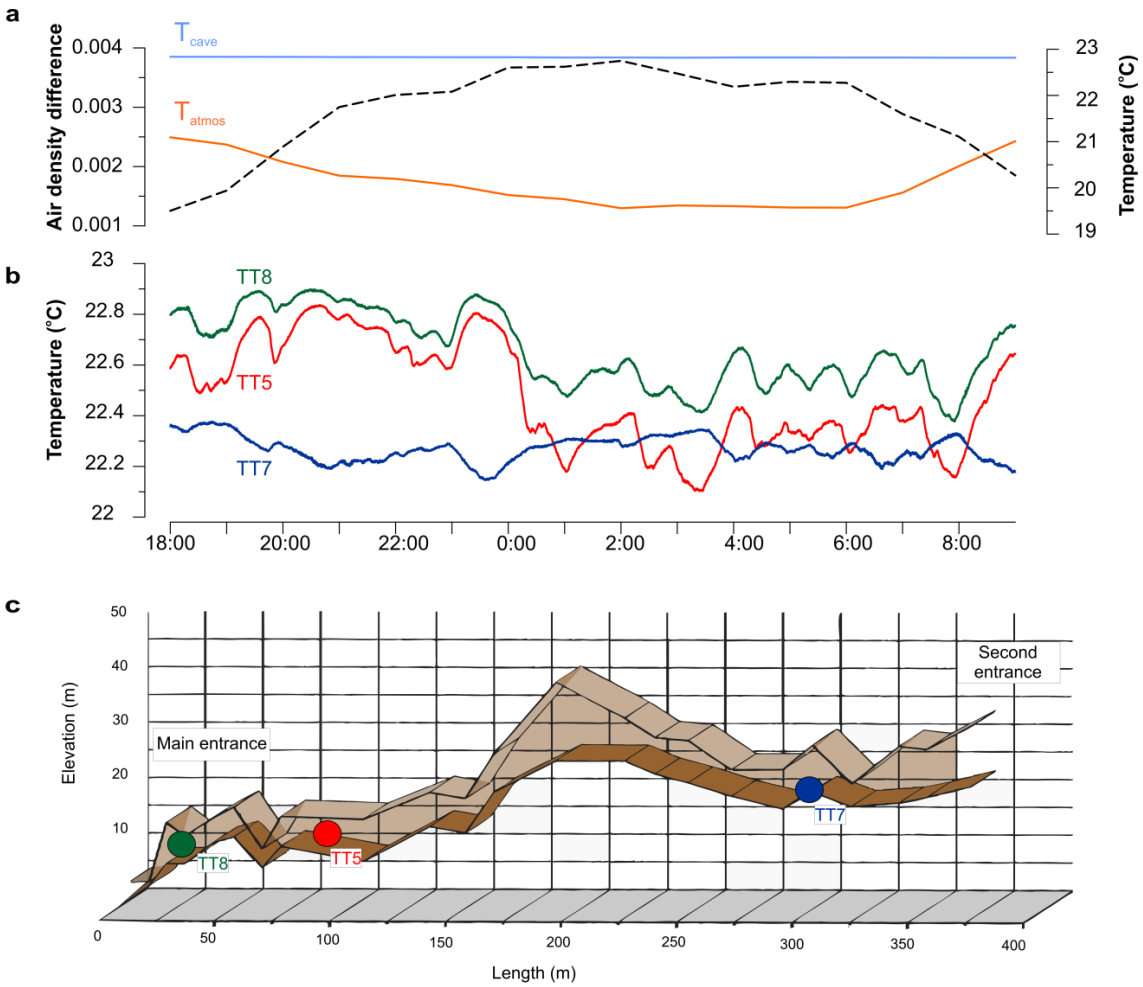

Figure 3.9 Winter high resolution experiment. 14 hour time series of **a)** hourly cave temperature, external air temperature and internal - external air density difference and **b)** 10 second temperature measurements of TT8, TT5 and TT7 **c)** location of TT8, TT5 and TT7 in the cave.

3.5.3 Cave atmosphere response to the July 7th 2012 earthquake

No clear change occurred in cave air pCO_2 or ^{222}Rn during or for the week following the earthquake (Fig. 3.10). A sharp increase in both ^{222}Rn and CO_2 occurs on the 20th of December (Fig. 3.3 b, c) but given the short half-life of radon (3.8 days) it is extremely unlikely that this is a delayed signal of the November 7th event. This increase could be explained instead by a coincident decrease in air density difference, associated with a moderate rainfall event, temporarily reducing inflow to the cave and resulting in a short-lived increase in CO_2 and ^{222}Rn.

A significant change in cave atmosphere might not have been observed due to the seasonal timing of the earthquake. As previously observed, in section 3.5.2, cave ventilation during the winter is dominated by inflow which acts to keep pCO_2 levels low. Seismic activity occurring during the summer season when outflow is dominant, may lead to a discernible increase in cave air ^{222}Rn and CO_2. Potentially a clearer influence would also be observed in a less well ventilated cave. Prior to the cave collapse and creation of the second entrance, and shortening of the cave at Yok Balum, ventilation would have been less effective and cave air pCO_2 and ^{222}Rn higher. Considerable seismic activity at this time may have created uncharacteristically high pCO_2 and ^{222}Rn values as a result of limited ventilation and should be a consideration when studying speleothems from Yok Balum deposited prior to the opening of the second entrance.

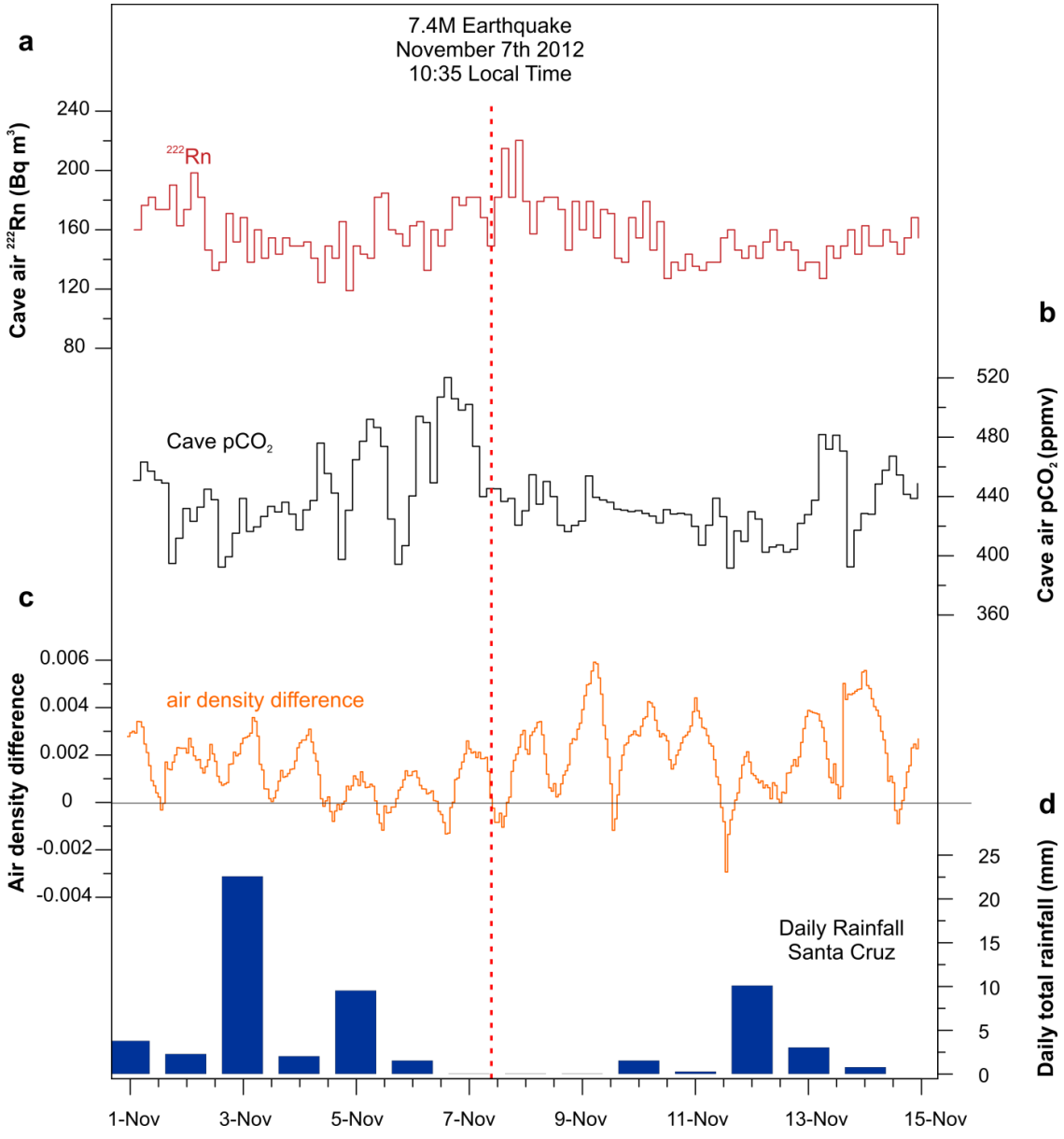

Figure 3.10 Response of cave air **a)** Rn^{222} **b)** CO_2 **c)** inside vs outside cave air density difference and **d)** daily rainfall at Santa Cruz during a 15 day time period surrounding the November 7th earthquake (red dashed line).

3.6 Study of Yok Balum hydrology

3.6.1 Karst hydrology

Karstified rock is heterogeneous, highly fractured and highly permeable, permitting numerous flow routes and connectivity patterns within the same karst system (Aquilina et al., 2006). Three levels of porosity exist within the karst (Ford and Williams, 2007): Primary porosity is associated with diffuse flow and related to inter-granular void space; secondary porosity is the flow of infiltrated water within joints and fractures; tertiary flow takes place in solution enhanced conduits and is the most rapid flow type. The extent and connectivity of these flow pathways within the karst will result in flow regimes which range from slow diffuse or matrix flow to rapid preferential flow (Bradley et al., 2010; Shuster and White, 1971). The heterogeneity of flow pathways within the karst above a cave system will result in highly diverse drip regimes which can display large spatial variability within a single cave system. Furthermore, these flow regimes may change seasonally if karst infiltration varies enough to activate alternative 'over-flow' flow routes (Bradley et al., 2010). Drip hydrological regimes have important implications for geochemical signals incorporated in speleothem carbonate as they control isotopic and trace element signal modification during water transfer from the soil zone to precipitation. Via close monitoring of stalagmite drip rates and local rainfall it is possible to identify stalagmites which respond rapidly to rainfall and are therefore likely to contain a high frequency climate signal. The importance of characterising the hydrological regime feeding a stalagmite is therefore an important pre-requisite for selection of appropriate samples for geochemical climate analysis and for interpreting climate signals present within speleothem carbonate.

Seven Yok Balum stalagmites were chosen for monitoring based primarily on their morphologies. Stalagmate drip loggers were used to record the hydrological regimes of seven stalagmites for varying periods between April 2011 and June 2013. See Figure 3.1 for locations and images of monitored stalagmites. Hourly drip rates were

converted using a drip volume estimate of 0.409ml per drip (Baldini et al., 2006b; Genty and Deflandre, 1998).

3.6.2 Results and Discussion

3.6.2.1 Classifying drip regimes

All monitored drips were active for the entirety of the monitoring period and were observed to be dripping all year round, even during the dry season, suggesting that drips must have a significant storage flow component. Statistical descriptions of the monitored drips are given in Table 3.1.

Table 3.1 Statistical properties of the seven monitored drip sites.

	N° of readings	Mean drip rate (drips hr^{-1})	Min drip rate (drips hr^{-1})	Max drip rate (drips hr^{-1})	Standard deviation	C.V	Drip group
YOK-L	13264	11	4	45	6	54	C
YOK-LD	15598	26	21	33	2	9	A
YOK-K	9109	46	39	52	2	5	A
YOK-SD	13548	12	10	14	1	6	A
YOK-G	3651	1176	1110	1440	24	2	B
YOK-I	11857	25	11	53	4	16	A
YOK-SK	11271.0	334	188	727	95	28	B

Considerable hydrological differences exist between the drips, even between drips in the same area of the cave. Mean drip rates between sites range from 12 drips hr^{-1} to 1176 drips hr^{-1} and standard deviations from 1 to 147, suggesting varying contributions of diffuse and fracture flow. The seven monitored speleothem drips from Yok Balum were classified using a model first devised by Smart and Friederich (1987) and later modified by Baker et al. (1997), which uses the relationship between maximum

discharge against the coefficient of variability (i.e relative standard deviation, CV) to group drips by hydrological characteristics ranging from seepage flow to considerable percolation flow (Baker et al., 1997; Baldini et al., 2006b; Smart and Friederich, 1987). The Yok Balum drips fall into seepage flow or seasonal flow categories based on this model (Fig. 3.11), as seen in other caves (Baldini et al., 2006b; Miorandi et al., 2010). The Smart and Friederich model is used to describe all degrees of hydrological flow within a cave, including rapid methods such as percolation stream and shaft flow, and it is therefore unsurprising that the drips forming "candlestick" shaped stalagmites fall into a narrow portion of the model classification. The seven drip regimes are grouped into three main groups (Fig. 3.12):

- Group A: Low-variability (CV < 20) and low discharge (< 10^{-5} L/sec)
- Group B: Modest-variability (CV of 20 – 40) and high discharge (>$^{10-5}$ L/sec)
- Group C: High-variability (CV > 50) and low discharge (< 10^{-5} L/sec)

Drips in Group A are dominated by diffuse seepage flow (i.e. the movement of water through small scale primary and secondary porosity in the karst aquifer (Baldini et al., 2006b)). YOK-SD is static in nature as it has a small CV (6) and constant variance over the logging period. Furthermore, it displays very low discharge rates (mean of 12 drips hr^{-1}) and shows no response to local rainfall, indicating that this drip is fed entirely by diffuse flow. YOK-LD has a discharge rate approximately twice that of YOK-SD and has greater variance. This is fitting with the proposed idea that drip rate and drip rate variability increase together (Baldini, 2004).

YOK-LD remains very constant, showing no response to seasonal or intense rainfall events. The period of lower variability (October 2011 – February 2012) is the result of the logger being displaced slightly during data download in October, causing the logger to be slightly less sensitive to drip variability. Conversely, YOK-I and YOK-K are also primarily fed by seepage reservoirs but display dramatic increases in drip rate, in response to rainfall events, which indicate that a preferential flow component is activated, presumably once a critical saturation or infiltration level is reached (Baker et al 2013). YOK-I is characterised by a stable baseline diffuse flow component,

punctuated by sharp, short lived increases in drip rate of ~90% (from ~27 to ~51 drips hr^{-1}) that occur in response to local rainfall events.

YOK-K is interesting as it has lower mean discharge than YOK-I (46 vs 25 drips hr^{-1}) yet a smaller variability (CV of 5 vs 16). This is probably due to the moderated response of YOK-K to rainfall. This suggests that YOK-K has a smaller fracture flow component than YOK-I and that the diffuse component is more responsive to local climate and karst recharge.

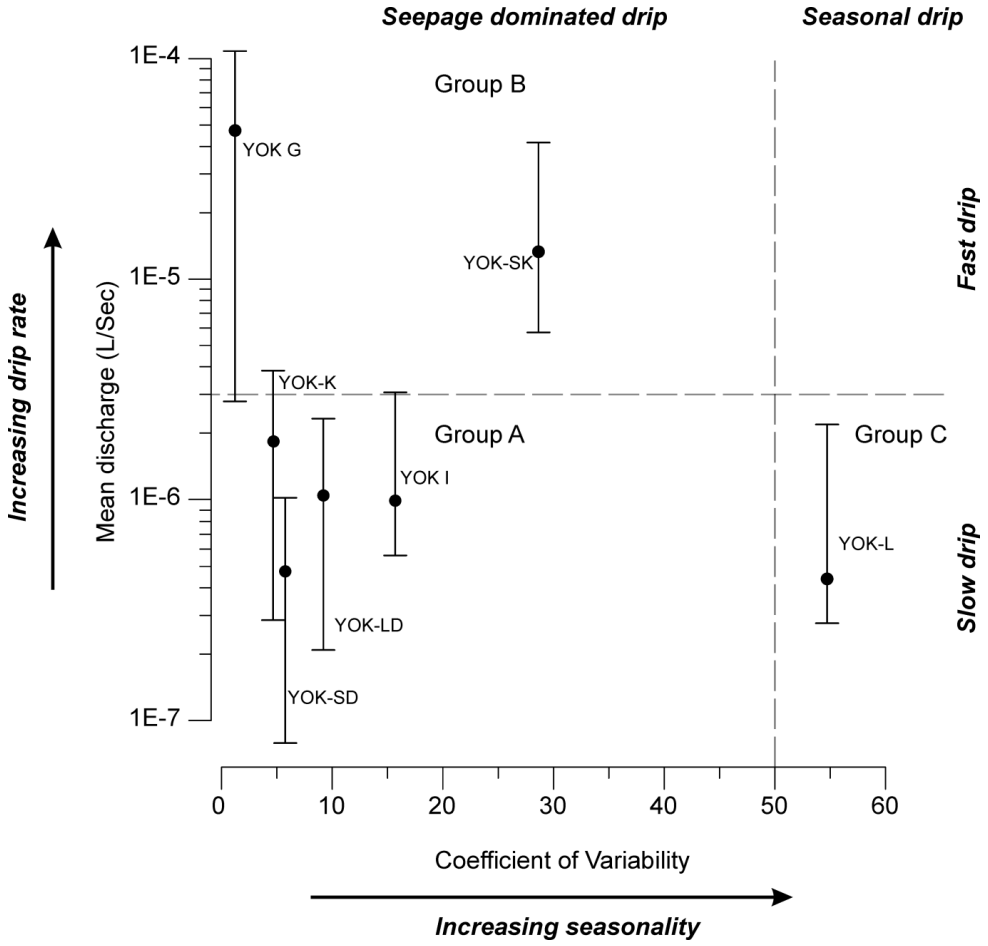

Figure 3.11 Mean discharge of monitored drip sites plotted against the coefficient of variation (standard deviation/mean x 100) (black circles) with maximum and minimum discharge expressed as positive and negative error bars. Groups A, B and C classify the drips in terms of variability and discharge. Long dashed lines separate the drips into seepage, seasonal and slow and fast categories. Adapted from Smart and Friederich (1987) and Baker et al. (1997).

Group B includes YOK-G and YOK-SK, two drips with high discharge rates and a modest variability, probably fed by large diffuse reservoirs which undergo seasonal change. YOK-SK displays a more ephemeral response to local rainfall events than YOK-G, suggesting that this drip has a larger preferential flow component. YOK-SK responds to local rainfall, with a lag time of approximately one day, in pulses which typically lasts between one and two weeks, depending on the duration of the rain event. A moderated drip hydrograph such as this is indicative of a fracture flow component which is restricted by aperture size at some point within the system. YOK-G drip rates increase steadily through the summer months as rainfall and infiltration increase, thereby increasing the reservoir store feeding the drip. This steady increase is punctuated by short lived peaks in drip rate, again linked to rain events and rapid fracture flow.

YOK-L is the only seasonal drip monitored, according to the modified Smart and Friederich model. YOK-L also has the lowest mean drip rate (11 drips hr^{-1}) but responds to local rainfall events in a matter of days in a manner similar to YOK-SK; likely due to their proximity and common hydrological components. YOK-L increases by as much as 400% of baseline diffuse values during periods of high infiltration and karst saturation. This is likely due to the introduction of a volume restricted preferential flow route by rainfall. Drip rates are kept low by the size of one or more aperture within the system.

The range of drip rates and varying responses to rainfall events suggests that the monitored speleothems would contain notably diverse climate signals, primarily as flow routing has a first order control on both isotopic mixing of waters and water saturation state. When considering samples for high resolution analysis it is important to consider the impact of ‘flashy’ hydrological responses to rainfall. Rapid increases in drip rate, related to prevailing climate conditions, indicate a switch in flow routing in the overlying karst. “Event” water such as this may be geochemically discreet from “non-event” diffuse water (Baker et al 2003) and it is therefore important to attempt to understand why such events occur and what effect they may have on precipitating carbonate geochemistry.

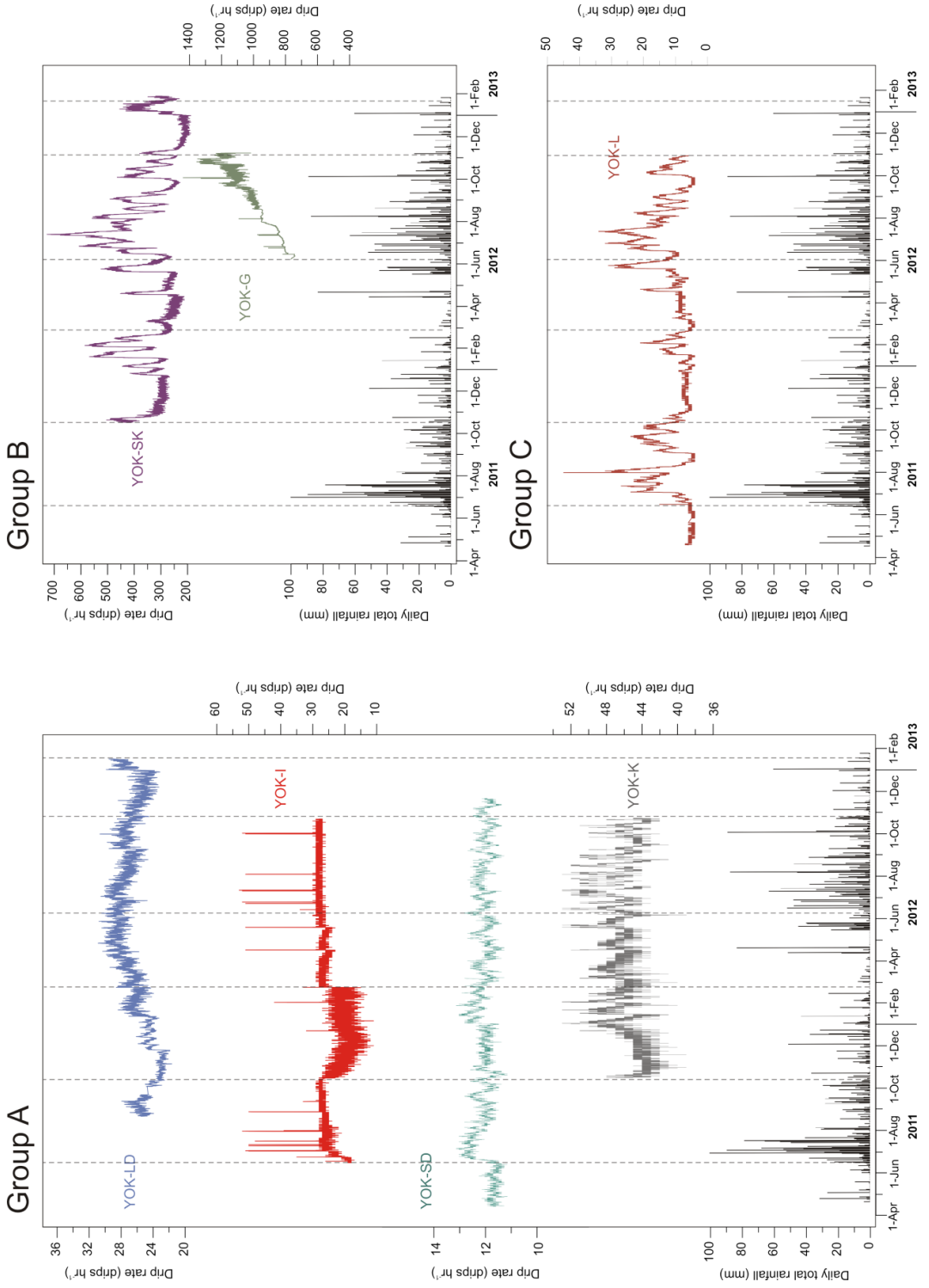

Figure 3.12 Hourly drip rate time series for the seven drips monitored in this study in respective groups and local daily rainfall at Santa Cruz Village. Dashed lines represent points of data download.

3.6.2.2 Identifying samples for high resolution geochemical analysis

Two stalagmites, YOK K and YOK L, were collected from Yok Balum cave in October 2012 after 18 months of monitoring. Based on their statistical drip properties and observed responses to rainfall events it was decided that these two stalagmites would produce two different but equally interesting climate records. YOK-L, which displays a stronger connection to the surface during periods of intense rainfall, is considered most likely to incorporate a stronger isotopic signature from deep convective storms and hurricanes. The static nature of YOK-LD and YOK-SD means that they are likely to have slow growth rates and contain long term, more muted geochemical climate signals in their carbonate. YOK-SK is likely to have a faster growth rate than its 'partner' YOK-L, but was left in the cave as it's morphology was less suitable. From external inspection it appeared that multiple growth axis shifts may have occurred during the growth of YOK-SK, which can cause problems during sample dissection and milling.

3.6.3 Seismic disturbance of drip regimes and implications for speleothem palaeoclimate studies

Three drip loggers were monitoring during the November 2012 earthquake: 'YOK-SK', 'YOK-SD' and 'YOK-LD'. Of these drips, two (YOK-LD and YOK-SD) were 'static' in nature (Baker et al., 1997; Smart and Friederich, 1987), as they displayed low drip rates and low variability (Fig. 3.11), indicative of a diffuse flow dominated hydrology. YOK-SK is classified as a 'seasonal' drip (Baker et al., 1997) because it responds to local rainfall events and seasonal climate variability, suggesting that a fracture flow pathway is activated once a threshold rainfall rate or karst saturation level is reached. YOK-SK responds to local rainfall with a lag time of <6 days, but displays greater variability during the wet season when the karst and soil are closer to saturation. None of the three loggers recorded any clear response to the seismic activity on November 7th (Fig. 3.13). None of these three loggers recorded any clear drip response to the seismic activity on November 7th (Fig. 11b). YOK-LD and YOK-SD, the two static drips, show no response, suggesting that diffuse flow regimes are not affected by seismic activity of

this magnitude. Similarly, YOK-SK, which at the time of the earthquake was displaying a peak in drip rate in response to rainfall events in the preceding days, shows no response outside what would be expected from the longer time series. This information indicates that more preferential flow routes are also unaffected by seismic activity of this nature. This observation is of significant value for speleothem palaeoclimate studies as it suggests that seismic activity does not affect hydrological flow pathways and hence alter carbonate geochemistry.

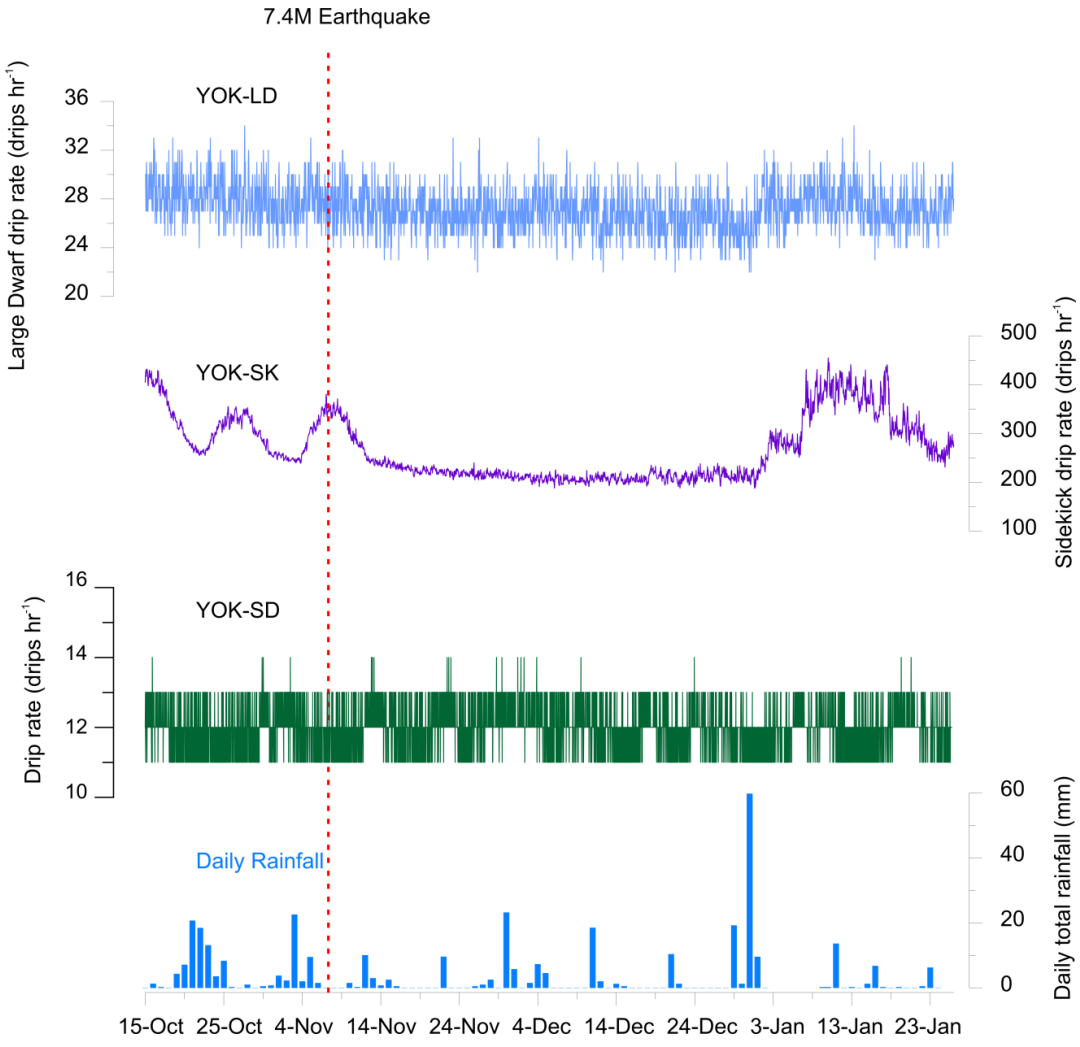

Figure 3.13 Eight-month time series of Large Dwarf, Sidekick and YOK G drip rates and daily rainfall at Santa Cruz Village between June 1012 and January 2013. November 7th earthquake indicated by red dashed line.

3.7 Conclusions

Yok Balum is an extremely well ventilated cave system which displays distinct seasonal ventilation regimes consistent with changes in air density differences between the cave and outside atmosphere. The winter regime is dominated by air inflow, low pCO_2 and lower karstic drawdown and CO_2 flux into the cave, while summer is dominated by air outflow, high karstic CO_2 drawdown and drip water degassing and a strong diurnal signal. Based on air temperature changes the degree of air exchange increases from the centre of the cave to the entrances and the second entrance experiences greater air exchange than the main entrance, presumably due to its size. By looking at thermal fluctuations of cave air on a ten-second timescale, direction of air movement is identified during summer and winter nights respectively and both entrances are found to display active dual-directional connections to the free atmosphere. The three datasets presented here; long term three-hourly CO_2, hourly temperature and the two high resolution studies all help to build a comprehensive understanding of ventilation at Yok Balum Cave. This will be pertinent to ongoing palaeoclimate research at this cave. Continued monitoring will help to discern inter-annual fluctuations and identify long term links between cave pCO_2 and local climate.

Hourly drip data is compared to local rainfall to discern hydrological regimes feeding individual stalagmites. Diverse hydrological regimes are observed, ranging from diffuse dominated flow to seasonal regimes. Two speleothem samples were selected based on both their morphologies and hydrological connections to the surface showing promise for high resolution proxy signal emplacement in the carbonate. This study could be extended and improved through investigation of how water saturation state varies with drip rate. This would further assist in the understanding of how flow regimes affect carbonate precipitation. Analysis of carbonate precipitated on the Iceland spars during the course of monitoring will hopefully provide seasonal, if not monthly, resolution dataset which can used to understand how fractionation responds to changes in drip rate and cave atmosphere.

Cave pCO_2 and ^{222}Rn did not show any discernable response to the November 7th earthquake. The well ventilated nature of the cave likely prevents any CO_2 and ^{222}Rn

build up which may be associated with the seismic activity. Likewise, none of the three drips displayed any discernible hydrological response to the earthquake, suggesting that seismic activity, even of considerable magnitude, has minimal hydrological repercussions at Yok Balum and is insufficient to result in perturbations in speleothem petrographical or geochemical records. The limited number of loggers precludes drawing firm conclusions for all drip types, however it is interesting that the three functioning loggers represent two end members of 'standard' drip types, from highly diffuse, slow and static drip rates (YOK-LD and YOK-SD), to highly variable and relatively fast drip rates (YOK-SK). It would be unsurprising if intermediate drip regimes were not affected by seismic activity of this magnitude either. Results presented here suggest that no hydrological disruption occurred and that seismic activity of this magnitude should not have severe implications for palaeoclimate reconstruction from stalagmites in Yok Balum, or caves in similar settings. The primary effect seismic activity may have on a speleothem record is to alter the growth axis position or orientation, rather than a direct disruption of the overlying hydrology. This could appear as a hiatus or sudden shift in isotope values if the growth axis movement was not accounted for during milling.

This study provides real time data of the effect of seismic activity on cave hydrology and atmosphere. In seismically active regions, determining this site specific response is a desirable outcome of cave monitoring studies designed to aid speleothem palaeoclimate proxy interpretation. This data provides encouraging evidence that seismic activity of this level does not have implications for speleothem palaeoclimate proxy interpretations from caves with similar ventilation dynamics as Yok Balum.

Chapter 4

Aerosol forcing of intertropical convergence zone position

A version of the Chapter has been submitted to Nature Geoscience authored by: Harriet E. Ridley[1], Yemane Asmerom[2], James U.L. Baldini[1], Sebastian F.M. Breitenbach[3], Valorie V. Aquino[2], Keith M. Prufer[4], Brendan J. Culleton[5], Victor Polyak[2], Franziska A. Lechleitner[3], Douglas J. Kennett[5], Minghua Zhang[6], Norbert Marwan[7], Colin G. Macpherson[1], Lisa M. Baldini[1], Tingyin Xiao[6], Jaime Awe[8] and Gerald H. Haug[3].

[1] *Department of Each Sciences, Durham University, Durham, UK.*
[2] *Department of Earth and Planetary Science, University of New Mexico, Albuquerque, NM, USA.*
[3] *Department of Earth Science, Eidgenössische Technische Hochschule (ETH), Zürich, Switzerland.*
[4] *Department of Anthropology, University of New Mexico, Albuquerque, NM, USA.*
[5] *Department of Anthropology, The Pennsylvania State University, University Park, PA, USA.*
[6] *Institute for Terrestrial and Planetary Atmospheres, School of Marine and Atmospheric Sciences, Stony Brook, NY USA*
[7] *Potsdam Institute for Climate Impact Research, Potsdam, Germany.*
[8] *Institute of Archaeology, Belmopan, Belize*

A version of this chapter has been submitted to *Nature Geoscience* with contributions from the following authors:

Harriet Ridley milled the speleothem samples and ran the stable isotope analyses, interpreted the data, conducted fieldwork and wrote the manuscript thereby contributing to over 85% of the work presented here.

James Baldini was also involved in data interpretation, fieldwork and provided comment on the manuscript.

Valorie Aquino, Yemane Asmerom and Victor Polyak conducted the Uranium-series analysis at the University of New Mexico.

Keith Prufer was involved in the collection of the stalagmite sample and fieldwork.

Douglas Kennett and Bendan Culleton performed radiocarbon analyses and were involved in the collection of the stalagmite.

Franziska Lechleitner performed high resolution re-milling and stable isotope analysis at ETH Zurich.

All other named co-authors **(Sebastian Breitenbach, Minghua Zhang, Norbert Marwan, Colin Macpherson, Lisa Baldini, Tingyin Xiao, Jaime Awe, and Gerald Haug)** contributed to the project and approved the final manuscript.

Aerosol forcing of intertropical convergence zone position

4.1 Abstract

Intertropical convergence zone (ITCZ) position is the dominant control on low-latitude precipitation distribution and is largely controlled by hemispheric temperature contrasts (Hwang et al., 2013; Broccoli et al., 2006). Recent modelling (Hwang et al., 2013; Rotstayn and Lohmann, 2002; Chang et al., 2011) and observational (Zhang et al., 2007; Lu et al., 2013) studies suggest that anthropogenic aerosols may have contributed to southward ITCZ shifts by moderating Northern Hemisphere (NH) relative to Southern Hemisphere (SH) warming (Hwang et al., 2013; Friedman et al., 2013; Booth et al., 2012). Despite this abundant evidence suggesting that NH-SH temperature contrasts affected low latitude rain belts over the last few decades, differentiating between anthropogenic forcing and century-scale natural variability is problematic and requires a record with nearly no chronological error and very high temporal resolution. Unfortunately, these types of records are extremely uncommon in tropical regions affected by the ITCZ. Here, we use an exceptionally well-dated and monthly-resolved 453 year-long stalagmite record from Belize to demonstrate that unprecedented rainfall decreases coincided with increasing anthropogenic aerosol emission rates. The record also suggests that short-lived drying occurred after large NH volcanic eruptions since 1550. These results strongly suggest that aerosol injections into the NH atmosphere result in southward ITCZ repositioning, and firmly implicate anthropogenic aerosol emissions as having caused 20th Century rainfall reductions in the northern tropics. Future changes in the distribution of aerosol emissions should therefore be a critical consideration when predicting regional susceptibility to severe rainfall variations.

4.2 Introduction

ITCZ position largely controls low latitude seasonal rainfall distribution. Relative ITCZ position is strongly influenced by hemispheric temperature contrasts and subsequent atmospheric restructuring, which draw the ITCZ toward the warmer hemisphere (Hwang et al., 2013; Broccoli et al., 2006; Zhang et al., 2007; Haug et al., 2001). Considerable proxy evidence positively links Northern Hemisphere temperature to low-latitude rainfall throughout the Holocene (Dykoski et al., 2005; Haug et al., 2001). Since 1900 however, limited instrumental evidence suggests a southward shift in ITCZ position (Rotstayn and Lohmann, 2002; Zhang et al., 2007), a trend possibly driven by asymmetrical hemispheric warming due to the cooling effect of anthropogenic aerosols (e.g., sulphates (Rotstayn and Lohmann, 2002; Chang et al., 2011) and black carbon (Zhang et al., 2008)) in the NH, but that could also arise from undetected natural variability. Climate models have attempted to assess the relative contributions of greenhouse gases (GHG) and aerosols to ITCZ displacement with contradictory results (Hwang et al., 2013; Friedman et al., 2013). Limited long-term instrumental climate records from low latitudes complicates detecting climate shifts attributable to anthropogenic influences, and consequently future precipitation projections remain ambiguous (Diffenbaugh and Field, 2013). Furthermore, chronological uncertainties associated with low latitude rainfall proxy records prevent establishing robust links between low-latitude rainfall amount and atmospheric aerosol distributions at a suitable resolution. Here, we discuss an exceptionally well-dated, monthly-scale stalagmite rainfall record from southern Belize, covering 456 years from 1550 to 2006 C.E., thus covering the critical transition into the Current Warm Period (CWP) with unprecedented detail and providing much needed evidence to support modelling work. This site is near the northernmost extent of the ITCZ, a remarkably sensitive location for reconstructing even minor variations in latitudinal extent of the ITCZ.

4.2.1 Oxygen isotopes as palaeoclimate proxies

Speleothem $\delta^{18}O$ values are affected by a relatively large number of factors, mostly linked to complex fractionation processes as water vapour travels from source region to sink (Lachniet, 2009). Isotope ratios of meteoric water are controlled by fractionation during phase change and diffuse exchange between liquid and vapour along its trajectory from source region to final infiltration. Generalised trends control the isotopic composition of meteoric water globally but added regional variability can produce differences of several parts per million (Bowen and Wilkinson, 2002; Lachniet, 2009; Vodila et al., 2011) due to temperature-related effects such as the amount, continental, and altitude effects (Dansgaard, 1964; Rozanski et al., 1993), as well as variability in moisture source location and moisture source $\delta^{18}O$ values (Kolodny et al., 2009; Kowalczk, 2009). Soil water $\delta^{18}O$ values, initially controlled by the $\delta^{18}O$ value of precipitation, can be significantly enriched by evaporation, a function of vegetation cover and local climate (Clark and Fritz, 1997; Fetter, 1994; Tang and Feng, 2001; Lachniet, 2009). Further modification of groundwater $\delta^{18}O$ value can occur via water mixing and residence in the karst (Fairchild et al., 2006). Upon entering the cave, fractionation during CO_2 degassing and associated carbonate precipitation are the two dominant processes affecting the final $\delta^{18}O$ value of speleothem carbonate (Lachniet, 2009). Evaporation induced kinetic fractionation is expected to be minimal in Yok Balum where relative humidity is >99%. The degree of kinetic fractionation has been assessed in Yok Balum Cave via Hendy tests by Kennett et al., (2012) who reported that some kinetic fractionation occurs during precipitation but that this is likely to have been stable over the last few thousand years because of near-constant cave temperature, humidity, and ventilation.

4.2.2 Carbon isotopes as palaeoclimate proxies

The stable isotope $\delta^{13}C$ from both marine and continental sources has been widely applied to palaeoclimate reconstruction for many decades, as a proxy for atmospheric CO_2 (e.g Shackleton et al., 1983; Cerling, 1984; Andrews, 2006; Berner, 2006) and as an indicator of bioproductivity (e.g Leng and Marshall 2004). In more recent years the $\delta^{13}C$ of speleothems has been utilized to infer past environmental and climate related changes (Frappier et al., 2002; Genty et al., 2006; McDermott, 2004; McDermott et al., 2005).

Speleothem carbon originates predominantly from biological CO_2 (typically with low $\delta^{13}C$ values) from the soil zone and from limestone bedrock dissolution (with typically higher $\delta^{13}C$ values). The final $\delta^{13}C$ value depends on several factors including: the photosynthetic pathway of overlying vegetation (Clark and Fritz, 1997), the bedrock contribution (Hendy, 1971; Dulinkski and Rozanski, 1990; Clark and Fritz, 1997), and drip rate in the cave, whereby lower drip rates result in higher speleothem $\delta^{13}C$ through increased fractionation associated with more pronounced CO_2 degassing (Hendy, 1971; Hellstrom et al., 1998; Dulinski and Rozanski, 1990; Wigley et al., 1978). At Yok Balum, the tropical climate results in high year-round biological activity and soil pCO_2 (Fig. 4.1). The vegetation above the cave is exclusively C3 and this is unlikely to have changed over the last 500 years. The more positive $\delta^{13}C$ bedrock isotopic contribution is thought to be proportional to the speleothem drip rate and prior carbonate precipitation (PCP) and hence water recharge to the karst, i.e. when conditions are drier, slower karstic through flow will result in a) reduced soil carbon contribution (through a reduction in soil microbial breakdown of organic matter and reduced root respiration), b) higher (more positive) $\delta^{13}C$ bedrock contributions, c) slower drip rates, and d) more extensive in-cave CO_2 degassing. These factors combine to produce more positive $\delta^{13}C$ carbonate values.

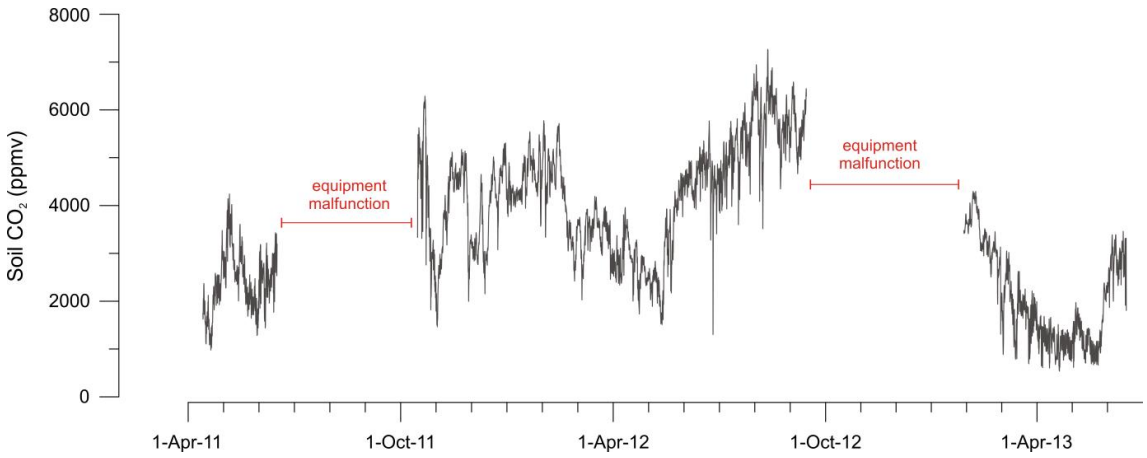

Figure 4.1 26-month time series of soil pCO_2 above the cave.

4.3 Methods

4.3.1 Stalagmite YOK-G

Stalagmite YOK-G was collected in June 2006, approximately 50m from the cave entrance, from atop a very large feature (a large stalagmite or amalgamation of various carbonate deposits) known as 'The Birthday Cake'. The 'Birthday Cake' area of the cave contains numerous active speleothems due to the presence of a doline, focussed recharge, and deeper organic soils directly above the site. Based on drip plate assessment, YOK-G was still actively precipitating carbonate at the time of collection. The 1090mm tall stalagmite was cut into three pieces. The top 384mm are discussed in this paper (Fig. 4.2). YOK-G was sectioned along the central growth axis to reveal the internal structure. YOK-G is clean and extremely well laminated (Fig. 4.3). Clear visual growth layers almost certainly correspond to seasonal changes in crystal arrangements with well-defined textures and fabrics (Frisia et al., 2000; Self and Hill, 2003). The mechanisms controlling changes in crystal fabrics are well-understood, particularly in calcite, and readers are directed to Frisia et al. (2000) for a comprehensive review. Because the cave environmental conditions are stable (i.e, cave CO_2 values and temperature do not vary markedly) the different laminae almost certainly result from shifts in carbonate saturation state associated with seasonal recharge variability and degassing rates associated with drip rate. Six powder samples were obtained along clear growth layers along the length of YOK-G for XRD analysis at ETH Zurich, which, when combined with petrographic analysis, indicate that YOK-G is entirely aragonitic.

4.3.2 Stable Isotope analysis

The top slab of stalagmite YOK-G was continuously milled at 0.1mm steps along the central growth axis using a computer-controlled ESI/New Wave Micromill with a standard 0.8mm tungsten carbide drill bit. Samples were milled to specifications of 0.1mm width, 10mm length and 1 mm depth, with the long axis parallel to growth layers. 220µg - 250µg of powder was transferred using an acetone-cleaned scalpel to round bottomed 12mL auto-sampler exetainer vials with butyl rubber septa (Labco,

High Wycombe, UK) for isotope ratio determination. The drill bit and milling track were cleaned after each sample using a compressed air gun. The location and angle of the sampling trench was moved accordingly to accommodate changes in growth axis orientation down the stalagmite (Fig. 4.2). A marker point was drilled every 10mm to facilitate navigation and measurement on the stalagmite.

Stable isotope analysis was conducted within the Department of Earth Sciences at Durham University using a Thermo-Finnigan (Bremen, Germany, now Thermo Fisher Scientific) MAT 253 Isotope-Ratio Mass Spectrometer with a Gasbench II (external precision of ca. 0.05-0.10‰). Fifty speleothem carbonate samples were loaded for each run. Carbonate samples were dissolved in 10 drops of orthophosphoric acid (H_3PO_4) under helium (grade 5) atmosphere. The solution was left to digest at 50^{o}C for two hours. The resultant gas mixture (CO_2 and He) was introduced to a gas chromatographic column and the CO_2 separated from the gas mixture. After passing the second water trap the analyte was introduced to the mass spectrometer. Each batch of sample powders were run with 14 standard powders; NBS18 (carbonatite), NBS19 (limestone), LS VEC (lithium carbonate) and an internal laboratory standard DCSO1 (Table 4.1). Normalisations and corrections were made to NBS19 and LS VEC. $^{13}C/^{12}C$ ratios are reported in standard delta notation relative to the Vienna Pee Dee Belemnite (‰ VPDB) standard. The external analytical precision is better than 0.1‰.

Table 4.1 Laboratory standards

Standard name	**Description**	**$\delta^{13}C/^{12}C$ (‰VPDB)**	**$\delta^{18}O/^{16}O$ (‰VPD)**
NBS18	Carbonatite	-5.1	-23.2
NBS19	Limestone	1.95	-2.2
DCS01	Internal Standard	-35.49	-17.15
LS VEC	Internal Standard	-46.5	-26.7

In total 3840 samples (0.1mm sample interval) were prepared and analysed along the length of YOK-G. Random samples were re-run to ensure reproducibility between the runs and lend confidence to the results.

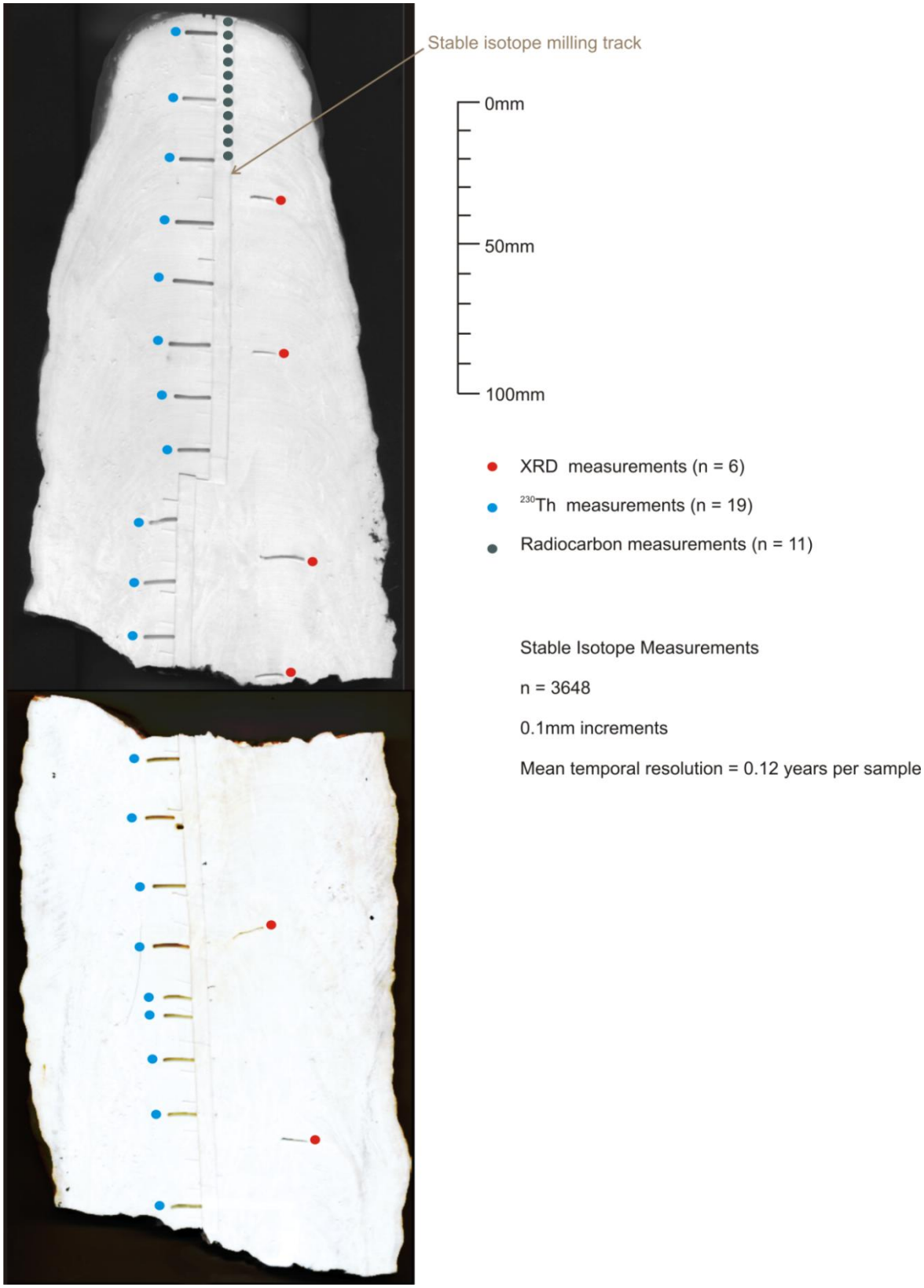

Figure 4.2 High resolution scan of YOK-G showing the isotope milling track, and 230Th and XRD sample locations.

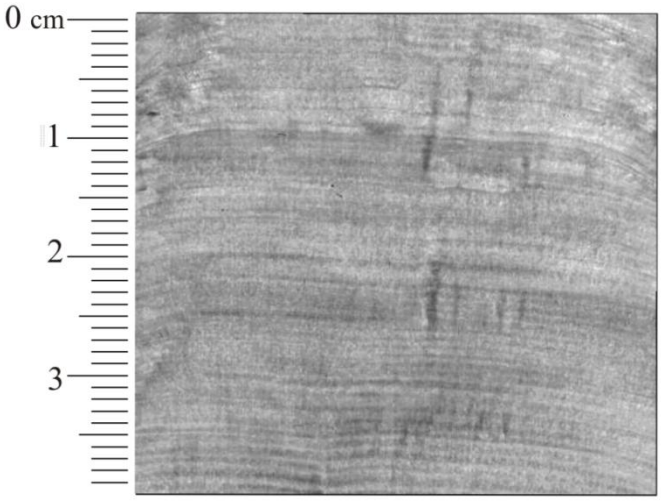

Figure 4.3 Example of visible annual laminations in YOK-G 40mm to 80mm from the top of the stalagmite.

4.3.3 Uranium-series analyses

Uranium-series (^{230}Th) dating of powders was performed at the University of New Mexico Radiogenic Isotope Laboratory. Milled powder samples (20-120 mg) and a drip water sample (13.3 g) were spiked with a solution containing ^{229}Th, ^{233}U, and ^{236}U, and uranium and thorium were separated using anion chemistry and analysed on a Thermo Neptune multicollector inductively coupled plasma mass spectrometer after the methods of Asmerom et al. (2010) and Cheng et al. (2013). Improved half-life values for ^{230}Th and ^{234}U were applied to these age results (Table 4.2).

4.3.4 Age Model and Time-Series Construction

Drip water and YOK-G carbonate powders extracted at 0.5 and 1.0 mm from the stalagmite top (years C.E. 2006 and 2004) were used to establish that stalagmite YOK-G detrital thorium has a high initial ^{230}Th/^{232}Th. This high initial value was found to be inversely correlated to ^{232}Th concentration such that initial ^{230}Th/^{232}Th$_{atomic}$ (ppm) = $323.67(X)^{-0.269}$, where X = concentration of ^{232}Th in pg/g, and the calculated initial ^{230}Th/^{232}Th$_{atomic}$ (ppm) has an assumed ± 10% absolute error (Fig. 4.4). Corrections are therefore made on ^{230}Th dates younger than C.E. 1800 due to higher ^{230}Th/^{232}Th ratios in this portion of the stalagmite. This correction does not significantly affect age results older than C.E. 1800 due to low ^{230}Th/^{232}Th ratios in the older carbonate.

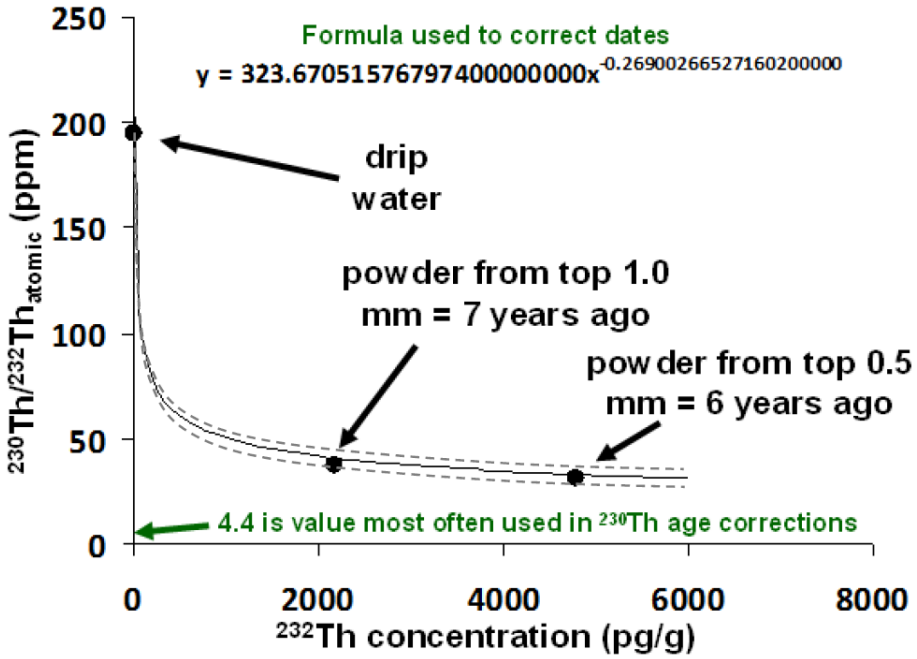

Figure 4.4 Detrital thorium correction. High values of $^{230}Th/^{232}Th_{atomic}$ (ppm) for a sample of drip water and two powders from the tip of stalagmite YOK-G were measured for = C.E. 2004 to 2006. Resulting $^{230}Th/^{232}Thatomic$ (ppm) values show a nonlinear relationship between detrital 232Th concentration and $^{230}Th/^{232}Th_{atomic}$ (ppm). Initial $^{230}Th/^{232}Th_{atomic}$ (ppm) value for each sample powder dated was determined by the curve shown above, where initial $^{230}Th/^{232}Th_{atomic}$ (ppm) = 323.67052 x (^{232}Th concentration (pg/g)) - 0.269003 (ppm) ± 10% (dashed curves).

Table 4.2 Uranium series data for stalagmite YOK-G.

distance from top (mm)	^{238}U (ng/g)	^{232}Th (pg/g)	$^{230}Th/^{232}Th$ (activity)	$^{230}Th/^{238}U$ (activity)	$\delta^{234}U_m$	$\delta^{234}U_i$	uncorrected Age (yrs B2006)	corrected Age (yrs B2006)	Year AD)
drip water	0.099 ± 0.005	4.7 ± 0.3	36 ± 3	0.56580 ± 0.01119	391 ± 3		55,376 ± 1410	6 ± 5699	2006
0.5	4481 ± 5	4794 ± 251	6 ± 1	0.00214 ± 0.00017	448 ± 1	448 ± 1	161 ± 13	6 ± 17	2006 ± 17
1	4380 ± 6	2171 ± 471	8 ± 2	0.00122 ± 0.00027	453 ± 1	453 ± 1	92 ± 20	8 ± 29	2004 ± 29
6	5200 ± 5	270 ± 57	32 ± 7	0.00054 ± 0.00003	467 ± 1	467 ± 1	40 ± 2	23 ± 5	1989 ± 5
27	4497 ± 9	86 ± 73	136 ± 116	0.00086 ± 0.00004	467 ± 1	467 ± 1	64 ± 3	55 ± 8	1957 ± 8
47	5154 ± 5	58 ± 60	331 ± 345	0.00121 ± 0.00003	483 ± 1	483 ± 1	89 ± 2	84 ± 6	1928 ± 6
68	6644 ± 7	27 ± 50	1110 ± 2057	0.00148 ± 0.00002	488 ± 1	488 ± 1	109 ± 1	106 ± 5	1906 ± 5
87	8352 ± 7	7 ± 42	6471 ± 39632	0.00173 ± 0.00001	464 ± 1	464 ± 1	129 ± 1	128 ± 4	1884 ± 4
107.5	5784 ± 5	59 ± 39	631 ± 422	0.00210 ± 0.00002	485 ± 1	485 ± 1	154 ± 2	150 ± 4	1862 ± 4
124.5	7773 ± 4	31 ± 50	1887 ± 3099	0.00242 ± 0.00003	489 ± 1	489 ± 1	178 ± 2	175 ± 4	1837 ± 4
141.5	17083 ± 20	117 ± 60	1206 ± 619	0.00270 ± 0.00002	508 ± 2	508 ± 2	195 ± 2	193 ± 2	1819 ± 2
165	6416 ± 5	4 ± 66	15952 ± 281458	0.00304 ± 0.00003	491 ± 1	492 ± 1	223 ± 2	222 ± 11	1790 ± 11
185	6754 ± 5	35 ± 57	2017 ± 3322	0.00338 ± 0.00003	486 ± 1	486 ± 1	248 ± 2	245 ± 5	1767 ± 5
203	7932 ± 7	17 ± 61	5051 ± 17887	0.00359 ± 0.00003	477 ± 1	477 ± 1	265 ± 2	264 ± 6	1748 ± 6
221	8387 ± 10	5 ± 55	21475 ± 258268	0.00385 ± 0.00002	474 ± 1	475 ± 1	285 ± 2	284 ± 7	1728 ± 7
241.5	10095 ± 25	8 ± 47	15310 ± 86993	0.00413 ± 0.00002	480 ± 1	481 ± 1	304 ± 2	304 ± 4	1708 ± 4
265	8099 ± 14	49 ± 47	2287 ± 2173	0.00457 ± 0.00003	481 ± 1	481 ± 1	337 ± 2	334 ± 4	1678 ± 4
285	8629 ± 15	64 ± 40	1982 ± 1241	0.00479 ± 0.00003	471 ± 1	472 ± 1	355 ± 2	352 ± 3	1660 ± 3
310	5674 ± 18	80 ± 66	1130 ± 937	0.00521 ± 0.00006	451 ± 2	451 ± 2	392 ± 4	386 ± 7	1626 ± 7
325	6238 ± 10	14 ± 53	7679 ± 30144	0.00546 ± 0.00005	471 ± 1	471 ± 1	405 ± 4	404 ± 7	1608 ± 7
343	7440 ± 11	106 ± 56	1253 ± 664	0.00583 ± 0.00003	469 ± 1	470 ± 1	434 ± 3	428 ± 4	1584 ± 4

yrs B2006 = years before AD 2006. All errors are absolute 2σ. Subsample sizes range from 20 to 200 mg. M = measured, and I = initial for $\delta^{234}U_m$ and $\delta^{234}U_i$. See SOI methods for initial $^{230}Th/^{232}Th$ values used to calculate corrected ages.

4.3.5 AMS ^{14}C Chronology and Bomb Carbon Modelling

An Incremental AMS ^{14}C study on the upper 48 mm of YOK-G was conducted to help constrain speleothem growth rates during the last 50 years. At Penn State University (PSU), carbonate samples we milled from the same surface sampled for U-Series dating and stable isotope work, offset from the stable isotope sampling axis. The surface was etched with dilute HCl to remove carbonate displaced when the speleothem was originally cut into a slab. The slab was mounted on a Sherline 5400 Micromill that allows for x-, y- and z-axis control to 10s of micrometers. Samples were drilled at 120-150 rpm with a 0.80mm carbide burr following individual growth increments visible in the speleothem to minimize time averaging. Based on the final age model, the samples represent roughly a single year of growth for samples before C.E. 1970 (0.84mm a^{-1}) and two years (0.42mm a^{-1}) after that. Drilling depth was maintained at 1 mm and between 8 and 12mg of carbonate were obtained for each sample. Two calcite ^{14}C blanks were also acid etched (~10% etch by mass) and drilled to produce powder to assess whether heat and pressure from the burr would cause exchange with modern ambient CO_2 and alter the ^{14}C content of the speleothem as observed in other cases (Hoffmann et al., 2010; Southon et al., 2012). Etched calcite chips were drilled at 150 rpm and 1000 rpm, respectively.

At the UC Irvine Keck Carbon Cycle AMS Facility (KCCAMS), carbonate powder was hydrolyzed with orthophosphoric acid under vacuum and the evolved CO_2 was reduced to graphite at 550°C using a modified hydrogen reduction method onto a Fe catalyst (Alfa Aesar mesh -325 lots JO2M27 and L16P22), with reaction water drawn off with $Mg(ClO4)_2$ (Santos et al., 2004; Santos et al., 2007). The Fe catalyst used is baked monthly at 300°C for 3 hours in air, and subsequently baked at 400°C in H_2 for 45 minutes prior to analysis to reduce modern carbon contamination. Solid graphite samples were pressed into Al targets and loaded on the target wheel with OX-1 (oxalic acid) and calcite blanks for AMS analysis. AMS ^{14}C measurements were made on a modified National Electronics Corporation compact spectrometer with a 0.5MV accelerator (NEC 1.5SDH-1)(Beverly et al., 2010). All ^{14}C ages were $\delta^{13}C$-corrected for mass dependent fractionation with measured values following Stuiver and Polach

(1977). Results are reported as fraction modern ($F^{14}C$) and $D^{14}C$ (‰) in Table S3. AMS measurements showed no appreciable difference between ^{14}C activity of the two blanks and the 150 rpm blank was used for the background correction for the YOK-G AMS ^{14}C samples.

The peak in atmospheric bomb carbon is attenuated within the YOK-G ^{14}C by a combination of: 1) biomass and soil carbon processes above Yok Balum Cave; 2) the proportion of dead carbon contributed to the speleothem carbonate; and 3) the possible mixing of dripwater and dissolution of secondary carbonates within the karst itself (Genty and Massault, 1997; Genty et al., 1998). Fractionation between soil CO_2 $\delta^{13}C$ (estimated at -22‰ VPDB) and speleothem $\delta^{13}C$ (averaging -8.5‰ VPDB) enriches $F^{14}C$ by 0.03105 (Saliége and Fontes, 1984). Accounting for fractionation and comparing the two pre-bomb samples (YG36 and YG48) to the early 20th century portion of the IntCal09 Northern Hemisphere curve (Reimer et al., 2009) in terms of $F^{14}C$ the dead carbon fraction (DCF) is estimated at ~15%. Correcting the measured values assuming a constant DCF, the first sample showing ^{14}C enrichment is YG 28 at 28mm from the tip, which would correspond to C.E. 1954-1956 in the Northern Hemisphere bomb ^{14}C compilations (Hua and Barbetti, 2004). This is in good agreement with the U-Series and carbon cycle counting chronologies, which also place 1955 at ~28 mm.

A simple model of the carbon reservoirs involved in speleothem carbonate deposition was developed following Genty et al. (1998) to help interpret the attenuated ^{14}C pulse in YOK-G (Fig. 4.5). The potential carbon reservoirs are: soil CO_2 from rapid-turnover soil organic matter (SOM, 1 year residence) that reflects the single year atmospheric ^{14}C; soil CO_2 from slow-turnover SOM (>1 year residence; average of atmospheric ^{14}C activity over the residence time); mixed dissolved carbonate in the epikarst zone; and DCF. Annual atmospheric ^{14}C content was estimated from C.E. 1850 to 1999 using the Northern Hemisphere Zone 2 bomb dataset (Hua and Barbetti, 2004) and the IntCal09 curve (Reimer et al., 2009), averaging the monthly values in the former and interpolating annual values for the latter in terms of $F^{14}C$. The contributions were varied in a series of iterations: rapid-turnover SOM from 5 to 75%; slow-turnover SOM residence time from 15 to 30 year; epikarst mixing from 0 to 15 yr.

The model with the best fit to the measured ^{14}C activity in YOK-G is consistent with a slow-turnover SOM contribution of 50% with a 30-yr residence time, and no epikarst mixing. The shape of the resulting curve matches the YOK-G record well (noting that the two peaks on the rising limb of the NH Zone 2 curve were not directly sampled in YOK-G), but the modelled $F^{14}C$ is elevated 3-4% above measured values (Fig. 4.5). This could be the result of the DCF increasing from 15% in the first half of the 20th century to roughly 18% after ca. C.E. 1960, as depicted in Figure 4.5. A shift in soil CO_2 $\delta^{13}C$, and hence less fractionation of ^{13}C and ^{14}C, is ruled out as a cause. This would require a transformation from C3 to C4 biomass above Yok Balum, for which there is no evidence.

Table 4.3 Incremental AMS ^{14}C measurements on YOK-G carbonate and calcite blanks.

Sample ID	depth (mm)	PSU#	UCIAMS#	$F^{14}C$	$D^{14}C$ (‰)
YG02	2	5150	111916	1.0332 ± 0.0019	33.2 ± 1.9
YG04	4	5151	111917	1.0636 ± 0.0026	63.6 ± 2.6
YG06	6	5152	111918	1.0886 ± 0.0015	88.6 ± 1.5
YG08	8	5153	111919	1.1019 ± 0.0017	101.9 ± 1.7
YG12	12	5154	111920	1.1326 ± 0.0016	132.6 ± 1.6
YG16	16	5155	111921	1.1279 ± 0.0017	127.9 ± 1.7
YG22	22	5156	111922	1.0657 ± 0.0017	65.7 ± 1.7
YG28	28	5157	111923	0.8905 ± 0.0013	-109.5 ± 1.3
YG36	36	5158	111924	0.8644 ± 0.0012	-135.6 ± 1.2
YG48	48	5159	111925	0.8639 ± 0.0014	-136.1 ± 1.4
Cal1 (150rpm)	na	5179	111945	0.0028 ± 0.0001	-997.2 ± 0.1
Cal2 (1000 rpm)	na	5180	111946	0.0024 ± 0.0001	-997.6 ± 0.1

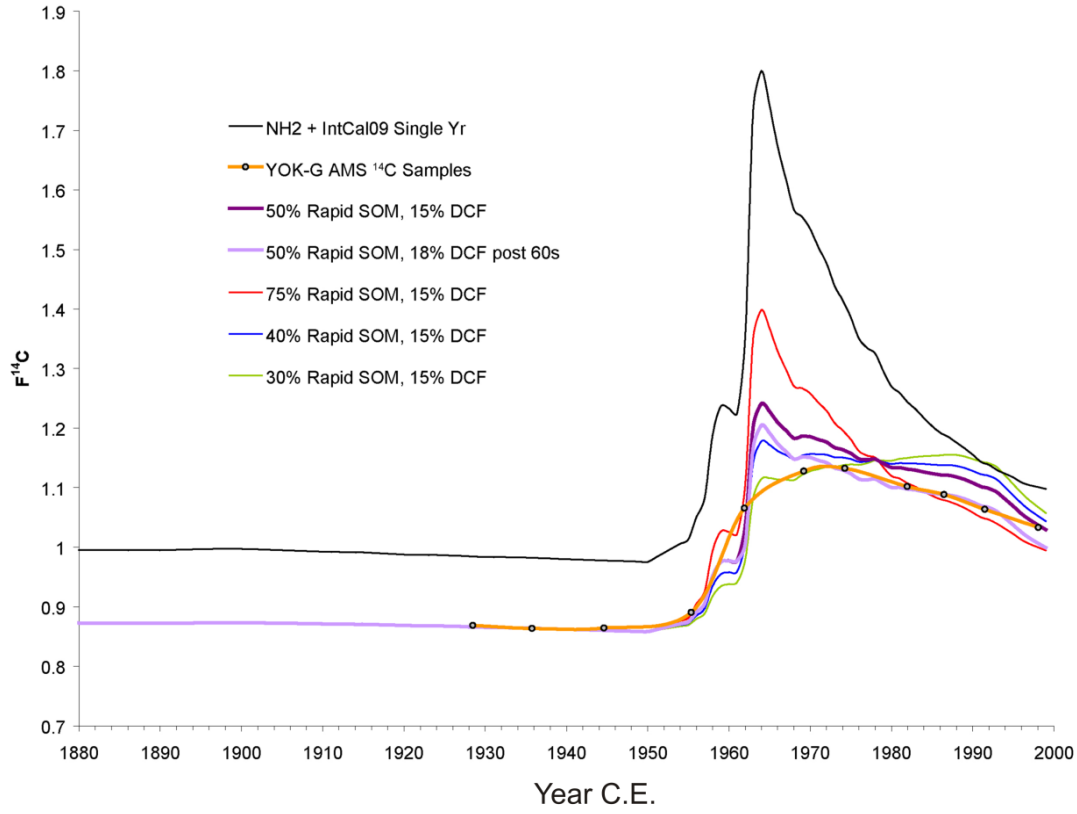

Figure 4.5 ^{14}C activity in YOK-G. Bomb ^{14}C activity in the YOK-G speleothem versus modelled ^{14}C mixtures of soil CO2 and dead carbon fraction (DCF) assuming 30-yr residence time for slow-turnover soil organic matter (SOM) and no mixing dripwater in the epikarst above Yok Balum Cave. YOK-G $F^{14}C$ values are plotted on the U-series timescale, where the rising limb of the bomb curve coincides with the Northern Hemisphere Zone 2 curve and modelled curves. The shape of the YOK-G ^{14}C curve most closely matches the assumption of 50% rapid turnover SOM CO2 (purple) but a closer correlation is found if the DCF increases from 15% to 18% after ca. C.E. 1960 (lavender).

4.3.6 $\delta^{13}C$ cycle chronology

YOK-G $\delta^{13}C$ is a function of CO_2 exchanges controlled primarily by rainfall and the amount of water entering the karst system. This mechanism has been found to be dominant in other tropical cave systems where rainfall variability controls speleothem $\delta^{13}C$ value via changes in drip rate (Yadava and Ramesh, 2005) and is supported here by comparison of the YOK-G record with nearby rainfall records from Punta Gorda (~30km to the south east). Rainfall and YOK-G $\delta^{13}C$ are negatively correlated on both monthly ($r_{pearsons} = -0.57$, $p < 0.001$) and annual ($r_{spearmans} = -0.41$, $p < 0.07$) timescales during the period that the records overlap (Fig. 4.7). The limited length of the Punta Gorda dataset limits the statistical significance of the relationship on annual timescales. While the contribution of biogenic carbon to the soil zone may account for some portion of the annual cycle, soil CO_2 productivity is driven more by water availability than temperature, which is essentially constant year round. Furthermore, the year round productivity of the tropical forest above the cave helps to eliminate large seasonal differences in the isotopic composition of soil CO_2. We therefore have confidence in $\delta^{13}C$ as being a proxy for karst recharge and rainfall. This interpretation is supported by the remarkable, demonstrably annual $\delta^{13}C$ cycles apparent throughout the record (Fig. 4.8) reflecting seasonal water recharge conditions, as well as by interpretations of other Belizean stalagmite $\delta^{13}C$ records as reflecting rainfall, notably Frappier et al. (2002), linking pronounced $\delta^{13}C$ increases to El Niño related rainfall reductions, and Webster et al.(Webster et al., 2007) linking $\delta^{13}C$ shifts over the last 3,300 years to rainfall. We note that these two studies represent the two published speleothem records from cave sites closest to Yok Balum cave (Actun Tunichil Muknal Cave, ~100km to the north, and Macal Chasm, ~80km to the north), and that both utilised $\delta^{13}C$ as a palaeorainfall proxy. The resolution of the Macal Chasm record is lower than that of YOK-G, however a clear positive relationship exists between the two (Fig 4.6). The Frappier ATM record is not sufficiently long as to permit successful comparison with YOK G.

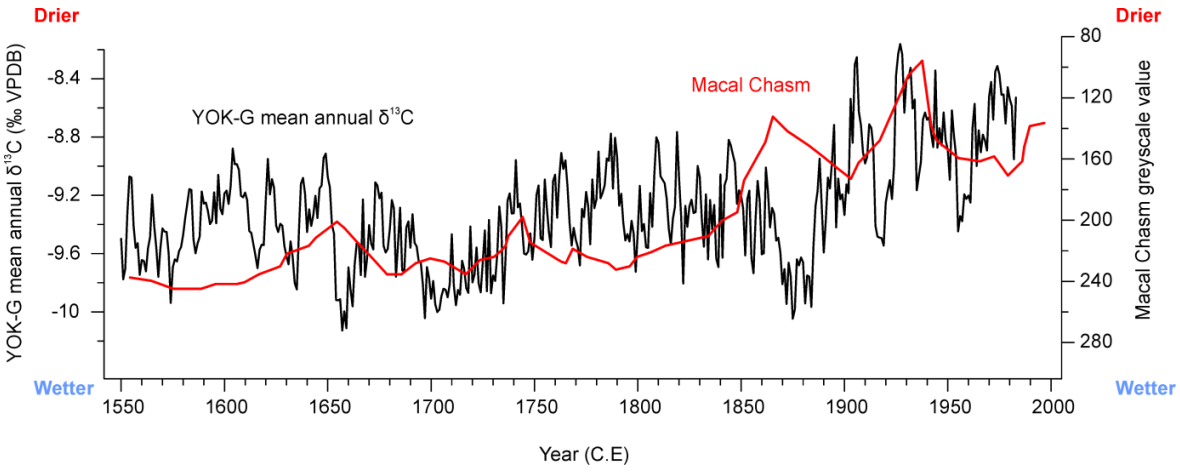

Figure 4.6 Mean annual YOK-G $\delta^{13}C$ and Macal Chasm greyscale record.

The ^{230}Th chronology suggests that YOK-G grew at a nearly constant rate of approximately 0.82mm a^{-1} between 1560 and 1983. The mean width of the $\delta^{13}C$ cycles present in the record is 0.83mm, indicating that the cycles are annual. Radiocarbon analyses permit identifying the rising limb of the radiocarbon bomb spike at 27mm depth. This provides an independent confirmation of the accuracy of the top ^{230}Th dates, and also provides a date with which to anchor the annual $\delta^{13}C$ chronology. Carbon cycles were counted from this chronological marker (1955). The highest $\delta^{13}C$ values in every cycle correspond with the end of the dry season (April) when the karst is most extensively drained and the lowest $\delta^{13}C$ values represent the peak of the wet season (July) (Fig. 4.8). Carbon cycle chronology is consistent with the ^{230}Th chronology, and is never outside the errors of any of the ^{230}Th dates. The $\delta^{13}C$ cycles therefore provide an accurate sub-seasonally resolved chronology. Only the top 6mm of the stalagmite failed to display $\delta^{13}C$ cycles. This spanned the time between 1983 and 2006 and is possibly due to a shift in hydrology. A further 270 carbonate samples were re-milled at a 30µm resolution on the top 8mm of YOK-G to both verify the sudden increase in $\delta^{13}C$ at 1983 and to determine whether annual $\delta^{13}C$ cycles would be visible at a higher resolution (Fig. 4.9). Analysis was performed at Eidgenössische Technische Hochschule (ETH) Zurich following methods similar to those previously described in section 3.3.2. This short interval (from 1984 to 2006) is therefore not included in the discussion due to increased chronological uncertainty.

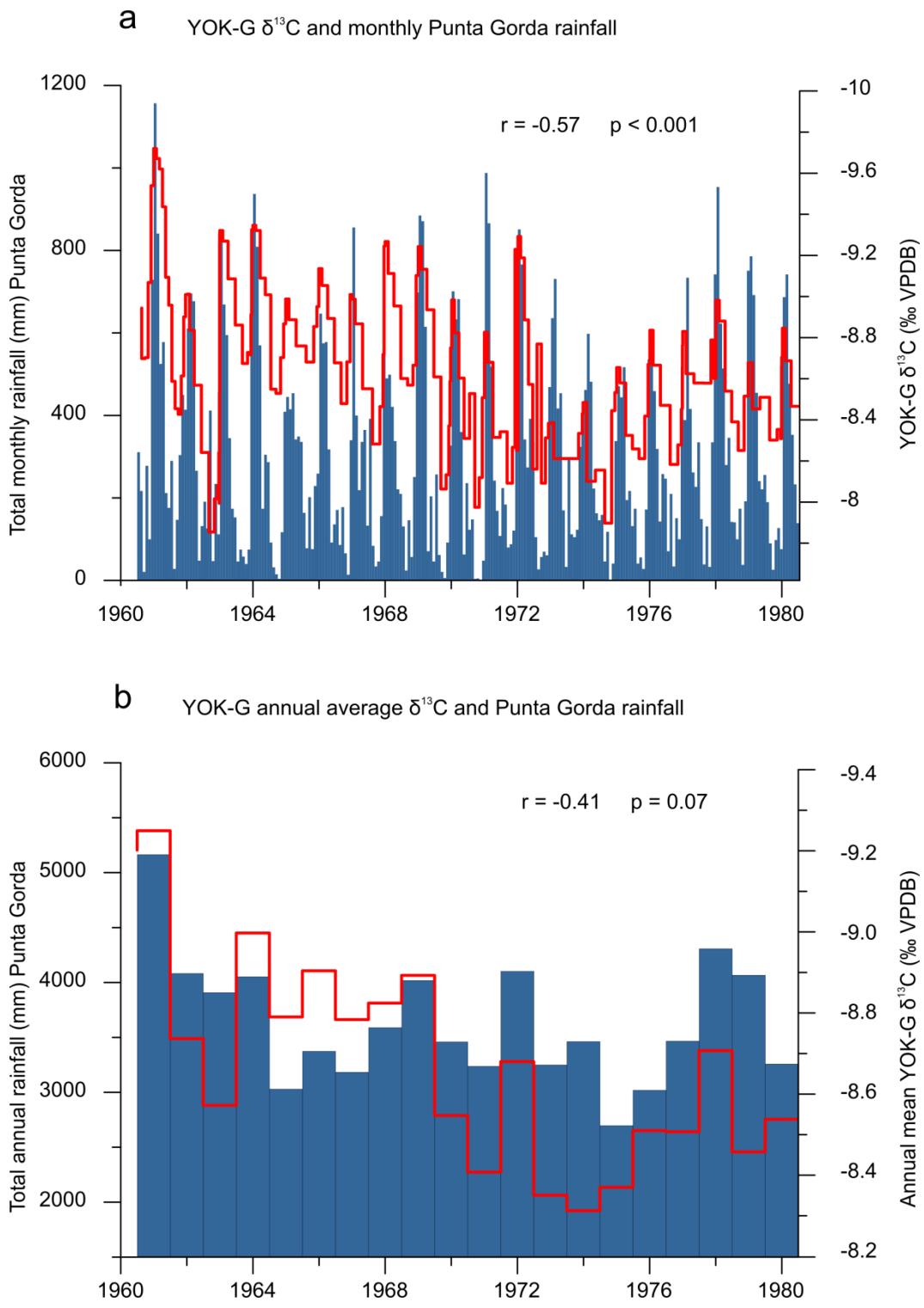

Figure 4.7 a) Monthly rainfall at Punta Gorda and YOK-G $\delta^{13}C$ (red line) **b)** Total annual rainfall recorded at Punta Gorda and mean annual YOK-G $\delta^{13}C$ for the period 1960-1980 (red line).

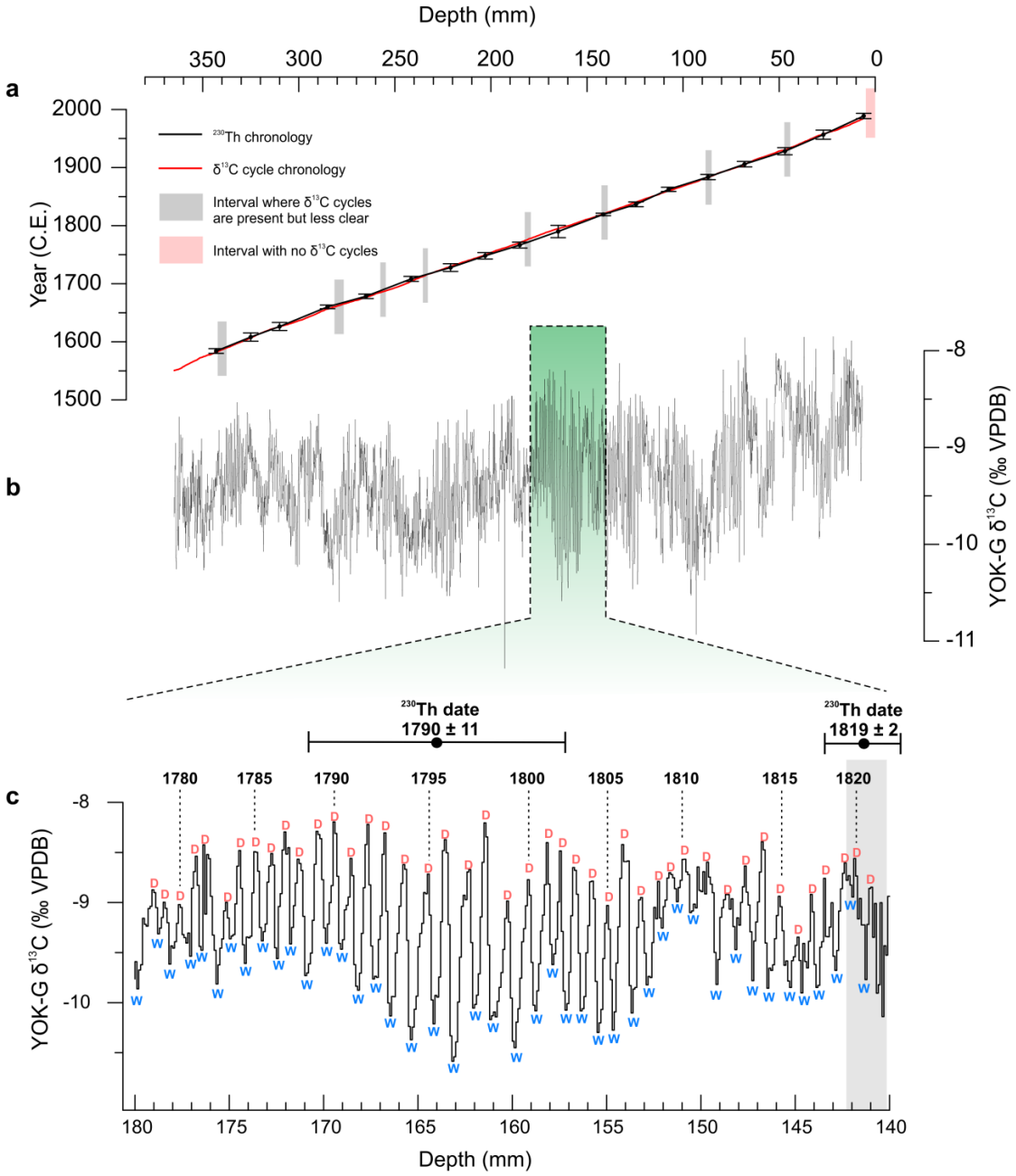

Figure 4.8 a) ^{230}Th dates with errors (black line) and δ^{13}C cycle chronology (red line). Shaded grey boxes indicate intervals where the δ^{13}C cycles are present but somewhat less clear. The shaded pink box indicates the interval (1983-2006) where δ^{13}C cycles are absent. Both chronological models are fitted with cubic splines. The ^{230}Th dates were used to verify the accuracy of the δ^{13}C cycle count chronology, but were not used directly in developing the chronological model. **b)** The YOK-G δ^{13}C record against depth spanning the last 456 years, with inset expanded in **c)** illustrating δ^{13}C annual cycles with peak wet ('W' = low δ^{13}C) and dry ('D' = higher δ^{13}C) season δ^{13}C values identified. These were used as a further chronological tool, permitting identification of season of deposition. The grey shaded area to the right illustrates cycles during an interval where the δ^{13}C cycles are less clear.

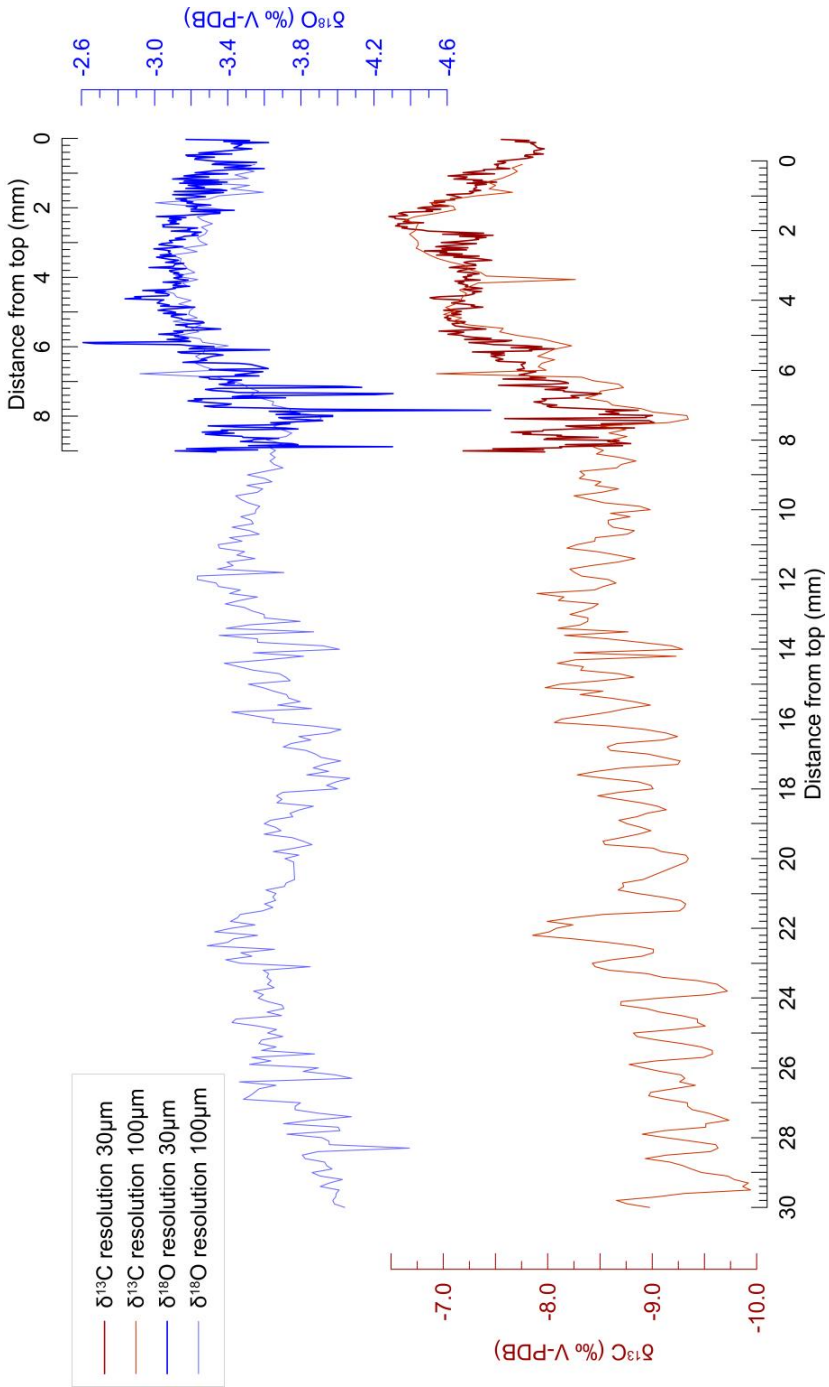

Figure 4.9. High resolution (30µm) resampling of the top 8mm of YOK-G and the original sampling (100µm resolution). Resampling conducted at ETH Zurich.

It is possible that the cycle amplitude and thus inferred seasonality is simply a product of different sampling resolutions across annual cycles of different wavelength. In short, because the spatial resolution of micromilling remained constant at 100 microns, more averaging of the $\delta^{13}C$ amplitude would occur for a year with less growth compared with a year with more. To test how much of an effect this phenomenon might have, numerical models were used to simulate stalagmite growth, and were then 'sampled'. Two annual growth rates similar to the minimum and maximum growth rates (500 and 1000 microns $year^{-1}$, respectively) observed in the YOK-G record were used in the models (Fig. 4.10). The synthetic $\delta^{13}C$ records derived from these two models are comparable to original $\delta^{13}C$ input dataset, illustrating that the amplitude of the $\delta^{13}C$ cycles is not significantly affected by this averaging effect. We then calculated the maximum amount that amplitudes of cycles with different wavelengths were muted by this averaging effect, and applied this maximum possible correction to the YOK-G $\delta^{13}C$ cycle amplitude dataset (Fig. 4.11). The resulting dataset is essentially indistinguishable from the original dataset, indicating that this averaging effect has no significant influence on $\delta^{13}C$ cycle amplitude within the range of growth rates observed within the YOK-G record.

By combining these three independent chronological techniques, U-Series, $\delta^{13}C$ cycle counting and identification of the atmospheric bomb spike, the YOK-G stable isotope record can be constrained to sub-annual precision.

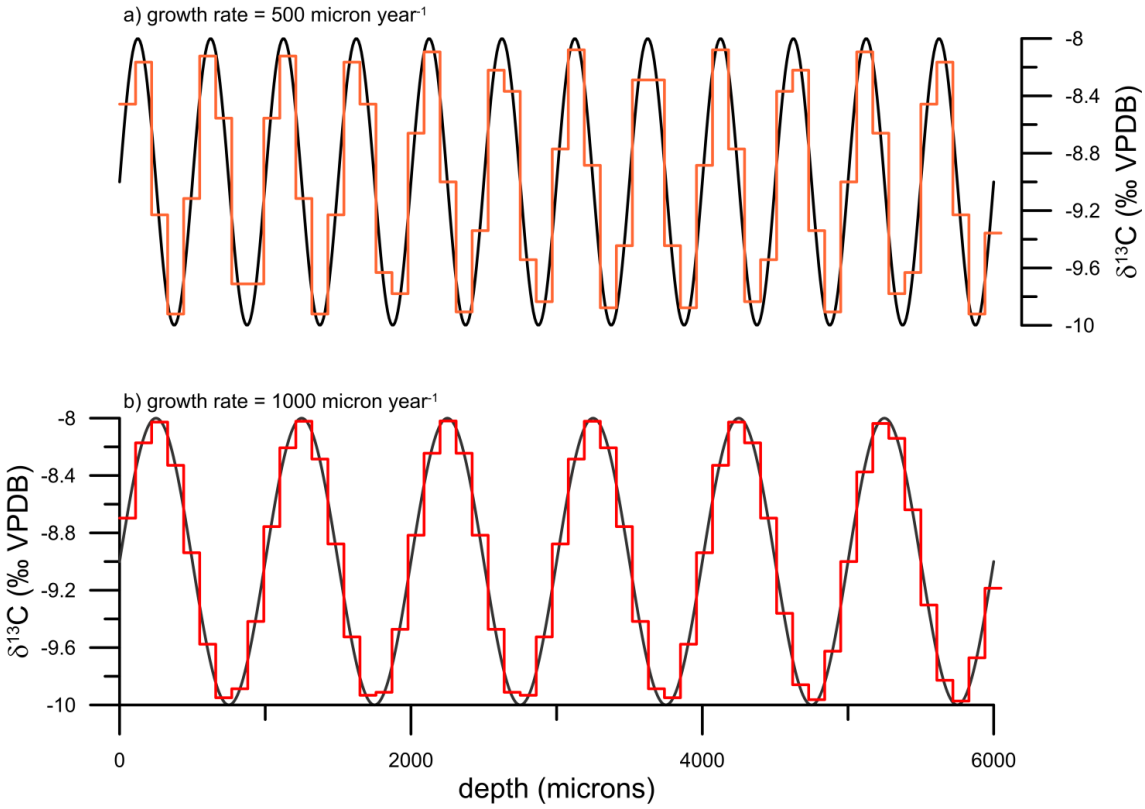

Figure 4.10 Modelled differential sample averaging effect induced by growth rate variability. Growth rate is modelled as varying between 500 and 1000 microns per year, similar to observed growth rate variability in stalagmite YOK-G, and the $\delta^{13}C$ amplitude of variability is 2‰, again consistent with YOK-G carbon isotope variability. The sampling interval is maintained at 100 microns irrespective of growth rate. The modelling demonstrates that differential growth rates produce very little difference in the amplitude of the $\delta^{13}C$ cycles as inferred after sampling. Thus, $\delta^{13}C$ cycle amplitude variability can be interpreted in terms of seasonality rather than a growth rate induced aliasing effect.

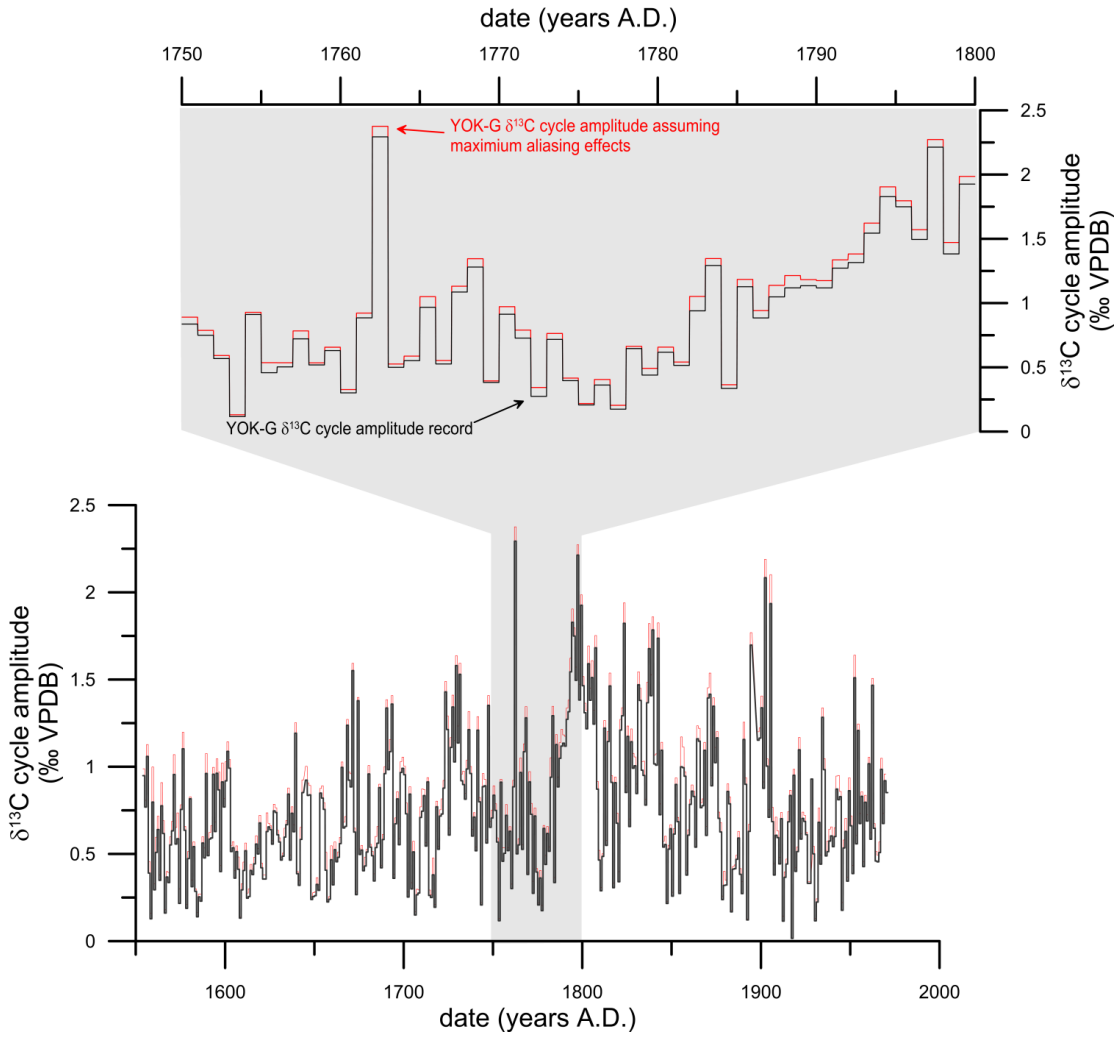

Figure 4.11 YOK-G $\delta^{13}C$ amplitude (black) and amplitude corrected for maximum aliasing effects (red). Both records are essentially identical, further demonstrating that growth rate induced aliasing is not an issue in interpreting the $\delta^{13}C$ cycles in terms of palaeoseasonality.

4.3.7 Environmental monitoring

Intensive monitoring for this project began at Yok Balum Cave in April 2011 following less intensive initial monitoring that began in 2006 (see Kennett *et al*., (2012) for details). Cave environment monitoring instruments were installed inside and above the cave to continuously monitor cave atmospheric parameters, drip hydrology, local meteorology, and soil environments. Locations of these instruments are illustrated in Chapter 3, Fig. 3.1. Rain gauges were set up in Santa Cruz village to allow for maintenance and because this was the nearest area to the cave without extensive tree cover. Small disturbances exist in some data sets due to equipment malfunction. These are highlighted in the results for each instrument.

a. Cave atmosphere

Within cave temperature measured at the large 'Birthday Cake' stalagmite is essentially constant (~22.9°C) and humidity is high (>95%) throughout the year. Within cave temperature approximates the external annual mean temperature (Fig. 3.2) and this plays an important role in determining the seasonal modes of ventilation in the cave. Figure 4.12 shows a 14-month time series of three-hourly cave air pCO_2 (corrected to barometric pressure) measured using a Vaisala MI70 Indicator coupled to a Vaisala GMP343 Carbocap CO_2 probe. This time series indicates that at no time did pCO_2 values reach elevated values sufficient to inhibit carbonate deposition. The cave ventilates on a daily basis (inset), most likely via diurnal density-induced gravitational overturning, which acts to keep pCO_2 levels low (means of 419ppmv and 515ppmv in January and June, respectively) compared to pCO_2 levels measured in many other caves (Baldini, 2010) and at levels insufficient to significantly alter the degree of kinetic fractionation due to the rate of CO_2 degassing. The two cave entrances and simple tunnel structure of the cave facilitate vigorous ventilation.

CO_2 variability is higher during the wet season than in the dry season, most likely due to a combination of increased CO_2 flux into the cave via drip water degassing and direct transfer from the active soil zone and a change in ventilation regime caused by

seasonal changes in air density gradient between the cave and outside atmosphere. It is very unlikely that during the last few thousand years pCO_2 levels were ever sufficiently high to restrict carbonate precipitation or alter the degree of kinetic fractionation. Hendy tests performed in Yok Balum Cave (Kennett et al., 2012) suggest that the $\delta^{13}C$ of precipitating carbonate is affected by some degree of kinetic fractionation. This stability of the cave CO_2 level and continuous ventilation mechanism suggest that changes in the degree of kinetic fractionation will be controlled by the amount of degassing permitted by the drip rate and hence karst recharge.

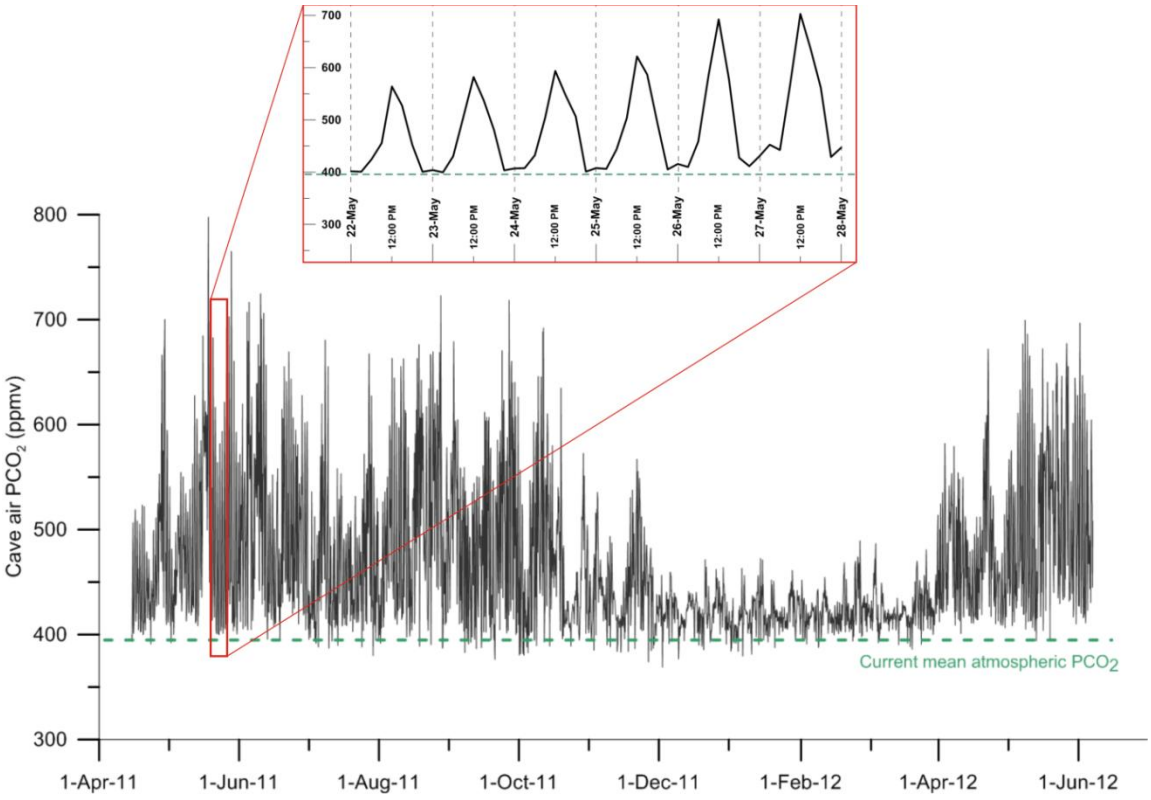

Figure 4.12 14-month time series of three hourly pCO2 in Yok Balum. Evidence that cave ventilates daily (insert) throughout the year and that pCO2 ¬values remain relatively low throughout the year.

b. YOK-G Drip rate

An automated drip logger was placed on the scar of YOK-G to measure drip discharge. Figure 4.13 shows a six-month time series of hourly YOK-G drip hydrology and total daily rainfall (at Santa Cruz village) from April 2012 to November 2013 (measured using both a HOBO weather station and Pluvimate rain gauge). YOK-G drip rate is typically high and highly variable, and displays both diffuse and fracture flow components. Drip rate slowly increases during the wet season (minimum 460 to maximum 1445 drips per hour) as the karst system becomes increasingly filled. Large rainfall events provoke a 'flashy' response in drip rate, indicative of quick transfer of water via fracture routes producing short-lived drip rate maxima. The high drip rate, even at the end of the dry season (April, May) suggests that a substantial diffuse flow component exists which is supplemented by fracture flow after pronounced rainfall events. YOK-G is therefore especially sensitive to variability in the fracture flow component, and thus records extreme high rainfall events as well as wet season droughts, but due to buffering by the diffuse flow component is less sensitive to dry season droughts.

The drip feeding YOK-G has a drip rate approximately 30 times greater than that of the drip feeding stalagmite YOK-I, located a few meters away in the same chamber (means of 921 and 25 drips per hour, respectively) (Kennett et al., 2012). This higher drip rate partially accounts for the higher growth rate of YOK-G compared to YOK-I (means of 830 microns and 200 microns per year, respectively) and for the less negative mean ^{13}C values of YOK-I carbonate. The difference in drip rates between these two stalagmites strongly indicates that the two drips are fed by considerably dissimilar hydrological pathways; consequently the two stalagmites record different components of the climate input signal (Baldini et al., 2006). YOK-G is fed by large diffuse and fracture flow components (Fig.4.14). YOK-I is fed by less fracture and diffuse flow, and consequently is more sensitive to short- and long-lived droughts but less sensitive to high rainfall events.

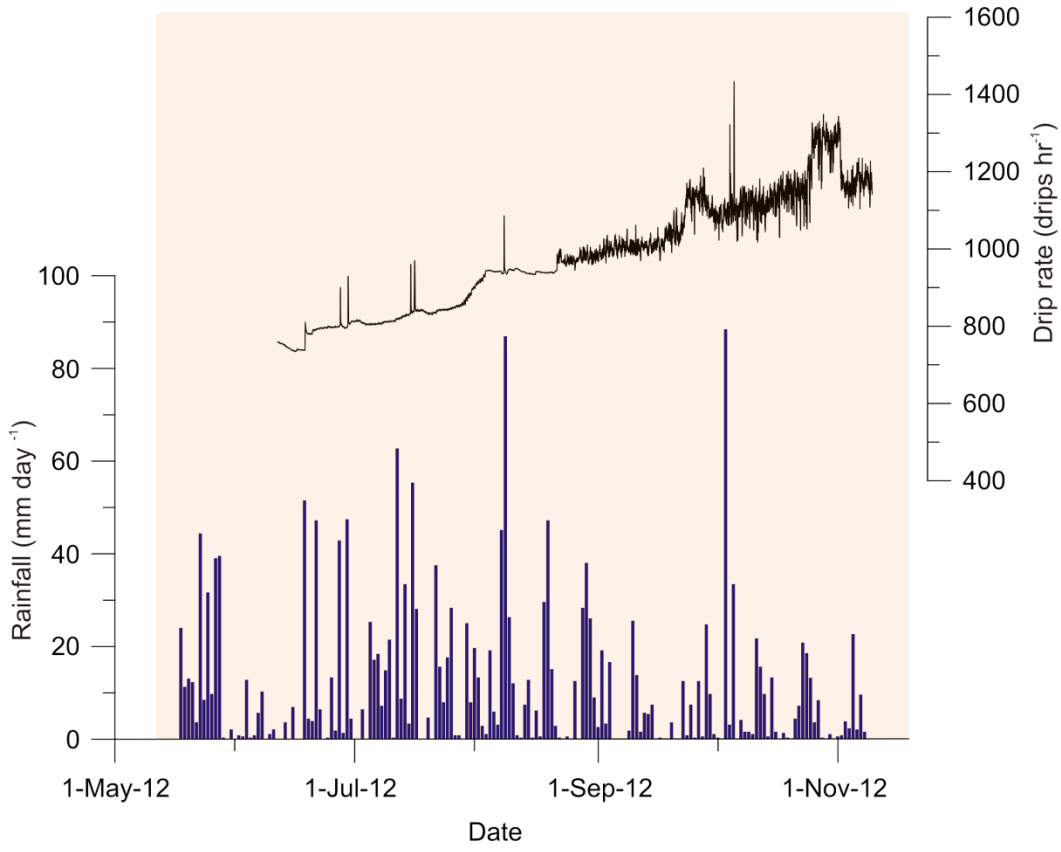

Figure 4.13 Six-month time series of hourly YOK-G drip rate and daily rainfall total from a rain gauge and HOBO meterological station located in Santa Cruz village (~3km north of Yok Balum). Drip regime provides evidence of diffuse (periods of smooth increase or decline) and fracture (short lived peaks) flow pathways.

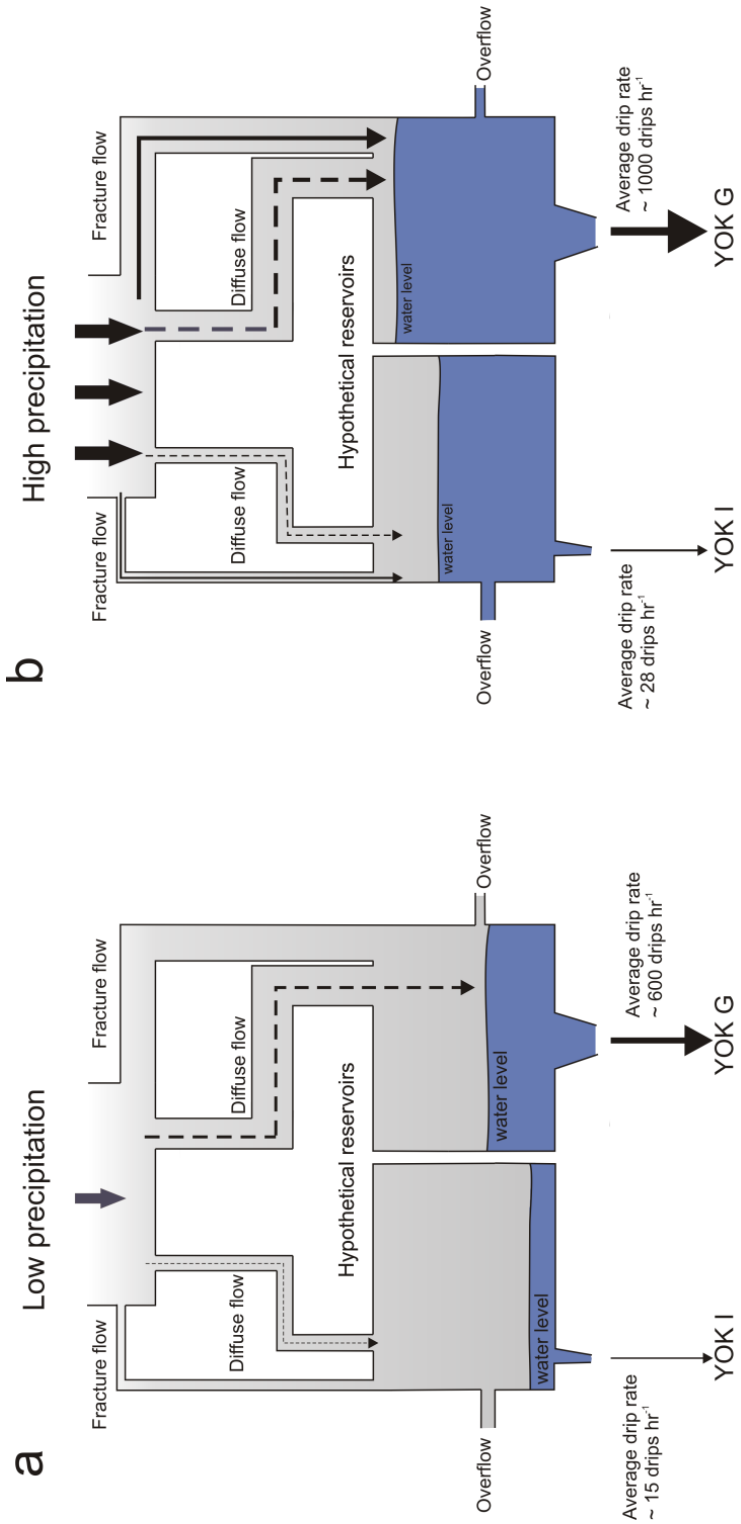

Figure 4.14 Hypothetical hydrology systems feeding YOK-I and YOK-G based on drip regimes. **(a)** Dominance of diffuse flow during low precipitation periods. **(b)** Initiation of fracture flow during high precipitation events. YOK-G has a larger reservoir than YOK-I and large diffuse and fracture components feeding the stalagmite. YOK-G has a larger aperture to the stalactite which feeds the stalagmite than that of YOK-I.

4.3.8 Aerosols

Dominant anthropogenic sulphate and nitrate aerosols are formed via oxidation of industrial oxides, primarily produced during coal consumption. Aerosols affect the climate both directly, via scattering and absorption of solar radiation, and indirectly, by affecting cloud cover (Koch and Del Genio, 2010) and cloud properties such as precipitation efficiency (Albrecht, 1989) and albedo (Twomey, 1974). Direct global mean aerosol forcing is currently estimated to be -0.5 ± 0.4 Wm^{-2}, and indirect global mean aerosol forcing at -0.7 with a range uncertainty of -0.3 to -1.8 Wm^{-2} (Forster and Ramaswamy, 2007). The combined net forcing acts to partially offset the positive radiative forcing of longer lived greenhouse gases (Forster and Ramaswamy, 2007; Leibensperger et al., 2012a). Due to the short lived nature of anthropogenic aerosols, their radiative forcing is strongly localised over source regions (Schulz et al., 2006), and anthropogenic aerosols are therefore thought to contribute to regional heterogeneity in climate change. Indeed observational studies provide considerable evidence that aerosols have lowered surface air temperatures, offsetting greenhouse warming (Qian and Giorgi, 2000; Wild et al., 2007; Ruckstuhl et al., 2008; Philipona et al., 2009). In two companion papers Leibenspeger et al. (2012a; 2012b) calculated that surface direct and indirect radiative forcing from US anthropogenic aerosols, strongly centred over the central and eastern US, peaked during the period 1970-1990 at -9 Wm^{-2} and was associated with a regional climate cooling of 0.5-1.0^{o}C on average during this period.

Patterns of atmospheric aerosol optical depth have displayed considerable temporal variability in accordance with varying temporal patterns of industrialization (Fig. 4.15). In order to account for the spatial and temporal heterogeneity caused by staggered patterns of industrialisation, we follow the rationale of Robertson et al. (2001) and use regional CO_2 emissions as a proxy for anthropogenic aerosol production. This provides better estimation of regional variability than single records of global aerosols derived from ice cores. Regional CO_2 emissions (Marland et al., 1994) for North America and Western Europe, scaled to 1992 values (Robertson et al., 2001) were utilised to assess relative regional contributions to the YOK-G record. Figure 4.15 illustrates the uneven distribution of atmospheric aerosols between the Northern and Southern Hemispheres, and that for regions spanning both hemispheres (e.g., Africa, Central and

South America) aerosol emissions are dominated by emissions in the northern parts of those regions.

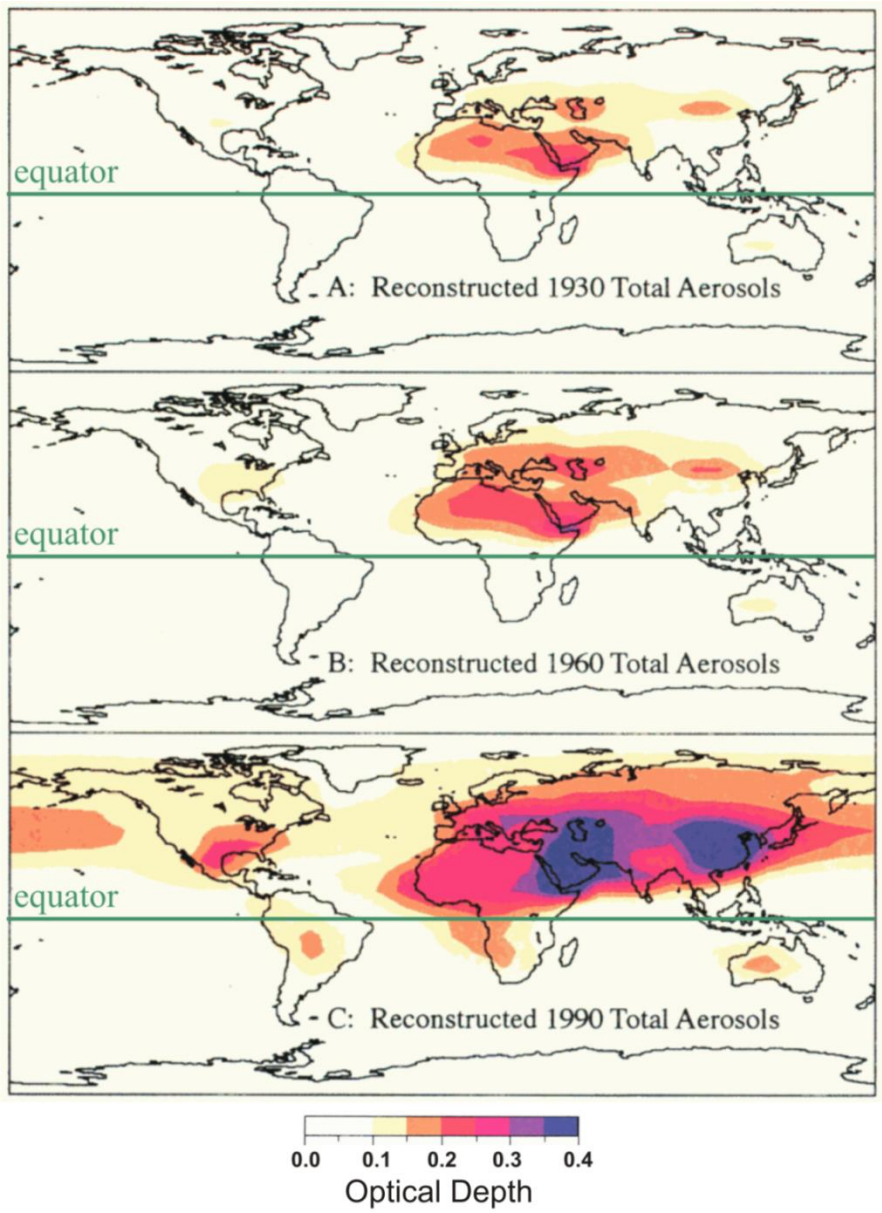

Figure 4.15 Reconstructed aerosols optical depth. Reconstructed aerosols optical depth due to tropospheric aerosols created by scaling modern distributions with regional CO_2 emission curves for (A) 1930 (B) 1960 and (C) 1990. Figure adapted from Robertson et al. (Robertson et al., 2001).

4.4 Results and discussion

Final $\delta^{18}O$ and $\delta^{13}C$ stable isotope records are displayed in Figure 4.16. The two records correlate ($r = 0.38$, $p < 0.001$) but not sufficiently to suggests that a) evaporation induced fractionation is the dominant control or b) that the two records are primarily controlled by the same environmental process or processes. As discussed in section 4.2.1 speleothem $\delta^{18}O$ values are affected by a relatively large number of factors, mostly linked to complex fractionation processes as water vapour travels from source region to sink (Lachniet, 2009). The YOK-G $\delta^{18}O$ record is positively correlated with existing NHT reconstructions (high $\delta^{18}O$ = high NHT), and particularly with the Esper et al. (2002) and Moberg *et al.* (2005) (Fig. 4.17). Tropical stalagmite $\delta^{18}O$ variability is typically interpreted as reflecting rainfall amount (Lachniet, 2009), and in Central America specifically to ITCZ related rainfall amount (Kennet *et al*., 2012). However, substantial research indicates that elevated NHT should have resulted in a more northerly summer ITCZ position (Friedman *et al*., 2013; Frierson *et al*., 2012, Kang *et al*., 2008; Yoshimori and Broccoli, 2008; Haug *et al*., 2003; Kang *et al.* 2009) the opposite of the NHT-$\delta^{18}O$ relationship suggested by the YOK-G record. The positive correlation between NHT and YOK-G $\delta^{18}O$ strongly indicates that regional temperature is the primary control on decadal to centennial scale $\delta^{18}O$ variability in YOK-G. Regional temperature will affect $\delta^{18}O$ values by influencing Caribbean sea surface temperatures and moisture mass evolution from the source region to the cave site. Elevated regional temperatures resulted in decreased fractionation during evaporation from the Caribbean Sea and during rainout along the moisture mass's trajectory, and both processes ultimately led to elevated rainfall $\delta^{18}O$.

On monthly- to annual-timescales Yok Balum cave drip water $\delta^{18}O$ values have been shown to reflect those of local rainfall, governed primarily by rainfall amount (Kennett *et al*., 2012). This is consistent with previous research (Lachniet and Patterson, 2009) which determined that temperature and amount effects are the dominant controls on rain and surface waters in Belize and Guatemala. However, it is apparent form the relationship between NHT and YOK-G $\delta^{18}O$ that on longer timescales, temperature controls on moisture mass evolution are typically dominant and rainfall amount have a

second order control $\delta^{18}O$ variability. Furthermore, the lack of definitive annual cycles in the $\delta^{18}O$ record further indicates that even on annual timescales the rainfall amount controlled $\delta^{18}O$ signal undergoes considerable modification either through evaporative processes at the surface or though mixing of isotopically distinct waters in the vadose zone. In short, the complex nature of $\delta^{18}O$ values in meteoric water in this region and the apparent signal modification which takes place in the soil and vadose zone complicates using $\delta^{18}O$ as a palaeo-rainfall record.

Conversely, stalagmite $\delta^{13}C$ in low latitude regions not experiencing temporal shifts in vegetation type (e.g., shifts from C3 to C4 vegetation) largely reflects effective rainfall amount and the hydrology of the drip feeding the stalagmite. As discussed in section 4.2.2 dry intervals promote prior carbonate precipitation (due to lower groundwater flow rates), increased bedrock carbon contributions, and reduced soil bioproductivity, all contributing to a more positive $\delta^{13}C$. Conversely, wetter conditions result in more negative $\delta^{13}C$. This interpretation is supported by interpretations of other Belizean stalagmite $\delta^{13}C$ records as reflecting rainfall as previously noted in Section 4.3.6. We stress that $\delta^{18}O$ is also an extremely useful complementary rainfall proxy, however unlike $\delta^{18}O$, fractionation processes occurring further afield are not a consideration when interpreting speleothem $\delta^{13}C$ values. We therefore believe that under the stable conditions observed at our site, $\delta^{13}C$ is more sensitive to subtle shifts in recharge and therefore here we utilise the YOK-G $\delta^{13}C$ record as a palaeorainfall proxy.

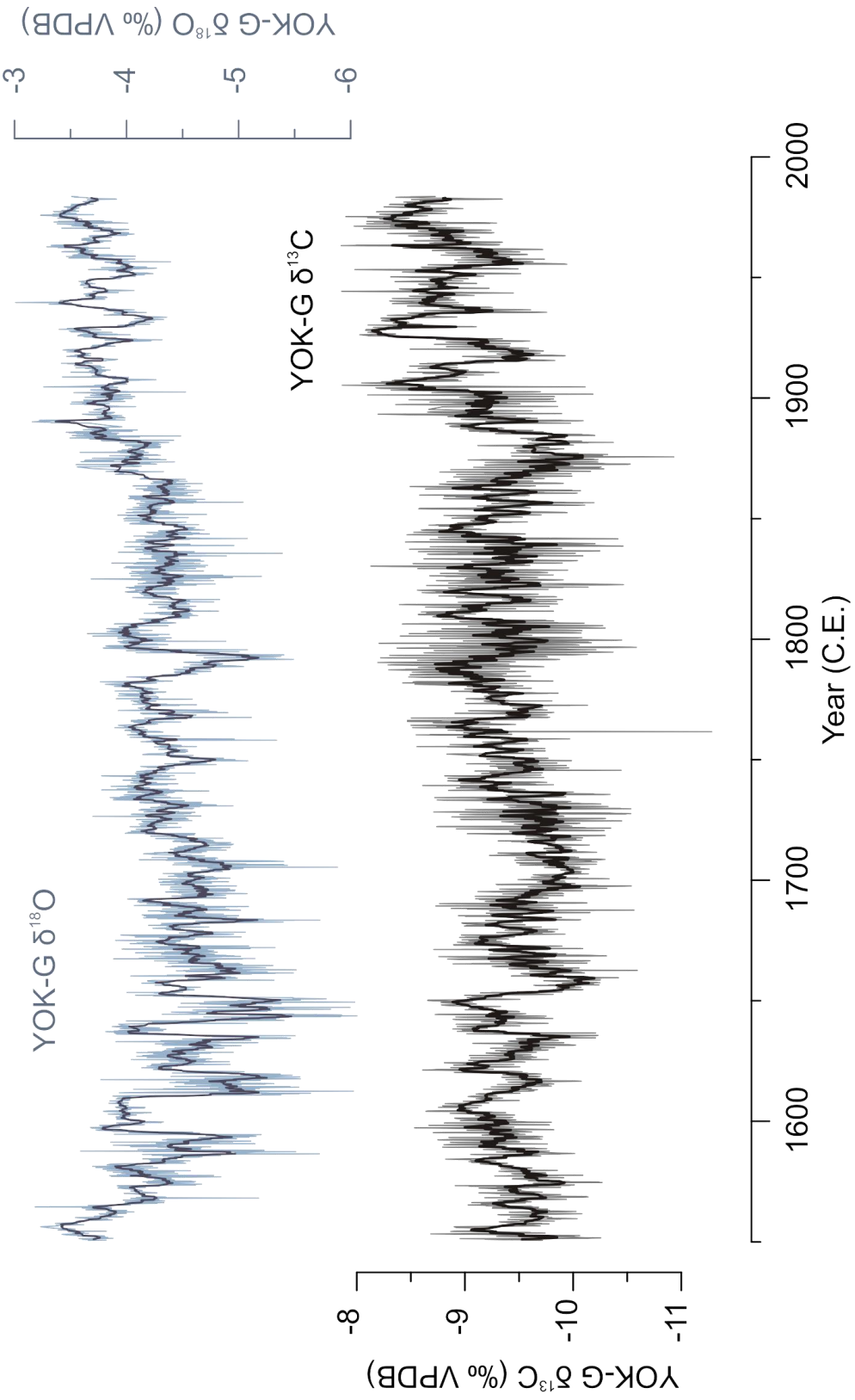

Figure 4.16. Final YOK-G $\delta^{18}O$ (blue line) and $\delta^{13}C$ (black line) stable isotope records, with 9 year running average (thick lines).

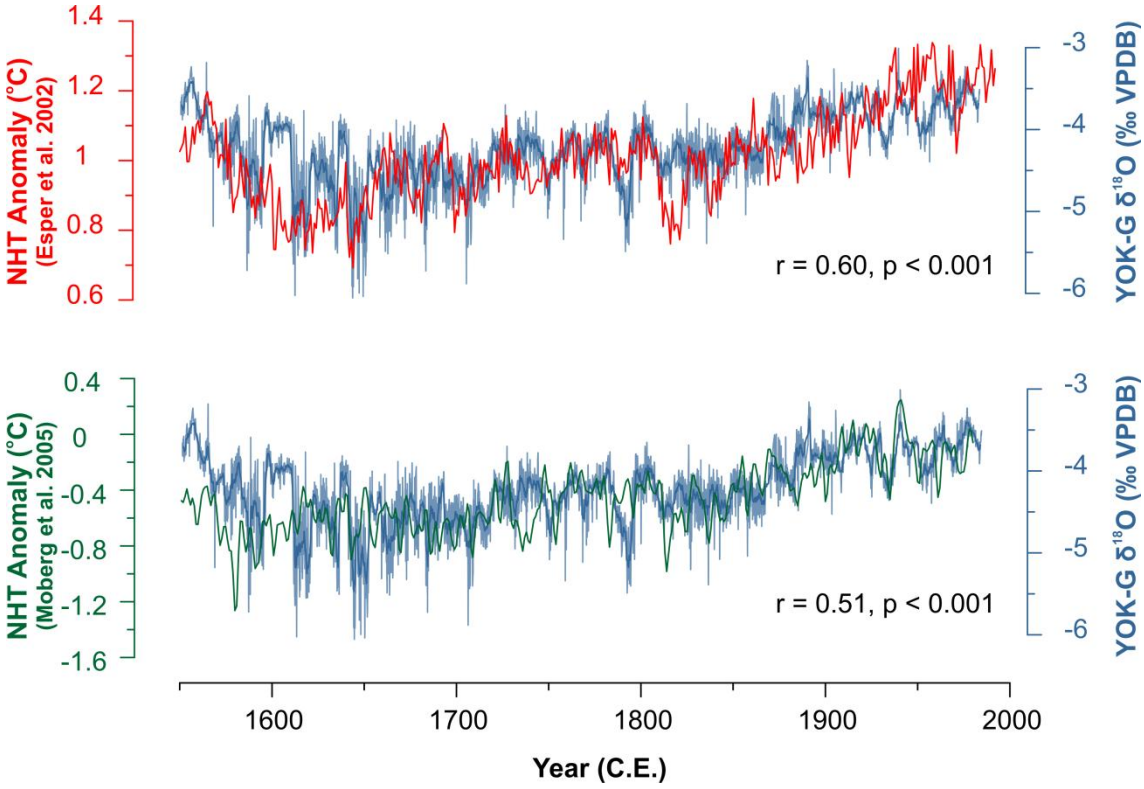

Figure 4.17 YOK-G $\delta^{18}O$ (blue) against Moberg et al. (2005) NHT reconstruction (green line) and Esper et al. (2002) NHT reconstruction (red line).

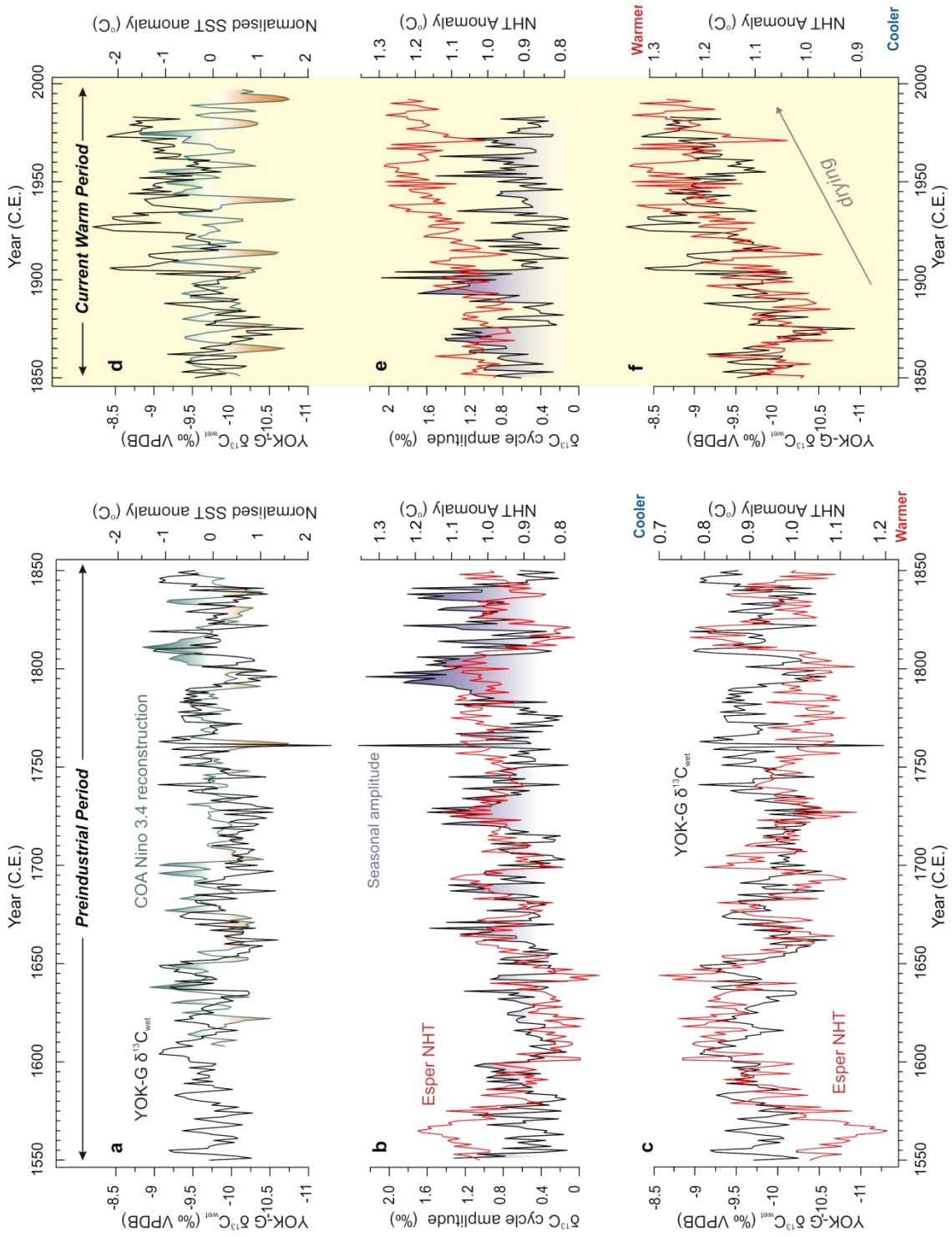

Figure 4.18 a) YOK-G $\delta^{13}C_{wet}$ record and the Niño 3.4 COA reconstruction (Wilson et al., 2010) for the period 1550 to 1850. **b)** Seasonality defined by the amplitude of each annual $\delta^{13}C$ from peak wet season to peak dry season and Esper NHT (Esper et al., 2002) for the period 1550-1850. **c)** YOK-G $\delta^{13}C_{wet}$ against NHT for the period 1550-1850. **d)** as in **(a)** but for the industrial interval of the record, 1851-1983. **e)** as in **(b)** but for the period 1851-1983. **f)** as in **(c)** but for the period 1851-1983.

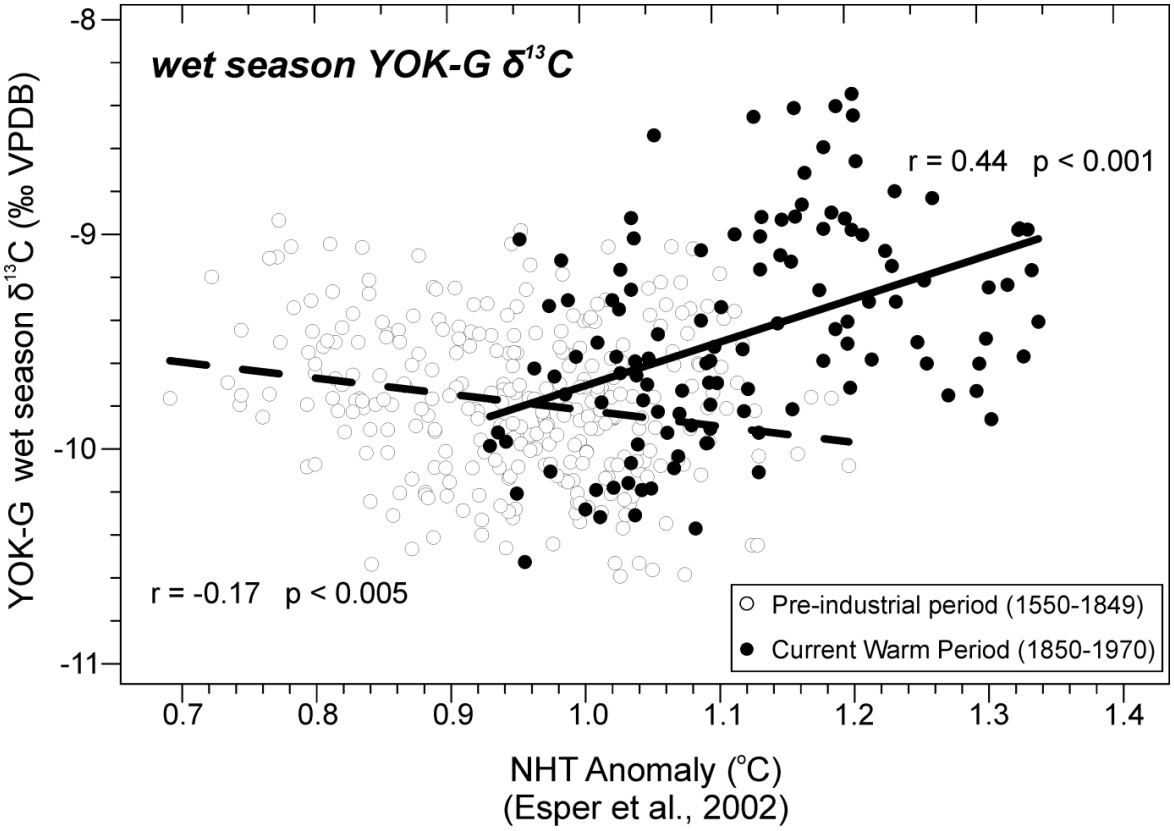

Figure 4.19 Scatterplot of YOK G $\delta^{13}C_{wet}$ versus Esper NHT (Esper et al., 2002) during the preindustrial period (1550-1849) (unfilled circles) showing weak significant negative correlation ($r = -0.19$, $p < 0.005$) and during the CWP (1850-1983) (black filled circles), which exhibits a switch to a significant positive correlation ($r = 0.43$, $p < 0.001$).

Both wet and dry season $\delta^{13}C$ values ($\delta^{13}C_{wet}$ and $\delta^{13}C_{dry}$) are clearly distinguishable in the YOK-G record (Fig. 4.8c), providing a rare opportunity to isolate rainfall amount during specific seasons at a low latitude site. YOK-G $\delta^{13}C_{wet}$ and the NINO3.4 Center of Action (COA) sea surface temperature (SST) reconstruction (Wilson et al., 2010) are anticorrelated ($r = -0.3$, $p < 0.001$ with a nine-year moving average applied) during the preindustrial period (1550-1850), suggesting that eastern equatorial Pacific SST exerted a significant control on Belizean rainfall (Fig. 4.18a). Additionally, a weak but significant negative relationship ($r = -0.19$, $p < 0.001$) exists between the Esper Northern Hemisphere Temperature (NHT) reconstruction (Esper et al., 2002) and δ^{13}Cwet during the preindustrial interval of the record (Fig. 4.18c). This suggests a warmer NH tends to draw the ITCZ to a more northerly position, consistent with the results of numerous previous studies (Friedman et al., 2013; Kang et al., 2008; Haug et al., 2001; Kang et al., 2009). No relationship exists between $\delta^{13}C_{dry}$ and NHT ($r = 0.05$, $p = 0.43$), again consistent with the interpretation of YOK-G $\delta^{13}C_{wet}$ as an ITCZ rainfall proxy. Elevated NHT tended to cause a more seasonal rainfall distribution (greater seasonality) during the preindustrial portion of the YOK-G record ($r = 0.32$, $p < 0.001$, with a nine-year moving average applied) (Fig. 4.18b). However, post-1850 all the $\delta^{13}C$ data (mean annual, wet season, and dry season) strongly suggest a steady drying trend coinciding with increasing NHT, suggesting a dramatic reversal in the relationship between NHT and ITCZ position) (Fig. 4.19) .

Additionally, post-1850 YOK-G annual mean $\delta^{13}C$ tracks trends in global GHG concentrations and anthropogenic aerosol emissions (Fig. 4.20). This indicates a southward ITCZ migration despite increasing NHT. This change in relationship also corroborates the notion that YOK-G $\delta^{13}C$ is a proxy for water recharge to the karst as opposed to temperature.

The timing of this relationship reversal suggests an anthropogenic link. Recent research highlights the competing effects of GHG and anthropogenic aerosols on low latitude rain belts, with GHG increases believed to force the ITCZ to the north, and aerosols to the south (Zhang et al., 2007; Friedman et al., 2013). Modelling studies suggest that a heterogeneous regional cooling effect induced by NH mid-latitude anthropogenic aerosol emissions drove the southward migration of the ITCZ over recent decade

(Hwang et al., 2013; Rotstayn and Lohmann, 2002; Chang et al., 2011; Friedman et al., 2013), leading to drought in the Sahel (Booth et al., 2012; Kawase et al., 2010) and parts of monsoonal Asia (Bollasina et al., 2011; Lau et al., 2006). The rainfall decreases implied by the YOK-G record closely follow patterns of regional industrialisation and aerosol emissions in North America and western Europe since ~1880 (Fig. 4.20 and Fig. 4.15). Peak US aerosol production during the period 1970-1990 is estimated to have had a direct radiative forcing of -6 Wm^{-2} over the central and eastern US resulting in relative cooling of 0.5-1.0^{o}C (Leibensperger et al., 2012b; Leibensperger et al., 2012a). Cooling over the North Atlantic region modifies atmospheric circulation to accommodate cross equatorial thermal contrasts and subsequently drives the ITCZ southward (Tokinaga and Xie, 2011).

4.4.1 Volcanic forcing

The YOK-G record also illustrates that very similar ITCZ repositioning occurred following large NH volcanic eruptions that injected sulphate aerosols into the atmosphere. Explosive volcanism has been shown to be a leading driver of natural climate variability over the last millennium (Crowley, 2000; Schneider et al., 2009; Ammann et al., 2007). SO_2 (sulphur dioxide) gas, produced by explosive volcanism, reacts with OH and H_2O in the stratosphere producing H_2O and H_2SO_4 (sulphuric acid) aerosols which interact with incoming and outgoing radiation and result in cooling via increased backscattering of solar radiation. Volcanic eruptions have been implicated as causing drought, famine and triggering long-term climatic shifts, such as the LIA (Oman et al., 2006; Anderson et al., 2008; Stothers, 2000), although eruption type, size and global location create considerable variability in the climatic response to volcanic forcing.

Explosive NH eruptions are thought to have affected the ITCZ through a similar mechanism as anthropogenic aerosols, causing preferential NH cooling, southward ITCZ migration, and consequently drying in Belize. We observed that for large eruptions, identifiable in the GISP2 record, NH eruptions are followed by an increase in

$\delta^{13}C$ (indicating drier conditions) for one or more years after (relative to values for monthly values the previous year (Year -1) (Fig. 4.20). With the exception of Westdhal (1978), all studied NH eruptions are associated with $\delta^{13}C$ increases from the previous year during the year of eruption or the following year (Year +1), indicating drier conditions. Specifically, NH eruptions seem to increase the severity of the dry season. We suggest that NH volcanic eruptions delay the start of the wet season which allows the karst to more thoroughly drain before the inception of the first hydrologically effective rainfall of the rainy season. We suggest that NH eruptions therefore reduce the duration of the wet season by shifting ITCZ position further to the south. Conversely, all three SH eruptions are associated with relative low $\delta^{13}C$ after the year of eruption, suggesting that the ITCZ was forced further to the north and the wet season extended. The observed ITCZ response to volcanic forcing varies, and is undoubtedly linked to the magnitude, type, chemistry, and location of the eruption, as well as to other non-volcanic processes. We note that the interaction of multiple eruptions may also be possible, complicating the attribution of any signal observed in Belize rainfall. Consequently Komage-Take (1640) and Awu (1641) are not included in this analysis as the response to these two large eruptions (occurring in different hemispheres) cannot be deconvolved.

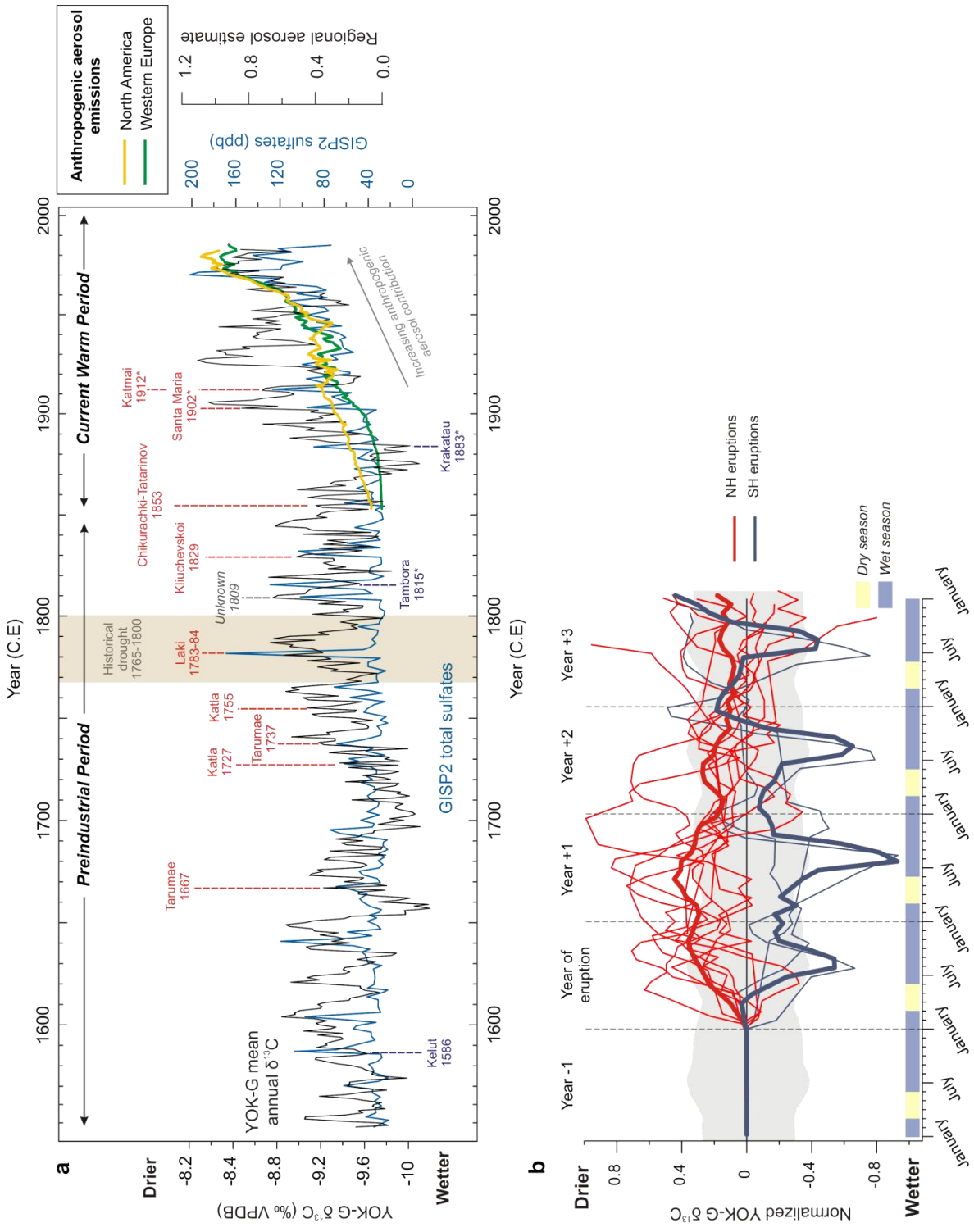
a
b
Year (C.E)
Preindustrial Period
Current Warm Period
Historical drought 1765-1800
Tarumae 1667
Kelut 1586
Katla 1727
Tarumae 1737
Katla 1755
Laki 1783-84
Unknown 1809
Kliuchevskoi 1829
Tambora 1815*
Chikurachki-Tatarinov 1853
Santa Maria 1902*
Katmai 1912*
Krakatau 1883*
Increasing anthropogenic aerosol contribution
GISP2 total sulfates
GISP2 sulfates (ppb)
Regional aerosol estimate
Anthropogenic aerosol emissions
North America
Western Europe
YOK-G mean annual δ13C
YOK-G δ13C (‰ VPDB)
Drier
Wetter
NH eruptions
SH eruptions
Dry season
Wet season
Year -1
Year of eruption
Year +1
Year +2
Year +3
Normalized YOK-G δ13C
January
July

Figure 4.20

Figure 4.20 a) Annual mean $\delta^{13}C$ (black) and GISP2 total sulphate record (blue) (Zielinski et al., 1994) for the period 1550-1983. Estimated aerosol production based on CO_2 emission rates relative to 1992 levels (Marland et al., 1994; Robertson et al., 2001) for western Europe (green) and North America (yellow) post 1850. Major NH eruptions (red labels) and SH eruptions (purple labels) identified within the GISP2 record. The dashed lines designate the date of the eruption thought to have caused the GISP2 sulphate peak rather than the sulphate peak itself; occasionally the eruption occurred the year preceding the sulphate peak in the ice core. The location of the volcano responsible for producing the large 1809 sulphate peak evident in the GISP2 record is unknown. (*) denotes eruptions with a Volcanic Explosivity Index of 6 or 7. The brown vertical bar indicates the timing of a large drought identified in the historical record (Kennett et al., 2012) **b)** Relative climate response to NH and SH eruptions exemplified by YOK-G $\delta^{13}C$ values (normalized to monthly means in the year prior to the eruption) in the year preceding the volcanic eruptions identified in panel a ('Year -1'), the year of the volcanic eruptions ('Year of eruption'), and three years following the eruptions ('Years +1, +2, and +3'). The grey shaded area represents one standard deviation from the monthly mean values over the entire preindustrial period. Thick lines represent the average δ13C response for NH eruptions (red line) and SH eruptions (blue line).

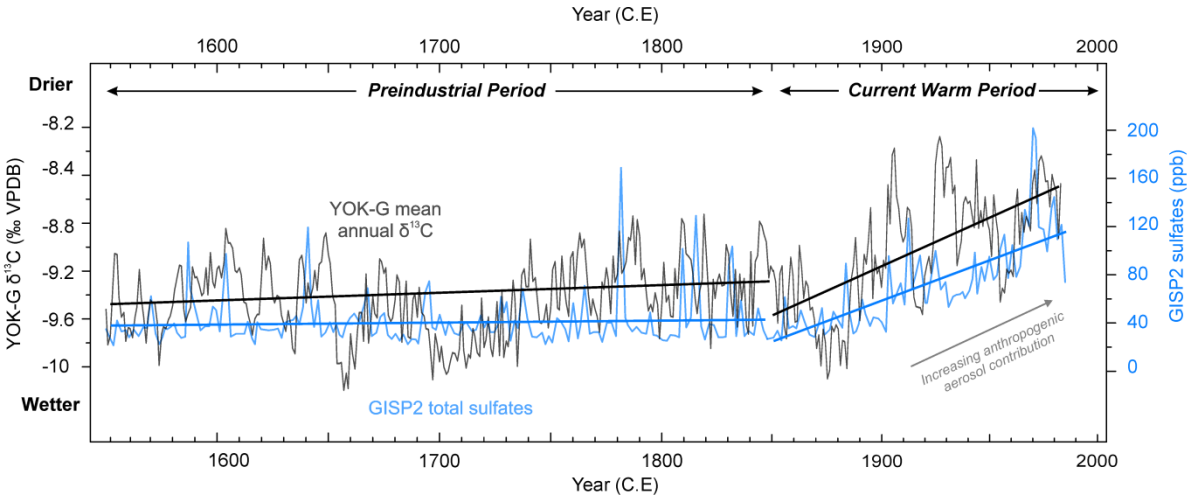

Figure 4.21 YOK-G mean annual $\delta^{13}C$ against GISP2 sulphate record. Linear trend lines for YOK-G $\delta^{13}C$ (black) and GISP2 (blue) for the preindustrial (1550-1849) and CWP (1850-1983).

Particularly noteworthy is the coincidence of the large and climatologically significant Laki eruption (1783-1784) with the height of the largest preindustrial drought in Belize since 1550 C.E., evident in both the YOK-G and the historical records. The Laki eruption has been implicated as the driver of drought in Africa, based on runoff estimations from sediments from the Nile (Oman et al., 2006), and several studies have attempted to constrain the climatic effects of volcanic eruptions at various latitudes (Robock, 2002; Fischer et al., 2007; Mann et al., 2005; Schneider et al., 2009; Highwood et al., 2003). This particular Laki eruption produced a peak estimated direct radiative forcing in August 1783 of -5.5 Wm^{-2} in the NH (Highwood et al., 2003), similar to the magnitude of the anthropogenic aerosol peak during 1970-1990 (-6 Wm^{-2}), and resulted in comparable drying in Belize. However, we note that the direct climate effects attributable to the Laki eruption were unlikely to have lasted more than three years (Highwood et al., 2003), so the 1783 eruption may have exacerbated or prolonged the 1765-1800 drought but was not the principal driver. SH volcanic eruptions, even those at low southerly latitudes, appear to force the ITCZ to the north. Most notable of these is the Tambora eruption in 1815, associated with increased Belizean rainfall the following year (Fig. 4.22). Of the twelve largest NH eruptions identified in the GISP2 ice core sulphate record since 1550 (Zielinski et al., 1994; White et al., 1997), all are associated with drying in Belize; conversely, all three large SH eruptions are associated with increased rainfall at our site (Fig. 4.20 and Fig. 4.22). Our data suggest that NH eruptions shortened the duration of the wet season, and SH eruptions extended wet season duration. The record provides compelling evidence that stratospheric sulphate aerosol injections associated with explosive volcanism resulted in short-lived ITCZ migration. Similarly, continuous NH anthropogenic aerosol emissions during the 20th Century drove sustained southward ITCZ repositioning.

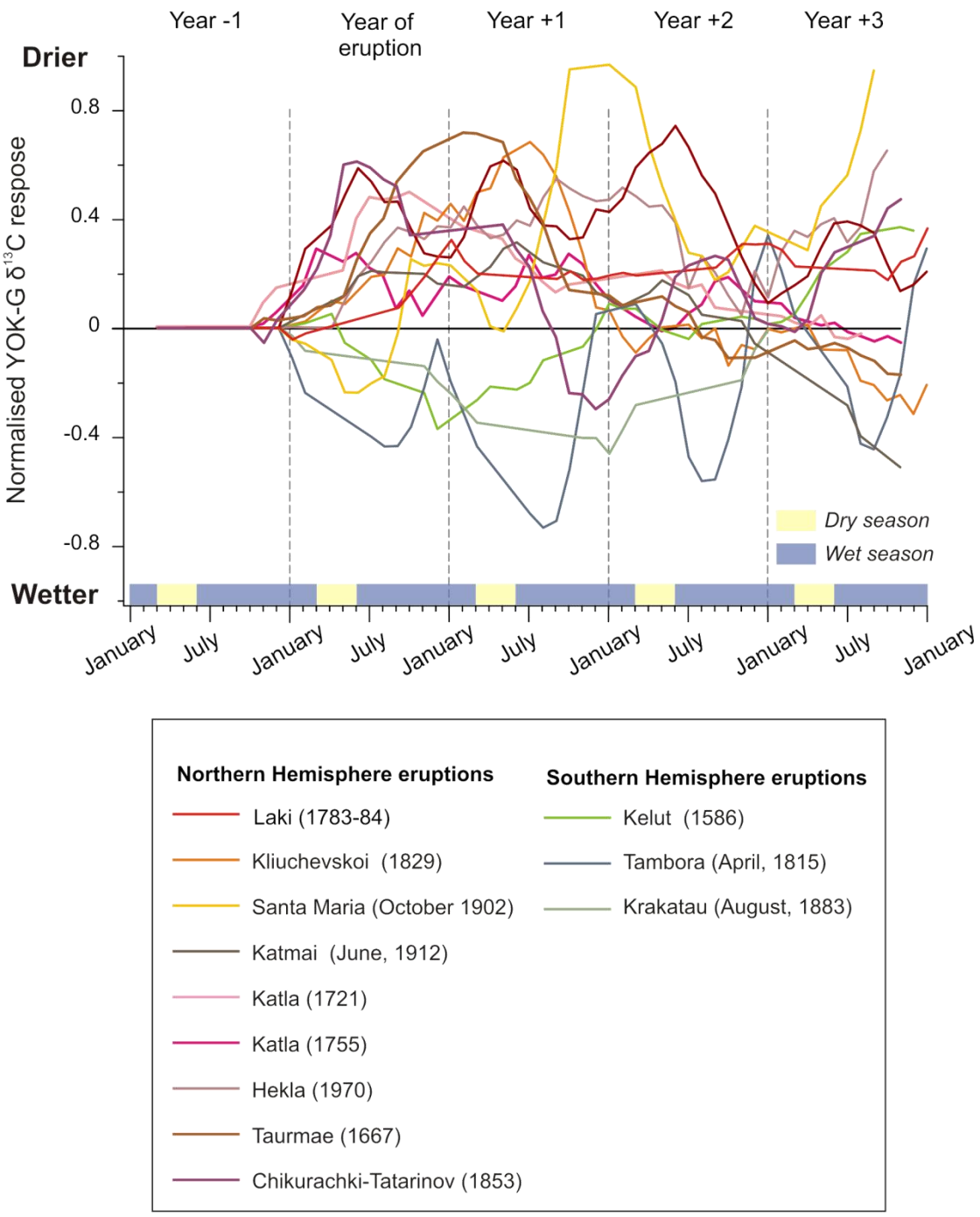

Figure 4.22 Response of YOK-G $\delta^{13}C$ to large volcanic events identified within the GISP2 record. Monthly YOK-G $\delta^{13}C$ (normalized to the respective month of the year prior to the eruption ('Year -1'). Shown are 'Year-1', the year of the eruption ('year of eruption') to three years after ('Year+1', 'Year+2', and 'Year+3') for nine NH volcanic eruptions and three SH eruptions.

4.5 Conclusions

This study presents a monthly resolved stable isotope record from a low-latitude cave site. The combination of three independent chronological controls, including annual geochemical cycles, provides a particularly robust and sub-annually resolved chronology. $\delta^{13}C$ is shown to reflect changes in rainfall and recharge to the karst, with wetter conditions producing to more negative speleothem $\delta^{13}C$ values. This monthly-resolved $\delta^{13}C$ rainfall record provides the strongest proxy evidence currently available that recent droughts in the northern tropics are attributable to extra-tropical anthropogenic forcing, supporting recent modelling studies. Rather than being a cyclic natural phenomenon, sustained rainfall reductions only occurred after atmospheric aerosols increased following regional industrialization in the NH. This concept is supported by evidence within the record that similar (albeit shorter lived) ITCZ repositioning occurred in response to sulphate aerosol forcing associated with large NH volcanic eruptions, probably caused by shortening of the wet season. Future modelling should focus on determining how shifts in regional aerosol emission rates might affect ITCZ position. This is particularly relevant to currently industrialising regions where large populations are dependent on seasonal rainfall, for example areas affected by the Indian and Asian Monsoons.

Chapter 5

Solar and volcanic influence on NAO state via interaction of the ITCZ

A version of the Chapter is being prepared for submission to Nature under the co-authorship of:

Sebastian F.M. Breitenbach[1], Harriet E. Ridley[2*], James U.L. Baldini[2], Keith M. Prufer[3], Franziska A. Lechleitner[1], Douglas J. Kennett[4] ,Kira Rehfeld[5], Norbert Marwan[6], Bedarth Goswami[6], Yemane Asmerom[7], Victor Polyak[7], Valorie V. Aquino[7] and Gerald H. Haug[1].*

** These authors contributed equally to this work*

[1] Department of Earth Science, Eidgenössische Technische Hochschule (ETH), Zürich, Switzerland.
[2] Department of Each Sciences, Durham University, Durham, UK.
[3] Department of Anthropology, University of New Mexico, Albuquerque, NM, USA.
[4] Department of Anthropology, The Pennsylvania State University, University Park, PA, USA.
[5] Alfred Wegner-Institute for Polar and Marine Research, Potsdam, Germany.
[6] Potsdam Institute for Climate Impact Research, Potsdam, Germany.
[7]Department of Earth and Planetary Science, University of New Mexico, Albuquerque, NM, USA.

A version of this chapter in currently being prepared for submission to *Nature or Nature Geoscience.*

Harriet Ridley wrote this chapter in its entirety using both the data presented in Chapter 4 and pre-existing data from Yok Balum Cave.

Sebastian Breitenbach and **James Baldini** contributed to the principal research ideas. **Kira Rehfeld** calculated the Median Absolute Deviation.

Franziska A. Lechleitner, Keith Prufer, Douglas Kennett, Valorie Aquino, Victor Polyak, Yemane Asmerom, Bedartha Goswami, Norbert Marwan, and **Gerald Haug** are all co-authors on the final manuscript.

Solar and volcanic forcing on NAO state via interaction of the ITCZ

5.1 Abstract

The North Atlantic Oscillation is the principal climate mode in the North Atlantic and has important influences on Atlantic/European climate. Here, we present a 2000 year, highly resolved and precisely dated ITCZ rainfall record from a speleothem in Belize. Agreement with existing NAO reconstructions confirms the validity of the record as a correlate NAO rainfall proxy and permits this new record to provide additional chronological control for existing reconstructions which are less well constrained. Deeper investigation of the record reveals a potential influence of solar activity and explosive volcanism on NAO atmospheric patterns in the North Atlantic region. We posit that these external forcings modify inter-hemispheric temperature contrasts resulting in meridional relocation of the ITCZ and subsequent atmospheric restructuring in the mid-latitude Atlantic region, producing NAO-like rainfall patterns. Comparison to rainfall proxies from other northerly low-latitude locations suggest that this is a global phenomenon and therefore has extensive implications for the low latitudes.

5.2 Introduction

The NAO represents the dominant mode of atmospheric variability in the North Atlantic region. Typically defined as the difference in normalised sea level pressure (SLP) between the Icelandic low (IL) and the Bermuda-Azores high (BAH), the NAO controls the strength and direction of wind fields and weather patterns across the north Atlantic mid latitudes. An NAO positive state (NAO+) is typically considered to be

a greater than normal SLP difference between the two Atlantic pressure centres, causing enhanced mid-latitude zonal flow across the Atlantic and Europe and anomalous southerly flow over the eastern United States. Alternatively, an NAO negative state (NAO-) is typically characterised by more relaxed atmospheric circulation, weaker and more southerly orientated westerly winds, wetter conditions in northern Africa and drier conditions in north-western Europe. This atmospheric mode therefore exerts a strong control on precipitation and temperature patterns across the North Atlantic basin and surrounding landmasses. Moreover, the NAO has a considerable influence on terrestrial and marine ecosystems and regional socio-economic activity (Hurrell et al., 2003; Trouet et al., 2009). Understanding past NAO behaviour as a means to better predict future scenarios is therefore of significant interest to the scientific community.

5.2.1 NAO reconstructions

NAO proxy reconstructions are essential to extend the limited instrumental time series to better characterise long term low-frequency variability and stability of the atmospheric patterns associated with the NAO (Cook et al., 1998; Cook et al., 2002; Glueck and Stockton, 2001; Luterbacher et al., 1999; Luterbacher et al., 2001; Meeker and Mayewski, 2002; Olsen et al., 2012; Proctor et al., 2000; Rodrigo et al., 2001; Trouet et al., 2009). Accurately reconstructing the NAO is challenging due to its dynamic nature and inherent assumptions of stationarity involved in interpreting proxies records beyond the instrumental record (Raible et al., 2006). Furthermore, the limited proxy data available from only a handful of sites impedes capturing the full NAO signal. As more NAO records are produced a more complete picture of past NAO activity may be derived for the whole North Atlantic region. Further difficulty arises as NAO proxy records are invariably rainfall records from regions where rainfall variability is thought to be associated with NAO pressure differences. These records may therefore be better described as NAO correlate records, rather than direct NAO records, although this is not widespread in the literature. In this chapter, NAO phases

will refer to rainfall signals associated with circulatory patterns induced by NAO related pressure anomalies.

One of the first high resolution reconstructions of the NAO was that of Proctor et al. (2000) (here referred to as Pr00). This record extended wintertime NAO activity (NAO_w) back approximately 1100 years to 900 AD, based on widths of precipitation controlled annual luminescent bands in stalagmite SU-96-7 from Uamh an Tartair Cave in northwest Scotland. Precipitation at the site is closely linked to the NAO with wetter winters associated with NAO+ conditions and consequently stronger westerly flow and cyclonic rainfall (Hurrell, 1995; Rodwell et al., 1999). Although this cave site is positioned at the northern NAO node, the site may still not capture the full NAO precipitation signal (Lehner et al., 2012). This could lead to potentially decade long periods of divergence between the NAO_w with classical NAO indices of SLP difference. Additionally, utilisation of a record from only one site limits distinguishing local variability from basin wide NAO activity.

Trouet et al. (2009) (here referred to as Tr09) used the precipitation proxy record of Pr00 and combined it with a drought proxy record from Morocco based on 326 time series of tree ring widths from cedars in the Atlas Mountains (Esper et al., 2007). This dual proxy record had the advantage of describing the two hydrological centres of action which arise from distinct NAO phases; wetter conditions in Scotland and Scandinavia and drier conditions in the western Mediterranean during a positive phase and vice versa for the negative (Hurrell, 1995; Wanner et al., 2001). One of the major findings of Tr09 was that the Medieval Climate Anomaly (MCA) was dominated by persistent NAO+ conditions, whereas the Little Ice Age, (LIA) experienced more substantial NAO- phases. This result however was not reproducible by climate models (Lehner et al., 2012) and the persistence of the MCA NAO+ phase has been questioned by later palaeoclimate reconstructions (Wassenburg et al., 2013). Olsen et al. (2012) (here referred to as On12) produced an extended record of NAO activity based on a high resolution lake sediment record from southwest Greenland. Variations in redox proxies (Mn/Fe ratios) are used to reconstruct lake hypolimnic anoxia, an indication of local temperature. This record is linked chronologically to the Tr09 record to produce a 5,200 year NAO index.

Wassenberg et al. (2013) (here referred to as Ws13) present an 1000 year NAO reconstruction from rainfall sensitive variations in magnesium (Mg) and strontium (Sr) in a Moroccan speleothem using a U-Th chronology which is entirely independent from Pr00. Dry conditions inferred from lower strontium concentrations in stalagmite GP5 from this Moroccan speleothem (from Grotte de Piste) are found during NAO+, when a strong BAH reduces moisture transport to north western Africa (Wassenburg et al., 2013).

These NAO reconstructions represent the longest and most cited proxy reconstructions to date. Interestingly, the Tr09 and On12 records are both tied to the chronology of Pr00, either by wiggle matching in the case of On12, or incorporation of the record in the case of Tr09. Although the Proctor chronology is based on annual speleothem laminae, it is constrained by only a single Thermal Ionisation Mass Spectrometer (TIMS) U-series date, with an error of ±174 years, and the authors state errors of ±20 years may exist in the chronology; therefore this potential chronological error extends to the Tr09 and On12 reconstructions. These interrelationships should be considered when using these records.

5.2.2 External forcing

Exogenous forcing is known to have exerted considerable control on multi-decadal variability in the Atlantic region (Ottera et al., 2010). Solar variability and explosive volcanism in particular have a significant forcing effect on radiative processes and climate variability (Fischer et al., 2007; Mann et al., 1998; Mann et al., 2005; Ottera et al., 2010).

Solar activity affects the radiative energy budget of the planet. Orbital forcing mechanisms control solar insolation on supra-millennial timescales (Berger, 1988; Berger and Loutre, 1991; Berger, 1978). On shorter timescale, sunspot activity and solar irradiance are likely to contribute to climate variability through alterations in the total global energy and distribution. Due to both current landmass distribution and deep vertical mixing in the southern oceans the NH warms substantially faster than the

SH. Hemispheric asymmetry, as discussed in Chapter 4, drives the strength and position of the ITCZ. Sunspot activity is known to vary on decadal timescales (Lean, 2000; Lean et al., 1995; Solanki and Unruh, 2013) and is therefore an important driver of climate variability on decadal to centennial timescales. A link between NAO and solar activity has been previously proposed (Lukianove and Alekseev, 2004).

As discussed in the previous chapter, explosive volcanism resulting in stratospheric sulphate loading partially drives climate on inter-annual and longer timescales via the scattering effect of sulphate aerosol particles on incoming solar shortwave radiation and absorption of near-infrared solar and outgoing long-wave radiation (Crowley, 2000; Ludlow et al., 2013; Robock, 2000; Robock, 2002; Schneider et al., 2009). The relative stability of the stratosphere promotes a longer atmospheric residence time and more extensive climatic impact. Furthermore, strong zonal winds result in rapid transport of sulphates around the globe potentially producing a global climate response (Robock, 2000).

As well as eruption magnitude and volume of aerosols released, the latitude, time of year and prevailing atmospheric modes and system states (e.g. ENSO phase) all influence the potential an eruption has to disrupt the climate (Kravitz and Robock, 2011; Schneider et al., 2009; Timmreck, 2012; Xu et al., 2013). This prevents discerning a single, quantifiable climate response to volcanic forcing although important dynamic responses reported include: winter warming in the NH continental landmasses after explosive low-latitude eruptions (Driscoll et al., 2012; Fischer et al., 2007; Schneider et al., 2009; Shindell et al., 2004; Shindell et al., 2003), weakened Asian monsoon circulation and southward ITCZ migration after high-latitude NH eruptions (Anchukaitis et al., 2010; Oman et al., 2006; Peng et al., 2010; Schneider et al., 2009). Coupled feedback mechanisms over decadal to centennial timescales may prolong or amplify volcanically perturbed climate disturbances (Miller et al., 2012; Ottera et al., 2010; Zanchettin et al., 2012; Zhong et al., 2011) and impact phases of ENSO and NAO (Adams et al., 2003; Czaja et al., 2002; Emile-Geay et al., 2008; Mann et al., 2005). Identification of these climate forcing mechanisms requires NAO proxy records with high resolutions and nearly perfect chronologies.

5.2.3 YOK-I record

Stalagmite YOK-I was collected in 2006 from Yok Balum Cave (Kennett et al., 2012), only a few meters from the site of YOK-G. The YOK-I chronology between 40BC and 2006AD is constrained by forty high precision ^{230}Th dates (error range ± 1 - 17 years) and has a temporal resolution of approximately one stable isotope point every six months (See Kennett et al. 2012 for details). The most recent 430 years (1553AD – 1983AD) of the YOK-I δ^{13}C record was tuned, within ^{230}Th sampling and analytical error, to the annually resolved YOK-G δ^{13}C record (Fig. 5.1) and fixed to the rising limb of the atmospheric bomb spike identified through high resolution radiocarbon analysis. Although the YOK-I and YOK-G records display characteristically different δ^{13}C variability, related to their significantly different hydrological regimes and different sampling resolutions (see Chapter 4 section 4.3.6), they do display general coherence and shared 'landmark' features can be identified within the two records. These were used as chronological marker points. Figure 5.2 displays the un-tuned and tuned YOK-I time series and dating errors.

YOK-I δ^{13}C is controlled predominantly by the amount of water recharge to the karst. Lower δ^{13}C values are associated with increased rainfall, via a lower bedrock isotopic contribution and decreased prior carbonate precipitation due to faster drip rates. Alternatively, decreased rainfall results in higher δ^{13}C values through prolonged contact with the bedrock due to slower karstic through-flow and increased prior carbonate precipitation. The hydrological regime feeding YOK-I is more diffuse than that feeding YOK-G. This, combined with the lower sampling resolution, acts as a low pass filter on climate signals, permitting longer frequency climate shifts to be recorded than YOK-G. This accounts for the larger magnitude variability observed in this record compared to the YOK-G δ^{13}C record. Spectral analysis of the YOK-I data reveal dominant spectral peaks at centennial periodicities and corroborate the concept that the YOK-I data retains long term climate signals due to the principally diffuse nature of the karst reservoir feeding the stalagmite. Alternatively, YOK-G δ^{13}C displays predominantly higher periodicity power spectra, on multi-decadal scales, indicating

that this stalagmite has greater connectivity with the surface and is therefore more susceptible to higher frequency shifts in rainfall.

Using the YOK-I $\delta^{13}C$ record we reconstruct an NAO index for the last 2,000 years using the Median Absolute Deviation (MAD). MAD is a measure of statistical dispersion similar to a z-score but more robust against outliers as deviations about the mean are not squared as in standard z-score processes. We invert the MAD reconstruction to reflect moisture conditions intuitively (i.e. negative MAD = negative NAO and reduced rainfall). The YOK-I_{MAD} can then be used as a tool for assessing the evolution of the NAO over the last 2000 years and facilitates comparison with existing reconstructions.

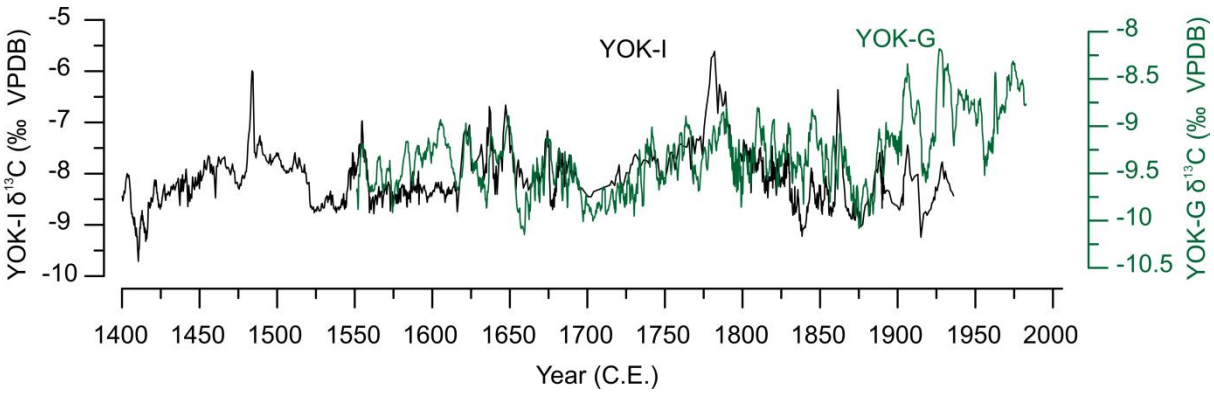

Figure 5.1 Comparison of YOK-I (black line) and YOK-G (green line) after tuning of the YOK-I chronology.

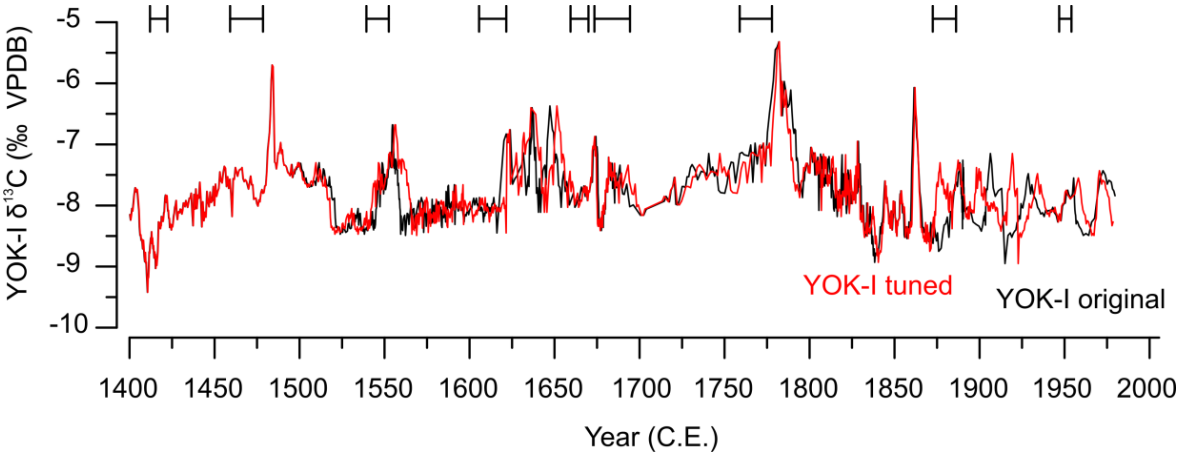

Figure 5.2 Original YOK-I record (black line) and new chronology tuned to YOK-G (red line).

5.3 Results

A weak link appears to exist between solar activity and NAO conditions, although the response is not consistent. The Oort, Sporer, Maunder and Dalton sunspot Grand Minima all trend towards more negative values (Fig. 5.4 and Fig. 5.5). An exception to this is the Wolfe Minimum which will be discussed in more detail later. The most notable dry period in the YOK-I_{MAD} record began at 660 AD and culminated in a substantial drought occurring from 1020 to 1120 AD, coincident with the Oort sunspot minimum (Solanki and Unruh, 2013). As discussed in the previous section, a solar activity minimum should result in a weaker and less northerly situated ITCZ, contributing to drier conditions in Belize. The early part of this drought has been linked to the collapse of the Classic Maya Civilization (Haug et al., 2003; Hodell et al., 2005; Kennett et al., 2012; Webster et al., 2007), although no firm causative climatological mechanism for the dry interval was proposed other than southward migration of the ITCZ. This interval coincides with a very strong NAO- phase appearing in both the Pr00 record and the YOK-I_{MAD} (Fig. 5.3a). Interestingly, this 11th Century drought occurred during the earlier part of the Medieval Climate Anomaly, when NHT was relatively high (Esper et al., 2002; Mann et al., 2009; Mann et al., 2008). A warmer NH, if no additional factors are considered, should result in a more northward ITCZ position and wetter conditions in low northern latitudes (Broccoli et al., 2006; Hwang et al., 2013; Zhang et al., 2007).

Figure 5.3 YOK-I_{MAD} record (black line), with ^{230Th} dates above against **a**) NAOw reconstruction from a speleothem in North West Scotland (Proctor et al, 2000). ^{230}Th dates shown above. **b)** NAOms reconstruction from stalagmite and tree rings data from Scotland and Morocco (Trouet et al 2009). Chronology is constrained by annual tree rings and incorporation of the NAOw record. **c)** NAO reconstruction from redox ratios in lake sediment from south western Greenland (Olsen et al 2012). Radiocarbon dates shown in blue. d**)** NAO reconstruction based on Sr concentrations in a stalagmite from Morocco. Radiocarbon dates are shown in red.

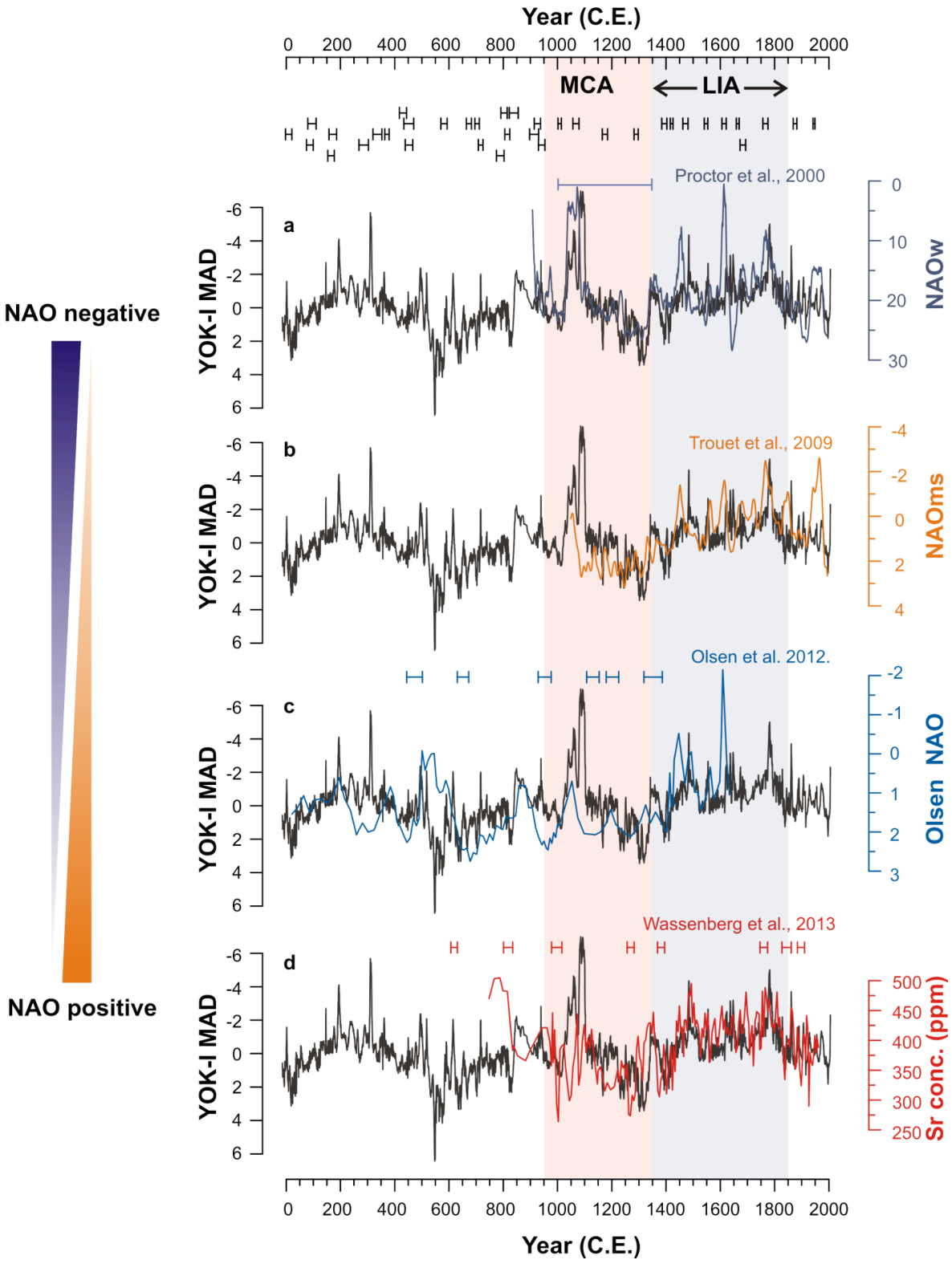
NAO negative
NAO positive
Year (C.E.)
0 200 400 600 800 1000 1200 1400 1600 1800 2000
MCA
LIA
Proctor et al., 2000
Trouet et al., 2009
Olsen et al. 2012.
Wassenberg et al., 2013
a
b
c
d
YOK-I MAD
-6 -4 -2 0 2 4 6
NAOw
0 10 20 30
NAOms
-4 -2 0 2 4
Olsen NAO
-2 -1 0 1 2 3
Sr conc. (ppm)
500 450 400 350 300 250
Year (C.E.)

Figure 5.3

Following the intense NAO- phase between 1020 and 1085AD, YOK-I_{MAD} indicates more variable NAO conditions during the later MCA (1100-1350 AD) and the onset of the Little Ice Age (LIA, 1350-1800 AD). Our record is further corroborated by Ws13 (Fig. 5.3d) who also observed that the NAO+ phase during the Medieval Climate Anomaly was not as pervasive as originally hypothesised by Tr09.

The excellent agreement between YOK-I_{MAD} and current NAO reconstructions (Fig. 5.3) provides considerable evidence that rainfall at Yok Balum is associated with phases of the NAO. The agreement between Pr00 and YOK-I_{MAD} is visually particularly striking, although the statistical relationship is only moderate ($r = 0.48$ $p<0.001$) (Fig. 5.4). The modest empirical correlations between YOK-I_{MAD} and previously published reconstructions is likely due to local responses to climate forcing, chronological uncertainties and differences in resolution, which is somewhat typical when dealing with palaeoclimate data. Shifting the Pr00 chronology also improves the coherence with the Tr09 and On12 records which are partly dependent on the chronology of Pr00. If the Tr09 record is tuned within potential chronological uncertainty, the relationship with YOK-I_{MAD} becomes even more remarkable (Fig. 5.5).

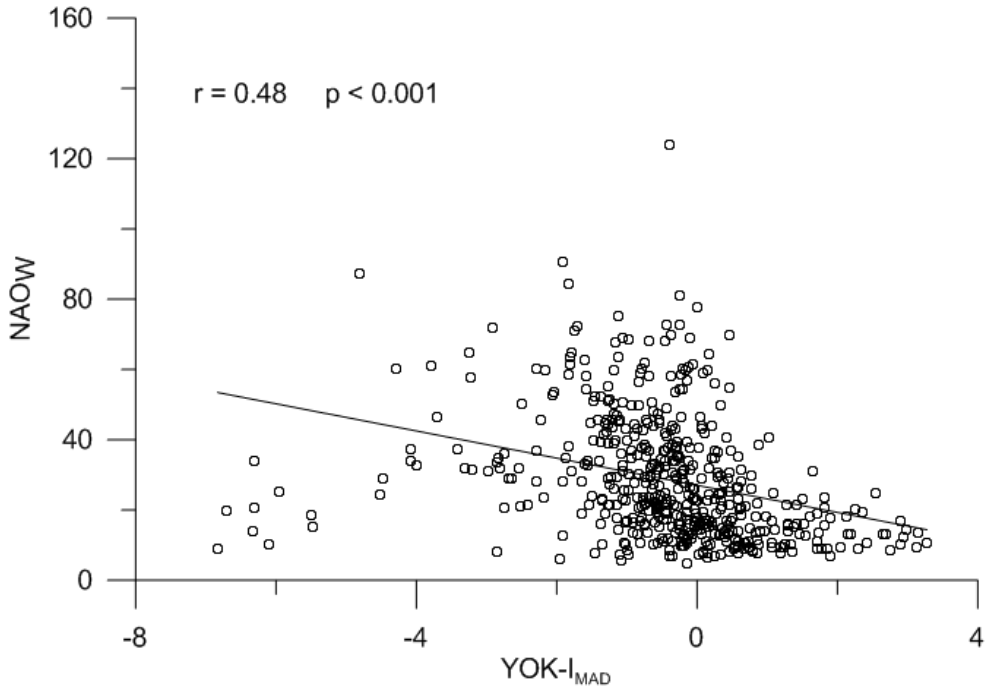

Figure 5.4 Pr00 NAO_w record against YOK-I_{MAD}

5.3.1 Volcanic forcing

NH eruptions are linked to southward displacement of the ITCZ due to localised cooling of the NH, and it is therefore posited that large NH eruptions both weakened the ITCZ and forced its southward migration due to preferential NH aerosol cooling, subsequently leading to short-lived drier conditions in northern low-latitudes. Hence, any large NH volcanic eruption should manifest as a sharp, short-lived excursion of 1-4 years, below baseline YOK-I_{MAD} values. To identify volcanically forced drying events in the YOK-I_{MAD} record, a low-pass 31-point Gaussian smoothing filter is applied to the data. A 31-point filter sufficiently smoothes the data to permit the identification of short-lived (<5 year) events from a local baseline value of an ~15 year sliding window, but is sufficiently robust against outlier points, high frequency noise and climate variability which may be linked to ENSO or other large scale modes. Any residuals more than three standard deviations below the mean residual value (i.e those residuals in the 10^{th} percentile) are identified as significant short lived drying events. Of the 32 residuals identified, all but two can be matched, within YOK-I or historical error, to 17 principal high latitude NH eruptions identified in the Smithsonian Institute, Global Volcanism Programme (Table 5.1., Fig. 5.5) (Some eruptions are associated with two or more residual points). The eruptions have a known, or estimated Volcanic Explosivity Index (VEI) of 5 or more, apart from The Eldgia eruption of AD934 which is thought to be only VEI 4 but long lived and therefore climatologically very significant. Twelve of the events identified can be matched to volcanic SO_4^{2-} signals in the GISP2 Ice Core (Zielinski, 2000; Zielinski et al., 1994; Zielinski et al., 1995) (Table 5.31.). The only peak which does not match appropriately with a large NH eruption is the residual at 1819. Various smaller (VEI 4) eruptions occurred around this time but it is difficult to assign this peak to a single eruption. This peak may also be a result of more positive baseline values during this time window, potentially caused by the massive VEI tropical eruption of Tambora in 1815. Recent wiggle matching efforts to constrain the date of the VEI 7 millennium eruption of Chaingbaishan Volcano (north-eastern China) have placed it between 850 and 1030AD (Dunlap et al., 1992; Horn and Schmincke, 2000; Zielinski et al., 1994). This eruption is thought to be one of the largest eruptions of the last 2000 years, injecting 4 Tg of SO_2 into the stratosphere (Horn and Schmincke, 2000)

and occurs, coincident with the onset of the Oort Solar Minimum, at the start of the largest NAO-phase recorded in the YOK-I_{MAD} and Pr00 records.

Visually, correlations can be made between tropical eruptions and positive YOK-I_{MAD} events). For example, one of the largest tropical eruptions of the last 2000 years, the Rabaul Caldera eruption in Papa New Guinea (VEI 6), occurred in 540AD (± 100) and is coincident with the most extreme NAO+ signal in the YOK-I_{MAD} record (Fig. 5.6). However, the relationship is less conclusive than for NH eruptions if the above methodology is applied. This could be due to several analytical and mechanistic issues including dating errors associated with specific eruptions and the filter methods applied here. Ejecta from explosive tropical eruptions rapidly encircle the globe causing a longer term, more widespread climate shift than high latitude NH eruptions. The filter method applied here may not facilitate identification of these effects in the same way as NH eruptions. Some of the largest aerosol injections of the past 1500 years occurred just before the onset of the Wolfe Minimum (Gao et al., 2008), many occurring in the tropics (Smithsonian Institute Global Volcanism Project).

Table 5.1 Allocation of eruptions to volcanic signals identified in YOK-I_{MAD}

Year (A.D) of signal in YOK-I	Name of eruption	Location	VEI	Date of eruption with error	Date discrepancy	Event identified in GISP2
1906.4	Ksudach	Kamchatka Peninsula, Russia	5	1907	1	yes
1861.5						
1828.7	Schiveluch	Kamchatka Peninsula, Russia	5	1829	0	yes
1819.1						
1782.0	Laki	Iceland	6	1783-4	1	yes
1780.9						
1779.8						
1647.2	Shiveluch	Kamchatka Peninsula, Russia	5	1650	-3	no
1636.8	Vesuvius; Kamaga Take	Italy; Japan	5	1631	-6	
1623.9	Katla	Iceland	5	1625	1	yes
1621.6						
1620.2						
1484.4	Mt St Helens	United States of America	5	1482	-2	yes
1483.9						
1483.3						
1342.1	Hekla	Iceland	5	1341	-1	yes
1251.7	Katla	Iceland	5	1262	10	yes
1250.7						
1100.5	Hekla	Iceland	5	1104	4	yes
1100.0						
1040.8	Changbaishan	Northern China	7	1026*	14	yes
938.9	Eldgia	Iceland	4	934 ± 2	-5	yes
518.0	Shiveluch	Kamchatka Peninsula, Russia	5	500 ± 50	-18	yes
517.4						
495.5	Vesuvius	Italy	5	495	-1	yes
495.5						
312.8	Ksudach	Kamchatka Peninsula, Russia	6	240 ± 100	-73	no
310.7						
310.0						
309.3						
146.4	Ksudach	Kamchatka Peninsula, Russia	6	155 ± 100	9	yes
145.7						

* Exact date debated

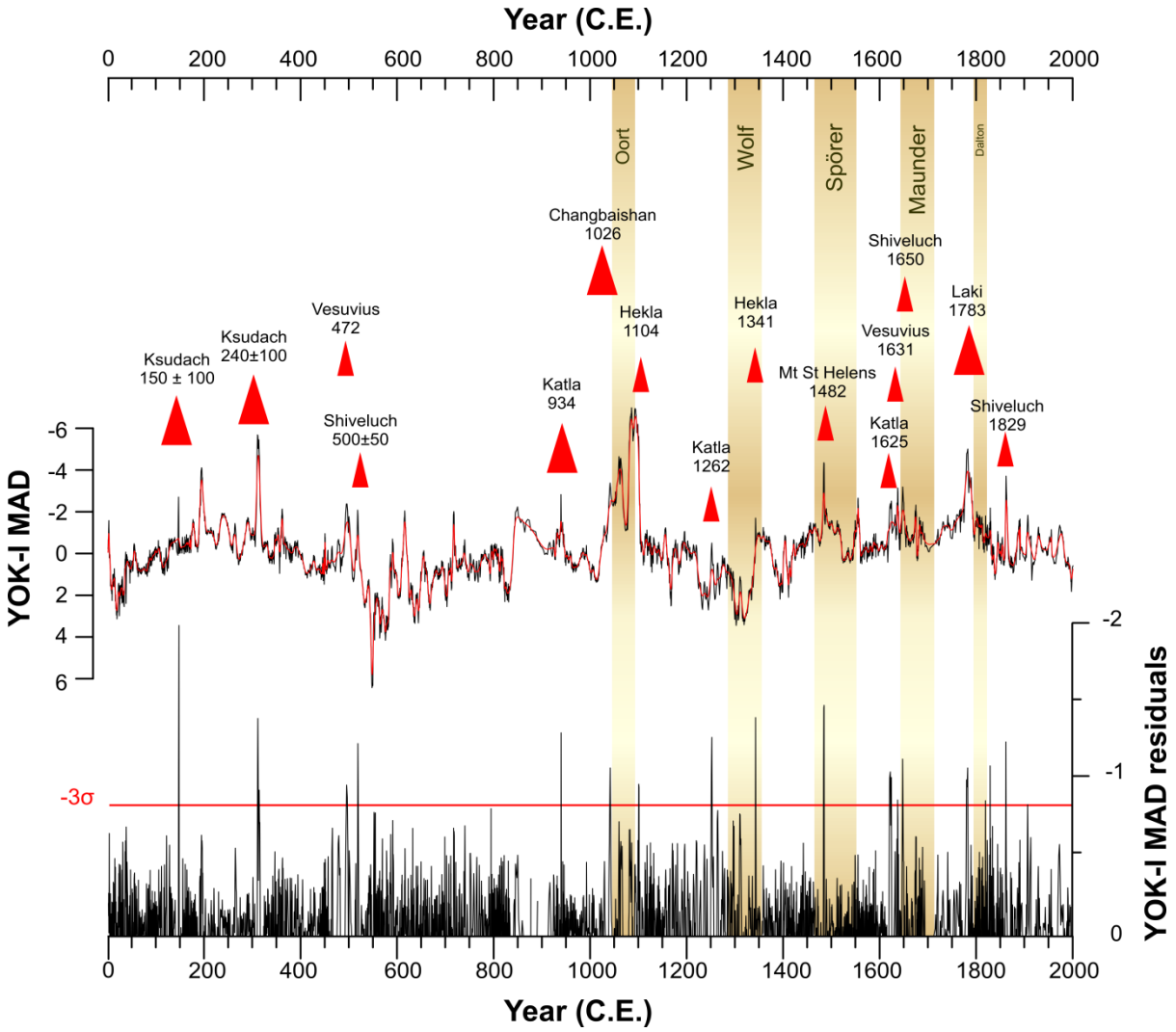

Figure 5.5 Residuals (black vertical bars) from 31 point Gaussian sliding filter (red line) applied to the YOK-I_{MAD} record. Red line indicates -3 sigma from the mean of the residuals and hence the 10th percentile. Red triangles denote volcanoes linked to residuals beyond -3 sigma. Larger triangles represent eruptions with a VEI of 6 or 7 and smaller triangles a VEI of 4 or 5. Volcanoes are named and the date of eruption with dating error (if applicable) is shown. Sunspot Grand Minima are also shown.

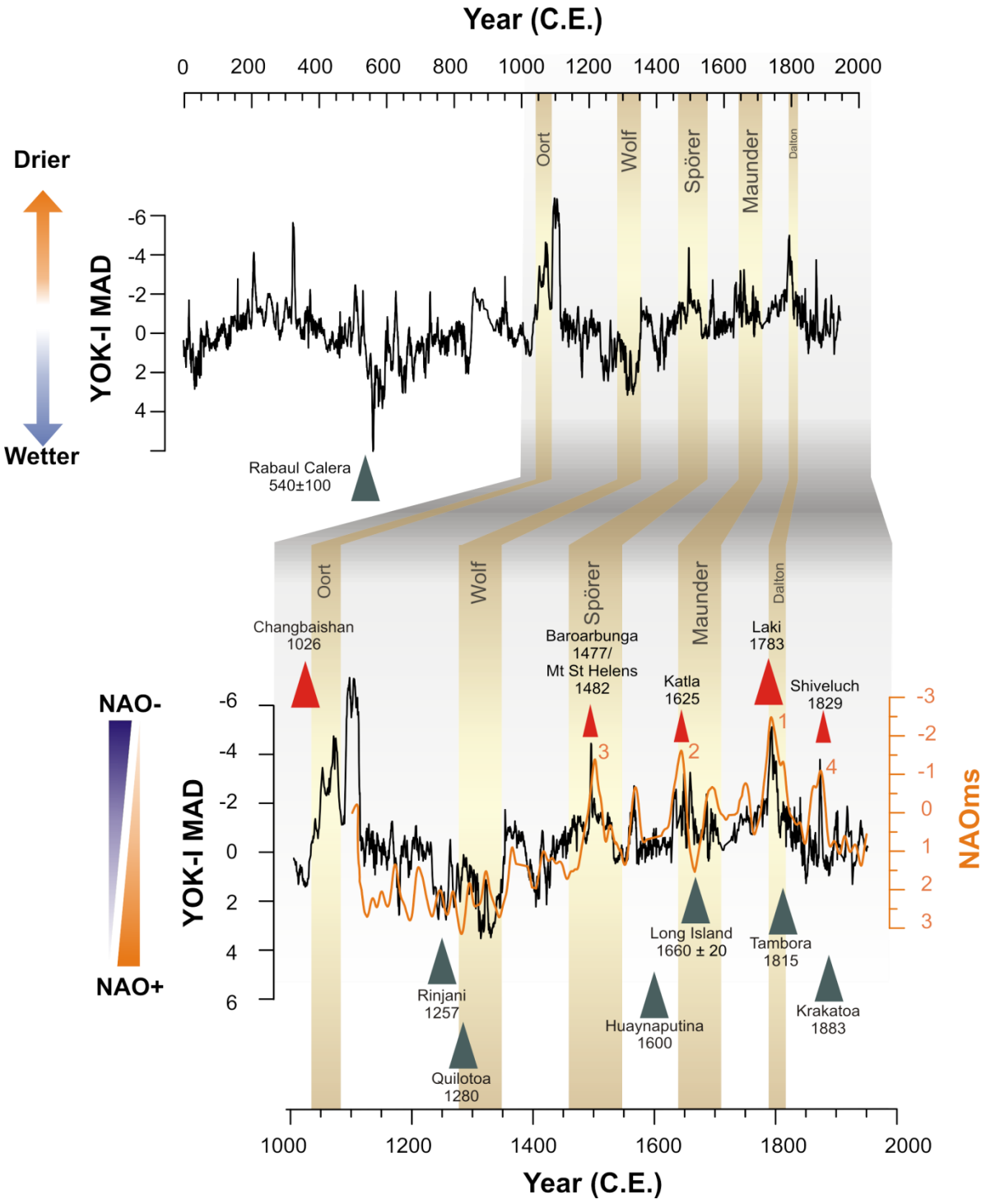

Figure 5.6 YOK-I_{MAD} with sunspot Grand Minima. Insert shows YOK-I_{MAD} and Tr09 NAOms for the last 1000 years. The four largest NAO- events linked to significant NH eruptions are numbered (1-4) and volcanoes shown using small (VEI 5) or large (VEI 6 or 7) red triangles. Large (VEI 6 or 7) tropical eruptions are shown below (green triangles). Tropical eruptions include: Rinjani (Indonesia), Quilotoa (Ecuador), Huaynaputina (Peru), Long Island (Papa New Guinea), Tambora (Indonesia) and Krakatoa (Indonesia).

Previous research suggests that NAO+ conditions can be induced by tropical eruptions (Shindell et al., 2004) which could potentially counteract solar forcing and cause the NAO+ signal during the onset of the Wolfe Minimum. Figure 5.5 compares YOK-I_{MAD} and Tr09 (tuned to YOK-I_{MAD}) to major NH and tropical volcanic eruptions over the last 1000 years. The four strongest NAO- phases visible in both records (numbered), are all linked to four of the most explosive NH eruptions. As expected, a tropical response is less easy to identify but it is notable that the occurrence of the large Quilotoa, Ecuador (1280AD, VEI 6) and Rinjani, Indonesia (1257AD, VEI 7) eruptions at the onset of the Wolfe Sunspot Minimum coincide with a more positive NAO state in both records, further supporting the concept that tropical volcanism may have counteracted the effect of solar forcing during this period. A similar trend is observed during the Maunder Minima when the Long Island, Papa New Guinea eruption (1660 ± 20 AD VEI 6) coincides with a switch from NAO- to NAO+ conditions. This is manifested particularly clearly in the Tr09 record. The resolution of the YOK-I_{MAD} record is somewhat unfortunate. With only two stable isotope points per year it is not possible to identify sub annual shifts that may be caused by volcanic activity. For example, as expressed in Chapter 4 section 4.4.3, if NH eruptions tend to shorten the wet season, this may not be expressed sufficiently with a bi-yearly resolved record.

Despite the difficulties inherent in assigning palaeo-volcanic events to shifts in regional climate, correlations between the YOK-I_{MAD} record and historical volcanic events does support modelling work which proposes a link between explosive volcanism in the tropics and high latitudes and North Atlantic climate. Furthermore, this record provides a longer and more highly resolved NAO record than the best cited, existing reconstructions and so will be of extensive use to the palaeoclimate community as further attempts are made to understand and predict North Atlantic climate variability.

5.3.2 Global picture

If the YOK-I_{MAD} record is interpreted as reasonable proxy for NAO state, as is strongly suggested in Figure 5.3, then given the apparent link between solar activity and volcanism it stands to reason that NAO phase in the North Atlantic is externally forced

by these factors (Fischer et al., 2007; Shindell et al., 2004). Such links between North Atlantic climate and tropical rainfall have been previously suggested (Deplazes et al., 2013; Souza and Cavalcanti, 2009; Trouet et al., 2009). Mechanistically, southward displacement of the ITCZ, due to either reduced solar activity or regional NH cooling by large NH volcanic eruptions, will draw the BAH to the south as the rising limb of the northern Hadley Cell relocates to the southward-displaced thermal equator. Subsequently, the westerlies will be weakened and/or displaced southward along with the falling limb of the Hadley Cell, thereby producing an NAO- pressure state (or the illusion of one in the case of simple BAH displacement) and respective rainfall signals in Morocco (wetter) and Scotland (drier). Alternatively, during periods of higher solar activity or tropical eruptions, warming over the NH draws the ITCZ to the north, forcing the BAH further north, strengthening and/or shifting the westerlies to the north, blocking moisture transport to Morocco and producing a NAO+ pressure state across the north Atlantic. This concept is shown schematically in Figure 5.7.

The involvement of the ITCZ could also explain why models have been unsuccessful in replicating NAO phases observed in proxy based reconstructions (Lehner et al., 2012). This mechanism involving initial ITCZ forcing leading to a reorganisation of NH pressure cells implies that large NAO shifts should have global manifestations. By comparing YOK-I_{MAD} to other low latitude rainfall reconstructions from southern China (Zhang et al., 2008), southern Oman (Fleitmann et al., 2004) and the Cariaco Basin (Haug et al., 2001) coherent evidence of meridional ITCZ migration on a global scale clearly exists (Fig. 5.8). The relationship with the Wanxiang Cave record is particularly clear and displays reasonable statistical correlation ($r = 0.30$, $p < 0.001$). The Wang Xiang record provides evidence of variability in the strength of the East Asian Monsoon over the last 1810 years and correlates with solar activity and NHT (Zhang et al., 2008). The Asian Monsoon was thought to be weaker during periods of cooler NHT (Dykoski et al., 2005; Heslop et al., 1999; Porter and An, 1995; Sirocko et al., 1996; Thompson et al., 1997; Wang et al., 2001; Yuan et al., 2004) when the ITCZ was displaced to the south (Haug et al., 2001; Hughen et al., 1996; Wang et al., 2004). This is observed throughout the Holocene in proxy records from Southeast Asia (Cheng et al., 2006; Dykoski et al., 2005; Yancheva et al., 2007) and Central America (Haug et al., 2001).

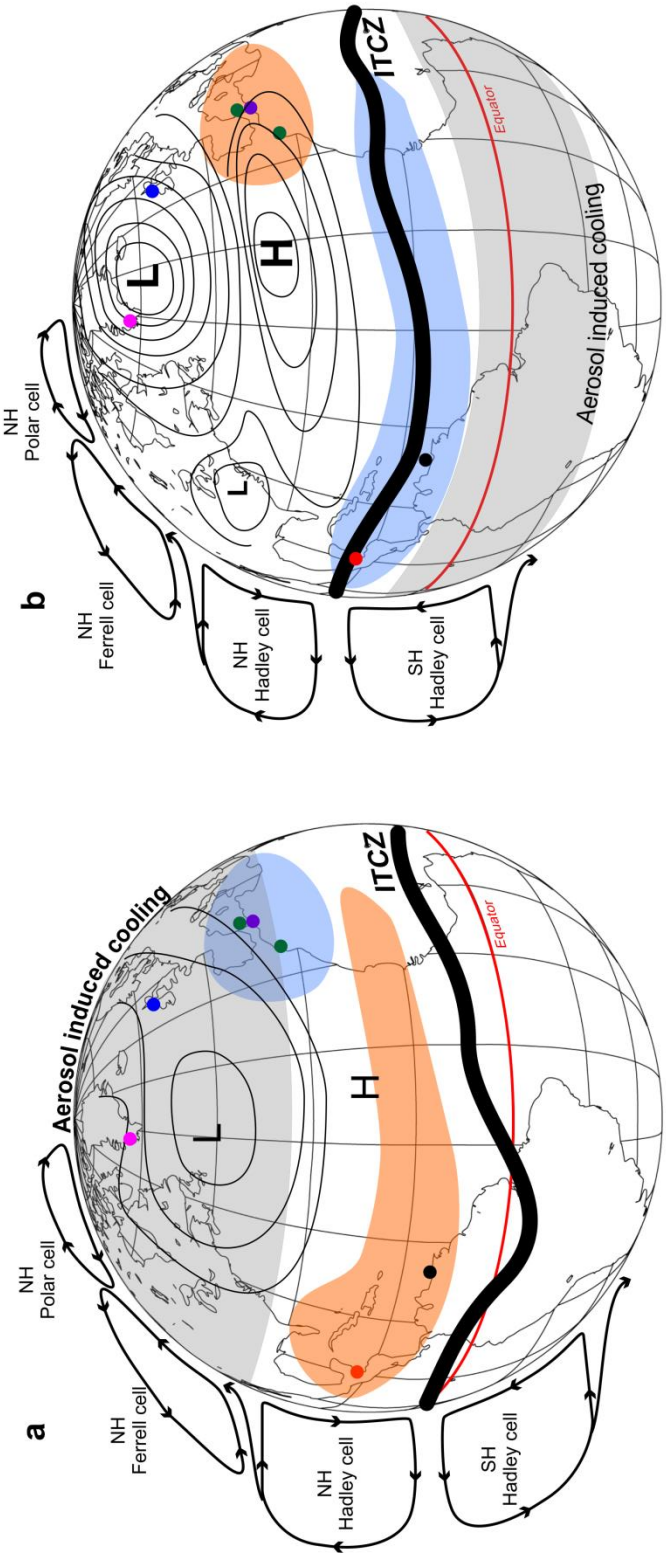

Figure 5.7 Schematic of **a)** NAO- conditions forced by southward ITCZ migration caused by aerosol induced NH cooling **b)** NAO+ conditions forced by northward ITCZ migration in response to aerosol cooling in the tropics and SH. Orange and blue shading denotes drier and wetter conditions respectively. Coloured dots denote the location of the Pr00 (blue), Tr09 (green), Ws13 (purple), On12 (pink) and YOK-I_{MAD} (red) proxies. The Cariaco basin is shown as a black dot.

Volcanic events identified from the YOK-I_{MAD} record are not represented in the Wang Xiang record, potentially due to the resolution of the Wang Xiang record being insufficient to successfully identify volcanic signals, or the response in YOK-I_{MAD} being a regional response. Interestingly, the peak at 1560AD in YOK-I_{MAD}, which was originally thought to be a volcanic signal, but was not identified by the filtering analysis as being so, is also expressed in the Wang Xiang Cave record (Fig. 5.8a). This suggests that this peak is a short term global shift rather than a more regionalised volcanic impact.

The relationships presented here between YOK-I_{MAD} and other low latitude palaeoclimate reconstructions provides convincing evidence of an intrinsic connection between solar forcing, volcanic activity, global ITCZ position and NAO state and lends confidence to the idea that NAO signals observed in the North Atlantic region may be driven by these external forcings through variations in ITCZ strength and position.

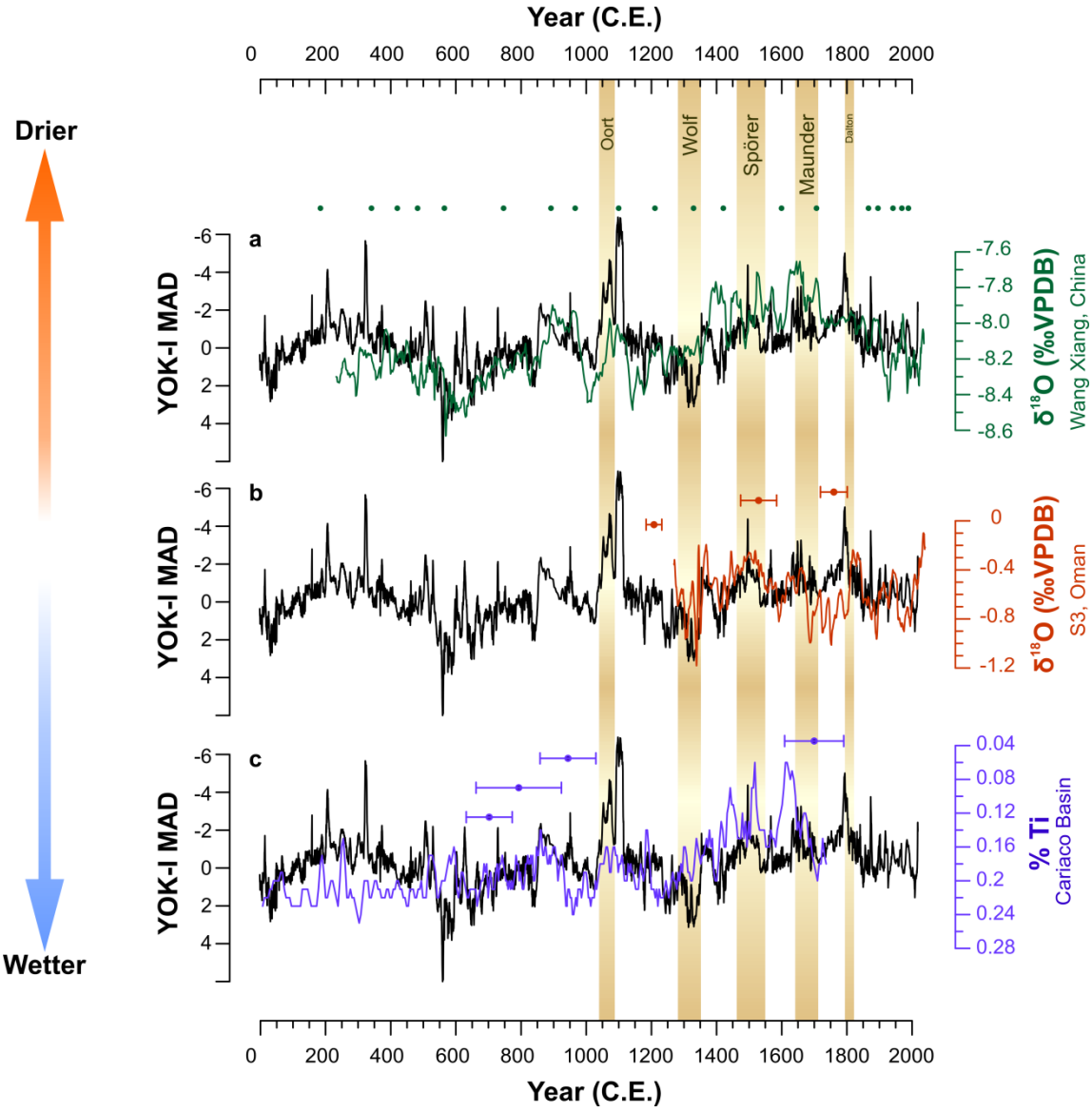

Figure 5.8 Grand Sunspot Minima and YOK-I_{MAD} (black lines) against **a)** Wanxiang Cave $\delta^{18}O$ record (with ^{230}Th dates) **b)** Stalagmite S3 $\delta^{18}O$ record (with ^{230}Th dates) **c)** Cariaco Basin Ti record (with ^{14}C dates).

5.4 Concluding remarks

The YOK-I_{MAD} reconstruction provides the longest, high-resolution NAO reconstruction yet available. Through comparison with existing NAO records we find that NAO state is clearly expressed in Belize rainfall with reduced precipitation being associated with NAO- phases and increased rainfall with NAO+ phases. The YOK-I_{MAD} reconstruction demonstrates that the 11th century drought in Belize was associated with the strongest NAO- in the last 2000 years and that the subsequent MCA was not characterised by NAO+ conditions as pervasive as previously proposed. The resolution of this record permits the identification of short-lived climate shifts related to NH volcanic eruptions. Research based on historical NAO data hinted at a link between explosive volcanism and the NAO, but the definite link remained elusive due to chronological uncertainties in existing NAO reconstructions. Comparison with other low-latitude rainfall proxy records suggests that NAO signals are linked to solar activity and explosive volcanism through strengthening and/or repositioning of the ITCZ with explosive high latitude eruptions being associated with southward displacement of the ITCZ and major atmospheric cells. This evidence provides a new and alternative view on the role of the NAO-climate mode and North Atlantic variability, and has important implications for future prediction and understanding of the NAO, particularly in terms of anthropogenic aerosol contributions. Future work should focus on quantifying how specific volcanic eruptions modify low latitude rain belts with regards to eruption type, size, duration, geographic location, time of eruption and the relative and combined forcing of volcanism and solar activity. It is also paramount that future work attempts to evaluate the forcing effect of solar activity and volcanism on the current anthropogenic climate state.

Chapter 6

Wider implications, overall conclusions and future research

Wider implications, overall conclusions and future research

6.1 Introduction

This thesis provided an analysis of rainfall variability and climate evolution in Central America and the North Atlantic over the last 2000 years based on geochemical evidence from two well-resolved Belizean stalagmites. Geochemical interpretations are supported by high resolution monitoring at the cave site and consequently Yok Balum Cave is identified as a suitable site for palaeoclimate study. The work presented is motivated by the need to develop highly resolved and well-constrained climate records from tropical regions to improve understanding of recent tropical climate variability.

Becasue this thesis is written as a series of papers, main conclusions relevant to each chapter are presented at the chapter's end. This chapter will draw together the main conclusions from the other chapters to address the core research topics outlined in Chapter 1 and to provide a concise overview of the contribution this body of work makes to tropical palaeoclimate research. The work presented here has stimulated new questions and presented potential avenues for further study. In light of this, suggestions for future work are made both specific to each chapter and for the body of work as a whole.

6.2 High resolution monitoring of tropical cave environmental parameters

Through analysis of high resolution environmental monitoring data from Yok Balum Cave, links are drawn between the cave environment, local climate and speleothem

growth (Chapter 3). This work is driven by an appreciation of the complexities of palaeoclimate proxy signal emplacement in speleothems and the subsequent need to understand *in-situ* conditions, such as cave hydrology and atmosphere, which control carbonate precipitation on various timescales (Baldini et al., 2008; Banner et al., 2007; Johnson et al., 2006; Kowalczk, 2009; Kowalczk and Froelich, 2010; Spötl et al., 2005). The Yok Balum Cave environment is extremely stable in terms of temperature, humidity and pCO_2. This provides a stable backdrop for palaeoclimate studies. The cave is characterised by a predictable and effective ventilation regime, forced primarily by temperature driven internal-external air density differences, which acts to keep pCO_2 levels low all year round. This eliminates potential seasonal bias in carbonate precipitation caused by variable degassing rates and simplifies proxy record interpretation in this respect. Likewise temperature and humidity remain effectively constant year-round and hence kinetic fractionation between drip water and carbonate associated with evaporation will be minimal. Hydrological links with the local climate are also explored and two speleothem samples collected based on their hydrological connection to the surface. These two speleothems were identified after 18 months of drip monitoring which exposed fast hydrological connections to the surface and reasonably high drip rates. These characteristics are more likely to be associated with fast speleothem growth rates (Banner et al., 2007) and minimal isotopic modification of isotopic signals from the surface (Bradley et al., 2010). This is desirable for very high resolution climate reconstruction and increases the likelihood that signals from synoptic scale weather events with unique isotopic signatures (e.g., hurricanes) will be preserved in the carbonate (Frappier, 2008).

The occurrence of a large magnitude earthquake during the monitoring provided a novel opportunity to assess the impact of seismic activity on cave hydrology and atmosphere and to determine whether seismic activity should be a consideration when studying speleothem records from seismically active regions. The results from active monitoring during an earthquake have not been previously reported and so the results of this section are somewhat novel. Neither the cave atmosphere nor drip rates of three characteristically different drips responded significantly to the earthquake. This information implies that seismic activity of this nature does not result in large

releases of ^{222}Rn or CO_2; which is theoretically possible if increased permeability allows release of geologic CO_2. However, the highly dynamic ventilation at Yok Balum may prevent substantial build-up of these gases may. Seismic activity should therefore not result in short-term speleothem growth stagnation or significant changes in drip water degassing rates associated with increased cave air pCO_2. This may not be the case in caves where ventilation is less effective or where seasonal stagnation occurs. In caves with similar ventilation dynamics and pCO_2 as Yok Balum however, seismic activity of the magnitude reported here should not disrupt carbonate precipitation.

The monitoring data obtained through this study significantly contributed to the interpretation and understanding of palaeoclimate proxy data from YOK-I (Kennett et al., 2012) and YOK-G (Ridley et al. (*in review*)). Particularly, the temperature and CO_2 data provided considerable evidence that no seasonal bias exists caused by changes in seasonally variable evaporative effects or CO_2 degassing rates. This is exceptionally important when considering sub annually resolved climate records. The monitoring data also provided vital information on the hydrological regimes feeding each stalagmite which accounted for the apparent disparity between the two $\delta^{13}C$ records (Chapters 4 and 5) and allowed the dominant climate signals from each record to be identified. This is an important step when working with multiple speleothem records as failure for two stalagmite records to replicate does not mean that they are not recording climate signals, only that they are recording different components of the climate system dependent on their hydrology.

The monitoring work presented here not only provides essential background information for speleothem based palaeoclimate studies at this cave site but also contributed to advances in cave monitoring techniques and equipment development. Caves, particularly in the tropics, are exceptionally challenging environments for electronic equipment. The monitoring methods detailed in this thesis describe effective techniques for evaluating remote tropical caves. The described equipment could be operated in other vadose-zone cave systems. This work also reinforces a 'monitor before sample' approach, whereby screening of stalagmites, initially based on morphology, over several months to years permits identification of samples suitable to specific palaoclimate problems. This not only avoids unnecessary use of research

resources, such as funds and materials for analysis of unsuitable samples, but also limits disruption to the cave environment and aesthetics.

From this work an understanding of the large scale ventilation and hydrological processes at Yok Balum is gained. A next step to further advance understanding of cave-carbonate systematics at Yok Balum would be to quantitatively assess how the described atmospheric and hydrologic changes affect isotopic signals in precipitated carbonate through changes in CO_2 degassing rates and changes in kinetic fractionation, on various timescales. This could be achieved through high resolution isotope analysis of the carbonate precipitated on the calcite spars place in the cave. Comparison between geochemical and petrographical characteristics of the precipitate and the monitoring information presented here will help to determine sub-seasonal changes in growth. It would also be pertinent to combine drip water and rainwater isotope data with the hydrological drip rate data presented here to attempt to model how isotopic signals are modified through different hydrological flow pathways within the cave. This will be valuable when interpreting the $\delta^{18}O$ signal from YOK-G, YOK-K and YOK-L.

6.3 Aerosol forcing of intertropical convergence zone position

Chapter 3 presents a 453-year rainfall record derived from $\delta^{13}C$ in stalagmite YOK-G. The YOK-G record is one of the best resolved palaeoclimate records to be developed from the tropics and importantly covers the transition from a natural to anthropogenically forced climate state. Southern Belize is exceptionally sensitive to rainfall changes associated with ITCZ strength and position and therefore the record provides an opportunity to observe how the tropical rain belt has shifted over Central America in response to external forcings, both natural and anthropogenic. The resolution of the record and the presence of well-preserved $\delta^{13}C$ cycles permit the record to be deconvolved to a seasonal level and $\delta^{13}C$ of the wet and dry seasons to be compared through time. To date this is quite a novel concept in tropical palaeoclimatology, which are typically lower resolution. Some of the most high profile tropical speleothem records, although covering much longer timescales than YOK-G,

have a resolution on the order of several years per stable isotope point (e.g. Dongge Cave, China (Dykoski et al., 2005); Wang Xiang Cave, China (Zhang et al., 2008); Tzabnah Cave, Mexico (Medina-Elizalde et al., 2010). Although these records provide invaluable information on past climate, they are insufficient to discern short-lived forcings, such volcanic eruptions, or inter-annual changes in seasonal rainfall.

As well as demonstrating the exceptional potential of speleothems as palaeoclimate proxy records, the YOK-G record provides some of the first palaeoclimate evidence in support of recent modelling and observational studies illustrating that anthropogenic aerosols have forced southward migration of the ITCZ (Chang et al., 2011; Hwang et al., 2013; Lu et al., 2013; Rotstayn and Lohmann, 2002; Zhang et al., 2007). The record shows that despite NH warming over the last 150 years, Belize has experienced reductions in wet season rainfall. This is the opposite trend to that observed during the pre-industrial period both in YOK-G and other low-latitude palaeoclimate records over the last two millennia (Dykoski et al., 2005; Haug et al., 2001). The drying trend revealed in the YOK-G record also tracks North America and European aerosol emissions, further corroborating the idea that aerosol radiative cooling of the NH has contributed to low-latitude rainfall reductions. This drying observed during the last 150 years associated with southward displacement of the ITCZ also occur after substantial NH volcanic eruptions. Volcanic aerosols, which are known to affect the Earth's radiative budget, appear to create an equivalent magnitude, but shorter-lived drying signal is observed in the YOK-G record during the pre-industrial. This idea is developed and further proved in Chapter 5 using the longer YOK-I record.

Aerosol forcing remains the largest source of uncertainty in climate prediction models for the coming century (IPCC, 2013) and yet it has been debated whether understanding their contribution is relevant for understanding present and future climate changes (Stevens, 2013). The YOK-G record provides the best proxy evidence to date that aerosol forcing does have considerable consequences for low latitude climate, despite the current dominance of greenhouse gases. Based on the results of this chapter it should be a priority of the climate science community to understand how ongoing aerosol production will affect other low-latitude regions.

The exceptional resolution and robust chronology of the YOK-G record provides exceptional opportunities for climatology. Not only does this record provide remarkable resolution data for climate models and multi-proxy reconstructions but also permits identification of synoptic-scale climate data which is only available from such a well resolved record, for example hurricane signals. The YOK-G $\delta^{18}O$ record, which is not discussed in great detail in this thesis, warrants attention. As described in Chapter 3 section 4.3.1, first order variability of YOK-G $\delta^{18}O$ is thought to be driven by regional temperature, which controls fractionation processes from the source region to the cave site. Furthermore the $\delta^{18}O$ record displays an exceptional correlation with NHT reconstructions, particularly Moberg et al. (2005) ($r = 0.51$, $p < 0.001$) and Esper et al. (2002) ($r = 0.6$, $p < 0.001$) (Fig. XX). It is hoped that the YOK-G record will be of use to the wider palaeoclimate community as a component of multi-proxy reconstructions of rainfall and temperature. YOK-G would be particularly valuable in such a composite record due to its low chronological uncertainty.

6.4 Solar and volcanic influence on NAO state via interaction of the ITCZ

Chapter 5 investigates the relationships between local rainfall, derived from speleothem records from Yok Balum, and large scale Atlantic climate variability and external forcing mechanisms over the last 2000 years. This chapter builds on the ideas developed in Chapter 4 regarding the influence of high-latitude volcanism on rainfall in Belize and extends them to the entire North Atlantic by considering the role of the NAO, ITCZ and the influence of solar activity.

The 2000 year $\delta^{13}C$ record from stalagmite YOK-I (Kennett et al., 2012) is tuned (within dating error) to the sub-annually resolved YOK-G record and the Median Absolute Deviation calculated in order to create a 2000-year long, bi-annually resolved NAO reconstruction (YOK-I_{MAD}). Strong correlation with existing NAO reconstructions from around the North Atlantic Basin supports the notion that this index is representative of NAO activity. The YOK-I_{MAD} reconstruction demonstrates that the 11th century drought in Belize, which has been linked to the demise of the Maya civilisation (Kennett et al., 2012; see Appendix A), was associated with the strongest NAO- in the last 2000 years

and is coincident with the Oort Sunspot Minimum and massive, high-latitude NH volcanic eruptions. Although it is widely believed that climate was a primary driver of the collapse of Maya polities in the 11th century, a mechanism accounting for the 'megadrought' has not been identified. YOK-I_{MAD} reconstruction provides a foundation for contextualising the climate anomaly which led to the collapse of this civilisation.

As well as providing a chronologically more robust NAO reconstruction, which can be used to anchor existing reconstructions, YOK-I_{MAD} also provides additional information to refine these reconstructions. The YOK-I_{MAD} indicates that the Medieval Climate Anomaly was not characterised by NAO+ conditions as pervasive as previously proposed by Trouet et al. (2009) which is an important result for characterising the Medieval Climate Anomaly (often considered the most analogous period of recent climate history to the Current Warm Period). The excellent agreement between YOK-I_{MAD} and existing NAO reconstructions provides a novel opportunity to observe how the ITCZ and NAO signals in the Atlantic are interconnected.

The bi-annual resolution of the YOK-I_{MAD} reconstruction permits the identification of short-lived climate shifts related to NH volcanic eruptions and therefore allows ideas presented in Chapter 4 to be further developed. As in YOK-G, YOK-I_{MAD} displays evidence of short lived drying events caused by ITCZ repositioning following large NH aerosol injections from explosive volcanism. The signal resulting from tropical and Southern Hemisphere eruptions is less conclusive, but it seems that both produce wetter conditions in Belize by forcing the ITCZ to the north and creating NAO+ conditions in the North Atlantic. Research based on historical NAO data hinted at a link between explosive volcanism and the NAO, but the definite link remained elusive due to chronological uncertainties in existing NAO reconstructions. This record provides some compelling evidence for this link and provides data to inform dynamic climate models.

It appears that the interaction of solar and volcanic forcings is important for predicting North Atlantic variability. Short lived forcing caused by volcanic activity can 'over-print' that of solar activity, which is a comparatively smaller radiative forcing. An example of this is during the Wölf Minimum, when despite low solar activity the ITCZ was forced

to the north by two enormous explosive large eruptions in Indonesia and Ecuador. Alternatively, volcanic eruptions can amplify solar forcings. Large NH eruptions appear to force more extreme NAO- conditions when combined with periods of low solar activity. This is an interesting observation which warrants further investigation, potentially with the involvement of volcanologists. Comparison with other low-latitude rainfall proxy records suggests that NAO signals are linked to solar activity and explosive volcanism through strengthening and/or repositioning of the ITCZ which occurs on a global scale. This provides a new and alternative view on the role of the NAO-climate mode and North Atlantic variability, which is typically thought to be driven from the North Atlantic zone itself. The results presented in this chapter therefore have important implications for future prediction and understanding of the NAO, particularly in terms of anthropogenic aerosol contributions.

As shown in Chapter 4, steadily increasing NH anthropogenic aerosols over the last century has disrupted rainfall in Belize by forcing the ITCZ further to the south. We do not however observed a strong NAO- over the last century, which could be expected simultaneous with southward ITCZ migration. Rapidly increasing GHG levels are likely responsible for the modification of the NAO phase observed during this industrialised period. GHG warming, which is particularly severe at higher latitudes, will affect atmospheric circulation and hence pressure variability across the Atlantic Basin. This stimulates interesting questions regarding the validity of considering current climate as a 'normal mode' for large scale climate variability.

There are two connected avenues of investigation arising from this chapter which warrant future work. Firstly, the YOK-I_{MAD} reconstruction could be used in conjunction with the YOK-G record in order to quantify how specific volcanic eruptions modify low latitude rain belts with regards to eruption type, size, duration, geographic location and time of eruption and how these interact with solar forcing. Further investigation into the local climate response to explosive volcanism through modelling and investigation of other proxy signals, for example trace elements, will be extremely beneficial in further understanding how local climate may be influenced by atmospheric aerosols, and may help to refine and/or extend the historic volcanism

record. It is also paramount that future work attempts to evaluate the forcing effect of volcanism and solar activity in the current anthropogenic climate state.

6.5 Concluding remarks

Combined, the chapters presented in this thesis present a comprehensive study of recent Central American and tropical Atlantic climate variability based on Belizean speleothem proxy records which are supported by relevant background information from a previously uncharacterised cave site. Evidence suggests that rainfall in Belize, which is highly sensitive to meridional migration and intensity changes of the ITCZ, is forced by solar and volcanic activity and that these responses are part of a larger-scale climate perturbation. The IPCC (2013) conclude that the total natural radiative forcing from solar irradiance changes and stratospheric volcanic aerosols made only a small contribution to the net radiative forcing throughout the last century, except for brief periods after large volcanic eruptions, such as Pinatubo. The anomalous relationship between YOK-G rainfall proxy record and NHT since 1850 therefore provides strong evidence of the impact of anthropogenic aerosols on low-latitude rainfall. The significance of the tropics in moderating extra-tropical climate variability is evidenced through comparison of geographically diverse proxy records. The apparent dominance of the ITCZ in controlling not only low-latitude rainfall, but also higher latitude climate is highlighted. From this research numerous opportunities for future study are apparent and the potential speleothems hold as tropical palaeoclimate proxy archives is clearly illustrated. As the number of palaeoclimate proxy records from the tropics increases, research should focus on combing these to obtain a more comprehensive picture of tropical climate variability throughout the Holocene.

References

Adams, B.J., Mann, M.E., Ammann, C.M., 2003. *Proxy evidence for an El Nino-like response to volcanic forcing*. Nature, 426(6964): 274-278.

Albrecht, B.A., 1989. *Aerosols, cloud microphysics, and fractional cloudiness*. Science, 245(4923): 1227-1230.

Alexander, M.A. et al., 2002. *The atmospheric bridge: The influence of ENSO teleconnections on air-sea interaction over the global oceans*. Journal of Climate, 15(16): 2205-2231.

Alley, R.B. et al., 2007. *Report of working group I of the Intergovernmental Panel on Climate Change summary for policymakers.*, Intergovernmental Panel on Climate Change.

Ammann, C.M., Joos, F., Schimel, D.S., Otto-Bliesner, B.L., Tomas, R.A., 2007. *Solar influence on climate during the past millennium: Results from transient simulations with the NCAR climate system model*. Proceedings of the National Academy of Sciences of the United States of America, 104(10): 3713-3718.

Anchukaitis, K.J. et al., 2010. *Influence of volcanic eruptions on the climate of the Asian monsoon region*. Geophysical Research Letters, 37.

Anderson, R.K., Miller, G.H., Briner, J.P., Lifton, N.A., DeVogel, S.B., 2008. *A millennial perspective on Arctic warming from C-14 in quartz and plants emerging from beneath ice caps*. Geophysical Research Letters, 35(1).

Aquilina, L., Ladouche, B., Dorfliger, N., 2006. *Water storage and transfer in the epikarst of karstic systems during high flow periods*. Journal of Hydrology, 327(3-4): 472-485.

Asmerom, Y., Polyak, V.J., Burns, S.J., 2010. *Variable winter moisture in the southwestern United States linked to rapid glacial climate shifts*. Nature Geoscience, 3(2): 114-117.

Badino, G., 2010. *Underground Meteorology - "What's the Weather Underground?"*. Acta Carsologica, 39(3): 427-448.

Baker, A., Barnes, W.L., Smart, P.L., 1997. *Variations in the discharge and organic matter content of stalagmite drip waters in Lower Cave, Bristol*. Hydrological Processes, 11: 1541-1555.

Baker, A.J., Mattey, D.P., Baldini, J.U.L., 2014. *Reconstructing modern stalagmite growth from cave monitoring, local meteorology, and experimental measurements of dripwater films*. Earth and Planetary Science Letters, 392(0): 239-249.

Baldini, J.U.L., 2004. *Geochemical and hydrological characterisation of stalagmites as palaeoclimate proxies, with an emphasis on trace element variablity.* PhD Thesis, University College Dublin, Dublin, 300 pp.

Baldini, J.U.L., 2010. *Cave atmosphere controls on stalagmite growth rate and palaeoclimate records*. Tufas and speleothems: Unravelling the microbial and physical controls, 336.

Baldini, J.U.L., McDermott, F., Clipson, N., 2006a. *Effects of high-frequency cave atmosphere pCO_2 variability on stalagmite climate proxy records*. Geochimica et Cosmochimica Acta, 70(18): A30-A30.

Baldini, J.U.L., McDermott, F., Fairchild, I.J., 2006b. *Spatial variability in cave drip water hydrochemistry: Implications for stalagmite paleoclimate records*. Chemical Geology, 235(3-4): 390-404.

Baldini, J.U.L., McDermott, F., Hoffmann, D.L., Richards, D.A., Clipson, N., 2008. *Very high-frequency and seasonal cave atmosphere P_{CO2} variability: Implications for stalagmite growth and oxygen isotope-based paleoclimate records*. Earth and Planetary Science Letters, 272(1-2): 118-129.

Banner, J.L., Guilfoyle, A., James, E.W., Stern, L.A., Musgrove, M., 2007. *Seasonal variations in modern speleothem calcite growth in Central Texas, USA*. Journal of Sedimentary Research, 77(7-8): 615-622.

Bard, E., Raisbeck, G.M., Yiou, F., Jouzel, J., 1997. *Solar modulation of cosmogenic nuclide production over the last millenium: comparison between ^{14}C and ^{10}Be*. Earth and Planetary Science Letters, 150: 453-462.

Bard, E., Raisbeck, G.M., Yiou, F., Jouzel, J., 2000. *Solar irradiance during the last 1200 years based on cosmogenic nuclides*. Tellus, 52B: 3.

Batiot-Guilhe, C., Seidel, J.L., Jourde, H., Hebrard, O., Bailly-Comte, V., 2007. *Seasonal variations of CO_2 and ^{222}Rn in a mediterranean sinkhole - spring (Causse d'Aumelas, SE France)*. International Journal of Speleology, 36(1): 51-56.

Beck, J.W. et al., 1992. *Sea-surface temperature from coral skeletal strontium calcium ratios*. Science, 257(5070): 644-647.

Becker, A. et al., 2006. *Speleoseismology: A critical perspective*. Journal of Seismology, 10(3): 371-388.

Berger, A., 1988. *Milankovitch theory and climate*. Reviews of Geophysics, 26(4): 624-657.

Berger, A., Loutre, M.F., 1991. *Insolation values for the climate of the last 10,000,000 years*. Quaternary Science Reviews, 10(4): 297-317.

Berger, A.L., 1978. *Long-term variations of daily insolation and quaternary climatic changes*. Journal of the Atmospheric Sciences, 35(12): 2362-2367.

Beverly, R.K. et al., 2010. *The Keck Carbon Cycle AMS Laboratory, University of California, Irvine: Status Report*. Radiocarbon, 52(2): 301-309.

Bollasina, M.A., Ming, Y., Ramaswamy, V., 2011. *Anthropogenic aerosols and the weakening of the South Asian summer monsoon*. Science, 334(6055): 502-505.

Bond-Lamberty, B., Thomson, A., 2010. *Temperature-associated increases in the global soil respiration record*. Nature, 464: 579-582.

Booth, B.B.B., Dunstone, N.J., Halloran, P.R., Andrews, T., Bellouin, N., 2012. *Aerosols implicated as a prime driver of twentieth-century North Atlantic climate variability*. Nature, 484(7393): 228-232.

Bourges, F., Mangin, A., d'Hulst, D., 2001. *Le gaz carbonique dans la dynamique de l'atmosphère des cavités karstique: l'exemple de l'Aven d'Orgnac (Ardèche)*. Earth and Planetary Sciences, 333: 685-692.

Bowen, G.J., Wilkinson, B., 2002. *Spatial distribution of $\delta^{18}O$ in meteoric precipitation.* . Geology, 30: 315-318.

Bradley, C., Baker, A., Jex, C.N., Leng, M.J., 2010. *Hydrological uncertainties in the modelling of cave drip-water $\delta^{18}O$ and the implications for stalagmite palaeoclimate reconstructions*. Quaternary Science Reviews, 29(17-18): 2201-2214.

Bradley, R.S., 1999. *Paleoclimatology: Reconstructing Climates of the Quaternary.* Academic, San Diego, California, 610 pp.

Breitenbach, S.F.M., Bernasconi, S.M., 2011. *Carbon and oxygen isotope analysis of small carbonate samples (20 to 100 µg) with a GasBench II preparation device*. Rapid Communications in Mass Spectrometry, 25(13): 1910-1914.

Briffa, K.R., Jones, P.D., Schweingruber, F.H., Osborn, T.J., 1998. *Influence of volcanic eruptions on Northern Hemisphere summer temperature over the past 600 years*. Nature, 393(6684): 450-455.

Broccoli, A.J., Dahl, K.A., Stouffer, R.J., 2006. *Response of the ITCZ to Northern Hemisphere cooling*. Geophysical Research Letters, 33(1).

Brook, G.A., Rafter, M.A., Railsback, L.B., Sheen, S., Lundberg, J., 1999. *A high-resolution proxy record of rainfall and ENSO since A.D. 1550 from layering in stalagmites from Anjohibe Cave, Madagascar*. The Holocene, 9(6): 695-705.

Cane, M.A., 1998. *Climate change - A role for the tropical Pacific*. Science, 282(5386): 59-+.

Cane, M.A., Sarachik, E.S., 1981. *The response of a linear baroclinic equatorial ocean to periodic forcing*. Journal of Marine Research, 39(4): 651-693.

Chang, C.Y., Chiang, J.C.H., Wehner, M.F., Friedman, A.R., Ruedy, R., 2011. *Sulfate aerosol control of tropical Atlantic climate over the twentieth century*. Journal of Climate, 24(10): 2540-2555.

Cheng, H. et al., 2009. *Ice Age Terminations*. Science, 326(5950): 248-252.

Cheng, H. et al., 2006. *A penultimate glacial monsoon record from Hulu Cave and two-phase glacial terminations*. Geology, 34(3): 217-220.

Cheng, H. et al., 2013. *Improvements in ^{230}Th dating, ^{230}Th and ^{234}U half-life values, and U–Th isotopic measurements by multi-collector inductively coupled plasma mass spectrometry*. Earth and Planetary Science Letters, 371–372(0): 82-91.

Chiang, J.C.H., 2009. *The Tropics in Paleoclimate*. Annual review of earth and planetary sciences, 37: 263-297.

Chiang, J.C.H., Bitz, C.M., 2005. *Influence of high latitude ice cover on the marine Intertropical Convergence Zone*. Climate Dynamics, 25(5): 477-496.

Chung, C.E., Ramanathan, V., 2006. *Weakening of North Indian SST gradients and the monsoon rainfall in India and the Sahel*. Journal of Climate, 19(10): 2036-2045.

Clark, I.D., Fritz, P., 1997. *Environmental isotopes in hydrogeology*. Lewis Publisher, New York, 328 pp.

CLIMAP, 1976. *Surface of Ice-Age Earth*. Science, 191(4232): 1131-1137.

Cobb, K.M., Adkins, J.F., Partin, J.W., Clark, B., 2007. *Regional-scale climate influences on temporal variations of rainwater and cave dripwater oxygen isotopes in northern Borneo*. Earth and Planetary Science Letters, 263(3-4): 207-220.

Cook, E.R., D'Arrigo, R.D., Briffa, K.R., 1998. *A reconstruction of the North Atlantic Oscillation using tree-ring chronologies from North America and Europe*. Holocene, 8(1): 9-17.

Cook, E.R., D'Arrigo, R.D., Mann, M.E., 2002. *A well-verified, multiproxy reconstruction of the winter North Atlantic Oscillation index since AD 1400*. Journal of Climate, 15(13): 1754-1764.

Cowan, B.D., Osborne, M.C., Banner, J.L., 2013. *Temporal variability of cave-air CO_2 in Central Texas*. Journal of Cave and Karst Studies, 75(1): 38-50.

Crowley, T., 2000. *Causes of climate change over the past 1,000 years*. Science, 289: 270-277.

Crowley, T., Kwang-Yul, K., 1996. *Comparison of proxy records of climate change and solar forcing*. Geophysical Research Letters, 23(4): 359-362.

Crowley, T.J., Unterman, M.B., 2012. *Technical details concerning development of a 1200-yr proxy index for global volcanism*. Earth Syst. Sci. Data Discuss., 5(1): 1-28.

Cruz, F.W. et al., 2005. *Insolation-driven changes in atmospheric circulation over the past 116,000 years in subtropical Brazil*. Nature, 434(7029): 63-66.

Czaja, A., van der Vaart, P., Marshall, J., 2002. *A diagnostic study of the role of remote forcing in tropical Atlantic variability*. Journal of Climate, 15(22): 3280-3290.

Dansgaard, W., 1964. *Stable isotopes in precipitation*. Tellus, 16(4): 436-468.

De Freitas, C.R., Littlbjohn, R.N., Clarkson, T.S., Kristament, I.S., 1982. *Cave climate: Assessment of airflow and ventilation*. Journal of Climatology, 2(4): 383-397.

Delaygue, G., Bard, E., 2011. *An Antarctic view of Beryllium-10 and solar activity for the past millennium*. Climate Dynamics, 36(11-12): 2201-2218.

Denis, A., Crémoux, F., 2002. *Using the entropy of curves to segment a time or spatial series*. Mathematical Geology, 34(8): 899-914.

Denis, A., Lastennet, R., Huneau, F., Malaurent, P., 2005. *Identification of functional relationships between atmospheric pressure and CO_2 in the cave of Lascaux using the concept of entropy of curves*. Geophysical Research Letters, 32(L05810): doi:10.1029/2004GL022226.

Deplazes, G. et al., 2013. *Links between tropical rainfall and North Atlantic climate during the last glacial period*. Nature Geoscience, 6(3): 213-217.

Diffenbaugh, N.S., Field, C.B., 2013. *Changes in ecologically critical terrestrial climate conditions*. Science, 341(6145): 486-492.

Driscoll, S., Bozzo, A., Gray, L.J., Robock, A., Stenchikov, G., 2012. *Coupled Model Intercomparison Project 5 (CMIP5) simulations of climate following volcanic eruptions*. Journal of Geophysical Research-Atmospheres, 117.

Dueñas, C., Fernández, M.C., Cañete, S., Carretero, J., Liger, E., 1999. *^{222}Rn concentrations, natural flow rate and the radiation exposure levels in the Nerja Cave*. Atmospheric Environment, 33(3): 501-510.

Dueñas, C., Fernández, M.C., Cañete, S., Pérez, M., Gordo, E., 2011. *Seasonal variations of radon and the radiation exposure levels in Nerja cave, Spain*. Radiation Measurements, 46(10): 1181-1186.

Dulinkski, M., Rozanski, K., 1990. *Formation of the $^{13}C/^{12}C$ isotpe ratios in speleothems: a semi-dynamic model*. Radiocarbon, 32: 7-16.

Dulinski, M., Rozanski, K., 1990. *Formation of C^{13}/C^{12} isotope ratios in speleothems - a semidynamic model*. Radiocarbon, 32(1): 7-16.

Dunbar, R., Cole, J., 1999. *Annual Records of Tropical Systems (ARTS); Recommendations for Research*. IGBP Science Series, Geneva.

Dunlap, C.E., Gill, J.B., Palacz, Z.A., 1992. *U/Th disequilibria in the large-volume, chemically-zoned, eruption of Baitoushan, 1010 AD.* . EOS, Transactions, American Geophysical Union, 73(43): 611.

Dykoski, C.A. et al., 2005. *A high-resolution, absolute-dated Holocene and deglacial Asian monsoon record from Dongge Cave, China*. Earth and Planetary Science Letters, 233(1-2): 71-86.

Emile-Geay, J., Seager, R., Cane, M.A., Cook, E.R., Haug, G.H., 2008. *Volcanoes and ENSO over the past millennium*. Journal of Climate, 21(13): 3134-3148.

Esper, J., Cook, E.R., Schweingruber, F.H., 2002. *Low-frequency signals in long tree-ring chronologies for reconstructing past temperature variability*. Science, 295(5563): 2250-2253.

Esper, J., Frank, D., Buntgen, U., Verstege, A., Luterbacher, J., 2007. *Long-term drought severity variations in Morocco*. Geophysical Research Letters, 34(17).

Faimon, J., Stelcl, J., Sas, D., 2006. *Anthropogenic CO_2-flux into cave atmosphere and its environmental impact: A case study in the Cisarska Cave (Moravian Karst, Czech Republic)*. Science of the Total Environment, 369(1-3): 231-245.

Faimon, J., Troppova, D., Baldik, V., Novotny, R., 2012. *Air circulation and its impact on microclimatic variables in the Cisarska Cave (Moravian Karst, Czech Republic)*. International Journal of Climatology, 32(4): 599-623.

Fairchild, I.J., 2002. *High-resolution speleothem trace element records: potential as climate proxies*. In: Carrasco, F., Duran, J.J., y Andreo, B. (Eds.), Karst and Environment, pp. 377-380.

Fairchild, I.J., Baker, A., 2012. *Speleothem Science: from process to past environments*. John Wiley and Sons Ltd, Oxford.

Fairchild, I.J. et al., 2006. *Modification and preservation of environmental signals in speleothems*. Earth-Science Reviews, 75(1-4): 105-153.

Fairchild, I.J., Treble, P.C., 2009. *Trace elements in speleothems as recorders of environmental change*. Quaternary Science Reviews, 28(5-6): 449-468.

Felis, T., Patzold, J., 2004. *Climate reconstructions from annually banded corals.* In: Shiyomi M, Kawahata H, Koizumi H, A, T., Y, A. (Eds.), Global Environmental Change in the Ocean and on Land. TERRAPUB, Tokyo, pp. 205-227.

Fetter, C.W., 1994. *Applied Hydrogeology*. Macmillan College Publishing Company, Inc., New York, 691 pp.

Field, M.S., 2007. *Risks to cavers and cave workers from exposures to low-level ionizing alpha radiation from Rn-222 decay in caves*. Journal of Cave and Karst Studies, 69(1): 207-228.

Fischer, E.M. et al., 2007. *European climate response to tropical volcanic eruptions over the last half millennium*. Geophysical Research Letters, 34(5).

Fleitmann, D. et al., 2004. *Palaeoclimatic interpretation of high-resolution oxygen isotope profiles derived from annually laminated speleothems from Southern Oman*. Quaternary Science Reviews, 23: 935-945.

Ford, D.C., Williams, P.W., 2007. *Karst geomorphology and hydrology*. Unwin Hyman Ltd., London.

Forster, P., Ramaswamy, V., 2007. *Changes in atmospheric constituents and in radiative forcing*. Climate Change 2007: The Physical Science Basis: 129-234.

Frappier, A., Sahagian, D., Gonzalez, L.A., Carpenter, S.J., 2002. *El Niño events recorded by stalagmite carbon isotopes*. Science, 298(5593): 565-565.

Frappier, A.B., 2008. *A stepwise screening system to select storm-sensitive stalagmites: Taking a targeted approach to speleothem sampling methodology*. Quaternary International, 187: 25-39.

Frappier, A.B., Sahagian, D., Carpenter, S.J., Gonzalez, L.A., Frappier, B.R., 2007. *Stalagmite stable isotope record of recent tropical cyclone events*. Geology, 35(2): 111-114.

Friedman, A.R., Hwang, Y.T., Chiang, J.C.H., Frierson, D.M.W., 2013. *Interhemispheric temperature asymmetry over the twentieth century and in future projections*. Journal of Climate, 26(15): 5419-5433.

Frierson, D.M.W., Hwang, Y.-T., 2011. *Extratropical influence on ITCZ Shifts in Slab Ocean Simulations of Global Warming*. Journal of Climate, 25(2): 720-733.

Frierson, D.M.W., Hwang, Y.T., 2012. *Extratropical Influence on ITCZ Shifts in Slab Ocean Simulations of Global Warming*. Journal of Climate, 25(2): 720-733.

Frisia, S., Borsato, A., Fairchild, I.J., McDermott, F., 2000. *Calcite fabrics, growth mechanisms, and environments of formation in speleothems from the Italian Alps and southwestern Ireland*. Journal of Sedimentary Research, 70(5): 1183-1196.

Frisia, S., Borsato, A., Preto, N., McDermott, F., 2003. *Late Holocene annual growth in three Alpine stalagmites records the influence of solar activity and the North Atlantic Oscillation on winter climate*. Earth and Planetary Science Letters, 6846.

Gagan, M.K. et al., 2000. *New views of tropical paleoclimates from corals*. Quaternary Science Reviews, 19(1-5): 45-64.

Gao, C., Robock, A., Ammann, C., 2008. *Volcanic forcing of climate over the past 1500 years: An improved ice core-based index for climate models*. Journal of Geophysical Research: Atmospheres, 113(D23): D23111.

Gao, C.C., Robock, A., Ammann, C., 2012. *Volcanic forcing of climate over the past 1500 years: An improved ice core-based index for climate models (vol 113, D2311, 2008)*. Journal of Geophysical Research-Atmospheres, 117.

Genty, D. et al., 2003. *Precise dating of Dansgaard-Oeschger climate oscillations in western Europe from stalagmite data*. Nature, 421: 833-837.

Genty, D., Deflandre, G., 1998. *Drip flow variations under a stalactite of the Père Noël cave (Belgium). Evidence of seasonal variations and air pressure constraints*. Journal of Hydrology, 211: 208-232.

Genty, D., Massault, M., 1997. *Bomb ^{14}C recorded in laminated speleothems: calculation of dead carbon proportion*. Radiocarbon., 39: 33-48.

Genty, D., Vokal, B., Obelic, B., Massault, M., 1998. *Bomb ^{14}C time history recorded in two modern stalagmites - importance for soil organic matter dynamics and bomb ^{14}C distribution over continents*. Earth and Planetary Science Letters, 160: 795-809.

Giannini, A., Kushnir, Y., Cane, M.A., 2001. *Seasonality in the impact of ENSO and the North Atlantic High on Caribbean Rainfall*. Physical Chemistry of the Earth, 26(2): 143-146.

Gill, A.E., 1980. *Some Simple Solutions for Heat-Induced Tropical Circulation*. Quarterly Journal of the Royal Meteorological Society, 106(449): 447-462.

Gilli, E., 1999. *Evidence of palaeoseismicity in a flowstone of the Observatoire cave (Monaco)*. Geodinamica Acta, 12(3-4): 159-168.

Gilli, E., Delange, P., 2001. *Utilisation des sp´el´eoth`emes comme indicateurs de n´eotectonique ou de la pal´eosismicit´e.* Tectonique Active et G´eomorphologie, Rev d'Analyse Spatiale Quantitative et Appliqu´ee, Spec. Publ.: 79-90.

Gilli, E., Serface, R., 1999. *Evidence of palaeoseismicity in the caves of Arizona and New Mexico*. Earth and Planetary Sciences, 329: 31-37.

Glueck, M.F., Stockton, C.W., 2001. *Reconstruction of the North Atlantic Oscillation, 1429-1983*. International Journal of Climatology, 21(12): 1453-1465.

Gregoric, A., Vaupotic, J., Gabrovsek, F., 2013. *Reasons for large fluctuation of radon and CO2 levels in a dead-end passage of a karst cave (Postojna Cave, Slovenia)*. Natural Hazards and Earth System Sciences, 13(2): 287-297.

Gregoric, A., Zidansek, A., Vaupotic, J., 2011. *Dependence of radon levels in Postojna Cave on outside air temperature*. Natural Hazards and Earth System Sciences, 11(5): 1523-1528.

Grottoli, A.G., Eakin, C.M., 2007. *A review of modern coral $\delta^{18}O$ and $\delta^{14}C$ proxy records*. Earth-Science Reviews, 81(1-2): 67-91.

Guilderson, T.P., Fairbanks, R.G., Rubenstone, J.L., 1994. *Tropical temperature-variations since 20,000 years ago - modulating interhemispheric climate-change*. Science, 263(5147): 663-665.

Haig, J., Nott, J., Reichart, G.-J., 2014. *Australian tropical cyclone activity lower than at any time over the past 550-1,500 years*. Nature, 505(7485): 667-671.

Hakl, J. et al., 1997. *Radon transport phenomena studied in karst caves - international experiences on radon levels and exposures*. Radiation Measurements, 28(1-6): 675-684.

Haug, G.H. et al., 2003. *Climate and the collapse of Maya civilization*. Science, 299(5613): 1731-1735.

Haug, G.H., Hughen, K.A., Sigman, D.M., Peterson, L.C., Rohl, U., 2001. *Southward migration of the intertropical convergence zone through the Holocene*. Science., 293(5533): 1304-1308.

Hegerl, G. et al., 2011. *Influence of human and natural forcing on European seasonal temperatures*. Nature Geoscience, 4(2): 99-103.

Hellstrom, J.C., McCulloch, M., Stone, J., 1998. *A detailed 31,000 year record of cliamte and vegatation change, from the isotope geochemistry of two New Zealand speleothems*. Quaternary Research, 50: 167.

Henderson, G.M., 2006. *Climate - Caving in to new chronologies*. Science, 313(5787): 620-622.

Hendy, C.H., 1971. *The isotopic geochemistry of speleothems - I The calculation of the effects of different modes of formation on the isotopic composition of speleothems and their applicability as palaeoclimatic indicators*. Geochimica et Cosmochimica Acta, 35: 801.

Heslop, D. et al., 1999. *Sub-millennial scale variations in East Asian monsoon systems recorded by dust deposits from the north-western Chinese Loess Plateau*. Physics and Chemistry of the Earth Part a-Solid Earth and Geodesy, 24(9): 785-792.

Hess, J.W., White, W.B., 1993. *Groundwater geochemistry of the carbonate karst aquifer, south-central Kentucky, USA*. Applied Geochemistry, 8(2): 189-204.

Hetzinger, S., Pfeiffer, M., Dullo, W.C., Halfar, J., 2010. *Rapid 20th century warming in the Caribbean and impact of remote forcing on climate in the northern tropical Atlantic as recorded in a Guadeloupe coral*. Palaeogeogr Palaeoclimatol Palaeoecol, 296(1-2): 14-14.

Highwood, E.J., Stevenson, D.S., Highwood, E.J., Stevenson, D.S., 2003. *Atmospheric impact of the 1783-1784 Laki eruption: Part II - climatic effect of sulphate aerosol*. Atmospheric Chemistry and Physics, 3: 1177-1189.

Hodell, D.A. et al., 2005. *Climate change on the Yucatan Peninsula during the Little Ice Age*. Quaternary Research, 63(2): 109-121.

Hoffmann, D.L. et al., 2010. *Towards radiocarbon calibration beyond 28 ka using speleothems from the Bahamas*. Earth and Planetary Science Letters, 289(1-2): 1-10.

Horn, S., Schmincke, H.U., 2000. *Volatile emission during the eruption of Baitoushan Volcano (China/North Korea) ca. 969 AD*. Bulletin of Volcanology, 61(8): 537-555.

Hua, Q., Barbetti, M., 2004. *Review of tropospheric bomb C^{14} data for carbon cycle modeling and age calibration purposes*. Radiocarbon, 46(3): 1273-1298.

Hughen, K.A., Overpeck , J.T., Peterson, L.C., Trumbore, S., 1996. *Rapid climate changes in the tropical Atlantic region during the last deglaciation*. Nature, 380: 51-54.

Hurrell, J.W., 1995. *Decadal trends in the North-Atlantic Oscillation - regional temperatures and precipitation*. Science, 269(5224): 676-679.

Hurrell, J.W., Kushnir, Y., Ottersen, G., Visbeck, M., 2003. *The North Atlantic Oscillation: climatic significance and environmental impact*. Geophys. Monogr. Ser., 134. AGU, Washington, DC, 279 pp.

Hwang, Y.T., Frierson, D.M.W., Kang, S.M., 2013. *Anthropogenic sulfate aerosol and the southward shift of tropical precipitation in the late 20th century*. Geophysical Research Letters, 40(11): 2845-2850.

IPCC, 2013. *Climate Change 2013: The physical science basis. Contribution of wrorking group I to the Fifth Assessment Report of the Intergovernmental Panel on Climate Change*. IPCC, 2013: Summary for Policymakers. Cambridge University Press, Cambridge, United Kingdom and New York, NY, USA.

Jansen, E. et al., 2007. *Palaeoclimate*. In: Solomon S et al. (Eds.), Climate Change 2007: The Physical Science Basis. Contribution of Working Group I to the Fourth Assessment Report of the Intergovernmental Panel on Climate Change. Cambridge University Press, Cambridge, pp. 433-497.

Johnson, K.R., Hu, C., Belshaw, N.S., Henderson, G.M., 2006. *Seasonal trace-element and stable-isotope variations in a Chinese speleothem: The potential for high-resolution paleomonsoon reconstruction*. Earth and Planetary Science Letters, 244(1-2): 394-407.

Jones, P.D., Mann, M.E., 2004. *Climate over past millennia*. Reviews of Geophysics, 42(2).

Kang, S.M., Frierson, D.M.W., Held, I.M., 2009. *The tropical response to extratropical thermal forcing in an idealized GCM: the importance of radiative feedbacks and convective parameterization*. Journal of the Atmospheric Sciences, 66(9): 2812-2827.

Kang, S.M., Held, I.M., Frierson, D.M.W., Zhao, M., 2008. *The response of the ITCZ to extratropical thermal forcing: idealized slab-ocean experiments with a GCM*. Journal of Climate, 21(14): 3521-3532.

Kawase, H. et al., 2010. *Physical mechanism of long-term drying trend over tropical North Africa*. Geophysical Research Letters, 37(9).

Kennett, D.J. et al., 2012. *Development and disintegration of Maya political systems in response to climate change*. Science, 338(6108): 788-791.

Koch, D., Del Genio, A.D., 2010. *Black carbon semi-direct effects on cloud cover: review and synthesis*. Atmospheric Chemistry and Physics, 10(16): 7685-7696.

Kolodny, Y., Calvo, R., Rosenfeld, D., 2009. *"Too low" $\delta^{18}O$ of paleo-meteoric, low latitude, water; do paleo-tropical cyclones explain it?* Palaeogeography Palaeoclimatology Palaeoecology, 280(3-4): 387-395.

Kowalczk, A., 2009. *High resolution microclimate study of Hollow Ridge Cave: Relationships between cave meteorology, air chemistry and hydrology and the impact of speleothem deposition.*, Florida State University, Thallahasse.

Kowalczk, A., Froelich, P., Gaffka, C., Tremaine, D., 2008. *High resolution time series cave ventilation processes and the effects of cave air chemistry and drip waters: speleoclimatology and proxy calibration.* Fall Meet. Suppl. Abstract PP51C-1521: Eos Transactions AGU, 89(53).

Kowalczk, A.J., Froelich, P.N., 2010. *Cave air ventilation and CO_2 outgassing by radon-222 modeling: How fast do caves breathe?* Earth and Planetary Science Letters, 289(1-2): 209-219.

Kravitz, B., Robock, A., 2011. *Climate effects of high-latitude volcanic eruptions: Role of the time of year*. Journal of Geophysical Research-Atmospheres, 116.

Lachniet, M.S., 2009. *Climatic and environmental controls on speleothem oxygen-isotope values*. Quaternary Science Reviews, 28(5-6): 412-432.

Lachniet, M. S. & Patterson, W. P. *Oxygen isotope values of precipitation and surface waters in northern Central America (Belize and Guatemala) are dominated by temperature and amount effects.* Earth and Planetary. Science Letters. 284, 435-446 (2009).

Lachniet, M.S. et al., 2004. *A 1500-year El Nino/Southern Oscillation and rainfall history for the Isthmus of Panama from speleothem calcite*. Journal of Geophysical Research-Atmospheres, 109(D20).

Lau, K.M., Kim, M.K., Kim, K.M., 2006. *Asian summer monsoon anomalies induced by aerosol direct forcing: the role of the Tibetan Plateau*. Climate Dynamics, 26(7-8): 855-864.

Lau, N.C., Nath, M.J., 2003. *Atmosphere-ocean variations in the Indo-Pacific sector during ENSO episodes*. Journal of Climate, 16(1): 3-20.

Lean, J., 2000. *Evolution of the sun's spectral irradiance since the Maunder Minimum*. Geophysical Research Letters, 27(16): 2425-2428.

Lean, J., Beer, J., Bradley, R.S., 1995. *Reconstruction of solar irradiance since 1610: Implications for climate change*. Geophysical Research Letters, 22(23): 3195-3198.

Lehner, F., Raible, C.C., Stocker, T.F., 2012. *Testing the robustness of a precipitation proxy-based North Atlantic Oscillation reconstruction*. Quaternary Science Reviews, 45: 85-94.

Leibensperger, E.M. et al., 2012a. *Climatic effects of 1950:2050 changes in US anthropogenic aerosols: Part 1: aerosol trends and radiative forcing*. Atmos. Chem. Phys., 12(7): 3333-3348.

Leibensperger, E.M. et al., 2012b. *Climatic effects of 1950:2050 changes in US anthropogenic aerosols: Part 2: climate response*. Atmos. Chem. Phys., 12(7): 3349-3362.

Lintner, B.R., Chiang, J.C.H., 2007. *Adjustment of the remote tropical climate to El Nino conditions*. Journal of Climate, 20(11): 2544-2557.

Lough, J.M., 2004. *A strategy to improve the contribution of coral data to high-resolution paleoclimatology*. Palaeogeography Palaeoclimatology Palaeoecology, 204(1-2): 115-143.

Lough, J.M., 2010. *Climate records from corals*. Wiley Interdisciplinary Reviews-Climate Change, 1(3): 318-331.

Lu, H.Y. et al., 2013. *Variation of East Asian monsoon precipitation during the past 21 k.y. and potential CO_2 forcing*. Geology, 41(9): 1023-1026.

Ludlow, F. et al., 2013. *Medieval Irish chronicles reveal persistent volcanic forcing of severe winter cold events, 431-1649 CE*. Environmental Research Letters, 8(2).

Luterbacher, J., Schmutz, C., Gyalistras, D., Xoplaki, E., Wanner, H., 1999. *Reconstruction of monthly NAO and EU indices back to AD 1675*. Geophysical Research Letters, 26(17): 2745-2748.

Luterbacher, J. et al., 2001. *Extending North Atlantic Oscillation reconstructions back to 1500*. Atmospheric Science Letters, 2(1-4): 114-124.

Luterbacher, J. et al., 2002. *Reconstruction of sea level pressure fields over the Eastern North Atlantic and Europe back to 1500*. Climate Dynamics, 18(7): 545-561.

Mann, M.E., 2007. *Climate over the past two millennia*. Annual Review of Earth and Planetary Sciences, 35: 111-136.

Mann, M.E., Bradley, R.S., Hughes, M.K., 1998. *Global-scale temperature patterns and climate forcing over the past six centuries*. Nature, 392: 779-787.

Mann, M.E., Cane, M.A., Zebiak, S.E., Clement, A., 2005. *Volcanic and solar forcing of the tropical Pacific over the past 1000 years*. Journal of Climate, 18(3): 447-456.

Mann, M.E., Woodruff, J.D., Donnelly, J.P., Zhang, Z., 2009. *Atlantic hurricanes and climate over the past 1,500 years*. Nature, 460(7257): 880-883.

Mann, M.E. et al., 2008. *Proxy-based reconstructions of hemispheric and global surface temperature variations over the past two millennia*. Proceedings of the National Academy of Sciences of the United States of America, 105(36): 13252-13257.

Marland, G., Andres, R.J., Boden, T.A., 1994. *Global, regional and national CO_2 emissions*. In: Boden, T.A., Kaiser, D.P., Sepanski, R.J., Stoss, F.W. (Eds.), Trends '93: A Compendium of Data on Global Change. Oak Ridge Nat. Lab., Oak Ridge, TN., pp. 505-584.

Mattey, D. et al., 2008. *A 53 year seasonally resolved oxygen and carbon isotope record from a modern Gibraltar speleothem: reconstructed drip water and relationship to local precipitation*. Earth and Planetary Science Letters, doi: 10.1016/j.epsl.2008.01.051.

Mattey, D.P. et al., 2010. *Seasonal microclimate control of calcite fabrics, stable isotopes and trace elements in modern speleothem from St Michaels Cave, Gibraltar*. Tufas and Speleothems: Unravelling the Microbial and Physical Controls, 336: 323-344.

McDermott, F., 2004. *Palaeo-climate reconstruction from stable isotope variations in speleothems: a review*. Quaternary Science Reviews, 23(7-8): 901-918.

McDonald, J., Drysdale, R., Hill, D., Chisari, R., Wong, H., 2007. *The hydrochemical response of cave drip waters to sub-annual and inter-annual climate variability, Wombeyan Caves, SE Australia*. Chemical Geology, 244(3-4): 605-623.

Medina-Elizalde, M. et al., 2010. *High resolution stalagmite climate record from the Yucatan Peninsula spanning the Maya terminal classic period*. Earth and Planetary Science Letters, 298(1-2): 255-262.

Meeker, L.D., Mayewski, P.A., 2002. *A 1400-year high-resolution record of atmospheric circulation over the North Atlantic and Asia*. Holocene, 12(3): 257-266.

Menichetti, M., 2013. *Karst processes and carbon flux in the Frasassi Caves, Italy*, 16th International Congress of Speleology, Brno, pp. 376-378.

Mickler, P.J. et al., 2004. *Stable isotopic variations in modern tropical speleothems: Evaluating equilibrium vs. kinetic effects*. Geochemica et Cosmochimica Acta, 68(21): 4381-4393.

Mickler, P.J., Stern, L.A., Banner, J.L., 2006. *Large kinetic isotope effects in modern speleothems*. Geological Society of America Bulletin, 118(1-2): 65-81.

Miller, G.H. et al., 2012. *Abrupt onset of the Little Ice Age triggered by volcanism and sustained by sea-ice/ocean feedbacks*. Geophysical Research Letters, 39.

Miller, T.E., 1996. *Geologic and hydrologic controls on karst and cave development in Belize*. Journal of Cave and Karst Studies, 58(2): 100-120.

Miorandi, R., Borsato, A., Frisia, S., Fairchild, I.J., Richter, D.K., 2010. *Epikarst hydrology and implications for stalagmite capture of climate changes at Grotta di Ernesto (NE Italy): results from long-term monitoring*. Hydrological Processes, DOI: 10.1002/hyp.7744.

Moberg, A., Sonechkin, D.M., Holmgren, K., Datsenko, N.M., Karlen, W., 2005. *Highly variable Northern Hemisphere temperatures reconstructed from low- and high-resolution proxy data*. Nature, 433(7026): 613-617.

Murthy, R. et al., 2003. *Carbon dioxide efflux from a 550 m^3 soil across a range of soil temperatures*. Forest Ecology and Management, 178(3): 311-327.

Muscheler, R. et al., 2007. *Solar activity during the last 1000 yr inferred from radionuclide records*. Quaternary Science Reviews, 26(1-2): 82-97.

Neukom, R., Gergis, J., 2012. *Southern Hemisphere high-resolution palaeoclimate records of the last 2000 years*. Holocene, 22(5): 501-524.

Oh, Y.H., Kim, G., 2011. *Factors controlling the air ventilation of a limestone cave revealed by Rn-222 and Rn-220 tracers*. Geosciences Journal, 15(1): 115-119.

Olsen, J., Anderson, N.J., Knudsen, M.F., 2012. *Variability of the North Atlantic Oscillation over the past 5,200 years*. Nature Geosci, 5(11): 808-812.

Oman, L., Robock, A., Stenchikov, G.L., Thordarson, T., 2006. *High-latitude eruptions cast shadow over the African monsoon and the flow of the Nile*. Geophysical Research Letters, 33(18).

Ottera, O.H., Bentsen, M., Drange, H., Suo, L.L., 2010. *External forcing as a metronome for Atlantic multidecadal variability*. Nature Geoscience, 3(10): 688-694.

Palmer, A.N., 2007. *Cave geology and speleogenesis over the past 65 years: Role of the national speleological society in advancing the science*. Journal of Cave and Karst Studies, 69(1): 3-12.

Peng, Y.B., Shen, C.M., Wang, W.C., Xu, Y., 2010. *Response of summer precipitation over Eastern China to large volcanic eruptions*. Journal of Climate, 23(3): 818-824.

Pfeiffer, M., Dullo, W.C., 2006. *Monsoon-induced cooling of the western equatorial Indian Ocean as recorded in coral oxygen isotope records from the Seychelles covering the period of 1840-1994 AD*. Quaternary Science Reviews, 25(9-10): 993-1009.

Pfeiffer, M., Dullo, W.C., Eisenhauer, A., 2004. *Variability of the Intertropical Convergence Zone recorded in coral isotopic records from the central Indian Ocean (Chagos Archipelago)*. Quaternary Research, 61(3): 245-255.

Pflitsch, A., Piaseki, J., 2003. *Detection of an airflow system in Niedzwiedia (Bear) Cave, Kletno, Poland.* Journal of Cave and Karst Studies, 65(3): 160-173.

Philander, S.G.H., 1981. *The response of equatorial oceans to a relaxation of the trade winds*. Journal of Physical Oceanography, 11(2): 176-189.

Philipona, R., Behrens, K., Ruckstuhl, C., 2009. *How declining aerosols and rising greenhouse gases forced rapid warming in Europe since the 1980s*. Geophysical Research Letters, 36.

Pokras, E.M., Mix, A.C., 1987. *Earths precession cycle and Quaternary climatic-change in tropical Africa*. Nature, 326(6112): 486-487.

Porter, S.C., An, Z.S., 1995. *Correlation between climate events in the North-Atlantic and China during last glaciation*. Nature, 375(6529): 305-308.

Prell, W.L., Kutzbach, J.E., 1987. *Monsoon variability over the past 150,000 years*. Journal of Geophysical Research-Atmospheres, 92(D7): 8411-8425.

Proctor, C.J., Baker, A., Barnes, W.L., 2002. *A three thousand year record of North Atlantic climate*. Climate Dynamics, ???????.

Proctor, C.J., Baker, A., Barnes, W.L., Gilmour, R.A., 2000. *A thousand year speleothem proxy record of North Atlantic climate from Scotland*. Climate Dynamics, 16(10-11): 815-820.

Przylibski, T.A., Ciezkowski, W., 1999. *Seasonal changes of radon concentration in the Niedzwiedzia Cave (SW Poland)*. Nuovo cimento della Societa Italiana Di Fisica C-Geophysics and Space Physics, 22(3-4): 463-469.

Qian, Y., Giorgi, F., 2000. *Regional climatic effects of anthropogenic aerosols? The case of Southwestern China*. Geophysical Research Letters, 27(21): 3521-3524.

Raible, C.C. et al., 2006. *Climate variability-observations, reconstructions, and model simulations for the Atlantic-European and Alpine region from 1500-2100 AD*. Climatic Change, 79(1-2): 9-29.

Reimer, P.J. et al., 2009. *Intcal09 and Marine09 Radiocarbon Age Calibration Curves, 0-50,000 Years Cal BP*. Radiocarbon, 51(4): 1111-1150.

Renault, P., 1970. *La formation des cavernes*. Que sai-je?, 1400. Presses universitaires de France.

Richards, D.A., Dorale, J.A., 2003. *U-series Chronology and Environmental Applications of Speleothems*. Reviews in Mineralogy and Geochemistry, 52(1): 407-460.

Robertson, A. et al., 2001. *Hypothesized climate forcing time series for the last 500 years*. Journal of Geophysical Research-Atmospheres, 106(D14): 14783-14803.

Robock, A., 2000. *Volcanic eruptions and climate*. Reviews of Geophysics, 38(2): 191-219.

Robock, A., 2002. *Pinatubo eruption - The climatic aftermath*. Science, 295(5558): 1242-1244.

Rodrigo, F.S., Pozo-Vazquez, D., Esteban-Parra, M.J., Castro-Diez, Y., 2001. *A reconstruction of the winter North Atlantic Oscillation index back to AD 1501 using, documentary data in southern Spain*. Journal of Geophysical Research-Atmospheres, 106(D14): 14805-14818.

Rodwell, M.J., Rowell, D.P., Folland, C.K., 1999. *Oceanic forcing of the wintertime North Atlantic Oscillation and European climate*. Nature, 398(6725): 320-323.

Rossignolstrick, M., 1985. *Mediterranean Quaternary Sapropels, an Immediate Response of the African Monsoon to Variation of Insolation*. Palaeogeography Palaeoclimatology Palaeoecology, 49(3-4): 237-263.

Rotstayn, L.D., Lohmann, U., 2002. *Tropical rainfall trends and the indirect aerosol effect*. Journal of Climate, 15(15): 2103-2116.

Rozanski, K., Araguas-Araguas, L., Gonfiantini, R., 1993. *Isotopic patterns in modern global precipitation*. In: Swart, P.K., Lohmann, K.C., McKenzie, J., Savin, S. (Eds.), Climate Change in Continental Isotopic Records. American Geophysical Union, Washington, D.C., pp. 1-36.

Ruckstuhl, C. et al., 2008. *Aerosol and cloud effects on solar brightening and the recent rapid warming*. Geophysical Research Letters, 35(12).

Ruddiman, W.F., 2001. *Earth's Climate, Past and Future*. W.H Freeman, New York, USA, 465 pp.

Saliége, J.F., Fontes, J., 1984. *Essai de détermination expérimentale du fractionnement des isotopes ^{13}C et ^{14}C du carbone au cours de processus naturels*. International Journal of Applied Radiation and Isotopes, 35: 55-62.

Sanchez-Canete, E.P., Serrano-Ortiz, P., Domingo, F., Kowalski, A.S., 2013. *Cave ventilation is influenced by variations in the CO_2-dependent virtual temperature*. International Journal of Speleology, 42(1): 1-8.

Santos, G.M., Southon, J.R., Druffel-Rodriguez, K.C., Griffin, S., Mazon, M., 2004. *Magnesium perchlorate as an alternative water trap in AMS graphite sample preparation: A report on sample preparation at KCCAMS at the University of California, Irvine*. Radiocarbon, 46(1): 165-173.

Santos, G.M., Southon, J.R., Griffin, S., Beaupre, S.R., Druffel, E.R.M., 2007. *Ultra small-mass AMS ^{14}C sample preparation and analyses at KCCAMS/UCI Facility*. Nuclear Instruments and Methods in Physics Research B, 259: 293-302.

Schneider, D.P., Ammann, C.M., Otto-Bliesner, B.L., Kaufman, D.S., 2009. *Climate response to large, high-latitude and low-latitude volcanic eruptions in the Community Climate System Model*. Journal of Geophysical Research-Atmospheres, 114.

Scholz, D., Hoffman, D., 2008. *$^{230}Th/U$-dating of fossil reef corals and speleothems.* . Quarternary Science Review, 57: 52-77.

Schulz, M. et al., 2006. *Radiative forcing by aerosols as derived from the AeroCom present-day and pre-industrial simulations*. Atmospheric Chemistry and Physics, 6: 5225-5246.

Sebela, S., Vaupotic, J., Kostak, B., Stemberk, J., 2010. *Direct measurement of present-day tectonic movement and associated radon flux in Postojna Cave, Slovenia*. Journal of Cave and Karst Studies, 72(1): 21-34.

Self, C.A., Hill, C.A., 2003. *How speleothems grow: an introduction to the ontogeny of cave minerals*. Journal of Cave and Karst Studies, 65(2): 130-151.

Sharp, Z.D., 2007. *Principles of stable isotope geochemistry*. Pearson Prentice Hall, Upper Sadfdle River, NJ.

Sherwin, C.M., Baldini, J.U.L., 2011. *Cave air and hydrological controls on prior calcite precipitation and stalagmite growth rates: Implications for palaeoclimate*

reconstructions using speleothems. Geochimica et Cosmochimica Acta, 75(14): 3915-3929.

Shindell, D.T., Schmidt, G.A., Mann, M.E., Faluvegi, G., 2004. *Dynamic winter climate response to large tropical volcanic eruptions since 1600*. Journal of Geophysical Research-Atmospheres, 109(D5).

Shindell, D.T., Schmidt, G.A., Miller, R.L., Mann, M.E., 2003. *Volcanic and solar forcing of climate change during the preindustrial era*. Journal of Climate, 16(24): 4094-4107.

Shuster, E.T., White, W.B., 1971. *Seasonal fluctuations in the chemistry of limestone springs: a possible means of characterizing carbonate aquifers*. Journal of Hydrology, 14: 93-128.

Sirocko, F., GarbeSchonberg, D., McIntyre, A., Molfino, B., 1996. *Teleconnections between the subtropical monsoons and high-latitude climates during the last deglaciation*. Science, 272(5261): 526-529.

Smart, P.L., Friederich, H., 1987. *Water movement and storage in the unsaturated zone of a maturely karstified carbonate aquifer, Mendip Hills, England*, Proceedings of the Environmental Problems in Karst Terranes and their Solutions Conference, KY, USA, pp. 57-87.

Smithson, P.A., 1991. *Interrelationships between cave and outside air temperatures*. Theoretical and Applied Climatology, 44(1): 65-73.

Solanki, S.K., Unruh, Y.C., 2013. *Solar irradiance variability*. Astronomische Nachrichten, 334(1-2): 145-150.

Southon, J.R., Noronha, A.L., Cheng, H., Edwards, R.L., Wang, Y., 2012. *A high-resolution record of atmospheric ^{14}C based on Hulu Cave speleothem H82*. Quarternary Science Review, 33: 32-41.

Souza, P., Cavalcanti, I.F.A., 2009. *Atmospheric centres of action associated with the Atlantic ITCZ position*. International Journal of Climatology, 29(14): 2091-2105.

Spötl, C., Fairchild, I.J., Tooth, A.F., 2005. *Cave air control on dripwater geochemistry, Obir Caves (Austria): implications for speleothem deposition in dynamically ventilated caves*. Geochimica et Cosmochimica Acta, 69(10): 2451-2468.

Spötl, C., Mattey, D., 2006. *Stable isotope microsampling of speleothems for palaeoenvironmental studies: A comparison of microdrill, micromill and laser ablation techniques*. Chemical Geology, 235(1-2): 48-58.

Steinhilber, F., Beer, J., Frohlich, C., 2009. *Total solar irradiance during the Holocene*. Geophysical Research Letters, 36.

Stevens, B., 2013. *Uncertain then, irrelevant now*. Nature, 503(7474): 47-48.

Stothers, R.B., 2000. *Climatic and demographic consequences of the massive volcanic eruption of 1258*. Climatic Change, 45(2): 361-374.

Stuiver, M., Polach, H.A., 1977. *Discussion: Reporting of ^{14}C data.* Radiocarbon, 19: 355-363.

Stute, M. et al., 1995. *Cooling of Tropical Brazil ($5^{o}C$) during the Last Glacial Maximum*. Science, 269(5222): 379-383.

Su, H., Neelin, J.D., Chou, C., 2001. *Tropical teleconnection and local response to SST anomalies during the 1997-1998 El Nino*. Journal of Geophysical Research-Atmospheres, 106(D17): 20025-20043.

Su, H., Neelin, J.D., Meyerson, J.E., 2004. *Tropical tropospheric, temperature and precipitation response to sea surface temperature forcing*. Earth's Climate: The Ocean-Atmosphere Interaction, 147: 379-392.

Suzuki, A. et al., 2006. *Coral records of the 1990s in the tropical northwest Pacific: ENSO, mass coral bleaching, and global warming*. Geochimica Et Cosmochimica Acta, 70(18): A631-A631.

Tang, K.L., Feng, X.H., 2001. *The effect of soil hydrology on the oxygen and hydrogen isotopic compositions of plants' source water*. Earth and Planetary Science Letters, 185(3-4): 355-367.

Thompson, L.G. et al., 1997. *Tropical climate instability: The last glacial cycle from a Qinghai-Tibetan ice core*. Science, 276(5320): 1821-1825.

Timmreck, C., 2012. *Modeling the climatic effects of large explosive volcanic eruptions*. Wiley Interdisciplinary Reviews-Climate Change, 3(6): 545-564.

Tokinaga, H., Xie, S.P., 2011. *Weakening of the equatorial Atlantic cold tongue over the past six decades*. Nature Geoscience, 4(4): 222-226.

Treble, P., Shelley, J.M.G., Chappell, J., 2003. *Comparison of high resolution sub-annual records of trace elements in a modern (1911-1992) speleothem with instrumental climate data from southwest Australia*. Earth and Planetary Science Letters, 216(1-2): 141-153.

Treble, P.C., Chappell, J., Gagan, M.K., McKeegan, K.D., Harrison, T.M., 2005. *In situ measurement of seasonal $\delta^{18}O$ variations and analysis of isotopic trends in a modem speleothem from southwest Australia*. Earth and Planetary Science Letters, 233(1-2): 17-32.

Trouet, V. et al., 2009. *Persistent positive North Atlantic Oscillation mode dominated the Medieval Climate Anomaly*. Science, 324(5923): 78-80.

Twomey, S., 1974. *Pollution and planetary albedo*. Atmospheric Environment, 8(12): 1251-1256.

Vieira, L.E.A., Solanki, S.K., Krivova, N.A., Usoskin, I., 2011. *Evolution of the solar irradiance during the Holocene*. Astronomy & Astrophysics, 531.

Virk, H.S., Singh, M., Ramola, R.C., 1997. *Radon monitoring for uranium exploration, earthquake prediction and environmental health hazard in Himachal Pradesh, India: an appraisial*. In: Virk, H.S. (Ed.), Rare gas geochemistry - applications in earth and environmental sciecnes. Amristar, Guru Nanak Dev University, pp. 89-99.

Vodila, G.V.G., Palcsu, L., Futo, I., Szanto, Z., 2011. *A 9-year record of stable isotope ratios of precipitation in Eastern Hungary: Implications on isotope hydrology and regional palaeoclimatology*. Journal of Hydrology, 400(1-2): 144-153.

Wackerbarth, A., Scholz, D., Fohlmeister, J., Mangini, A., 2010. *Modelling the $\delta^{18}O$ value of cave drip water and speleothem calcite.* Earth and Planetary Science Letters, 299: 387-397.

Wang, X.F. et al., 2004. *Wet periods in northeastern Brazil over the past 210 kyr linked to distant climate anomalies*. Nature, 432(7018): 740-743.

Wang, Y.J. et al., 2001. *A high-resolution absolute-dated late Pleistocene monsoon record from Hulu Cave, China*. Science, 294: 2345-2348.

Wang, Y.J. et al., 2005a. *The Holocene Asian monsoon: Links to solar changes and North Atlantic climate*. Science, 308(5723): 854-857.

Wang, Y.M., Lean, J.L., Sheeley, N.R., 2005b. *Modeling the sun's magnetic field and irradiance since 1713*. Astrophysical Journal, 625(1): 522-538.

Wanner, H. et al., 2001. *North Atlantic Oscillation-concepts and studies*. Surveys in Geophysics, 22: 321-382.

Wassenburg, J.A. et al., 2013. *Moroccan speleothem and tree ring records suggest a variable positive state of the North Atlantic Oscillation during the Medieval Warm Period*. Earth and Planetary Science Letters, 375: 291-302.

Weber, S.L., 2005. *A timescale analysis of the Northern Hemisphere temperature response to volcanic and solar forcing*. Clim. Past, 1(1): 9-17.

Webster, J.W. et al., 2007. *Stalagmite evidence from Belize indicating significant droughts at the time of Preclassic Abandonment, the Maya Hiatus, and the Classic Maya collapse*. Palaeogeography Palaeoclimatology Palaeoecology, 250(1-4): 1-17.

White, D.E., White, J.M.C., Steig, E.J., Barlow, L.K., 1997. *Reconstructing annual and seasonal climatic responses from volcanic events since AD 1270 as recorded in the deuterium signal from the Greenland Ice Sheet Project 2 ice core*. Journal of Geophysical Research-Atmospheres, 102(D16): 19683-19694.

Wigley, T.M.L., 1967. *Non-steady flow through a porous medium and cave breathing*. Journal of Geophysical Research, 72: 3199-3205.

Wigley, T.M.L., Plumer, L.N., Pearson, F.J., 1978. *Mass transfer and carbon isotope evolution in natural water system*. Geochimica et Cosmochimica Acta, 42(1117-11139).

Wild, M., Ohmura, A., Makowski, K., 2007. *Impact of global dimming and brightening on global warming*. Geophysical Research Letters, 34(4).

Wilson, R. et al., 2010. *Reconstructing ENSO: the influence of method, proxy data, climate forcing and teleconnections*. Journal of Quaternary Science, 25(1): 62-78.

Wong, C.I., Banner, J.L., Musgrove, M., 2011. *Seasonal dripwater Mg/Ca and Sr/Ca variations driven by cave ventilation: Implications for and modeling of speleothem paleoclimate records*. Geochimica Et Cosmochimica Acta, 75(12): 3514-3529.

Wu, Y. et al., 2003. *Radon concentration: A tool for assessing the fracture network at Guanyinyan study area, China*. Water Sa, 29(1): 49-53.

Xu, J.D. et al., 2013. *Climatic impact of the Millennium eruption of Changbaishan volcano in China: New insights from high-precision radiocarbon wiggle-match dating*. Geophysical Research Letters, 40(1): 54-59.

Yadava, M.G., Ramesh, R., 2005. *Monsoon reconstruction from radiocarbon dated tropical Indian speleothems*. The Holocene, 15(1): 48-59.

Yancheva, G. et al., 2007. *Influence of the intertropical convergence zone on the East Asian monsoon*. Nature, 445(7123): 74-77.

Yoshimori, M. & Broccoli, A. J. *Equilibrium response of an atmosphere-mixed layer ocean model to different radiative forcing agents: Global and zonal mean response*. Journal of Climate. 21, 4399-4423 (2008).

Yuan, D. et al., 2004. *Timing, duration, and transitions of the last interglacial Asian monsoon*. Science, 304: 575-578.

Zanchettin, D. et al., 2012. *Bi-decadal variability excited in the coupled ocean-atmosphere system by strong tropical volcanic eruptions*. Climate Dynamics, 39(1-2): 419-444.

Zebiak, S.E., Cane, M.A., 1987. *A model El-Nino Southern Oscillation*. Monthly Weather Review, 115(10): 2262-2278.

Zhang, P.Z. et al., 2008. *A test of climate, sun, and culture relationships from an 1810-year chinese cave record*. Science, 322(5903): 940-942.

Zhang, X. et al., 2007. *Detection of human influence on twentieth-century precipitation trends*. Nature, 448(7152): 461-465.

Zhong, Y. et al., 2011. *Centennial-scale climate change from decadally-paced explosive volcanism: a coupled sea ice-ocean mechanism*. Climate Dynamics, 37(11-12): 2373-2387.

Zielinski, G.A., 2000. *Use of paleo-records in determining variability within the volcanism–climate system*. Quaternary Science Reviews, 19(1–5): 417-438.

Zielinski, G.A. et al., 1994. *Record of volcanism since 7000-BC from the GISP2 Greenland ice core and implications for the volcano-climate system*. Science, 264(5161): 948-952.

Zielinski, G.A. et al., 1995. *The Gisp Ice Core Record of Volcanism since 7000-Bc - Reply*. Science, 267(5195): 257-258.

Appendix A

Development and Disintegration of Maya Political Systems in Response to Climate Change

Douglas J. Kennett *et al.*

Science **338**, 788 (2012);
DOI: 10.1126/science.1226299

Science (print ISSN 0036-8075; online ISSN 1095-9203) is published weekly, except the last week in December, by the American Association for the Advancement of Science, 1200 New York Avenue NW, Washington, DC 20005.

deposited mineral phases within fissures and cracks. The martian weathering products are the most likely source of the required LREE, incompatible, and volatile elements. Upon impact, preferential, shock-induced melting occurred in the target rock along fractures where weathering products were concentrated. This melting produced the black glass and retained in it chemical signatures characteristic of the martian surface. Shock melting also trapped a component derived from the martian atmosphere, as revealed by stepped combustion–mass spectrometry. About 0.7 My ago, the sample was ejected from Mars and eventually landed on Earth in July 2011. The martian weathering features in Tissint described here are compatible with spacecraft observations on Mars, including those made by the NASA Viking landers, MER Spirit rover, and ESA's Mars Express orbiter (*5*, *21*–*23*).

References and Notes

1. D. D. Bogard, P. Johnson, *Science* **221**, 651 (1983).
2. R. H. Becker, R. O. Pepin, *Earth Planet. Sci. Lett.* **69**, 225 (1984).
3. A. H. Treiman, J. D. Gleason, D. D. Bogard, *Planet. Space Sci.* **48**, 1213 (2000).
4. G. Crozaz, M. Wadhwa, *Geochim. Cosmochim. Acta* **65**, 971 (2001).
5. Supplementary materials are available on *Science* Online.
6. P. Rochette *et al.*, *Meteorit. Planet. Sci.* **40**, 529 (2005).
7. A. O. Nier, M. B. McElroy, *J. Geophys. Res.* **82**, 4341 (1977).
8. I. A. Franchi, I. P. Wright, A. S. Sexton, C. T. Pillinger, *Meteorit. Planet. Sci.* **34**, 657 (1999).
9. J. Blichert-Toft, J. D. Gleason, P. Télouk, F. Albarède, *Earth Planet. Sci. Lett.* **173**, 25 (1999).
10. G. Dreibus *et al.*, *Meteorit. Planet. Sci.* **35**, A49 (2000).
11. J. A. Barrat, J. Blichert-Toft, R. W. Nesbitt, F. Keller, *Meteorit. Planet. Sci.* **36**, 23 (2001).
12. C. R. Neal, L. A. Taylor, J. C. Ely, J. C. Jain, M. A. Nazarov, *Lunar Planet. Sci.* **32**, 1671 (2001).
13. B. Marty, K. Hashizume, M. Chaussidon, R. Wieler, *Space Sci. Rev.* **106**, 175 (2003).
14. T. Owen *et al.*, *J. Geophys. Res.* **82**, 4635 (1977).
15. J.-A. Barrat *et al.*, *Geochim. Cosmochim. Acta* **66**, 3505 (2002).
16. V. Sautter *et al.*, *Earth Planet. Sci. Lett.* **195**, 223 (2002).
17. P. Beck *et al.*, *Geochim. Cosmochim. Acta* **70**, 2127 (2006).
18. D. W. Mittlefehldt, M. M. Lindstrom, *Geochim. Cosmochim. Acta* **67**, 1911 (2003).
19. M. N. Rao, L. E. Borg, D. S. McKay, S. J. Wentworth, *Geophys. Res. Lett.* **26**, 3265 (1999).
20. E. L. Walton, P. J. Jugo, C. D. K. Herd, M. Wilke, *Geochim. Cosmochim. Acta* **74**, 4829 (2010).
21. R. E. Arvidson, J. L. Gooding, H. J. Moore, *Rev. Geophys.* **27**, 39 (1989).
22. L. A. Haskin *et al.*, *Nature* **436**, 66 (2005).
23. A. Gendrin *et al.*, *Science* **307**, 1587 (2005).
24. J. A. Barrat *et al.*, *Geochim. Cosmochim. Acta* **83**, 79 (2012).
25. K. Marti, J. S. Kim, A. N. Thakur, T. J. McCoy, K. Keil, *Science* **267**, 1981 (1995).

Acknowledgments: We acknowledge D. N. Menegas and family for their generous donation enabling the acquisition of Tissint (BM.2012,M1), M. Aoudjehane for fieldwork, A. Aaranson for field information, J. Gibson for assistance with oxygen isotope analysis, L. Labenne for loan of a sample, and A. Irving for 400 mg of powdered sample. This study was funded at Hassan II University Casablanca, Faculté des Sciences Ain Chock, by Centre de Recherches Scientifiques et Techniques Morocco and CNRS France (Projet International de Coopération Scientifique, Sciences de l'Univers 01/10), and by Comité Mixte Inter Universitaire Franco-Marocain Volubilis (MA/11/252); CRPG Nancy, France, by the CNES, CNRS, and European Research Council under the European Community's Seventh Framework Programme (FP7/2007-2013 no. 267255); Université de Bretagne Occidentale–Institut Universitaire Européen de la Mer, Plouzané, France, by the Programme National de Planétologie, Institut National des Sciences de l'Univers; Open University, by Science and Technology Facilities Council grant to the Planetary and Space Sciences Discipline; and University of Alberta, by the Natural Sciences and Engineering Research Council of Canada (grant 261740-03).

Supplementary Materials

www.sciencemag.org/cgi/content/full/science.1224514/DC1
Materials and Methods
Supplementary Text
Figs. S1 to S11
Tables S1 to S13
References (*26*–*35*)

9 May 2012; accepted 25 September 2012
Published online 11 October 2012;
10.1126/science.1224514

Development and Disintegration of Maya Political Systems in Response to Climate Change

Douglas J. Kennett,[1]*† Sebastian F. M. Breitenbach,[2]* Valorie V. Aquino,[3] Yemane Asmerom,[4] Jaime Awe,[5] James U.L. Baldini,[6] Patrick Bartlein,[7] Brendan J. Culleton,[1] Claire Ebert,[1] Christopher Jazwa,[1] Martha J. Macri,[8] Norbert Marwan,[9] Victor Polyak,[4] Keith M. Prufer,[3] Harriet E. Ridley,[6] Harald Sodemann,[10] Bruce Winterhalder,[11] Gerald H. Haug[2]

The role of climate change in the development and demise of Classic Maya civilization (300 to 1000 C.E.) remains controversial because of the absence of well-dated climate and archaeological sequences. We present a precisely dated subannual climate record for the past 2000 years from Yok Balum Cave, Belize. From comparison of this record with historical events compiled from well-dated stone monuments, we propose that anomalously high rainfall favored unprecedented population expansion and the proliferation of political centers between 440 and 660 C.E. This was followed by a drying trend between 660 and 1000 C.E. that triggered the balkanization of polities, increased warfare, and the asynchronous disintegration of polities, followed by population collapse in the context of an extended drought between 1020 and 1100 C.E.

The Classic Maya (300 to 1000 C.E.) left a remarkable historical record inscribed on well-dated stone monuments. Wars, marriages, and accessions of kings and queens are tied to long count calendar dates and correlate with specific days in the Christian calendar (Goodman-Thompson-Martinez correlation). The termination of this tradition between 800 and 1000 C.E. marks the widespread collapse of Classic Maya political systems. Multidecadal drought has been implicated, but remains controversial because of dating uncertainties and insufficient temporal resolution in paleoclimatic records. Lake sediments from the Yucatan Peninsula provided the first evidence of substantial drying in the Terminal Classic (*1*). However, disturbances to lake sediment sequences caused by prehistoric deforestation and agricultural expansion during the Classic Period complicate reproducing these results near the largest and most politically important Maya centers (such as Tikal and Caracol). Several studies more distant from the Maya lowlands (ML) support either relatively dry conditions or a series of droughts during the Terminal Classic (*2*–*5*), but the relevance of these records for the ML remains unclear (*6*).

Cave deposits in the ML show great promise for paleoclimatic reconstruction (*7*–*9*). The challenge lies in developing long, continuous records from rapidly growing stalagmites that can be dated precisely by using ^{234}U-^{230}Th (U-Th). Here, we present a subannually resolved rainfall record from an exceptionally well-dated stalagmite collected from Yok Balum (YB) Cave in Belize (16°12'30.780" N, 89°4'24.420" W, 366 m above sea level) (*10*). YB cave is located 1.5 km from the Classic Period Maya site of Uxbenká. Three other important Maya centers (Pusilha, Lubaantun, Nim Li Punit) are within 30 km (fig. S1); Tikal and other major Classic Period population centers (such as Caracol, Copan, and Calakmul) are

[1]Department of Anthropology, Pennsylvania State University, University Park, PA 16802, USA. [2]Department of Earth Science, Eidgenössische Technische Hochschule (ETH), CH-8092 Zürich, Switzerland. [3]Department of Anthropology, University of New Mexico, Albuquerque, NM 87131, USA. [4]Department of Earth and Planetary Sciences, University of New Mexico, Albuquerque, NM 87131, USA. [5]Institute of Archaeology, National Institute of Culture and History, Belmopan, Belize. [6]Department of Earth Sciences, University of Durham, Durham DH1 3LE, UK. [7]Department of Geography, University of Oregon, Eugene, OR 97403, USA. [8]Department of Native American Studies, University of California, Davis, Davis, CA 95616, USA. [9]Potsdam Institute for Climate Impact Research, Post Office Box 60 12 03, 14412 Potsdam, Germany. [10]Institute for Atmospheric and Climate Science, ETH, CH-8092 Zürich, Switzerland. [11]Department of Anthropology, University of California, Davis, Davis, CA 95616, USA.

*These authors contributed equally to this work.
†To whom correspondence should be addressed. E-mail: djk23@psu.edu

within 200 km and are influenced by the same climate systems (fig. S8). Age control of our climate reconstruction is comparable in precision with the historical record, providing a foundation for examining the complex nature of political dynamics in response to climate change.

In 2006, we collected a 56-cm-long stalagmite (YOK-I) from 50 m inside the western entrance of the cave (figs. S2 and S3). Forty U-Th dates indicate that the upper 415 mm of the stalagmite grew continuously between 40 B.C.E. and 2006 C.E. (table S2 and fig. S4). Analytical precision for the U-Th dates ranges from ±1 to ±17 years, and time averaging related to sample drilling is ~20 years (table S3 and fig. S5). The climate record is based on >4200 oxygen isotope ($\delta^{18}O$) measurements taken continuously in 0.1-mm increments, representing a mean temporal resolution of 0.5 years (table S4 and fig. S6). Monitoring data from YB cave combined with Hendy tests on stalagmite and glass drip plate carbonate indicate that $\delta^{18}O$ values reflect rainfall amount above the cave and that minor kinetic effects exist that increase $\delta^{18}O$ values, possibly enhancing the signal when climate conditions are dry (figs. S9 to S14). The $\delta^{18}O$ record ranges from –5.2 to –2.5 per mil (‰) and oscillates on decadal to multicentennial scales (Fig. 1). Multidecadal droughts occur between ~200 to 300, 820 to 870, 1020 to 1100, and 1530 to 1580 C.E., and the high-resolution YOK-I record permits the identification of other shorter and occasionally very severe droughts, particularly centered on AD 420, 930, and 1800. The $\delta^{18}O$ record is considered unreliable in the 20th century and not a reflection of drought conditions (fig. S7) (*10*).

We argue that climate variability was predominantly driven by Intertropical Convergence Zone (ITCZ) migration and changes in El Niño frequency, the linkage being a general perturbation of tropical climate (Walker Circulation) accompanying El Niño–Southern Oscillation (ENSO)–time scale variability. During El Niño years, the ITCZ is positioned over the eastern equatorial Pacific, and boreal summer moisture delivery to the ML decreases (*11*). Strengthened vertical wind shear linked to ITCZ position during El Niño years reduces the number of tropical depressions, storms, and hurricanes crossing the ML. Power spectral analyses of the YOK-I $\delta^{18}O$ record shows statistically significant periodicities centered on 3 to 8 years, which is consistent with a strong ENSO signal (fig. S15). Previous research used titanium concentrations in marine sediments from the Cariaco Basin to reconstruct ITCZ-related rainfall changes over the ML (*2*, *11*). We tuned the past 2000 years of the Cariaco Ti chronology within that record's errors using our high-precision U-Th chronology (Fig. 1B and fig. S16). A correlation may exist between the YOK-I $\delta^{18}O$ record and other lower-resolution records from the ML, including Lake Chichancanab sediment density record (Fig. 1C) (*12*), Lake Punta Laguna ostracod $\delta^{18}O$ record (Fig. 1D) (*13*), and the Macal Chasm speleothem luminescence record (Fig. 1E) (*8*). However, statistically significant correlations between these records are difficult to demonstrate because the chronological uncertainties of older records allow for a range of correlation coefficients. Given these uncertainties, we cannot definitively link these regional records, but visually similar trends are evident on multidecadal time scales (fig. S17).

We hypothesize that precipitation-induced changes in agricultural productivity mediated the tendency toward political integration or disintegration in the ML. Droughts recorded in the Yucatan between 1535 and 1575 C.E. (*14*) correspond to one of four multidecadal droughts evident in the YOK-I record (Fig. 2). The interval from 1535 to 1542 C.E. was particularly dry. Historical accounts link this drought to reduced agricultural productivity, famine, disease, death, and population relocation. Some estimates suggest that drought-related agricultural disaster caused nearly a million deaths in Mexico in 1535 C.E. (*15*), illustrating how meteorologically dry conditions presage agricultural drought with severe effects scaled to population density and level of agricultural intensification.

A dry period comparable with the historical drought of 1535 C.E. is evident in the YOK-I record

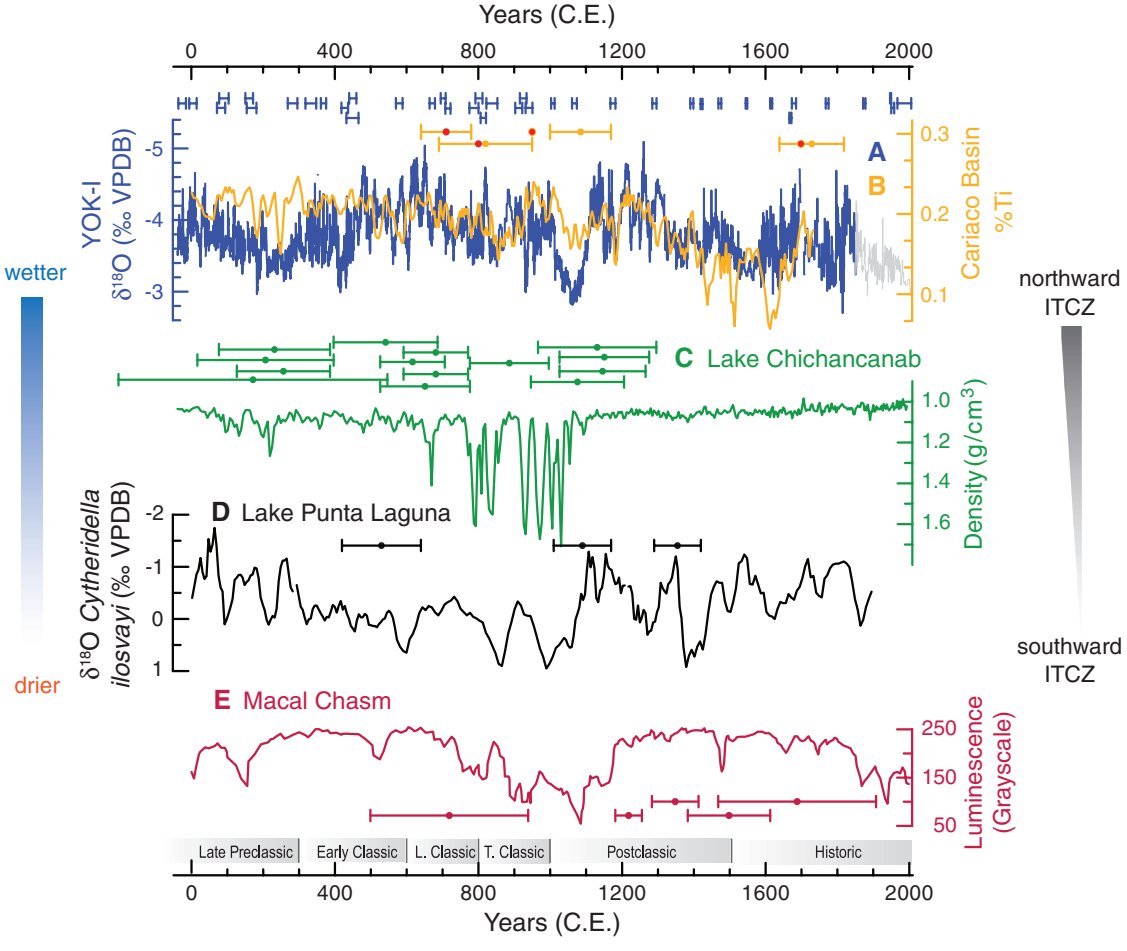

Fig. 1. Comparison of (**A**) stalagmite YOK-I $\delta^{18}O$ with (**B**) Tuned (red dots) (*10*) bulk sediment titanium record from the Cariaco Basin, Venezuela (*11*). (**C**) Lake Chichancanab sediment density record (*12*). (**D**) Lake Punta Laguna ostracod (*Cytheridella ilosvayi*) $\delta^{18}O$ record (*13*). (**E**) Macal Chasm speleothem luminescence record (*8*). Similarities in the YOK-I and Cariaco records suggest that rainfall variability was strongly modulated by ITCZ migration. Age models for each record are based on calibrated ^{14}C or U-Th, with error bars showing the relative chronological precision of each record. Smoothed records that emphasize multidecadal trends are shown in fig. S17. The light gray line denotes uncertainties in the 20th- century $\delta^{18}O$ record (details and climate archive locations are available in the supplementary materials).

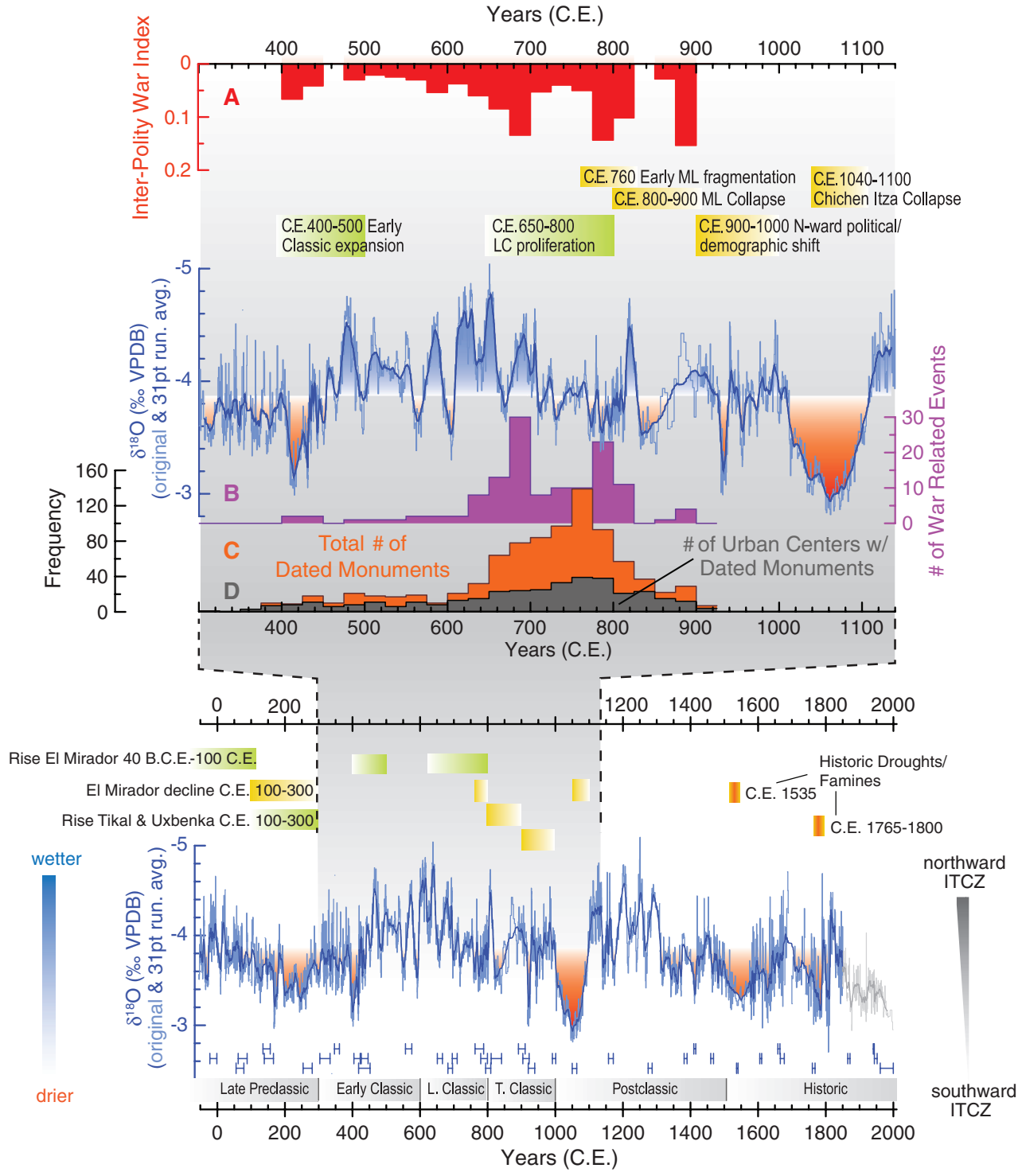

Fig. 2. (Bottom) YOK-I $\delta^{18}O$ climate record spanning the past 2000 years (40 B.C.E. to 2006 C.E.) shown relative to Maya chronology and major historical events. Blue bars just below the $\delta^{18}O$ curve indicate the small error for each of the 40 U-Th dates used to constrain the chronology of the $\delta^{18}O$ climate record (*10*). Drier-than-average conditions during this interval are shown in orange. Two historically recorded droughts in the 16th- and 18th-century C.E. accord well with the YOK-I record, and the earliest multidecadal drought in the record (200 to 300 C.E.) corresponds with decline of the large center of El Mirador and a major sociopolitical reorganization in the ML. (Top) The YOK-I $\delta^{18}O$ climate record between 300 and 1140 C.E. shown relative to major historic events along with (**A**) An interpolity warfare index based on the number of war-related events between Maya sites or rulers relative to the total number of events recorded during each interval. (**B**) Raw number of war-related events. (**C**) Frequency distribution of long-count dated monuments in the ML. (**D**) Total number of urban centers with dated monuments through time as a proxy for the development and disintegration of complex polities in the ML. All hieroglyphic data are from the Maya Hieroglyphic database (raw data is available in the supplementary materials) (*28*) and are binned in 25-year intervals. The light gray line denotes uncertainties in the 20th-century $\delta^{18}O$ record (*10*).

at the end of the Preclassic Period (200 to 300 C.E.). Maya populations had expanded across the ML during the Middle and Late Preclassic Periods (1000 B.C.E. to 100 C.E.), exploiting productive agricultural soils and seasonal wetlands (*16, 17*). Multiple fully developed polities emerged in the ML (*18*), including the large center of El Mirador in northern Guatemala (*19*). The drying trend evident in the YOK-I record starting at 100 C.E. culminated in a century-long dry interval (200 to 300 C.E.) that corresponds to the demise of El Mirador, which is consistent with the hypothesis that drought played a role in the political realignment and reorganization of ML population centers between 150 to 300 C.E. (*12*). Several ML polities persisted, however, and became more integrated and grew in size, including Uxbenká (*20*).

Tikal, already established in the central Peten (Guatemala) as an important regional center during the Middle and Late Preclassic (1000 B.C.E. to 300 C.E.), emerged as a dominant sociopolitical force in the wake of the climatic and social instability of the 3rd and 4th centuries C.E. (*21*). Tikal, Calakmul, and other important sites in the central Peten were positioned near seasonal wetlands under intensive use (*22*). High rainfall during the Early Classic evident in the YOK-I record (Fig. 2) maintained these wetlands and seasonally recharged constructed water storage systems (reservoirs and tanks) (*23*). This helps to explain the growing geopolitical influence of polities like Tikal, Calakmul, Caracol, and Naranjo. Many of the best-recorded ruling Maya lineages were founded around 440 to 500 C.E. (*24*) during this interval of anomalously high rainfall. The overall number of monument-bearing political centers and indications of war among them also increased throughout the Early Classic (300 to 650 C.E.) (Fig. 2).

Terminal Classic Period droughts have been cited as causes of societal collapse in the Maya lowlands (*1*). The YOK-I record is consistent with this hypothesis, showing a multidecadal drought at this time (820 to 870 C.E.). This finding is consistent with arguments for a ~40% reduction in summer rainfall during the Terminal Classic Period (*9*). Multidecadal drought between 820 and 870 C.E. was part of a broader regional drying trend starting 640 C.E., culminating at 1020 C.E. in a century-long dry period that is the most pronounced in our record. The early stages of this drying trend correspond with an increase in interpolity warfare (Fig. 2, A and B) and expansion in the number of competing political centers, enumerated here from long count-dated historical texts (Fig. 2, C and D, and tables S7 and S8). War-related events increased during a dry interval between 640 and 660 C.E., but then peaked after a lag during a wetter interval between 660 and 700 C.E. Climate drying after 640 C.E. may have exacerbated environmental degradation that occurred with 5th- and 6th-century C.E. population expansion under a wetter climatic regime. Drying constrained agricultural productivity, stimulated inter-polity warfare (*25*), and promoted political competition and fissioning that was ultimately unsustainable.

The first evidence for political fragmentation occurred in the Petexbatun region between 760 and 800 C.E. (*26*), corresponding with a dry interval in the YOK-I record, peak population densities throughout the region (145 people per km^2) (*27*), and the maximum spatial extent of monument-bearing urban centers (Fig. 2, C and D). Historical texts on stone monuments were dedicated in at least 39 centers from 750 to 775 C.E., with rulers commissioning monuments at several large centers at unprecedented rates. These texts point to a dynamic and unstable geopolitical landscape centered on status rivalry, war, and strategic alliances (*28*). A precipitous drop in the number of texts at key centers (such as Tikal) between 775 and 800 C.E. was the precursor to a 50% drop in the number of centers with text-dated monuments between 800 and 825 C.E., which is evidence for widespread failure of these political systems. Increasing interpolity warfare (Fig. 2A) is most evident in the historical record between 780 and 800 C.E. Political power became decentralized as the institution of divine kingship collapsed between 780 and 900 C.E. Less is known about the fate of the people integrated into these polities, but depopulation took centuries and entailed migration, reorganization (*29*, *30*), and persistence in the environs surrounding abandoned cities (such as Mopan Valley, Guatemala) (*21*). Centers of political importance shifted to the northern parts of the Yucatan Peninsula as carved stone monuments were commissioned less frequently in the central Peten; the tradition ended at Chichen Itza sometime between 1000 and 1100 C.E. during the longest and driest interval of the past 2000 years.

ITCZ migration–influenced climate variability in the ML as recorded in YOK-I aids in understanding the complex socio-natural processes associated with Maya political dynamics during the past 2000 years. Population increases and the expansion of Classic Maya polities were favored by anomalously high rainfall and increased agricultural productivity between 440 and 660 C.E. High-density Maya populations were increasingly susceptible to the agricultural consequences of climate drying. We propose that a two-stage collapse commenced with the 660 C.E. drying trend. It triggered the balkanization of polities, increased warfare, and abetted overall sociopolitical destabilization. Political disintegration in the Petexbatun region foreshadows two multidecadal dry intervals that further reduced agricultural yields and caused more widespread political disintegration between 800 and 900 C.E. This was followed by a second stage of more gradual population decline and then punctuated population reductions during the most extreme dry interval in the YOK-I record between 1020 and 1100 C.E. The linkage between extended 16th-century drought, crop failures, death, famine, and migration in Mexico provides a historic analog evident in the YOK-I record for the sociopolitical tragedy and human suffering experienced by the 11th-century Maya. It also helps explain why the cultural elaboration evident during the Classic Period never fully redeveloped.

References and Notes

1. D. A. Hodell, J. H. Curtis, M. Brenner, *Nature* **375**, 391 (1995).
2. G. H. Haug *et al.*, *Science* **299**, 1731 (2003).
3. S. E. Metcalfe, M. D. Jones, S. J. Davies, A. Noren, A. MacKenzie, *Holocene* **20**, 1195 (2010).
4. D. W. Stahle *et al.*, *Geophys. Res. Lett.* **38**, L05703 (2011).
5. M. S. Lachniet, J. P. Bernal, Y. Asmerom, V. Polyak, D. Piperno, *Geology* **40**, 259 (2012).
6. J. Aimers, D. Hodell, *Nature* **479**, 44 (2011).
7. A. B. Frappier, D. Sahagian, S. J. Carpenter, L. A. González, B. R. Frappier, *Geology* **35**, 111 (2007).
8. J. W. Webster *et al.*, *Palaeogeogr. Palaeoclimatol. Palaeoecol.* **250**, 1 (2007).
9. M. Medina-Elizalde, E. J. Rohling, *Science* **335**, 956 (2012).
10. Materials and methods are available as supplementary material on *Science* Online.
11. G. H. Haug, K. A. Hughen, D. M. Sigman, L. C. Peterson, U. Röhl, *Science* **293**, 1304 (2001).
12. D. A. Hodell, M. Brenner, J. H. Curtis, *Quat. Sci. Rev.* **24**, 1413 (2005).
13. J. H. Curtis, D. A. Hodell, M. Brenner, *Quat. Res.* **46**, 37 (1996).
14. B. Mendoza, V. García-Acosta, V. Velasco, E. Jáuregui, R. Díaz-Sandoval, *Clim. Change* **83**, 151 (2007).
15. V. García-Acosta, J. M. Pérez-Zevallos, A. Molina del Villar, *Desastres Agrícolas en México. Catálogo Histórico. Tomo I: Épocas Prehispánica y Colonial* (Fondo de Cultura Económica and CIESAS, México, 2003), pp. 958–1822.
16. N. P. Dunning *et al.*, *Ann. Assoc. Am. Geogr.* **92**, 267 (2002).
17. S. Luzzadder-Beach, T. P. Beach, N. P. Dunning, *Proc. Natl. Acad. Sci. U.S.A.* **109**, 3646 (2012).
18. F. Estrada-Belli, *The First Maya Civilization: Ritual and Power Before the Classic Period* (Routledge, London, 2011).
19. R. D. Hansen, S. Bozarth, J. Jacob, D. Wahl, T. Schreiner, *Ancient Mesoamerica* **13**, 273 (2002).
20. B. J. Culleton, K. M. Prufer, D. J. Kennett, *J. Archeologic. Sci.* **39**, 1572 (2012).
21. J. P. Laporte, V. Fialko, *Ancient Mesoamerica* **6**, 41 (1995).
22. T. Beach *et al.*, *Quat. Sci. Rev.* **28**, 1710 (2009).
23. V. L. Scarborough *et al.*, *Proc. Natl. Acad. Sci. U.S.A.* **109**, 12408 (2012).
24. S. Martin, N. Grube, *Chronicle of the Maya Kings and Queens* (Thames & Hudson, London, 2008).
25. D. Webster, *The Fall of the Ancient Maya: Solving the Mystery of the Maya Collapse* (Thames and Hudson, London, 2002).
26. A. Demarest, *Ancient Maya: The Rise and Fall of a Rainforest Civilization* (Cambridge Univ. Press, Cambridge, 2004).
27. T. P. Culbert, D. S. Rice, Eds., *Precolumbian Population History in the Maya Lowlands* (Univ. of New Mexico Press, Albuquerque, 1990).
28. J. L. Munson, M. J. Macri, *J. Anthropol. Archaeol.* **28**, 424 (2009).
29. J. A. Sabloff, *Proc. Am. Philos. Soc.* **151**, 11 (2007).
30. P. M. Rice, D. S. Rice, in *The Terminal Classic in the Maya Lowlands: Collapse, Transition, and Transformation*, A. A. Demarest, P. M. Rice, D. S. Rice, Eds. (Univ. Press of Colorado, Boulder, CO, 2004), pp. 125–139.

Acknowledgments: We thank D. Hodell, M. Brenner, J. Yaeger, J. Lohse, J. Kennett, D. Webster, and three anonymous reviewers for their useful comments. Thanks to H. Meyer (AWI Potsdam for isotope analysis of rain and drip water. This research was supported by NSF (HSD-0827305, BCS-0940744, and EAR-0326902), European Research Council (240167), Swiss National Foundation (CRSI22-132646/1), the German Science Foundation (DFG FOR1380 "HIMPAC"), and the Alphawood Foundation.

Supplementary Materials

www.sciencemag.org/cgi/content/full/338/6108/788/DC1
Materials and Methods
Figs. S1 to S17
Tables S1 to S8
References (*31–211*)

19 June 2012; accepted 26 September 2012
10.1126/science.1226299

Appendix B

Sample depth (mm)	Date (C.E.)	$\delta^{13}C$ (‰VPDB)	$\delta^{18}O$ (‰VPDB)	Sample depth (mm)	Date (C.E.)	$\delta^{13}C$ (‰VPDB)	$\delta^{18}O$ (‰VPDB)
0.10		-7.76	-3.55	4.70		-7.24	-3.25
0.20		-7.66	-3.46	4.80		-7.57	-3.20
0.30		-7.71	-3.54	4.90		-7.54	-3.24
0.40		-7.64	-3.44	5.00		-7.70	-3.13
0.50		-7.56	-3.51	5.10		-7.94	-3.25
0.60		-7.42	-3.16	5.20		-8.08	-3.26
0.70		-7.50	-3.52	5.30		-8.23	-3.40
0.80		-7.44	-3.42	5.40		-8.06	-3.27
0.90		-7.66	-3.60	5.50		-7.98	-3.27
1.00		-7.32	-3.35	5.60		-7.90	-3.22
1.10		-7.08	-3.29	5.70		-8.07	-3.25
1.20		-6.87	-3.00	5.80		-7.94	-3.22
1.30		-7.10	-3.22	5.90		-7.91	-3.27
1.40		-7.12	-3.38	6.00		-7.99	-3.34
1.50		-6.94	-3.33	6.10		-6.93	-2.92
1.60		-6.73	-3.23	6.20		-8.33	-3.34
1.70		-6.63	-3.26	6.30		-8.43	-3.41
1.80		-6.76	-3.32	6.40		-8.68	-3.48
1.90		-6.74	-3.26	6.50	1983.54	-8.72	-3.51
2.00		-6.73	-3.29	6.60	1983.48	-8.50	-3.57
2.10		-6.68	-3.28	6.70	1983.40	-8.48	-3.53
2.20		-6.72	-3.23	6.80	1983.29	-8.36	-3.58
2.30		-6.75	-3.25	6.90	1983.16	-8.57	-3.65
2.40		-6.76	-3.29	7.00	1983.00	-8.62	-3.64
2.50		-6.74	-3.16	7.10	1982.84	-8.89	-3.74
2.60		-6.81	-3.23	7.20	1982.68	-9.01	-3.75
2.70		-6.87	-3.09	7.30	1982.54	-9.33	-3.90
2.80		-6.95	-3.15	7.40	1982.45	-9.35	-3.91
2.90		-7.07	-3.14	7.50	1982.38	-9.16	-3.75
3.00		-7.22	-3.16	7.60	1982.29	-8.50	-3.65
3.10		-7.23	-3.18	7.70	1982.07	-8.75	-3.69
3.20		-7.36	-3.22	7.80	1981.77	-8.59	-3.75
3.30		-7.41	-3.11	7.90	1981.54	-8.76	-3.72
3.40		-8.27	-3.24	8.00	1981.44	-8.61	-3.61
3.50		-7.33	-3.15	8.10	1981.38	-8.60	-3.70
3.60		-7.25	-3.18	8.20	1981.29	-8.44	-3.62
3.70		-7.15	-3.03	8.30	1981.12	-8.53	-3.66
3.80		-7.22	-3.11	8.40	1980.92	-8.47	-3.63
3.90		-7.19	-3.12	8.50	1980.71	-8.69	-3.66
4.00		-7.16	-3.20	8.60	1980.54	-8.85	-3.63
4.10		-7.12	-3.13	8.70	1980.45	-8.70	-3.65
4.20		-7.02	-3.22	8.80	1980.43	-8.66	-3.70
4.30		-7.11	-3.19	8.90	1980.42	-8.31	-3.60
4.40		-7.00	-3.19	9.00	1980.39	-8.35	-3.51
4.50		-7.18	-3.23	9.10	1980.29	-8.30	-3.60
4.60		-7.09	-3.10	9.20	1980.06	-8.51	-3.64

Sample depth (mm)	Date (C.E.)	$\delta^{13}C$ (‰VPDB)	$\delta^{18}O$ (‰VPDB)	Sample depth (mm)	Date (C.E.)	$\delta^{13}C$ (‰VPDB)	$\delta^{18}O$ (‰VPDB)
9.30	1979.77	-8.45	-3.50	13.90	1972.65	-9.19	-3.92
9.40	1979.54	-8.68	-3.59	14.00	1972.54	-9.29	-4.01
9.50	1979.42	-8.52	-3.56	14.10	1972.46	-8.25	-3.54
9.60	1979.29	-8.25	-3.44	14.20	1972.42	-9.23	-3.81
9.70	1979.11	-8.39	-3.47	14.30	1972.37	-8.27	-3.62
9.80	1978.92	-8.54	-3.51	14.40	1972.29	-8.09	-3.38
9.90	1978.72	-8.88	-3.58	14.50	1972.13	-8.34	
10.00	1978.54	-8.98	-3.55	14.60	1971.92	-8.31	-3.54
10.10	1978.44	-8.60	-3.55	14.70	1971.70	-8.68	-3.68
10.20	1978.38	-8.79	-3.47	14.80	1971.54	-8.83	-3.72
10.30	1978.29	-8.58	-3.53	14.90	1971.45	-8.51	-3.74
10.40	1978.07	-8.58	-3.54	15.00	1971.38	-8.12	-3.51
10.50	1977.77	-8.62	-3.42	15.10	1971.29	-7.97	-3.59
10.60	1977.54	-8.83	-3.52	15.20	1971.16	-8.53	-3.65
10.70	1977.44	-8.76	-3.57	15.30	1971.00	-8.31	-3.72
10.80	1977.43	-8.46	-3.41	15.40	1970.83	-8.60	-3.73
10.90	1977.42	-8.45	-3.48	15.50	1970.67	-8.82	-3.80
11.00	1977.39	-8.28	-3.35	15.60	1970.54	-8.98	-3.67
11.10	1977.29	-8.18	-3.36	15.70	1970.46	-8.75	-3.86
11.20	1977.06	-8.47	-3.49	15.80	1970.42	-8.59	-3.42
11.30	1976.76	-8.67	-3.45	15.90	1970.41	-8.37	
11.40	1976.54	-8.84	-3.55	16.00	1970.37	-8.13	-3.65
11.50	1976.45	-8.67	-3.40	16.10	1970.29	-8.06	-3.64
11.60	1976.39	-8.42	-3.43	16.20	1970.13	-8.61	-3.87
11.70	1976.29	-8.21	-3.34	16.30	1969.92	-8.94	-4.02
11.80	1976.12	-8.26	-3.71	16.40	1969.71	-9.13	-3.95
11.90	1975.92	-8.32	-3.23	16.50	1969.54	-9.24	-3.79
12.00	1975.71	-8.58	-3.23	16.60	1969.45	-9.10	-3.85
12.10	1975.54	-8.65	-3.34	16.70	1969.38	-8.67	-3.75
12.20	1975.44	-8.53	-3.35	16.80	1969.29	-8.57	-3.70
12.30	1975.39	-8.44	-3.47	16.90	1969.13	-8.60	-3.83
12.40	1975.29	-7.90	-3.41	17.00	1968.92	-8.95	-3.88
12.50	1975.08	-8.16	-3.56	17.10	1968.71	-9.11	-3.91
12.60	1974.80	-8.10	-3.47	17.20	1968.54	-9.27	-4.02
12.70	1974.54	-8.48	-3.39	17.30	1968.45	-9.24	-3.93
12.80	1974.43	-8.43	-3.49	17.40	1968.42	-8.72	-3.87
12.90	1974.40	-8.33	-3.53	17.50	1968.38	-8.46	-3.95
13.00	1974.29	-8.21	-3.60	17.60	1968.29	-8.28	-3.83
13.10	1973.54	-8.39	-3.60	17.70	1968.06	-8.55	-4.07
13.20	1973.45	-8.38	-3.80	17.80	1967.77	-8.87	-3.99
13.30	1973.38	-8.31	-3.51	17.90	1967.54	-8.99	-3.94
13.40	1973.29	-8.09	-3.39	18.00	1967.44	-9.01	-4.00
13.50	1973.17	-8.77	-3.87	18.10	1967.39	-8.68	-3.70
13.60	1973.04	-8.16	-3.35	18.20	1967.29	-8.48	-3.67
13.70	1972.91	-8.57	-3.56	18.30	1967.12	-8.68	-3.70
13.80	1972.78	-8.89	-3.56	18.40	1966.92	-8.89	-3.67

Sample depth (mm)	Date (C.E.)	$\delta^{13}C$ (‰VPDB)	$\delta^{18}O$ (‰VPDB)	Sample depth (mm)	Date (C.E.)	$\delta^{13}C$ (‰VPDB)	$\delta^{18}O$ (‰VPDB)
18.50	1966.71	-9.05	-3.87	23.10	1961.82	-9.44	-3.64
18.60	1966.54	-9.14	-3.79	23.20	1961.72	-9.62	-3.62
18.70	1966.44	-8.95	-3.74	23.30	1961.63	-9.67	-3.65
18.80	1966.39	-8.85	-3.76	23.40	1961.54	-9.72	-3.54
18.90	1966.29	-8.68	-3.63	23.50	1961.46	-9.54	-3.59
19.00	1966.06	-8.76	-3.60	23.60	1961.38	-9.07	-3.57
19.10	1965.76	-8.89	-3.66	23.70	1961.29	-8.70	-3.62
19.20	1965.54	-8.99	-3.69	23.80	1961.20	-8.70	-3.70
19.30	1965.44	-8.87	-3.60	23.90	1961.09	-8.94	-3.71
19.40	1965.38	-8.70	-3.75	24.00	1960.99	-9.07	-3.61
19.50	1965.29	-8.53	-3.81	24.10	1960.88	-9.28	-3.69
19.60	1965.15	-8.55	-3.86	24.20	1960.77	-9.43	-3.44
19.70	1964.99	-9.01	-3.77	24.30	1960.66	-9.43	-3.42
19.80	1964.83	-9.09	-3.65	24.40	1960.54	-9.51	-3.56
19.90	1964.67	-9.32	-3.79	24.50	1960.42	-9.21	-3.67
20.00	1964.54	-9.35	-3.71	24.60	1960.29	-8.82	-3.62
20.10	1964.46	-9.33	-3.76	24.70	1960.15	-8.85	-3.70
20.20	1964.42	-8.91	-3.77	24.80	1959.99	-9.05	-3.59
20.30	1964.40	-8.72	-3.72	24.90	1959.83	-9.28	-3.57
20.40	1964.36	-8.73	-3.71	25.00	1959.68	-9.47	-3.66
20.50	1964.29	-8.67	-3.61	25.10	1959.54	-9.57	-3.58
20.60	1964.14	-8.86	-3.66	25.20	1959.45	-9.58	-3.87
20.70	1963.92	-9.09	-3.65	25.30	1959.42	-9.49	-3.53
20.80	1963.70	-9.27	-3.66	25.40	1959.38	-9.03	-3.64
20.90	1963.54	-9.32	-3.60	25.50	1959.29	-8.78	-3.52
21.00	1963.45	-9.31	-3.65	25.60	1959.17	-8.92	-3.90
21.10	1963.45	-9.26	-3.59	25.70	1959.04	-9.08	-3.81
21.20	1963.45	-8.53	-3.47	25.80	1958.92	-9.28	-3.99
21.30	1963.44	-8.23	-3.45	25.90	1958.79	-9.31	-4.08
21.40	1963.44	-7.99	-3.41	26.00	1958.66	-9.26	-3.46
21.50	1963.44	-8.24	-3.55	26.10	1958.54	-9.41	-3.66
21.60	1963.42	-8.08	-3.42	26.20	1958.42	-9.20	-3.57
21.70	1963.38	-8.02	-3.33	26.30	1958.29	-8.99	-3.55
21.80	1963.29	-7.85	-3.56	26.40	1958.17	-8.97	-3.52
21.90	1963.12	-8.24	-3.43	26.50	1958.07	-9.13	-3.49
22.00	1962.90	-8.57	-3.40	26.60	1957.97	-9.34	-3.80
22.10	1962.68	-8.84	-3.29	26.70	1957.88	-9.34	-3.77
22.20	1962.54	-9.01	-3.66	26.80	1957.79	-9.38	-3.77
22.30	1962.47	-9.01	-3.47	26.90	1957.71	-9.54	-3.90
22.40	1962.42	-8.90	-3.53	27.00	1957.63	-9.64	-4.08
22.50	1962.37	-8.61	-3.39	27.10	1957.54	-9.73	-3.86
22.60	1962.29	-8.43	-3.47	27.20	1957.47	-9.51	-3.70
22.70	1962.20	-8.45	-3.85	27.30	1957.42	-9.51	-4.00
22.80	1962.10	-8.59	-3.59	27.40	1957.36	-9.11	-4.01
22.90	1962.01	-8.96	-3.62	27.50	1957.29	-8.90	-3.72
23.00	1961.91	-9.09	-3.61	27.60	1957.08	-9.13	-3.92

Sample depth (mm)	Date (C.E.)	$\delta^{13}C$ (‰VPDB)	$\delta^{18}O$ (‰VPDB)	Sample depth (mm)	Date (C.E.)	$\delta^{13}C$ (‰VPDB)	$\delta^{18}O$ (‰VPDB)
27.70	1956.75	-9.37	-3.95	32.30	1950.93	-9.02	-3.95
27.80	1956.54	-9.61	-3.96	32.40	1950.73	-9.10	-3.93
27.90	1956.47	-9.63	-4.39	32.50	1950.54	-9.17	-4.03
28.00	1956.42	-9.56	-3.89	32.60	1950.43	-9.13	-4.08
28.10	1956.36	-9.14	-3.81	32.70	1950.39	-8.58	-3.85
28.20	1956.29	-8.93	-3.82	32.80	1950.29	-8.31	-3.89
28.30	1956.20	-9.17	-3.93	32.90	1949.92	-8.63	-3.96
28.40	1956.11	-9.29	-3.94	33.00	1949.54	-9.01	-3.95
28.50	1956.01	-9.38	-3.97	33.10	1949.51	-9.03	-3.86
28.60	1955.91	-9.47	-3.86	33.20	1949.49	-8.97	-3.82
28.70	1955.82	-9.72	-3.91	33.30	1949.46	-8.79	-3.85
28.80	1955.72	-9.79	-4.03	33.40	1949.44	-8.71	-3.72
28.90	1955.63	-9.92	-3.96	33.50	1949.41	-8.72	-3.67
29.00	1955.54	-9.87	-3.91	33.60	1949.29	-8.66	-3.73
29.10	1955.47	-9.94	-4.01	33.70	1949.05	-8.87	-3.67
29.20	1955.42	-9.30	-3.99	33.80	1948.76	-8.73	-3.64
29.30	1955.36	-9.04	-3.99	33.90	1948.54	-8.98	-3.68
29.40	1955.29	-8.66	-3.97	34.00	1948.44	-8.52	-3.60
29.50	1955.15	-8.77	-3.98	34.10	1948.39	-8.42	-3.57
29.60	1954.93	-8.97	-4.04	34.20	1948.29	-8.35	-3.62
29.70	1954.71	-9.04	-3.95	34.30	1948.06	-8.78	-3.60
29.80	1954.54	-9.16	-4.07	34.40	1947.77	-8.85	-3.63
29.90	1954.45	-9.13	-4.00	34.50	1947.54	-9.11	-3.69
30.00	1954.39	-8.95	-4.18	34.60	1947.50	-9.11	-3.68
30.10	1954.29	-8.60	-3.99	34.70	1947.46	-8.93	-3.68
30.20	1954.12	-8.61	-3.77	34.80	1947.44	-8.85	-3.72
30.30	1953.91	-9.03	-4.27	34.90	1947.29	-8.57	-3.60
30.40	1953.70	-9.38	-4.22	35.00	1947.04	-8.58	-3.60
30.50	1953.54	-9.49	-4.10	35.10	1946.79	-8.74	-3.59
30.60	1953.45	-9.21	-3.94	35.20	1946.54	-8.84	-3.65
30.70	1953.38	-8.54	-3.78	35.30	1946.29	-8.66	-3.68
30.80	1953.29	-7.98	-3.66	35.40	1946.08	-8.67	-3.73
30.90	1953.17	-8.18	-4.03	35.50	1945.92	-8.78	-3.67
31.00	1953.03	-8.51	-4.05	35.60	1945.82	-8.89	-3.76
31.10	1952.88	-8.66	-3.84	35.70	1945.74	-8.86	-3.73
31.20	1952.72	-8.67	-4.01	35.80	1945.68	-8.86	-3.62
31.30	1952.54	-8.81	-3.93	35.90	1945.62	-9.08	-3.71
31.40	1952.29	-8.42	-3.91	36.00	1945.54	-9.22	-3.80
31.50	1952.12	-8.52	-3.93	36.10	1945.47	-9.22	-3.75
31.60	1951.97	-8.67	-3.99	36.20	1945.43	-9.17	-3.75
31.70	1951.82	-9.06	-4.19	36.30	1945.38	-8.62	-3.74
31.80	1951.68	-9.38	-4.20	36.40	1945.29	-8.39	-3.81
31.90	1951.54	-9.52	-4.24	36.50	1945.08	-8.42	-3.82
32.00	1951.42	-9.20	-4.07	36.60	1944.77	-8.64	-3.85
32.10	1951.29	-8.85	-4.06	36.70	1944.54	-8.67	-4.07
32.20	1951.13	-8.97	-4.16	36.80	1944.42	-8.48	-3.84

Sample depth (mm)	Date (C.E.)	$\delta^{13}C$ (‰VPDB)	$\delta^{18}O$ (‰VPDB)	Sample depth (mm)	Date (C.E.)	$\delta^{13}C$ (‰VPDB)	$\delta^{18}O$ (‰VPDB)
36.90	1944.29	-7.86	-3.70	41.50	1937.45	-9.07	-3.76
37.00	1944.14	-8.07	-3.79	41.60	1937.38	-8.89	-3.75
37.10	1943.99	-8.59	-3.80	41.70	1937.29	-8.77	-3.71
37.20	1943.84	-8.97	-3.76	41.80	1937.13	-8.88	-3.76
37.30	1943.69	-9.03	-3.93	41.90	1936.92	-9.06	-3.89
37.40	1943.54	-9.45	-3.73	42.00	1936.71	-9.40	-3.92
37.50	1943.41	-8.81	-3.67	42.10	1936.54	-9.61	-4.07
37.60	1943.29	-8.58	-3.65	42.20	1936.45	-9.27	-3.85
37.70	1943.12	-8.66	-3.62	42.30	1936.41	-8.98	-3.84
37.80	1942.92	-8.84	-3.72	42.40	1936.37	-8.79	-3.80
37.90	1942.72	-8.98	-3.69	42.50	1936.29	-8.62	-3.83
38.00	1942.54	-9.09	-3.71	42.60	1936.13	-8.82	-3.83
38.10	1942.44	-8.84	-3.64	42.70	1935.93	-9.30	-3.97
38.20	1942.38	-8.67	-3.66	42.80	1935.72	-9.59	-4.09
38.30	1942.29	-8.49	-3.64	42.90	1935.54	-9.76	-4.08
38.40	1942.12	-8.53	-3.67	43.00	1935.51	-9.65	-4.18
38.50	1941.91	-8.75	-3.82	43.10	1935.48	-9.42	-4.12
38.60	1941.70	-8.81	-3.83	43.20	1935.45	-8.97	-4.01
38.70	1941.54	-8.87	-3.80	43.30	1935.42	-8.71	-3.89
38.80	1941.45	-8.83	-3.73	43.40	1935.39	-8.62	-3.92
38.90	1941.39	-8.52	-3.67	43.50	1935.29	-8.47	-3.98
39.00	1941.29	-8.33	-3.59	43.60	1934.92	-8.57	-3.95
39.10	1941.15	-8.54	-3.65	43.70	1934.54	-8.72	-3.85
39.20	1941.00	-8.85	-3.81	43.80	1934.44	-8.60	-3.91
39.30	1940.84	-8.76	-3.57	43.90	1934.42	-8.53	-3.80
39.40	1940.69	-8.88	-3.59	44.00	1934.40	-8.38	-4.02
39.50	1940.54	-8.91	-3.57	44.10	1934.29	-8.28	-4.13
39.60	1940.42	-8.69	-3.41	44.20	1934.05	-8.70	-4.17
39.70	1940.29	-8.30	-3.40	44.30	1933.76	-8.78	-4.17
39.80	1940.06	-8.37	-3.40	44.40	1933.54	-8.93	-4.31
39.90	1939.77	-8.55	-3.44	44.50	1933.44	-8.82	-4.36
40.00	1939.54	-8.94	-3.01	44.60	1933.39	-8.63	-4.22
40.10	1939.44	-8.85	-3.51	44.70	1933.29	-8.25	-4.19
40.20	1939.38	-8.74	-3.49	44.80	1933.12	-8.22	-4.17
40.30	1939.29	-8.37	-3.45	44.90	1932.92	-8.28	-4.07
40.40	1939.16	-8.33	-3.50	45.00	1932.71	-8.37	-4.23
40.50	1939.03	-8.64	-3.47	45.10	1932.54	-8.46	-4.33
40.60	1938.88	-8.59	-3.31	45.20	1932.44	-8.37	-4.22
40.70	1938.72	-8.87	-3.59	45.30	1932.39	-8.33	-4.25
40.80	1938.54	-8.99	-3.57	45.40	1932.29	-8.23	-4.20
40.90	1938.29	-8.47	-3.56	45.50	1932.07	-8.23	-4.09
41.00	1938.11	-8.47	-3.56	45.60	1931.78	-8.30	-4.06
41.10	1937.95	-8.64	-3.62	45.70	1931.54	-8.46	-4.04
41.20	1937.80	-9.07	-3.68	45.80	1931.44	-8.48	-4.24
41.30	1937.66	-9.21	-3.68	45.90	1931.39	-8.44	-4.03
41.40	1937.54	-9.25	-3.71	46.00	1931.29	-8.35	-4.07

Sample depth (mm)	Date (C.E.)	$\delta^{13}C$ (‰VPDB)	$\delta^{18}O$ (‰VPDB)	Sample depth (mm)	Date (C.E.)	$\delta^{13}C$ (‰VPDB)	$\delta^{18}O$ (‰VPDB)
46.10	1931.04	-8.34	-4.02	50.70	1927.42	-8.18	-3.51
46.20	1930.73	-8.48	-4.04	50.80	1927.29	-8.10	-3.87
46.30	1930.54	-8.60	-4.21	50.90	1927.07	-8.16	-3.61
46.40	1930.47	-8.60	-4.11	51.00	1926.78	-8.23	-3.75
46.50	1930.41	-8.50	-4.04	51.10	1926.54	-8.36	-3.75
46.60	1930.35	-8.42	-4.04	51.20	1926.44	-8.34	-3.92
46.70	1930.29	-8.10	-3.95	51.30	1926.42	-8.34	-3.65
46.80	1930.22	-8.23	-3.95	51.40	1926.39	-8.24	-3.59
46.90	1930.15	-8.30	-3.94	51.50	1926.29	-8.03	-4.03
47.00	1930.09	-8.37	-3.92	51.60	1926.05	-8.07	-3.57
47.10	1930.02	-8.41	-3.95	51.70	1925.75	-8.12	-3.56
47.20	1929.95	-8.34	-3.98	51.80	1925.54	-8.47	-3.74
47.30	1929.88	-8.43	-4.07	51.90	1925.42	-8.40	-3.62
47.40	1929.81	-8.54	-4.05	52.00	1925.29	-8.35	-3.70
47.50	1929.74	-8.76	-4.03	52.10	1925.17	-8.37	-3.76
47.60	1929.67	-8.93	-4.04	52.20	1925.04	-8.54	-3.70
47.70	1929.61	-9.07	-4.04	52.30	1924.92	-8.90	-3.77
47.80	1929.54	-9.08	-4.01	52.40	1924.79	-9.05	-3.83
47.90	1929.49	-9.11	-3.94	52.50	1924.66	-9.13	-3.77
48.00	1929.45	-9.05	-3.94	52.60	1924.54	-9.35	-3.93
48.10	1929.43	-8.83	-3.87	52.70	1924.44	-9.26	-4.09
48.20	1929.41	-8.78	-3.77	52.80	1924.37	-8.85	-4.00
48.30	1929.41	-8.89	-3.93	52.90	1924.29	-8.74	-4.11
48.40	1929.41	-8.86	-3.87	53.00	1924.18	-8.82	-4.32
48.50	1929.40	-8.73	-3.86	53.10	1924.05	-8.92	-3.81
48.60	1929.39	-8.53	-3.87	53.20	1923.92	-9.27	-4.03
48.70	1929.37	-8.30	-3.68	53.30	1923.78	-9.34	-3.91
48.80	1929.34	-8.38	-3.66	53.40	1923.65	-9.60	-4.22
48.90	1929.29	-8.15	-3.73	53.50	1923.54	-9.54	-4.11
49.00	1929.22	-8.19	-3.61	53.60	1923.45	-9.54	-3.97
49.10	1929.14	-8.30	-3.61	53.70	1923.38	-9.13	-4.03
49.20	1929.04	-8.25	-3.55	53.80	1923.29	-8.85	-3.92
49.30	1928.94	-8.28	-3.66	53.90	1923.18	-8.82	-3.93
49.40	1928.83	-8.20	-3.47	54.00	1923.05	-8.92	-3.83
49.50	1928.72	-8.28	-3.47	54.10	1922.92	-9.14	-3.81
49.60	1928.63	-8.38	-3.50	54.20	1922.79	-9.19	-3.84
49.70	1928.54	-8.41	-3.51	54.30	1922.66	-9.22	-3.87
49.80	1928.48	-8.41	-3.46	54.40	1922.54	-9.42	-3.89
49.90	1928.45	-8.09	-3.40	54.50	1922.45	-9.20	-3.79
50.00	1928.42	-8.20	-3.65	54.60	1922.38	-8.93	-3.85
50.10	1928.37	-8.14	-3.65	54.70	1922.29	-8.72	-3.84
50.20	1928.29	-8.08	-3.77	54.80	1922.16	-8.95	-3.86
50.30	1928.14	-8.08	-3.58	54.90	1922.01	-9.07	-3.78
50.40	1927.94	-8.17	-3.61	55.00	1921.84	-9.22	-3.69
50.50	1927.72	-8.15	-3.49	55.10	1921.68	-9.31	-3.75
50.60	1927.54	-8.20	-3.54	55.20	1921.54	-9.41	-3.85

Sample depth (mm)	Date (C.E.)	$\delta^{13}C$ (‰VPDB)	$\delta^{18}O$ (‰VPDB)	Sample depth (mm)	Date (C.E.)	$\delta^{13}C$ (‰VPDB)	$\delta^{18}O$ (‰VPDB)
55.30	1921.46	-9.40	-3.90	59.90	1916.45	-9.42	-3.73
55.40	1921.41	-9.29	-3.73	60.00	1916.42	-9.51	-3.76
55.50	1921.37	-8.93	-3.73	60.10	1916.39	-9.58	-3.69
55.60	1921.29	-8.83	-3.68	60.20	1916.29	-9.38	-3.80
55.70	1921.13	-9.02	-3.75	60.30	1916.08	-9.46	-3.92
55.80	1920.92	-9.37	-3.75	60.40	1915.79	-9.69	-3.90
55.90	1920.71	-9.54	-3.72	60.50	1915.54	-9.83	-3.81
56.00	1920.54	-9.59	-3.72	60.60	1915.52	-9.62	-3.82
56.10	1920.45	-9.23	-3.73	60.70	1915.51	-9.56	-3.80
56.20	1920.41	-9.45	-3.66	60.80	1915.49	-9.44	-3.72
56.30	1920.37	-8.97	-3.60	60.90	1915.48	-9.40	-3.71
56.40	1920.29	-8.49	-3.60	61.00	1915.46	-9.12	-3.72
56.50	1920.12	-9.36	-3.48	61.10	1915.43	-9.03	-3.62
56.60	1919.90	-9.55	-3.43	61.20	1915.29	-9.00	-3.61
56.70	1919.69	-9.64	-3.52	61.30	1914.54	-9.27	-3.67
56.80	1919.54	-9.73	-3.54	61.40	1914.52	-9.04	-3.69
56.90	1919.47	-9.67	-3.59	61.50	1914.49	-8.82	-3.55
57.00	1919.43	-9.73	-3.60	61.60	1914.47	-8.65	-3.42
57.10	1919.41	-9.67	-3.58	61.70	1914.45	-8.88	-3.46
57.20	1919.37	-9.60		61.80	1914.42	-8.86	-3.48
57.30	1919.29	-9.21	-3.53	61.90	1914.29	-8.58	-3.47
57.40	1919.17	-9.31	-3.47	62.00	1914.03	-8.87	-3.63
57.50	1919.05	-9.34	-3.59	62.10	1913.75	-8.84	-3.55
57.60	1918.91	-9.41	-3.59	62.20	1913.54	-8.93	-3.56
57.70	1918.78	-9.51		62.30	1913.45	-8.75	-3.54
57.80	1918.65	-9.60	-3.63	62.40	1913.43	-8.86	-3.66
57.90	1918.54	-9.70	-3.63	62.50	1913.42	-8.76	-3.72
58.00	1918.45	-9.63	-3.68	62.60	1913.39	-8.63	-3.77
58.10	1918.38	-9.49	-3.59	62.70	1913.29	-8.49	-3.67
58.20	1918.29	-9.30	-3.64	62.80	1913.12	-8.63	-3.67
58.30	1918.17	-9.32	-3.65	62.90	1912.92	-8.71	-3.77
58.40	1918.01	-9.42	-3.64	63.00	1912.71	-8.78	-3.80
58.50	1917.84	-9.67	-3.54	63.10	1912.54	-8.93	-3.55
58.60	1917.68	-9.82	-3.64	63.20	1912.47	-8.61	-3.71
58.70	1917.54	-9.93	-3.68	63.30	1912.43	-8.60	-3.65
58.80	1917.45	-9.91	-3.50	63.40	1912.29	-8.57	-3.63
58.90	1917.42	-9.77	-3.64	63.50	1912.04	-8.79	-3.77
59.00	1917.41	-9.44	-3.59	63.60	1911.79	-8.88	-3.69
59.10	1917.40	-9.20	-3.52	63.70	1911.54	-9.03	-3.85
59.20	1917.37	-9.16	-3.50	63.80	1911.29	-8.92	-3.67
59.30	1917.29	-8.98	-3.47	63.90	1911.08	-8.91	-3.81
59.40	1917.08	-9.10	-3.60	64.00	1910.94	-9.00	-3.78
59.50	1916.77	-9.20	-3.56	64.10	1910.84	-9.13	-3.79
59.60	1916.54	-9.60	-3.66	64.20	1910.77	-9.06	-3.78
59.70	1916.51	-9.60	-3.72	64.30	1910.71	-9.27	-3.73
59.80	1916.48	-9.60	-3.70	64.40	1910.64	-8.47	-3.50

Sample depth (mm)	Date (C.E.)	$\delta^{13}C$ (‰VPDB)	$\delta^{18}O$ (‰VPDB)	Sample depth (mm)	Date (C.E.)	$\delta^{13}C$ (‰VPDB)	$\delta^{18}O$ (‰VPDB)
64.50	1910.54	-9.31	-3.69	69.10	1903.45	-8.62	-3.91
64.60	1910.42	-9.07	-3.69	69.20	1903.38	-8.47	-3.68
64.70	1910.29	-8.61	-3.78	69.30	1903.29	-8.32	-3.71
64.80	1910.07	-8.89	-3.77	69.40	1903.16	-8.59	-3.81
64.90	1909.77	-8.92	-3.72	69.50	1903.00	-8.91	-3.79
65.00	1909.54	-9.17	-3.76	69.60	1902.84	-9.14	-3.87
65.10	1909.44	-8.91	-3.73	69.70	1902.68	-9.42	-3.99
65.20	1909.41	-8.94	-3.81	69.80	1902.54	-9.70	-4.02
65.30	1909.38	-8.89	-3.82	69.90	1902.46	-9.64	-4.53
65.40	1909.29	-8.73	-3.69	70.00	1902.42	-9.55	-4.07
65.50	1909.12	-8.78	-3.74	70.10	1902.40	-9.04	-3.97
65.60	1908.92	-8.90	-3.91	70.20	1902.37	-8.75	-3.73
65.70	1908.72	-8.82	-3.43	70.30	1902.29	-8.69	-3.53
65.80	1908.54	-9.02	-4.02	70.40	1902.13	-9.00	-3.69
65.90	1908.44	-8.61	-3.98	70.50	1901.91	-9.15	-3.69
66.00	1908.42	-8.66	-3.84	70.60	1901.69	-9.29	-3.88
66.10	1908.39	-8.59	-3.97	70.70	1901.54	-10.18	-3.81
66.20	1908.29	-8.42	-3.96	70.80	1901.47	-9.70	-3.82
66.30	1907.92	-8.78	-3.88	70.90	1901.43	-9.45	-3.87
66.40	1907.54	-8.94	-4.26	71.00	1901.40	-9.00	-4.03
66.50	1907.44	-8.35	-4.12	71.10	1901.37	-8.75	-3.73
66.60	1907.40	-8.40	-4.11	71.20	1901.29	-8.10	-3.79
66.70	1907.29	-8.33	-4.01	71.30	1901.18	-8.70	-3.68
66.80	1907.04	-8.97	-3.96	71.40	1901.05	-8.93	-3.76
66.90	1906.76	-8.23	-3.97	71.50	1900.91	-9.06	-3.95
67.00	1906.54	-8.42	-3.88	71.60	1900.77	-9.31	-3.93
67.10	1906.42	-8.32	-3.90	71.70	1900.65	-9.67	-4.00
67.20	1906.29	-8.04	-3.97	71.80	1900.54	-9.83	-4.07
67.30	1906.11	-8.24	-3.96	71.90	1900.47	-9.71	-3.82
67.40	1905.92	-8.27	-3.99	72.00	1900.42	-9.38	-3.72
67.50	1905.72	-8.38	-4.00	72.10	1900.37	-9.03	-3.72
67.60	1905.54	-8.55	-3.86	72.20	1900.29	-8.95	-3.63
67.70	1905.41	-8.35	-3.82	72.30	1900.16	-9.07	-3.83
67.80	1905.29	-7.86	-3.71	72.40	1900.00	-9.19	-3.84
67.90	1905.06	-8.41	-3.88	72.50	1899.83	-9.19	-4.05
68.00	1904.76			72.60	1899.67	-9.37	-3.88
68.10	1904.54	-10.11	-3.26	72.70	1899.54	-9.82	-3.88
68.20	1904.45	-9.01	-3.85	72.80	1899.46	-9.73	-3.97
68.30	1904.41	-8.88	-3.92	72.90	1899.42	-9.79	-3.97
68.40	1904.37	-8.66	-3.90	73.00	1899.37	-8.88	-3.83
68.50	1904.29	-8.18	-3.79	73.10	1899.29	-8.48	-3.94
68.60	1904.15	-8.19	-3.81	73.20	1899.18	-8.72	-3.62
68.70	1903.99	-8.22	-3.77	73.30	1899.04	-8.76	-3.64
68.80	1903.82	-8.44	-3.82	73.40	1898.91	-9.01	-3.62
68.90	1903.67	-8.61	-3.87	73.50	1898.77	-9.28	-3.86
69.00	1903.54	-9.03	-3.92	73.60	1898.65	-9.59	-3.72

Sample depth (mm)	Date (C.E.)	$\delta^{13}C$ (‰VPDB)	$\delta^{18}O$ (‰VPDB)	Sample depth (mm)	Date (C.E.)	$\delta^{13}C$ (‰VPDB)	$\delta^{18}O$ (‰VPDB)
73.70	1898.54	-9.84	-3.99	78.30	1893.83		
73.80	1898.45	-9.71	-3.88	78.40	1893.67	-9.40	-3.88
73.90	1898.38	-9.14	-3.62	78.50	1893.54	-9.89	-3.82
74.00	1898.29	-8.68	-3.51	78.60	1893.46	-9.77	-3.84
74.10	1898.19	-8.87	-3.66	78.70	1893.43	-9.67	-3.86
74.20	1898.08	-8.93	-3.61	78.80	1893.41	-9.23	-3.81
74.30	1897.97			78.90	1893.37	-8.63	-3.80
74.40	1897.86	-9.39	-3.61	79.00	1893.29	-8.20	-3.61
74.50	1897.75	-9.30	-3.67	79.10	1893.13	-8.42	-3.65
74.60	1897.64	-9.45	-3.85	79.20	1892.90	-8.75	-3.78
74.70	1897.54	-9.51	-3.71	79.30	1892.68	-9.03	-3.96
74.80	1897.45	-9.28	-3.50	79.40	1892.54	-9.47	-3.87
74.90	1897.38	-8.53	-3.78	79.50	1892.47	-9.34	-3.86
75.00	1897.29	-8.36	-3.63	79.60	1892.42	-9.32	-3.84
75.10	1897.14	-8.87	-3.81	79.70	1892.36	-9.09	-3.91
75.20	1896.93	-9.15	-3.74	79.80	1892.29	-8.84	-3.81
75.30	1896.71	-9.42	-3.85	79.90	1892.20	-8.94	-3.82
75.40	1896.54	-9.61	-3.91	80.00	1892.12	-8.92	-3.74
75.50	1896.45	-9.86	-3.95	80.10	1892.03	-9.08	-3.97
75.60	1896.41			80.20	1891.94	-9.17	-3.74
75.70	1896.41	-9.70	-4.08	80.30	1891.85	-9.56	-3.85
75.80	1896.40			80.40	1891.75	-9.61	-3.99
75.90	1896.37	-8.79	-3.88	80.50	1891.65	-9.61	-3.89
76.00	1896.29			80.60	1891.54	-9.67	-3.88
76.10	1896.13			80.70	1891.42		
76.20	1895.91			80.80	1891.29		
76.30	1895.69			80.90	1891.18	-8.96	-3.90
76.40	1895.54			81.00	1891.07	-9.02	-3.76
76.50	1895.46			81.10	1890.96	-9.10	-3.87
76.60	1895.43			81.20	1890.85	-9.23	-3.98
76.70	1895.40			81.30	1890.75	-9.87	-3.23
76.80	1895.37			81.40	1890.64	-9.91	-3.22
76.90	1895.29	-8.67	-3.73	81.50	1890.54	-10.09	-3.54
77.00	1895.16	-8.77	-3.71	81.60	1890.45	-9.98	-3.28
77.10	1895.00	-8.91	-3.76	81.70	1890.38	-9.50	-3.22
77.20	1894.82	-9.14	-3.84	81.80	1890.29	-9.19	-3.23
77.30	1894.66	-9.62	-3.81	81.90	1890.15	-9.44	-3.16
77.40	1894.54			82.00	1889.94	-9.42	-3.32
77.50	1894.47			82.10	1889.73	-9.72	-3.34
77.60	1894.43			82.20	1889.54	-9.98	-3.67
77.70	1894.42			82.30	1889.44	-8.84	
77.80	1894.40			82.40	1889.39	-8.84	
77.90	1894.36			82.50	1889.29	-8.82	
78.00	1894.29	-8.68	-3.81	82.60	1888.92	-9.00	
78.10	1894.17	-8.65	-3.66	82.70	1888.54	-9.13	-3.84
78.20	1894.01	-8.78	-3.89	82.80	1888.42	-8.88	

Sample depth (mm)	Date (C.E.)	$\delta^{13}C$ (‰VPDB)	$\delta^{18}O$ (‰VPDB)
82.90	1888.29	-8.86	
83.00	1888.10	-8.88	-3.96
83.10	1887.90	-9.03	-3.88
83.20	1887.70	-9.03	-3.65
83.30	1887.54	-9.34	
83.40	1887.44	-9.33	
83.50	1887.38	-9.36	
83.60	1887.29	-8.96	-3.84
83.70	1887.15	-9.15	-3.80
83.80	1886.99	-9.24	-3.69
83.90	1886.82	-9.03	-3.61
84.00	1886.67	-9.34	-4.10
84.10	1886.54	-9.63	-3.73
84.20	1886.45	-9.61	-3.79
84.30	1886.38	-9.24	-3.70
84.40	1886.29	-9.04	-4.05
84.50	1886.17	-9.20	-4.05
84.60	1886.05	-9.13	-3.54
84.70	1885.91	-9.73	-3.63
84.80	1885.78	-9.31	-3.46
84.90	1885.65	-9.69	-3.86
85.00	1885.54	-9.75	-3.49
85.10	1885.45	-9.73	-3.59
85.20	1885.38	-9.68	-3.93
85.30	1885.29	-9.28	-3.55
85.40	1885.18	-9.30	-3.73
85.50	1885.05	-9.56	-3.77
85.60	1884.91	~~-10.08~~	-3.91
85.70	1884.78	-9.87	-3.62
85.80	1884.65	-10.14	-3.76
85.90	1884.54	-10.19	-3.81
86.00	1884.45	-10.20	-3.52
86.10	1884.38	-9.85	-3.62
86.20	1884.29	-9.77	-4.48
86.30	1884.19	-9.80	-3.55
86.40	1884.08	-9.79	-3.81
86.50	1883.97	-9.88	-3.75
86.60	1883.86	-9.79	-4.12
86.70	1883.75	-9.86	-3.67
86.80	1883.64	-9.86	-3.93
86.90	1883.54	-9.93	-3.65
87.00	1883.46	-9.93	-3.59
87.10	1883.41	-9.72	-3.49
87.20	1883.36	-9.66	-3.58
87.30	1883.29	-9.51	-3.76
87.40	1883.17	-9.55	-3.94
87.50	1883.01	-9.64	-3.67
87.60	1882.84	-9.58	-3.75
87.70	1882.67	-9.58	-3.97
87.80	1882.54	-9.79	-3.77
87.90	1882.46	-9.81	-4.42
88.00	1882.42	-9.70	-4.16
88.10	1882.37	-9.84	-4.15
88.20	1882.29	-9.62	-3.78
88.30	1882.16	-10.08	-3.85
88.40	1882.00	-9.84	-4.02
88.50	1881.83	-9.94	-4.12
88.60	1881.67	-9.85	-4.25
88.70	1881.54	-10.37	-4.38
88.80	1881.46	-10.03	-4.32
88.90	1881.42	-10.14	-3.94
89.00	1881.37	-9.85	-4.19
89.10	1881.29	-9.58	-4.15
89.20	1881.16	-9.88	-4.24
89.30	1881.00	-9.84	-4.28
89.40	1880.83	-9.94	-4.22
89.50	1880.67	-9.93	-4.30
89.60	1880.54	-9.98	-3.99
89.70	1880.47	-10.00	-4.26
89.80	1880.43	-9.62	-4.12
89.90	1880.38	-9.29	-4.08
90.00	1880.29	-9.12	-3.99
90.10	1880.15	-9.37	-4.28
90.20	1880.00	-9.50	-4.29
90.30	1879.84	-9.61	-4.31
90.40	1879.69	-9.68	-4.05
90.50	1879.54	-9.78	-4.14
90.60	1879.42	-9.61	-4.30
90.70	1879.29	-9.46	-4.21
90.80	1878.93	-9.92	-4.02
90.90	1878.54	-9.80	-4.04
91.00	1878.41	-9.73	-3.96
91.10	1878.29	-9.48	-4.15
91.20	1878.05	-9.48	-3.92
91.30	1877.77	-9.56	-4.16
91.40	1877.54	-9.66	-4.04
91.50	1877.43	-9.64	-3.59
91.60	1877.41	-9.60	-4.19
91.70	1877.38	-9.54	-4.12
91.80	1877.29	-9.42	-3.94
91.90	1877.05	-10.05	-4.13
92.00	1876.75	-9.81	-4.05

Sample depth (mm)	Date (C.E.)	$\delta^{13}C$ (‰VPDB)	$\delta^{18}O$ (‰VPDB)	Sample depth (mm)	Date (C.E.)	$\delta^{13}C$ (‰VPDB)	$\delta^{18}O$ (‰VPDB)
92.10	1876.54	-10.32	-4.15	96.70	1871.69	-9.97	-4.13
92.20	1876.46	-10.08	-4.27	96.80	1871.54	-10.00	-4.08
92.30	1876.42	-10.03	-4.28	96.90	1871.47	-9.90	-3.58
92.40	1876.37	-9.88	-4.04	97.00	1871.43	-9.73	-3.56
92.50	1876.29	-9.69	-4.30	97.10	1871.40	-10.26	
92.60	1876.17	-9.79	-4.14	97.20	1871.36	-9.48	
92.70	1876.04	-10.27	-3.85	97.30	1871.29	-9.08	
92.80	1875.91	-9.43	-4.12	97.40	1871.20	-9.17	
92.90	1875.78	-10.19	-4.07	97.50	1871.09	-9.82	
93.00	1875.65	-10.31	-4.15	97.60	1870.98	-9.94	
93.10	1875.54	-10.93	-4.09	97.70	1870.85	-10.24	
93.20	1875.45	-10.37	-3.99	97.80	1870.70	-10.21	-3.69
93.30	1875.38	-9.83	-4.02	97.90	1870.54	-10.28	
93.40	1875.29	-9.61	-4.14	98.00	1870.29	-8.87	
93.50	1875.17	-9.70	-4.19	98.10	1870.13	-9.59	
93.60	1875.01	-9.85	-3.69	98.20	1869.99	-9.53	-4.10
93.70	1874.84	-9.85	-4.01	98.30	1869.86	-9.65	
93.80	1874.68	-10.13	-4.17	98.40	1869.74	-9.88	
93.90	1874.54	-10.19	-4.30	98.50	1869.63	-10.03	-4.02
94.00	1874.45	-9.97	-4.05	98.60	1869.54	-10.16	
94.10	1874.41	-10.07	-4.22	98.70	1869.47	-9.72	-3.82
94.20	1874.41	-10.23	-4.35	98.80	1869.42	-9.75	-4.33
94.30	1874.41	-10.00	-4.17	98.90	1869.37	-9.00	
94.40	1874.41	-9.15	-4.09	99.00	1869.29	-8.77	-3.94
94.50	1874.37	-9.14	-3.89	99.10	1869.16	-9.35	-3.94
94.60	1874.29	-9.03	-3.64	99.20	1869.00	-9.18	
94.70	1874.07	-9.45	-3.63	99.30	1868.83	-9.67	-3.97
94.80	1873.76	-9.98	-3.89	99.40	1868.67	-9.81	
94.90	1873.54	-10.21	-3.59	99.50	1868.54	-9.98	
95.00	1873.46	-10.23	-4.43	99.60	1868.45	-9.72	
95.10	1873.42	-9.35	-4.23	99.70	1868.38	-9.38	-3.90
95.20	1873.37	-9.30	-4.03	99.80	1868.29	-8.92	
95.30	1873.29	-9.19	-3.98	99.90	1868.16	-9.27	-4.15
95.40	1873.15	-9.39	-4.21	100.00	1868.00	-9.32	
95.50	1872.99	-9.73	-4.04	100.10	1867.83	-9.51	
95.60	1872.83	-10.28	-4.06	100.20	1867.67	-9.88	
95.70	1872.67	-10.31	-4.22	100.30	1867.54	-9.99	
95.80	1872.54	-10.53	-4.27	100.40	1867.46	-9.90	
95.90	1872.46	-10.36	-3.99	100.50	1867.41	-9.76	
96.00	1872.43	-10.51	-3.78	100.60	1867.37	-9.32	
96.10	1872.41	-10.28	-4.00	100.70	1867.29	-8.90	
96.20	1872.40	-9.70	-3.55	100.80	1867.16	-9.02	-4.19
96.30	1872.37	-9.32	-3.85	100.90	1867.00	-9.20	
96.40	1872.29	-9.18	-3.91	101.00	1866.82	-9.44	
96.50	1872.13	-9.19	-4.05	101.10	1866.66	-9.68	
96.60	1871.91	-9.66	-4.06	101.20	1866.54	-9.73	

Sample depth (mm)	Date (C.E.)	$\delta^{13}C$ (‰VPDB)	$\delta^{18}O$ (‰VPDB)	Sample depth (mm)	Date (C.E.)	$\delta^{13}C$ (‰VPDB)	$\delta^{18}O$ (‰VPDB)
101.30	1866.46	-9.68		105.90	1861.45	-9.57	-4.32
101.40	1866.41	-9.43	-4.12	106.00	1861.37	-9.42	-4.33
101.50	1866.36	-9.15	-4.27	106.10	1861.29	-9.24	-4.22
101.60	1866.29	-8.96	-4.53	106.20	1861.17	-9.33	-4.33
101.70	1866.18	-8.97	-4.35	106.30	1861.02	-9.33	-4.32
101.80	1866.06	-9.01	-4.46	106.40	1860.85	-9.73	-4.64
101.90	1865.92	-9.01	-4.46	106.50	1860.68	-9.70	-4.38
102.00	1865.78	-9.21	-4.38	106.60	1860.54	-10.04	-4.26
102.10	1865.65	-9.39	-4.46	106.70	1860.46	-10.01	-4.23
102.20	1865.54	-9.60	-4.32	106.80	1860.42	-9.80	-4.35
102.30	1865.47	-9.63	-4.44	106.90	1860.40	-9.68	-4.23
102.40	1865.43	-9.61	-4.54	107.00	1860.36	-9.36	-4.54
102.50	1865.40	-9.28	-4.23	107.10	1860.29	-9.18	-4.21
102.60	1865.36	-9.14	-4.35	107.20	1860.13	-9.21	-4.51
102.70	1865.29	-8.83	-4.44	107.30	1859.92	-9.29	-4.31
102.80	1865.14	-9.17	-4.30	107.40	1859.70	-8.58	-4.38
102.90	1864.93	-9.30	-4.24	107.50	1859.54	-9.59	-4.57
103.00	1864.71	-9.85	-4.44	107.60	1859.46	-9.45	-4.59
103.10	1864.54	-9.91	-4.22	107.70	1859.43	-9.56	-4.20
103.20	1864.46	-9.82	-4.68	107.80	1859.42	-9.51	-4.22
103.30	1864.42	-9.69	-4.45	107.90	1859.42	-9.23	-4.30
103.40	1864.38	-9.19	-4.50	108.00	1859.41	-9.41	-4.02
103.50	1864.29	-8.76	-4.33	108.10	1859.37	-9.08	-4.05
103.60	1864.13	-8.83	-4.52	108.20	1859.29	-8.81	-4.29
103.70	1863.92	-8.93	-4.34	108.30	1859.16	-9.09	-4.04
103.80	1863.70	-9.43	-4.25	108.40	1858.99	-8.92	-4.03
103.90	1863.54	-9.65	-4.09	108.50	1858.82	-9.17	-4.16
104.00	1863.46	-9.55	-4.06	108.60	1858.66	-9.09	-4.03
104.10	1863.42	-9.61	-4.18	108.70	1858.54	-9.41	-4.28
104.20	1863.38	-9.05	-4.57	108.80	1858.47	-9.33	-4.44
104.30	1863.29	-8.49	-4.26	108.90	1858.43	-9.33	-4.25
104.40	1863.12	-8.67	-4.44	109.00	1858.38	-8.95	-4.42
104.50	1862.90	-8.99	-4.19	109.10	1858.29	-8.80	-4.02
104.60	1862.68	-9.07	-4.36	109.20	1858.17	-8.88	-4.49
104.70	1862.54	-9.17	-4.28	109.30	1858.04	-9.14	-4.30
104.80	1862.46	-8.93	-4.53	109.40	1857.92	-9.34	-4.70
104.90	1862.38	-8.90	-4.08	109.50	1857.79	-9.27	-4.07
105.00	1862.29	-8.63	-4.30	109.60	1857.66	-9.39	-4.53
105.10	1862.20	-8.94	-4.51	109.70	1857.54	-9.58	-4.34
105.20	1862.10	-8.91	-4.14	109.80	1857.42	-9.41	-4.29
105.30	1862.01	-9.53	-4.31	109.90	1857.29	-9.20	-4.62
105.40	1861.91	-9.74	-4.30	110.00	1857.17	-9.33	-4.13
105.50	1861.82	-9.93	-4.37	110.10	1857.04	-9.32	-4.28
105.60	1861.73	-9.99	-4.43	110.20	1856.92	-9.66	-4.17
105.70	1861.63	-9.08	-4.67	110.30	1856.79	-9.88	-5.04
105.80	1861.54	-10.07	-4.15	110.40	1856.67	-9.94	-4.42

Sample depth (mm)	Date (C.E.)	$\delta^{13}C$ (‰VPDB)	$\delta^{18}O$ (‰VPDB)	Sample depth (mm)	Date (C.E.)	$\delta^{13}C$ (‰VPDB)	$\delta^{18}O$ (‰VPDB)
110.50	1856.54	-10.19	-4.32	115.10	1851.37	-9.05	-4.05
110.60	1856.45	-9.94	-4.48	115.20	1851.29	-8.81	-4.10
110.70	1856.41	-9.94	-4.35	115.30	1851.17	-8.93	-4.01
110.80	1856.41	-10.09	-4.60	115.40	1851.04	-8.92	-4.17
110.90	1856.40	-10.04	-4.25	115.50	1850.91	-9.15	-4.17
111.00	1856.40	-9.52	-4.23	115.60	1850.77	-9.45	-4.18
111.10	1856.37	-9.33	-4.40	115.70	1850.65	-9.48	-4.24
111.20	1856.29	-9.25	-4.09	115.80	1850.54	-9.53	-4.26
111.30	1856.09	-9.44	-4.29	115.90	1850.45	-9.30	-4.26
111.40	1855.79	-9.68	-4.40	116.00	1850.38	-9.06	-4.55
111.50	1855.54	-10.11	-4.12	116.10	1850.29	-8.92	-3.99
111.60	1855.44	-10.02	-4.23	116.20	1850.19	-8.88	-4.09
111.70	1855.40	-9.23	-4.12	116.30	1850.08	-9.07	-4.44
111.80	1855.29	-9.11	-4.32	116.40	1849.97	-9.14	-3.97
111.90	1854.92	-9.55	-4.23	116.50	1849.84	-9.20	-4.18
112.00	1854.54	-9.58	-4.06	116.60	1849.69	-9.23	-4.13
112.10	1854.43	-9.61	-4.13	116.70	1849.54	-9.31	-4.23
112.20	1854.39	-9.11	-4.30	116.80	1849.29	-9.06	-4.24
112.30	1854.29	-8.58	-4.31	116.90	1849.10	-9.05	-3.98
112.40	1854.04	-8.57	-4.26	117.00	1848.94	-9.18	-4.16
112.50	1853.74	-9.08	-4.00	117.10	1848.79	-9.07	-4.19
112.60	1853.54	-9.36	-4.28	117.20	1848.66	-9.21	-4.24
112.70	1853.46	-9.20	-4.26	117.30	1848.54	-9.58	-4.28
112.80	1853.42	-9.35	-4.21	117.40	1848.46	-9.45	-4.53
112.90	1853.40	-9.24	-4.30	117.50	1848.42	-9.42	-4.12
113.00	1853.37	-9.25	-4.23	117.60	1848.41	-9.43	-4.44
113.10	1853.29	-9.08	-4.25	117.70	1848.40	-9.40	-4.49
113.20	1853.18	-9.18	-4.38	117.80	1848.37	-9.06	-4.30
113.30	1853.05	-9.30	-4.21	117.90	1848.29	-8.93	-4.28
113.40	1852.91	-9.54	-4.23	118.00	1848.07	-9.10	-4.04
113.50	1852.78	-9.71	-4.06	118.10	1847.76	-9.14	-4.03
113.60	1852.65	-9.79	-4.42	118.20	1847.54	-9.19	-4.23
113.70	1852.54	-9.93	-4.39	118.30	1847.46	-9.18	-4.58
113.80	1852.47	-9.84	-4.01	118.40	1847.42	-9.18	-4.64
113.90	1852.43	-9.95	-4.19	118.50	1847.42	-9.15	-4.36
114.00	1852.40	-9.59	-3.99	118.60	1847.42	-8.88	-4.34
114.10	1852.36	-9.28	-4.29	118.70	1847.41	-8.73	-4.40
114.20	1852.29	-9.24	-4.38	118.80	1847.38	-8.78	-4.35
114.30	1852.14	-9.26	-4.18	118.90	1847.29	-8.67	
114.40	1851.92	-9.48	-4.23	119.00	1847.16	-8.87	
114.50	1851.69	-9.49	-4.71	119.10	1847.00	-8.84	-4.45
114.60	1851.54	-9.70	-4.07	119.20	1846.84	-8.76	-4.52
114.70	1851.47	-9.70	-4.29	119.30	1846.68	-8.99	-4.46
114.80	1851.44	-9.56	-4.18	119.40	1846.54	-9.08	-4.42
114.90	1851.42	-9.33	-4.00	119.50	1846.45	-8.95	-4.45
115.00	1851.41	-9.22	-3.92	119.60	1846.42	-8.99	-4.46

Sample depth (mm)	Date (C.E.)	$\delta^{13}C$ (‰VPDB)	$\delta^{18}O$ (‰VPDB)	Sample depth (mm)	Date (C.E.)	$\delta^{13}C$ (‰VPDB)	$\delta^{18}O$ (‰VPDB)
119.70	1846.38	-8.88	-4.52	124.30	1840.45	-9.43	
119.80	1846.29	-8.86	-4.61	124.40	1840.42	-9.38	-4.11
119.90	1845.92	-8.98	-4.52	124.50	1840.40	-9.08	-4.08
120.00	1845.54	-9.15	-4.60	124.60	1840.37	-8.60	-4.39
120.10	1845.44	-8.94	-4.45	124.70	1840.29	-8.45	-3.99
120.20	1845.42	-8.72	-4.65	124.80	1840.15	-8.88	-4.17
120.30	1845.41	-9.20	-4.43	124.90	1839.99	-9.43	-4.15
120.40	1845.39	-8.64	-4.58	125.00	1839.82	-9.92	-4.21
120.50	1845.29	-8.60	-4.69	125.10	1839.66	-10.14	-4.25
120.60	1845.11	-8.62	-4.40	125.20	1839.54	-10.20	-4.28
120.70	1844.90	-8.82	-4.29	125.30	1839.47	-10.07	-4.23
120.80	1844.69	-8.93	-4.34	125.40	1839.42	-9.73	-4.30
120.90	1844.54	-9.07	-4.35	125.50	1839.37	-9.25	-4.57
121.00	1844.46	-9.02	-4.35	125.60	1839.29	-9.19	-4.13
121.10	1844.42	-8.90	-4.31	125.70	1839.18	-9.26	-4.28
121.20	1844.37	-8.59	-4.57	125.80	1839.05	-9.72	-4.43
121.30	1844.29	-8.53	-4.18	125.90	1838.92	-10.07	-4.53
121.40	1844.16	-8.70	-4.20	126.00	1838.78	-10.20	-4.96
121.50	1844.00	-9.08	-4.65	126.10	1838.65		-4.46
121.60	1843.83	-9.32	-4.28	126.20	1838.54	-10.46	-4.35
121.70	1843.67	-9.51	-4.57	126.30	1838.46	-10.17	-4.39
121.80	1843.54	-9.56	-4.74	126.40	1838.42	-9.55	-4.22
121.90	1843.46	-9.42	-4.41	126.50	1838.37	-8.89	-4.04
122.00	1843.43	-9.34	-4.41	126.60	1838.29	-8.68	-3.98
122.10	1843.41	-8.75	-4.24	126.70	1838.14	-9.04	-4.19
122.20	1843.37	-8.54	-4.59	126.80	1837.93	-9.29	-4.18
122.30	1843.29	-8.46	-4.41	126.90	1837.72	-9.56	-4.21
122.40	1843.13	-8.89	-4.30	127.00	1837.54	-9.89	-4.38
122.50	1842.91	-9.16	-4.42	127.10	1837.44	-9.73	-4.30
122.60	1842.70	-9.45	-4.06	127.20	1837.39	-8.90	-4.16
122.70	1842.54	-9.48	-4.39	127.30	1837.29	-8.49	-4.08
122.80	1842.45	-9.47	-4.53	127.40	1837.07	-9.00	-4.08
122.90	1842.38	-8.99	-4.41	127.50	1836.77	-9.70	-4.30
123.00	1842.29	-8.75	-4.43	127.60	1836.54	-10.25	-4.15
123.10	1842.17	-8.76	-4.17	127.70	1836.44	-10.17	-4.39
123.20	1842.05	-8.98	-4.52	127.80	1836.41	-9.68	-4.31
123.30	1841.92	-9.60	-4.62	127.90	1836.39	-8.75	-4.23
123.40	1841.79	-9.97	-4.67	128.00	1836.29	-8.57	-4.60
123.50	1841.66	-10.28	-5.08	128.10	1836.05	-8.91	-3.93
123.60	1841.54	-10.41	-4.38	128.20	1835.75	-9.60	-4.37
123.70	1841.45	-9.94		128.30	1835.54	-10.02	-5.39
123.80	1841.38	-9.24	-4.56	128.40	1835.45	-8.93	-4.49
123.90	1841.29	-8.68	-4.11	128.50	1835.41	-9.72	-4.71
124.00	1841.07	-8.89	-4.08	128.60	1835.37	-9.03	-4.33
124.10	1840.77	-9.19	-4.29	128.70	1835.29	-8.65	-4.16
124.20	1840.54	-9.46	-4.27	128.80	1835.15	-8.67	-4.22

Sample depth (mm)	Date (C.E.)	$\delta^{13}C$ (‰VPDB)	$\delta^{18}O$ (‰VPDB)	Sample depth (mm)	Date (C.E.)	$\delta^{13}C$ (‰VPDB)	$\delta^{18}O$ (‰VPDB)
128.90	1834.99	-9.10	-4.24	133.50	1829.54	-9.41	-3.98
129.00	1834.83	-9.54	-4.44	133.60	1829.46	-9.31	-4.44
129.10	1834.67	-9.85	-4.54	133.70	1829.41	-8.96	-4.16
129.20	1834.54	-10.09	-4.48	133.80	1829.37	-9.12	-4.03
129.30	1834.46	-10.09	-4.89	133.90	1829.29	-8.56	-4.62
129.40	1834.43	-9.98	-4.23	134.00	1829.16	-8.87	-4.16
129.50	1834.41	-9.56	-4.67	134.10	1829.00	-9.02	-4.39
129.60	1834.37	-9.49	-4.49	134.20	1828.84	-9.26	-4.31
129.70	1834.29	-9.31	-4.40	134.30	1828.68	-9.64	-4.30
129.80	1834.13	-9.38	-4.22	134.40	1828.54	-9.95	-4.51
129.90	1833.92	-9.51	-4.36	134.50	1828.46	-9.41	-4.35
130.00	1833.71	-9.48	-4.23	134.60	1828.42	-9.46	-4.22
130.10	1833.54	-9.57	-4.46	134.70	1828.38	-9.06	-4.16
130.20	1833.45	-9.50	-4.39	134.80	1828.29	-8.95	-4.69
130.30	1833.38	-8.79	-4.26	134.90	1828.07	-9.08	-4.05
130.40	1833.29	-8.62	-4.11	135.00	1827.76	-9.66	-4.12
130.50	1833.13	-8.88	-4.35	135.10	1827.54	-9.76	-4.10
130.60	1832.92	-9.30	-4.66	135.20	1827.46	-9.67	-4.36
130.70	1832.71	-9.71	-4.63	135.30	1827.42	-9.31	-4.33
130.80	1832.54	-10.04	-4.27	135.40	1827.38	-9.16	-4.38
130.90	1832.44	-9.99	-4.37	135.50	1827.29	-8.77	-4.03
131.00	1832.41	-9.99	-4.67	135.60	1827.15	-8.91	-4.14
131.10	1832.40	-9.56	-4.34	135.70	1826.99	-8.98	-4.12
131.20	1832.38	-9.23	-4.69	135.80	1826.82	-9.38	-4.53
131.30	1832.29	-9.06	-4.27	135.90	1826.67	-9.51	-4.46
131.40	1832.06	-9.09	-4.48	136.00	1826.54	-9.82	-4.37
131.50	1831.75	-9.35	-4.09	136.10	1826.45	-9.53	-4.86
131.60	1831.54	-9.90	-4.60	136.20	1826.38	-9.14	-4.29
131.70	1831.47	-9.80	-3.87	136.30	1826.29	-8.67	-4.04
131.80	1831.43	-9.84	-4.53	136.40	1826.16	-8.80	-4.43
131.90	1831.42	-9.75	-4.43	136.50	1826.00	-8.83	-5.20
132.00	1831.41	-9.47	-4.41	136.60	1825.84	-9.43	-4.29
132.10	1831.37	-9.15	-4.66	136.70	1825.68	-9.51	-4.52
132.20	1831.29	-8.52	-4.39	136.80	1825.54	-9.67	-4.14
132.30	1831.17	-8.67	-4.07	136.90	1825.45	-9.65	-4.95
132.40	1831.04	-9.21	-4.24	137.00	1825.38	-9.07	-4.32
132.50	1830.91	-9.32	-4.47	137.10	1825.29	-9.02	-4.23
132.60	1830.78	-9.55	-4.41	137.20	1825.13	-9.03	-4.74
132.70	1830.65	-9.48	-4.33	137.30	1824.92	-9.00	-3.68
132.80	1830.54	-9.60	-4.72	137.40	1824.70	-9.67	-4.12
132.90	1830.45	-9.42	-4.46	137.50	1824.54	-9.91	-4.41
133.00	1830.38	-8.77	-4.29	137.60	1824.46	-9.85	-4.10
133.10	1830.29	-8.13	-4.43	137.70	1824.42	-9.77	-4.58
133.20	1830.13	-8.32	-4.00	137.80	1824.40	-9.78	-4.60
133.30	1829.92	-8.85	-4.70	137.90	1824.37	-9.12	-4.59
133.40	1829.70	-8.90	-4.06	138.00	1824.29	-8.74	-4.78

Sample depth (mm)	Date (C.E.)	$\delta^{13}C$ (‰VPDB)	$\delta^{18}O$ (‰VPDB)	Sample depth (mm)	Date (C.E.)	$\delta^{13}C$ (‰VPDB)	$\delta^{18}O$ (‰VPDB)
138.10	1824.16	-8.90	-4.40	142.70	1818.68	-9.48	-4.46
138.20	1824.00	-8.98	-4.51	142.80	1818.54	-9.68	-4.13
138.30	1823.82	-9.20	-4.17	142.90	1818.41	-9.54	-4.22
138.40	1823.66	-9.61	-4.23	143.00	1818.29	-9.00	-4.17
138.50	1823.54	-9.70	-4.20	143.10	1818.17	-9.25	-4.16
138.60	1823.47	-9.54	-4.27	143.20	1818.06	-9.34	-4.27
138.70	1823.43	-9.18	-4.35	143.30	1817.96	-9.34	-4.15
138.80	1823.41	-9.49	-4.39	143.40	1817.85	-8.76	-4.30
138.90	1823.37	-8.98	-4.51	143.50	1817.75	-9.39	-4.35
139.00	1823.29	-8.85	-4.15	143.60	1817.64	-9.45	
139.10	1823.16	-9.20	-4.19	143.70	1817.54	-9.83	
139.20	1823.00	-9.80	-4.10	143.80	1817.46	-9.85	-4.36
139.30	1822.83	-10.20	-4.79	143.90	1817.41	-9.62	-4.24
139.40	1822.67	-10.31	-4.42	144.00	1817.37	-9.09	-4.34
139.50	1822.54	-10.47	-4.33	144.10	1817.29	-8.92	-4.05
139.60	1822.45	-10.31	-4.47	144.20	1816.93	-9.39	
139.70	1822.38	-9.73	-4.62	144.30	1816.54	-9.65	
139.80	1822.29	-8.64	-4.45	144.40	1816.44	-9.59	-4.41
139.90	1822.16	-8.98	-4.15	144.50	1816.41	-9.41	-4.83
140.00	1822.01	-8.94	-4.07	144.60	1816.41	-9.90	-4.54
140.10	1821.84	-9.53	-4.13	144.70	1816.39	-9.58	-4.37
140.20	1821.68	-9.43	-4.23	144.80	1816.29	-9.35	-4.46
140.30	1821.54	-10.14	-4.32	144.90	1816.11	-9.43	-4.56
140.40	1821.45	-9.00	-4.33	145.00	1815.89	-9.54	-4.49
140.50	1821.42	-9.82	-4.00	145.10	1815.68	-9.58	
140.60	1821.41	-9.91	-4.13	145.20	1815.54	-9.85	-4.53
140.70	1821.40	-9.01	-4.44	145.30	1815.47	-9.78	
140.80	1821.37	-9.35	-4.03	145.40	1815.44	-9.58	-4.78
140.90	1821.29	-8.85	-4.26	145.50	1815.42	-9.63	-4.42
141.00	1821.09	-8.86	-4.03	145.60	1815.41	-9.28	-4.38
141.10	1820.80	-9.22	-4.47	145.70	1815.37	-9.04	-4.24
141.20	1820.54	-9.77	-4.18	145.80	1815.29	-8.94	-4.30
141.30	1820.52	-9.22	-4.44	145.90	1815.17	-9.13	-4.39
141.40	1820.49			146.00	1815.05	-9.36	-4.51
141.50	1820.47	-8.96	-4.27	146.10	1814.91	-9.62	-4.53
141.60	1820.45	-9.16	-4.08	146.20	1814.78	-9.68	-4.51
141.70	1820.42	-8.74	-4.10	146.30	1814.65	-9.66	-4.45
141.80	1820.29	-8.56	-4.17	146.40	1814.54	-9.86	-4.56
141.90	1819.54	-8.94	-3.99	146.50	1814.45	-9.40	-4.52
142.00	1819.45	-8.83	-4.10	146.60	1814.38	-8.47	-4.20
142.10	1819.42	-8.73	-4.01	146.70	1814.29	-8.39	-4.28
142.20	1819.39	-8.78	-4.44	146.80	1814.16	-8.70	-4.39
142.30	1819.29	-8.60	-4.12	146.90	1814.00	-8.99	-4.39
142.40	1819.14	-8.71	-4.21	147.00	1813.83	-9.19	-4.39
142.50	1818.98	-8.86	-4.12	147.10	1813.67	-9.38	-4.47
142.60	1818.83	-9.08	-4.32	147.20	1813.54	-9.78	-4.62

Sample depth (mm)	Date (C.E.)	$\delta^{13}C$ (‰VPDB)	$\delta^{18}O$ (‰VPDB)	Sample depth (mm)	Date (C.E.)	$\delta^{13}C$ (‰VPDB)	$\delta^{18}O$ (‰VPDB)
147.30	1813.46	-9.29	-4.47	151.90	1808.70	-9.04	-4.56
147.40	1813.41	-9.02	-4.37	152.00	1808.54	-9.25	-4.36
147.50	1813.37	-8.90	-4.34	152.10	1808.42	-9.15	-4.25
147.60	1813.29	-8.64	-4.31	152.20	1808.29	-8.79	-4.11
147.70	1813.16	-8.84	-4.28	152.30	1808.17	-9.16	-4.21
147.80	1813.00	-9.00	-4.29	152.40	1808.04	-9.05	-4.17
147.90	1812.82	-9.23	-4.56	152.50	1807.92	-9.40	-4.29
148.00	1812.66	-9.15	-4.45	152.60	1807.79	-9.75	-4.24
148.10	1812.54	-9.47	-4.55	152.70	1807.66	-9.74	-4.36
148.20	1812.46	-9.24	-4.58	152.80	1807.54	-9.82	-4.30
148.30	1812.41	-8.96	-4.37	152.90	1807.44	-9.51	-4.15
148.40	1812.36	-9.07	-4.47	153.00	1807.37	-9.19	-4.19
148.50	1812.29	-8.92	-4.47	153.10	1807.29	-8.95	-4.22
148.60	1812.18	-8.92	-4.47	153.20	1807.16	-8.97	-4.23
148.70	1812.05	-8.97	-4.59	153.30	1807.00	-9.25	-4.23
148.80	1811.91	-9.05	-4.59	153.40	1806.83	-9.85	-4.40
148.90	1811.77	-9.15	-4.55	153.50	1806.67	-9.86	-4.44
149.00	1811.65	-9.57	-4.66	153.60	1806.54	-10.10	-4.39
149.10	1811.54	-9.82	-4.82	153.70	1806.46	-9.83	-4.31
149.20	1811.47	-9.50	-4.57	153.80	1806.43	-8.58	-3.95
149.30	1811.43	-8.90	-4.54	153.90	1806.40	-8.59	-3.90
149.40	1811.40	-8.82	-4.44	154.00	1806.37	-8.59	-3.90
149.50	1811.36	-8.75	-4.44	154.10	1806.29	-8.42	-3.89
149.60	1811.29	-8.60	-4.43	154.20	1806.16	-8.76	-4.10
149.70	1811.19	-8.91	-4.38	154.30	1806.00	-9.24	-4.02
149.80	1811.06	-8.69	-4.26	154.40	1805.83	-9.60	-4.13
149.90	1810.92	-8.89	-4.41	154.50	1805.67	-10.09	-4.15
150.00	1810.78	-8.88	-4.57	154.60	1805.54	-10.27	-4.37
150.10	1810.65	-8.64	-4.16	154.70	1805.45	-9.77	-4.05
150.20	1810.54	-9.05	-4.44	154.80	1805.38	-9.27	-4.02
150.30	1810.47	-9.02	-4.52	154.90	1805.29	-9.03	-3.97
150.40	1810.43	-9.08	-4.51	155.00	1805.16	-9.21	-3.94
150.50	1810.42	-9.10	-4.59	155.10	1805.00	-9.56	-4.05
150.60	1810.40	-8.72	-4.35	155.20	1804.83	-10.07	-4.10
150.70	1810.36	-8.69	-4.40	155.30	1804.67	-10.20	-4.10
150.80	1810.29	-8.57	-4.30	155.40	1804.54	-10.30	-4.09
150.90	1810.14	-8.57	-4.39	155.50	1804.45	-9.79	-4.08
151.00	1809.93	-8.78	-4.51	155.60	1804.38	-8.96	-3.82
151.10	1809.71	-8.85	-4.63	155.70	1804.29	-8.79	-3.84
151.20	1809.54	-8.99	-4.44	155.80	1804.16	-8.79	-3.86
151.30	1809.46	-8.86	-4.56	155.90	1804.00	-9.23	-3.89
151.40	1809.43	-8.75	-4.44	156.00	1803.83	-9.50	-3.98
151.50	1809.39	-8.72	-4.42	156.10	1803.67	-9.94	-4.12
151.60	1809.29	-8.70	-4.37	156.20	1803.54	-10.06	-4.23
151.70	1809.11	-8.76	-4.47	156.30	1803.46	-10.08	-4.12
151.80	1808.90	-8.98	-4.55	156.40	1803.42	-9.51	-3.98

Sample depth (mm)	Date (C.E.)	$\delta^{13}C$ (‰VPDB)	$\delta^{18}O$ (‰VPDB)	Sample depth (mm)	Date (C.E.)	$\delta^{13}C$ (‰VPDB)	$\delta^{18}O$ (‰VPDB)
156.50	1803.37	-8.92	-3.86	161.10	1798.48	-10.17	-4.05
156.60	1803.29	-8.68	-3.90	161.20	1798.44	-9.42	-3.95
156.70	1803.16	-8.65	-3.83	161.30	1798.38	-8.35	-3.96
156.80	1803.00	-9.13	-3.93	161.40	1798.29	-8.20	-3.97
156.90	1802.84	-9.70	-4.04	161.50	1798.17	-8.60	-4.00
157.00	1802.68	-10.01	-4.11	161.60	1798.04	-9.14	-4.05
157.10	1802.54	-10.07	-4.11	161.70	1797.92	-9.71	-4.27
157.20	1802.45	-9.89	-4.06	161.80	1797.79	-9.93	-4.26
157.30	1802.38	-9.29	-3.86	161.90	1797.67	-10.02	-4.37
157.40	1802.29	-8.48	-3.65	162.00	1797.54	-10.05	-4.24
157.50	1802.12	-8.99	-3.88	162.10	1797.42	-9.40	-4.04
157.60	1801.91	-9.37	-4.38	162.20	1797.29	-8.67	-3.86
157.70	1801.70	-9.51	-3.97	162.30	1797.17	-8.70	-3.82
157.80	1801.54	-9.62	-4.28	162.40	1797.07	-8.97	-3.81
157.90	1801.45	-9.42	-4.08	162.50	1796.98	-8.93	-3.83
158.00	1801.38	-8.82	-3.81	162.60	1796.90	-9.04	-3.87
158.10	1801.29	-8.40	-3.70	162.70	1796.82	-9.55	-4.04
158.20	1801.17	-8.82	-4.08	162.80	1796.75	-9.99	-4.06
158.30	1801.04	-9.13	-3.92	162.90	1796.68	-10.39	-4.10
158.40	1800.90	-9.28	-3.96	163.00	1796.61	-10.54	-4.12
158.50	1800.77	-9.61	-4.02	163.10	1796.54	-10.59	-4.29
158.60	1800.65	-9.88	-4.12	163.20	1796.47	-10.33	-4.18
158.70	1800.54	-10.08	-4.13	163.30	1796.42	-9.22	-3.95
158.80	1800.46	-10.03	-4.40	163.40	1796.36	-8.50	-3.79
158.90	1800.41	-9.60	-4.34	163.50	1796.29	-8.37	-3.80
159.00	1800.36	-8.93	-4.13	163.60	1796.19	-8.48	-3.80
159.10	1800.29	-8.77	-3.92	163.70	1796.06	-9.19	-3.96
159.20	1800.19	-9.03	-4.02	163.80	1795.92	-9.74	-4.13
159.30	1800.08	-9.26	-4.01	163.90	1795.77	-9.94	-4.10
159.40	1799.97	-9.39	-4.21	164.00	1795.64	-9.93	-4.08
159.50	1799.85	-9.76	-4.07	164.10	1795.54	-10.21	-5.08
159.60	1799.74	-10.06	-4.35	164.20	1795.46	-9.97	-4.67
159.70	1799.63	-10.19	-4.26	164.30	1795.37	-9.13	-4.44
159.80	1799.54	-10.45	-4.22	164.40	1795.29	-8.72	-4.61
159.90	1799.47	-10.38	-4.21	164.50	1795.21	-8.91	-4.00
160.00	1799.42	-9.95	-4.13	164.60	1795.12	-8.90	-4.63
160.10	1799.36	-9.20	-3.97	164.70	1795.04	-9.21	-4.21
160.20	1799.29	-8.99	-3.98	164.80	1794.96	-9.31	-4.21
160.30	1799.21	-9.16	-4.23	164.90	1794.87	-9.44	-4.27
160.40	1799.11	-9.47	-4.89	165.00	1794.79	-9.94	-5.00
160.50	1799.02	-9.70	-3.92	165.10	1794.71	-10.07	-4.27
160.60	1798.92	-9.85	-4.02	165.20	1794.62	-10.24	-4.32
160.70	1798.82	-9.99	-4.05	165.30	1794.54	-10.37	-4.39
160.80	1798.72	-10.14	-4.14	165.40	1794.47	-10.24	-4.83
160.90	1798.63	-10.09	-4.10	165.50	1794.42	-9.38	-4.68
161.00	1798.54	-10.13	-4.11	165.60	1794.36	-8.67	-4.08

Sample depth (mm)	Date (C.E.)	$\delta^{13}C$ (‰VPDB)	$\delta^{18}O$ (‰VPDB)	Sample depth (mm)	Date (C.E.)	$\delta^{13}C$ (‰VPDB)	$\delta^{18}O$ (‰VPDB)
165.70	1794.29	-8.62	-4.60	170.30	1789.29	-8.29	-4.57
165.80	1794.20	-8.81	-4.60	170.40	1789.16	-8.62	-4.73
165.90	1794.10	-9.04	-4.72	170.50	1789.00	-9.18	-4.86
166.00	1793.98	-9.31	-4.81	170.60	1788.83	-9.51	-4.98
166.10	1793.87	-9.50	-4.87	170.70	1788.67	-9.61	-5.00
166.20	1793.75	-9.94	-4.94	170.80	1788.54	-9.70	-5.05
166.30	1793.64	-9.94	-4.97	170.90	1788.46	-9.73	-4.91
166.40	1793.54	-10.13	-5.08	171.00	1788.43	-9.14	-4.71
166.50	1793.45	-10.00	-5.40	171.10	1788.41	-8.68	-4.61
166.60	1793.38	-9.09	-4.87	171.20	1788.37	-8.61	-4.51
166.70	1793.29	-8.30	-4.62	171.30	1788.29	-8.57	-4.54
166.80	1793.18	-8.52	-4.97	171.40	1788.13	-8.81	-4.64
166.90	1793.06	-9.13	-4.88	171.50	1787.92	-9.03	-4.66
167.00	1792.92	-9.37	-5.18	171.60	1787.71	-9.25	-4.73
167.10	1792.79	-9.75	-5.38	171.70	1787.54	-9.41	-4.75
167.20	1792.66	-9.74	-5.29	171.80	1787.45	-8.45	-4.42
167.30	1792.54	-9.76	-5.32	171.90	1787.39	-8.52	-4.46
167.40	1792.45	-9.43	-4.98	172.00	1787.29	-8.30	-4.43
167.50	1792.38	-8.82	-5.15	172.10	1787.12	-8.48	-4.47
167.60	1792.29	-8.22	-4.69	172.20	1786.91	-8.91	-4.63
167.70	1792.16	-8.42	-4.92	172.30	1786.70	-9.04	-4.68
167.80	1792.00	-8.85	-5.12	172.40	1786.54	-9.56	-4.75
167.90	1791.83	-9.31	-5.33	172.50	1786.45	-9.45	-4.66
168.00	1791.67	-9.70	-5.29	172.60	1786.38	-8.63	-4.43
168.10	1791.54	-9.88	-5.49	172.70	1786.29	-8.51	-4.43
168.20	1791.46	-9.84	-5.27	172.80	1786.15	-8.64	-4.45
168.30	1791.41	-9.62	-5.01	172.90	1785.99	-8.80	-4.44
168.40	1791.37	-8.73	-4.92	173.00	1785.82	-9.22	-4.54
168.50	1791.29	-8.56	-4.73	173.10	1785.67	-9.29	-4.62
168.60	1791.16	-8.95	-5.09	173.20	1785.54	-9.38	-4.62
168.70	1791.00	-9.03	-4.67	173.30	1785.45	-9.25	-4.63
168.80	1790.84	-9.07	-4.91	173.40	1785.38	-8.69	-4.51
168.90	1790.67	-9.37	-4.79	173.50	1785.29	-8.50	-4.37
169.00	1790.54	-9.47	-4.83	173.60	1785.17	-8.49	-4.32
169.10	1790.46	-9.41	-4.83	173.70	1785.05	-8.90	-4.42
169.20	1790.41	-8.74	-4.55	173.80	1784.92	-9.34	-4.43
169.30	1790.37	-8.31	-4.51	173.90	1784.79	-9.35	-4.38
169.40	1790.29	-8.19	-4.54	174.00	1784.66	-9.34	-4.46
169.50	1790.13	-8.83	-4.77	174.10	1784.54	-9.61	-4.32
169.60	1789.92	-9.00	-4.80	174.20	1784.45	-9.42	-4.30
169.70	1789.70	-9.21	-4.86	174.30	1784.38	-8.86	-4.12
169.80	1789.54	-9.41	-4.84	174.40	1784.29	-8.48	-4.00
169.90	1789.46	-9.25	-4.81	174.50	1784.13	-8.64	-4.16
170.00	1789.42	-8.77	-4.68	174.60	1783.92	-9.01	-4.13
170.10	1789.40	-8.36	-4.62	174.70	1783.71	-9.32	-4.17
170.20	1789.37	-8.32	-4.59	174.80	1783.54	-9.33	-4.18

Sample depth (mm)	Date (C.E.)	$\delta^{13}C$ (‰VPDB)	$\delta^{18}O$ (‰VPDB)	Sample depth (mm)	Date (C.E.)	$\delta^{13}C$ (‰VPDB)	$\delta^{18}O$ (‰VPDB)
174.90	1783.45	-9.36	-4.25	179.50	1777.82	-9.16	-4.12
175.00	1783.38	-9.15	-4.21	179.60	1777.73	-9.62	-4.16
175.10	1783.29	-9.00	-4.18	179.70	1777.63	-9.67	-4.24
175.20	1783.16	-9.08	-4.28	179.80	1777.54	-9.86	-4.17
175.30	1783.00	-9.36	-4.28	179.90	1777.47	-9.59	-4.21
175.40	1782.84	-9.46	-4.27	180.00	1777.43	-9.76	-4.26
175.50	1782.68	-9.62	-4.22	180.10	1777.40	-9.70	-4.22
175.60	1782.54	-9.81	-4.41	180.20	1777.36	-9.55	-4.24
175.70	1782.45	-9.48	-4.26	180.30	1777.29	-9.22	-3.93
175.80	1782.42	-9.33	-4.33	180.40	1776.95	-9.24	-4.03
175.90	1782.41	-8.94	-3.99	180.50	1776.54	-9.35	-4.20
176.00	1782.38	-8.56	-3.97	180.60	1776.43	-9.32	-3.93
176.10	1782.29	-8.52	-3.77	180.70	1776.41	-9.28	-3.98
176.20	1782.08	-9.12	-3.97	180.80	1776.29	-9.18	-4.27
176.30	1781.78	-8.42	-4.27	180.90	1775.90	-9.27	-4.28
176.40	1781.54	-9.48	-4.19	181.00	1775.54	-9.37	-4.28
176.50	1781.44	-9.44	-4.06	181.10	1775.44	-9.17	-4.24
176.60	1781.39	-8.83	-3.91	181.20	1775.41	-9.26	-4.06
176.70	1781.29	-8.54	-3.81	181.30	1775.38	-9.05	-4.19
176.80	1781.05	-8.69	-3.88	181.40	1775.29	-9.01	-3.91
176.90	1780.75	-8.86	-4.01	181.50	1775.11	-9.09	-4.59
177.00	1780.54	-9.54	-4.05	181.60	1774.91	-9.25	-4.22
177.10	1780.45	-9.30	-4.03	181.70	1774.70	-9.27	-4.12
177.20	1780.42	-9.40	-4.03	181.80	1774.67	-9.38	-4.19
177.30	1780.42	-9.35	-4.09	181.90	1774.63	-9.41	-4.20
177.40	1780.41	-9.32	-3.89	182.00	1774.59	-9.40	-4.13
177.50	1780.38	-9.05	-3.92	182.10	1774.56	-9.30	-4.04
177.60	1780.29	-9.02	-3.99	182.20	1774.52	-9.30	-4.10
177.70	1780.15	-9.21	-3.98	182.30	1774.46	-9.80	-4.20
177.80	1780.00	-9.39	-4.15	182.40	1774.29	-9.18	-4.26
177.90	1779.83	-9.45	-4.16	182.50	1774.04	-9.20	-4.07
178.00	1779.68	-9.43	-4.17	182.60	1773.79	-9.34	-4.10
178.10	1779.54	-9.61	-4.21	182.70	1773.54	-9.40	-4.10
178.20	1779.45	-9.20	-4.24	182.80	1773.29	-9.00	-4.19
178.30	1779.39	-9.06	-4.03	182.90	1773.08	-9.25	-4.12
178.40	1779.29	-9.00	-4.28	183.00	1772.93	-9.46	-4.36
178.50	1779.06	-9.15	-4.17	183.10	1772.82	-9.43	-4.05
178.60	1778.75	-9.25	-4.11	183.20	1772.75	-9.30	-4.22
178.70	1778.54	-9.31	-4.10	183.30	1772.69	-9.57	-4.62
178.80	1778.45	-9.05	-3.90	183.40	1772.62	-9.67	-4.27
178.90	1778.37	-8.90	-4.23	183.50	1772.54	-10.13	-4.35
179.00	1778.29	-8.87	-4.09	183.60	1772.47	-9.86	-4.30
179.10	1778.20	-9.04	-4.21	183.70	1772.43	-9.97	-4.47
179.20	1778.10	-9.06	-4.35	183.80	1772.41	-9.67	-4.17
179.30	1778.01	-9.24	-4.23	183.90	1772.37	-9.78	-4.23
179.40	1777.92	-9.22	-4.34	184.00	1772.29	-9.42	-4.23

Sample depth (mm)	Date (C.E.)	$\delta^{13}C$ (‰VPDB)	$\delta^{18}O$ (‰VPDB)	Sample depth (mm)	Date (C.E.)	$\delta^{13}C$ (‰VPDB)	$\delta^{18}O$ (‰VPDB)
184.10	1771.54	-9.72	-4.13	188.70	1766.54	-9.55	-4.42
184.20	1771.44	-9.58	-4.12	188.80	1766.45	-9.22	-4.10
184.30	1771.39	-9.44	-4.10	188.90	1766.38	-8.89	-4.17
184.40	1771.29	-9.44	-4.13	189.00	1766.29	-8.47	-4.04
184.50	1771.11	-9.59	-4.14	189.10	1766.09	-8.78	-4.17
184.60	1770.91	-9.55	-4.13	189.20	1765.78	-8.47	-4.04
184.70	1770.71	-9.69	-4.17	189.30	1765.54	-9.23	-4.48
184.80	1770.54	-9.76	-4.73	189.40	1765.51	-9.12	-4.07
184.90	1770.44	-9.48	-4.07	189.50	1765.48	-8.85	-4.17
185.00	1770.39	-9.52	-3.93	189.60	1765.45	-9.06	-4.32
185.10	1770.29	-9.03	-4.38	189.70	1765.42	-9.08	-4.23
185.20	1769.91	-9.35	-4.81	189.80	1765.39	-9.03	-4.20
185.30	1769.54	-9.82	-4.73	189.90	1765.29	-8.71	-4.10
185.40	1769.46	-9.79	-4.90	190.00	1765.06	-9.10	-4.18
185.50	1769.42	-9.76	-4.35	190.10	1764.77	-9.32	-4.28
185.60	1769.41	-9.56	-4.25	190.20	1764.54	-9.47	-4.22
185.70	1769.40	-9.62	-4.38	190.30	1764.44	-9.34	-4.12
185.80	1769.37	-9.25	-4.14	190.40	1764.42	-9.14	-4.14
185.90	1769.29	-8.91	-4.13	190.50	1764.39	-8.70	-4.01
186.00	1769.17	-8.91	-4.13	190.60	1764.29	-8.50	-3.93
186.10	1769.05	-9.28	-4.39	190.70	1764.05	-8.65	-3.97
186.20	1768.92	-9.35	-4.14	190.80	1763.75	-9.01	-3.99
186.30	1768.78	-9.55	-4.50	190.90	1763.54	-9.07	-4.10
186.40	1768.66	-9.74	-4.44	191.00	1763.46	-8.74	-4.03
186.50	1768.54	-9.76	-4.37	191.10	1763.42	-8.91	-4.06
186.60	1768.46	-9.74	-4.62	191.20	1763.41	-9.02	-4.16
186.70	1768.43	-9.49	-4.61	191.30	1763.37	-9.22	-4.06
186.80	1768.41	-9.47	-4.37	191.40	1763.29	-8.51	-3.90
186.90	1768.40	-9.53	-4.52	191.50	1763.15	-8.78	-4.03
187.00	1768.37	-9.43	-4.58	191.60	1762.99	-8.90	-4.04
187.10	1768.29	-9.38	-4.42	191.70	1762.82	-9.16	-4.07
187.20	1767.91	-9.54	-4.35	191.80	1762.67	-9.08	-4.08
187.30	1767.54	-9.78	-4.44	191.90	1762.54	-9.34	-4.11
187.40	1767.47	-9.73	-5.11	192.00	1762.46	-9.10	-4.16
187.50	1767.43	-9.58	-4.65	192.10	1762.41	-9.16	-4.19
187.60	1767.42	-9.68	-4.79	192.20	1762.37	-9.07	-4.03
187.70	1767.42	-9.77	-4.47	192.30	1762.29	-8.84	-3.99
187.80	1767.41	-9.41	-4.48	192.40	1762.16	-9.03	-3.99
187.90	1767.37	-9.01	-4.52	192.50	1762.00	-8.92	-4.02
188.00	1767.29	-8.50	-4.32	192.60	1761.83	-9.19	-4.12
188.10	1767.19	-8.99	-4.16	192.70	1761.67	-9.55	-4.26
188.20	1767.08	-9.30	-4.47	192.80	1761.54	-11.28	-4.31
188.30	1766.97	-9.30	-4.54	192.90	1761.46	-9.23	-4.13
188.40	1766.86	-9.36	-4.22	193.00	1761.43	-9.43	-4.16
188.50	1766.75	-9.30	-4.24	193.10	1761.41	-9.16	-4.32
188.60	1766.64	-9.38	-4.26	193.20	1761.40	-9.24	-4.14

Sample depth (mm)	Date (C.E.)	$\delta^{13}C$ (‰VPDB)	$\delta^{18}O$ (‰VPDB)	Sample depth (mm)	Date (C.E.)	$\delta^{13}C$ (‰VPDB)	$\delta^{18}O$ (‰VPDB)
193.30	1761.36	-9.17	-4.04	197.90	1756.46	-9.11	-4.38
193.40	1761.29	-8.99	-4.15	198.00	1756.29	-8.86	-4.36
193.50	1761.17	-8.99	-4.09	198.10	1755.92	-9.24	-4.49
193.60	1761.01	-9.10	-4.15	198.20	1755.54	-9.34	-4.30
193.70	1760.84	-9.17	-4.10	198.30	1755.52	-8.56	-4.62
193.80	1760.68	-9.03	-4.12	198.40	1755.51	-9.22	-4.34
193.90	1760.54	-9.43	-4.18	198.50	1755.49	-9.26	-4.49
194.00	1760.46	-9.26	-4.14	198.60	1755.48	-9.27	-4.33
194.10	1760.43	-9.43	-4.16	198.70	1755.46	-9.00	-4.25
194.20	1760.41	-8.68	-4.03	198.80	1755.29	-8.84	-4.28
194.30	1760.37	-8.93	-4.08	198.90	1754.54	-9.74	-4.45
194.40	1760.29	-8.55	-4.01	199.00	1754.46	-9.51	-4.36
194.50	1760.06	-9.04	-4.18	199.10	1754.42	-9.54	-4.34
194.60	1759.75	-9.03	-4.48	199.20	1754.37	-9.55	-4.39
194.70	1759.54	-9.23	-4.22	199.30	1754.29	-9.28	-4.29
194.80	1759.47	-9.18	-4.14	199.40	1754.18	-9.31	-4.53
194.90	1759.42	-9.23	-4.22	199.50	1754.08	-9.63	-4.38
195.00	1759.37	-9.12	-4.09	199.60	1753.97	-9.55	-4.54
195.10	1759.29	-8.93	-4.03	199.70	1753.86	-9.56	-4.46
195.20	1759.18	-9.00	-4.17	199.80	1753.75	-9.52	-4.40
195.30	1759.07	-9.11	-4.16	199.90	1753.64	-9.74	-4.46
195.40	1758.96	-9.57	-4.25	200.00	1753.54	-9.74	-4.48
195.50	1758.85	-9.44	-4.27	200.10	1753.45	-9.37	-4.45
195.60	1758.74	-9.58	-4.28	200.20	1753.38	-9.38	-4.55
195.70	1758.64	-9.70	-4.37	200.30	1753.29	-9.29	-4.40
195.80	1758.54	-9.97	-4.96	200.40	1753.08	-9.31	-4.53
195.90	1758.45	-9.64	-4.37	200.50	1752.78	-9.25	-4.34
196.00	1758.37	-9.44	-4.35	200.60	1752.54	-9.63	-4.42
196.10	1758.29	-9.34	-4.22	200.70	1752.42	-9.01	-4.20
196.20	1758.20	-9.50	-4.22	200.80	1752.29	-8.83	-4.17
196.30	1758.09	-9.36	-5.34	200.90	1752.11	-8.94	-4.14
196.40	1757.98	-9.67	-4.23	201.00	1751.90	-8.97	-4.31
196.50	1757.87	-9.59	-4.26	201.10	1751.70	-9.11	-4.60
196.60	1757.76	-9.52	-4.35	201.20	1751.54	-9.33	-4.53
196.70	1757.65	-9.56	-4.24	201.30	1751.41	-9.25	-4.46
196.80	1757.54	-9.68	-4.18	201.40	1751.29	-9.21	-4.39
196.90	1757.46	-9.58	-4.29	201.50	1751.18	-9.22	-4.41
197.00	1757.43	-9.31	-4.13	201.60	1751.07	-9.27	-4.39
197.10	1757.40	-9.24	-4.23	201.70	1750.96	-9.33	-4.58
197.20	1757.36	-9.24	-4.18	201.80	1750.85	-9.53	-4.55
197.30	1757.29	-9.16	-4.34	201.90	1750.75	-9.55	-4.64
197.40	1756.54	-9.58	-4.25	202.00	1750.64	-9.68	-4.63
197.50	1756.52	-9.47	-4.30	202.10	1750.54	-9.77	-4.87
197.60	1756.51	-9.37	-4.30	202.20	1750.45	-9.57	-4.68
197.70	1756.49	-9.37	-4.30	202.30	1750.38	-9.60	-4.57
197.80	1756.47	-9.23	-4.31	202.40	1750.29	-9.20	-4.69

Sample depth (mm)	Date (C.E.)	$\delta^{13}C$ (‰VPDB)	$\delta^{18}O$ (‰VPDB)	Sample depth (mm)	Date (C.E.)	$\delta^{13}C$ (‰VPDB)	$\delta^{18}O$ (‰VPDB)
202.50	1750.17	-9.21	-4.58	207.10	1744.54	-9.72	-4.32
202.60	1750.01	-9.50	-4.97	207.20	1744.45	-9.69	-4.17
202.70	1749.84	-9.71	-4.70	207.30	1744.44	-9.30	-4.15
202.80	1749.68	-9.79	-4.95	207.40	1744.43	-9.46	-4.37
202.90	1749.54	-9.98	-4.90	207.50	1744.42	-9.66	-4.61
203.00	1749.46	-9.98	-5.08	207.60	1744.42	-9.47	-4.28
203.10	1749.41	-9.67	-4.75	207.70	1744.41	-9.37	-4.08
203.20	1749.37	-9.34	-4.59	207.80	1744.37	-9.26	-4.20
203.30	1749.29	-9.24	-4.47	207.90	1744.29	-9.15	-4.24
203.40	1749.13	-9.57	-4.57	208.00	1744.16	-9.21	-4.13
203.50	1748.91	-9.67	-4.57	208.10	1743.99	-9.39	-4.11
203.60	1748.69	-9.61	-4.71	208.20	1743.82	-9.31	-4.09
203.70	1748.54	-9.85	-4.67	208.30	1743.67	-9.42	-4.13
203.80	1748.47	-9.73	-4.58	208.40	1743.54	-9.70	-4.31
203.90	1748.43	-9.42	-4.48	208.50	1743.47	-9.48	-4.17
204.00	1748.38	-9.23	-4.47	208.60	1743.43	-9.28	-4.15
204.10	1748.29	-9.01	-4.34	208.70	1743.41	-9.12	-4.43
204.20	1748.17	-9.34	-4.53	208.80	1743.37	-9.16	-4.18
204.30	1748.04	-9.29	-4.43	208.90	1743.29	-8.81	-3.78
204.40	1747.92	-9.67	-4.80	209.00	1743.13	-8.89	-3.87
204.50	1747.79	-9.61	-4.61	209.10	1742.92	-9.30	-4.38
204.60	1747.66	-9.67	-4.55	209.20	1742.70	-9.54	-4.09
204.70	1747.54	-9.94	-4.37	209.30	1742.54	-9.73	-4.24
204.80	1747.42	-9.82	-4.36	209.40	1742.45	-9.39	-4.14
204.90	1747.29	-9.23	-4.42	209.50	1742.38	-9.24	-4.12
205.00	1747.17	-9.30	-4.13	209.60	1742.29	-8.84	-4.05
205.10	1747.06	-9.43	-4.16	209.70	1742.15	-8.94	-4.20
205.20	1746.96	-9.50	-4.31	209.80	1741.99	-9.01	-4.32
205.30	1746.86	-9.70	-4.24	209.90	1741.82	-9.02	-4.44
205.40	1746.76	-9.31	-4.18	210.00	1741.67	-8.98	-4.41
205.50	1746.65	-9.81	-4.27	210.10	1741.54	-9.05	-4.13
205.60	1746.54	-9.96	-4.43	210.20	1741.45	-8.99	-3.97
205.70	1746.42	-9.90	-4.37	210.30	1741.38	-8.98	-4.03
205.80	1746.29	-9.31	-4.30	210.40	1741.29	-8.85	-4.07
205.90	1746.18	-9.60	-4.37	210.50	1741.18	-8.84	-4.07
206.00	1746.06	-9.38	-4.30	210.60	1741.05	-8.91	-4.06
206.10	1745.96	-9.38	-4.30	210.70	1740.92	-9.05	-4.13
206.20	1745.85	-9.53	-4.38	210.80	1740.78	-9.07	-4.13
206.30	1745.75	-9.84	-4.30	210.90	1740.65	-9.68	-4.17
206.40	1745.64	-9.78	-4.36	211.00	1740.54	-9.76	-4.26
206.50	1745.54	-10.44	-4.36	211.10	1740.46	-9.59	-4.27
206.60	1745.45	-9.67	-4.17	211.20	1740.43	-9.59	-4.26
206.70	1745.38	-9.36	-4.18	211.30	1740.42	-9.48	-4.20
206.80	1745.29	-9.09	-4.16	211.40	1740.40	-9.13	-4.23
206.90	1745.08	-9.29	-4.09	211.50	1740.37	-9.02	-4.04
207.00	1744.77	-9.23	-4.35	211.60	1740.29	-8.96	-4.08

Sample depth (mm)	Date (C.E.)	$\delta^{13}C$ (‰VPDB)	$\delta^{18}O$ (‰VPDB)	Sample depth (mm)	Date (C.E.)	$\delta^{13}C$ (‰VPDB)	$\delta^{18}O$ (‰VPDB)
211.70	1740.16	-9.23	-4.11	216.30	1735.29	-9.38	-4.36
211.80	1740.00	-9.58	-4.46	216.40	1734.92	-9.62	-4.11
211.90	1739.83	-9.65	-4.16	216.50	1734.54	-9.93	-3.95
212.00	1739.67	-9.35	-4.22	216.60	1734.44	-9.86	-4.39
212.10	1739.54	-9.82	-4.36	216.70	1734.41	-9.65	-4.02
212.20	1739.45	-9.58	-4.15	216.80	1734.41	-9.53	-4.11
212.30	1739.38	-9.10	-4.14	216.90	1734.39	-8.96	-4.13
212.40	1739.29	-8.61	-4.01	217.00	1734.29	-8.72	-3.85
212.50	1739.18	-9.10	-4.15	217.10	1734.11	-9.09	-4.49
212.60	1739.05	-9.13	-4.05	217.20	1733.90	-9.17	-3.88
212.70	1738.92	-9.12	-3.86	217.30	1733.70	-9.49	-3.97
212.80	1738.78	-8.96	-4.08	217.40	1733.54	-9.73	-4.11
212.90	1738.65	-9.31	-4.07	217.50	1733.46	-9.60	-4.24
213.00	1738.54	-9.44	-4.01	217.60	1733.42	-9.50	-4.19
213.10	1738.46	-9.36	-4.12	217.70	1733.41	-9.36	-4.05
213.20	1738.41	-9.42	-4.20	217.80	1733.37	-9.02	-3.91
213.30	1738.36	-9.19	-4.21	217.90	1733.29	-8.74	-3.88
213.40	1738.29	-8.92	-4.09	218.00	1733.13	-8.87	-4.29
213.50	1738.17	-9.03	-4.05	218.10	1732.91	-9.30	-4.52
213.60	1738.01	-9.12	-4.17	218.20	1732.69	-9.87	-4.37
213.70	1737.83	-9.20	-3.92	218.30	1732.54	-9.98	-4.46
213.80	1737.67	-9.51	-4.38	218.40	1732.47	-9.79	-4.29
213.90	1737.54	-9.56	-4.17	218.50	1732.43	-9.95	-4.43
214.00	1737.47	-9.48	-3.96	218.60	1732.41	-9.91	-4.42
214.10	1737.43	-9.45	-4.38	218.70	1732.39	-9.67	-4.12
214.20	1737.42	-9.15	-3.78	218.80	1732.36	-9.26	-4.67
214.30	1737.41	-9.09	-3.91	218.90	1732.29	-9.17	-4.23
214.40	1737.37	-8.90	-4.50	219.00	1732.20	-9.36	-4.12
214.50	1737.29	-8.85	-4.22	219.10	1732.09	-9.39	-4.15
214.60	1737.16	-9.17	-4.23	219.20	1731.98	-9.60	-4.16
214.70	1737.00	-9.26	-4.74	219.30	1731.85	-10.05	-4.66
214.80	1736.83	-9.58	-4.43	219.40	1731.70	-10.09	-4.36
214.90	1736.67	-9.56	-4.01	219.50	1731.54	-10.26	-4.41
215.00	1736.54	-10.00	-4.41	219.60	1731.29	-9.36	-4.80
215.10	1736.45	-9.87	-4.43	219.70	1731.16	-9.76	-4.30
215.20	1736.38	-9.52	-4.01	219.80	1731.04	-9.39	-4.37
215.30	1736.29	-9.40	-4.41	219.90	1730.93	-9.50	-4.44
215.40	1736.18	-9.61	-4.14	220.00	1730.82	-9.48	-4.63
215.50	1736.05	-9.94	-4.37	220.10	1730.72	-9.83	-4.95
215.60	1735.92	-9.94	-4.17	220.20	1730.63	-10.07	-4.58
215.70	1735.79	-10.19	-4.32	220.30	1730.54	-10.32	-4.57
215.80	1735.66	-10.09	-4.29	220.40	1730.46	-10.25	-4.65
215.90	1735.54	-10.34	-4.30	220.50	1730.38	-9.66	-4.28
216.00	1735.46	-10.28	-4.33	220.60	1730.29	-9.40	-4.33
216.10	1735.41	-9.73	-3.99	220.70	1730.19	-9.44	-4.22
216.20	1735.37	-9.57	-3.98	220.80	1730.09	-9.55	-4.29

Sample depth (mm)	Date (C.E.)	$\delta^{13}C$ (‰VPDB)	$\delta^{18}O$ (‰VPDB)	Sample depth (mm)	Date (C.E.)	$\delta^{13}C$ (‰VPDB)	$\delta^{18}O$ (‰VPDB)
220.90	1729.98	-9.76	-4.45	225.50	1724.45	-10.17	-4.30
221.00	1729.87	-10.08	-4.54	225.60	1724.41	-9.94	-4.20
221.10	1729.76	-10.44	-4.60	225.70	1724.37	-9.51	-4.14
221.20	1729.65	-10.28	-4.47	225.80	1724.29	-9.34	-4.21
221.30	1729.54	-10.53	-4.59	225.90	1724.07	-9.45	-4.15
221.40	1729.45	-10.17	-4.32	226.00	1723.77	-9.83	-4.27
221.50	1729.38	-9.36	-4.13	226.10	1723.54	-10.06	-4.46
221.60	1729.29	-9.00	-4.15	226.20	1723.45	-9.99	-4.24
221.70	1729.08	-9.22	-4.11	226.30	1723.42	-10.04	-4.21
221.80	1728.77	-9.58	-4.26	226.40	1723.41	-9.88	-4.28
221.90	1728.54	-9.85	-4.31	226.50	1723.38	-9.67	-4.16
222.00	1728.45	-9.73	-4.47	226.60	1723.29	-9.46	-4.11
222.10	1728.41	-9.60	-4.29	226.70	1723.11	-9.50	-4.27
222.20	1728.37	-8.90	-4.18	226.80	1722.89	-9.64	-4.20
222.30	1728.29	-8.71	-4.16	226.90	1722.68	-9.94	-4.36
222.40	1728.16	-9.21	-4.61	227.00	1722.54	-9.97	-4.13
222.50	1728.00	-9.74	-4.45	227.10	1722.47	-9.87	-4.20
222.60	1727.83	-10.34	-4.54	227.20	1722.42	-9.99	-4.20
222.70	1727.67	-10.40	-4.58	227.30	1722.36	-9.41	-4.16
222.80	1727.54	-10.53	-4.56	227.40	1722.29	-8.75	-4.25
222.90	1727.46	-10.38	-4.39	227.50	1722.20	-8.74	-4.03
223.00	1727.43	-10.49	-4.51	227.60	1722.12		
223.10	1727.42	-9.90	-4.24	227.70	1722.03	-9.71	-4.20
223.20	1727.41	-9.35	-4.07	227.80	1721.94	-9.73	-4.49
223.30	1727.38	-9.10	-4.05	227.90	1721.85		
223.40	1727.29	-8.95	-4.04	228.00	1721.75	-10.11	-4.35
223.50	1727.07	-9.25	-4.21	228.10	1721.65	-9.83	-4.36
223.60	1726.76	-9.53	-4.37	228.20	1721.54	-10.35	-4.25
223.70	1726.54	-9.90	-4.66	228.30	1721.42	-10.02	-4.26
223.80	1726.45	-9.92	-3.70	228.40	1721.29	-8.92	-4.21
223.90	1726.38	-9.44	-4.19	228.50	1721.15	-9.25	-4.09
224.00	1726.29	-8.88	-4.18	228.60	1721.00	-9.41	-4.24
224.10	1726.15	-8.98	-4.19	228.70	1720.84	-9.82	-4.23
224.20	1725.99	-9.30	-4.31	228.80	1720.69	-10.18	-4.25
224.30	1725.82	-9.74	-4.53	228.90	1720.54	-10.29	-4.20
224.40	1725.67	-9.92	-4.44	229.00	1720.45	-10.23	-4.22
224.50	1725.54	-10.30	-4.46	229.10	1720.41	-9.78	-4.11
224.60	1725.46	-10.28	-4.49	229.20	1720.37	-9.60	-4.04
224.70	1725.41	-10.10	-4.30	229.30	1720.29	-9.41	-4.11
224.80	1725.37	-9.69	-4.55	229.40	1720.07	-9.46	-4.25
224.90	1725.29	-8.96	-4.20	229.50	1719.76	-9.60	-4.01
225.00	1725.16	-8.97	-4.09	229.60	1719.54	-9.75	-4.03
225.10	1725.01	-9.32	-4.39	229.70	1719.45	-9.63	-3.99
225.20	1724.84	-9.88	-4.38	229.80	1719.38	-9.29	-4.61
225.30	1724.68	-10.19	-4.58	229.90	1719.29	-9.02	-4.39
225.40	1724.54	-10.45	-4.38	230.00	1719.15	-9.18	-4.17

Sample depth (mm)	Date (C.E.)	$\delta^{13}C$ (‰VPDB)	$\delta^{18}O$ (‰VPDB)	Sample depth (mm)	Date (C.E.)	$\delta^{13}C$ (‰VPDB)	$\delta^{18}O$ (‰VPDB)
230.10	1718.99	-9.45	-4.36	234.70	1713.41	-9.93	-4.58
230.20	1718.82	-9.47	-4.61	234.80	1713.38	-9.80	-4.43
230.30	1718.67	-9.89	-4.39	234.90	1713.29	-9.73	-4.84
230.40	1718.54	-10.28	-4.51	235.00	1713.06	-9.73	-4.59
230.50	1718.46	-10.30	-4.42	235.10	1712.76	-9.96	-4.39
230.60	1718.41	-10.26	-4.47	235.20	1712.54	-10.02	-4.49
230.70	1718.36	-10.13	-4.54	235.30	1712.45	-10.02	-4.89
230.80	1718.29	-9.56	-4.22	235.40	1712.38	-10.03	-4.42
230.90	1718.17	-9.66	-4.36	235.50	1712.29	-9.75	-4.50
231.00	1718.01	-9.69	-4.47	235.60	1712.15	-9.94	-4.43
231.10	1717.84	-9.74	-4.47	235.70	1712.00	-9.77	-4.48
231.20	1717.68	-10.01	-4.54	235.80	1711.84	-9.98	-4.71
231.30	1717.54	-10.09	-4.52	235.90	1711.68	-10.11	-4.49
231.40	1717.45	-9.98	-4.57	236.00	1711.54	-10.22	-4.34
231.50	1717.42	-9.77	-4.48	236.10	1711.52	-10.01	-4.65
231.60	1717.41	-9.63	-4.84	236.20	1711.50	-9.81	-4.44
231.70	1717.41	-9.79	-4.86	236.30	1711.48	-9.79	-4.25
231.80	1717.40	-9.84	-4.54	236.40	1711.46	-9.78	-4.39
231.90	1717.37	-9.76	-4.43	236.50	1711.44	-9.64	-4.27
232.00	1717.29	-9.56	-4.26	236.60	1711.44	-9.74	-4.39
232.10	1717.07	-10.03	-4.52	236.70	1711.40	-9.66	-4.67
232.20	1716.76	-9.74	-4.70	236.80	1711.29	-9.31	-4.28
232.30	1716.54	-10.08	-4.75	236.90	1710.93	-9.47	-4.15
232.40	1716.52	-9.96	-4.70	237.00	1710.54	-9.75	-4.32
232.50	1716.49	-10.00	-4.57	237.10	1710.42	-9.31	-4.58
232.60	1716.47	-9.82	-4.77	237.20	1710.29	-9.23	-4.53
232.70	1716.44	-9.59	-4.43	237.30	1710.04	-9.58	-4.70
232.80	1716.44	-9.76	-4.52	237.40	1709.76	-9.89	-4.52
232.90	1716.39	-9.59	-4.64	237.50	1709.54	-10.02	-4.56
233.00	1716.29	-9.31	-4.54	237.60	1709.44	-9.86	-4.49
233.10	1716.15	-9.50	-4.41	237.70	1709.40	-10.05	-4.40
233.20	1715.99	-9.43	-4.41	237.80	1709.37	-9.68	-4.23
233.30	1715.84	-9.54	-4.79	237.90	1709.29	-9.47	-4.78
233.40	1715.69	-9.53	-4.49	238.00	1709.12	-9.69	-4.81
233.50	1715.54	-9.83	-4.93	238.10	1708.92	-9.89	-4.37
233.60	1715.42	-9.71	-4.84	238.20	1708.71	-10.23	-4.75
233.70	1715.29	-9.64	-4.67	238.30	1708.54	-10.29	-4.79
233.80	1714.92	-9.80	-4.95	238.40	1708.51	-10.25	-4.74
233.90	1714.54	-10.15	-4.93	238.50	1708.49	-10.09	-4.77
234.00	1714.41	-9.87	-4.56	238.60	1708.46	-9.56	-4.11
234.10	1714.29	-9.77	-4.51	238.70	1708.43	-9.54	-4.36
234.20	1714.11	-9.82	-4.70	238.80	1708.40	-9.51	-4.51
234.30	1713.91	-9.89	-4.46	238.90	1708.29	-9.46	-4.35
234.40	1713.71	-9.92	-4.56	239.00	1708.06	-10.16	-5.24
234.50	1713.54	-9.98	-4.92	239.10	1707.77	-10.11	-5.40
234.60	1713.44	-9.82	-4.66	239.20	1707.54	-10.22	-4.55

Sample depth (mm)	Date (C.E.)	$\delta^{13}C$ (‰VPDB)	$\delta^{18}O$ (‰VPDB)	Sample depth (mm)	Date (C.E.)	$\delta^{13}C$ (‰VPDB)	$\delta^{18}O$ (‰VPDB)
239.30	1707.42	-9.93	-4.81	243.90	1700.54	-10.33	-4.60
239.40	1707.29	-9.48	-4.60	244.00	1700.45	-9.68	-4.81
239.50	1707.11	-9.50	-4.43	244.10	1700.38	-9.63	-4.29
239.60	1706.90	-9.52	-4.87	244.20	1700.29	-9.49	-4.75
239.70	1706.70	-9.88	-5.06	244.30	1699.92	-9.71	-4.59
239.80	1706.54	-10.22	-4.74	244.40	1699.54	-9.92	-4.40
239.90	1706.44	-10.04	-5.40	244.50	1699.45	-9.69	-4.58
240.00	1706.38	-9.99	-4.41	244.60	1699.42	-9.75	-4.32
240.10	1706.29	-9.51	-4.94	244.70	1699.38	-9.84	-4.91
240.20	1706.15	-9.74	-5.44	244.80	1699.29	-9.67	-4.67
240.30	1706.00	-9.78	-4.60	244.90	1699.14	-9.79	-4.29
240.40	1705.84	-9.94	-4.76	245.00	1698.99	-9.78	-4.30
240.50	1705.68	-9.87	-4.58	245.10	1698.83	-9.93	-4.75
240.60	1705.54	-10.01	-4.74	245.20	1698.68	-9.87	-4.76
240.70	1705.45	-9.85	-4.76	245.30	1698.54	-10.02	-4.48
240.80	1705.38	-10.06	-5.88	245.40	1698.42	-9.75	-4.43
240.90	1705.29	-9.73	-4.77	245.50	1698.29	-9.29	-4.43
241.00	1705.07	-9.88	-4.72	245.60	1698.15	-9.30	-4.30
241.10	1704.78	-10.03	-5.04	245.70	1698.00	-9.74	-4.41
241.20	1704.54	-10.15	-4.83	245.80	1697.84	-10.22	-4.61
241.30	1704.44	-9.98	-4.74	245.90	1697.68	-10.22	-4.70
241.40	1704.39	-9.94	-4.91	246.00	1697.54	-10.54	-4.98
241.50	1704.29	-9.88	-4.67	246.10	1697.45	-10.47	-4.73
241.60	1704.05	-9.91	-4.84	246.20	1697.40	-10.29	-4.79
241.70	1703.76	-9.99	-4.84	246.30	1697.37	-9.63	-4.63
241.80	1703.54	-10.08	-4.86	246.40	1697.29	-9.58	-4.56
241.90	1703.45	-10.00	-4.51	246.50	1697.13	-9.70	-4.39
242.00	1703.39	-10.07	-4.57	246.60	1696.92	-9.82	-4.62
242.10	1703.29	-9.93	-4.74	246.70	1696.71	-9.91	-4.71
242.20	1703.12	-9.95	-4.63	246.80	1696.54	-10.31	-4.61
242.30	1702.92	-10.07	-4.66	246.90	1696.45	-10.13	-4.61
242.40	1702.72	-9.94	-4.33	247.00	1696.42	-9.93	-4.92
242.50	1702.54	-10.14	-4.61	247.10	1696.38	-9.66	-4.81
242.60	1702.41	-9.96	-4.47	247.20	1696.29	-9.32	-4.39
242.70	1702.29	-9.63	-4.43	247.30	1696.13	-9.42	-4.44
242.80	1701.90	-9.70	-4.69	247.40	1695.92	-9.72	-4.97
242.90	1701.54	-9.91	-4.37	247.50	1695.70	-10.01	-4.66
243.00	1701.45	-9.79	-4.77	247.60	1695.54	-10.09	-4.90
243.10	1701.41	-9.94	-4.77	247.70	1695.45	-9.95	-4.96
243.20	1701.37	-9.80	-4.46	247.80	1695.42	-9.69	-4.47
243.30	1701.29	-9.61	-4.47	247.90	1695.38	-9.41	-4.90
243.40	1701.17	-9.65	-4.79	248.00	1695.29	-9.12	-4.39
243.50	1701.04	-9.89	-4.60	248.10	1695.12	-9.29	-4.35
243.60	1700.92	-10.04	-4.81	248.20	1694.90	-9.70	-4.47
243.70	1700.79	-9.99	-4.92	248.30	1694.69	-9.79	-4.47
243.80	1700.66	-10.19	-4.62	248.40	1694.54	-9.90	-4.81

Sample depth (mm)	Date (C.E.)	$\delta^{13}C$ (‰VPDB)	$\delta^{18}O$ (‰VPDB)	Sample depth (mm)	Date (C.E.)	$\delta^{13}C$ (‰VPDB)	$\delta^{18}O$ (‰VPDB)
248.50	1694.46	-9.64	-5.04	253.10	1689.45	-9.67	-4.07
248.60	1694.42	-9.91	-5.08	253.20	1689.38	-9.16	-4.38
248.70	1694.37	-9.52	-4.72	253.30	1689.29	-8.73	-4.31
248.80	1694.29	-9.35	-4.65	253.40	1689.19	-9.11	-4.37
248.90	1694.17	-9.50	-4.66	253.50	1689.09	-9.28	-5.09
249.00	1694.05	-9.56	-4.49	253.60	1688.99	-9.54	-4.82
249.10	1693.91	-9.74	-4.53	253.70	1688.88	-9.53	-4.40
249.20	1693.78	-9.77	-4.83	253.80	1688.77	-9.69	-4.40
249.30	1693.65	-9.49	-4.88	253.90	1688.66	-9.75	-4.88
249.40	1693.54	-9.91	-4.79	254.00	1688.54	-9.86	-4.70
249.50	1693.45	-9.71	-4.70	254.10	1688.42	-9.33	-4.46
249.60	1693.38	-9.39	-4.40	254.20	1688.29	-8.87	-4.60
249.70	1693.29	-9.09	-4.58	254.30	1688.17	-9.19	-4.65
249.80	1693.16	-9.30	-4.48	254.40	1688.04	-9.02	-4.32
249.90	1693.00	-9.50	-4.71	254.50	1687.92	-9.19	-4.91
250.00	1692.83	-9.72	-4.66	254.60	1687.79	-9.54	-4.87
250.10	1692.67	-9.70	-4.86	254.70	1687.66	-9.64	-4.67
250.20	1692.54	-9.77	-4.89	254.80	1687.54	-10.56	-4.78
250.30	1692.46	-9.75	-4.53	254.90	1687.45	-10.06	-5.02
250.40	1692.42	-9.71	-4.40	255.00	1687.41	-10.20	-4.81
250.50	1692.37	-9.29	-4.43	255.10	1687.38	-9.83	-4.60
250.60	1692.29	-9.10	-4.03	255.20	1687.35	-9.70	-4.66
250.70	1692.16	-9.20	-4.01	255.30	1687.29	-9.23	-4.19
250.80	1691.99	-9.13	-4.18	255.40	1687.18	-9.41	-4.50
250.90	1691.82	-9.42	-4.23	255.50	1687.06	-9.60	-4.53
251.00	1691.66			255.60	1686.92	-9.81	-4.31
251.10	1691.54	-9.55	-4.12	255.70	1686.77	-9.68	-4.57
251.20	1691.45	-9.56	-4.10	255.80	1686.65	-9.88	-4.69
251.30	1691.38	-9.32	-4.13	255.90	1686.54	-10.16	-4.70
251.40	1691.29	-9.19	-4.25	256.00	1686.47	-10.14	-4.35
251.50	1691.19	-9.19	-4.12	256.10	1686.42	-9.96	-4.54
251.60	1691.08	-9.27	-4.10	256.20	1686.37	-9.69	-4.63
251.70	1690.97	-9.45	-4.34	256.30	1686.29	-9.20	-4.58
251.80	1690.86	-9.71	-4.47	256.40	1686.18	-9.35	-4.54
251.90	1690.75	-9.78	-4.11	256.50	1686.05	-9.29	-4.54
252.00	1690.64	-10.08	-4.37	256.60	1685.91	-9.41	-4.87
252.10	1690.54	-10.12	-4.63	256.70	1685.77	-9.24	-4.34
252.20	1690.46	-10.13	-4.30	256.80	1685.64	-9.31	-4.33
252.30	1690.42	-10.02	-4.54	256.90	1685.54	-9.52	-4.14
252.40	1690.37	-9.04	-4.18	257.00	1685.46	-9.44	-4.25
252.50	1690.29	-8.76	-4.28	257.10	1685.37	-9.53	-4.47
252.60	1690.17	-8.85	-4.27	257.20	1685.29	-8.94	-5.00
252.70	1690.00	-9.20	-4.30	257.30	1685.20	-9.11	-4.16
252.80	1689.83	-9.49	-4.53	257.40	1685.11	-9.07	-4.52
252.90	1689.66	-9.77	-4.69	257.50	1685.01	-9.00	-4.68
253.00	1689.54	-9.82	-4.21	257.60	1684.91	-9.28	-4.67

Sample depth (mm)	Date (C.E.)	$\delta^{13}C$ (‰VPDB)	$\delta^{18}O$ (‰VPDB)	Sample depth (mm)	Date (C.E.)	$\delta^{13}C$ (‰VPDB)	$\delta^{18}O$ (‰VPDB)
257.70	1684.82	-9.37	-4.18	262.30	1679.38	-9.51	-4.36
257.80	1684.72	-9.52	-4.41	262.40	1679.29	-9.37	-4.47
257.90	1684.63	-9.68	-4.89	262.50	1679.14	-9.76	-4.68
258.00	1684.54	-9.87	-4.62	262.60	1678.92	-9.61	-4.61
258.10	1684.47	-9.89	-4.63	262.70	1678.71	-9.80	-4.54
258.20	1684.41	-9.61	-4.98	262.80	1678.54	-9.83	-4.76
258.30	1684.36	-9.66	-4.15	262.90	1678.45	-9.81	-4.62
258.40	1684.29	-9.45	-4.93	263.00	1678.44	-9.64	-4.82
258.50	1684.20	-9.52	-4.81	263.10	1678.43	-9.66	-4.70
258.60	1684.10	-9.53	-4.65	263.20	1678.42	-9.44	-4.69
258.70	1683.99	-9.71	-4.28	263.30	1678.42	-9.40	-4.67
258.80	1683.88	-9.79	-5.22	263.40	1678.41	-9.46	-5.06
258.90	1683.76	-9.79	-5.15	263.50	1678.37	-9.48	-4.79
259.00	1683.64	-9.92	-4.90	263.60	1678.29	-9.29	-4.71
259.10	1683.54	-10.07	-5.13	263.70	1678.14	-9.68	-4.47
259.20	1683.47	-10.05	-5.15	263.80	1677.93	-9.71	-4.68
259.30	1683.43	-9.85	-5.02	263.90	1677.72	-9.49	-4.79
259.40	1683.42	-10.05	-4.92	264.00	1677.54	-9.93	-4.96
259.50	1683.42	-9.93	-5.73	264.10	1677.45	-9.64	-4.90
259.60	1683.40	-9.48	-5.23	264.20	1677.42	-9.59	-4.69
259.70	1683.37	-9.26	-5.50	264.30	1677.41	-9.64	-4.68
259.80	1683.29	-9.19	-4.91	264.40	1677.38	-9.41	-4.74
259.90	1682.93	-9.48	-4.62	264.50	1677.29	-8.97	-3.95
260.00	1682.54	-9.53	-5.40	264.60	1676.92	-9.21	-4.09
260.10	1682.44	-9.51	-4.84	264.70	1676.54	-9.46	-4.95
260.20	1682.40	-9.27	-4.90	264.80	1676.43	-9.25	-5.03
260.30	1682.29	-8.97	-4.51	264.90	1676.38	-9.45	-4.25
260.40	1682.04	-8.98	-4.31	265.00	1676.37	-9.15	-4.66
260.50	1681.75	-9.12	-4.57	265.10	1676.36	-9.25	-4.23
260.60	1681.54	-9.55	-4.65	265.20	1676.35	-9.19	-4.87
260.70	1681.44	-9.56	-4.30	265.30	1676.34	-9.10	-4.23
260.80	1681.38	-9.24	-4.33	265.40	1676.33	-9.13	-4.08
260.90	1681.29	-9.01	-4.20	265.50	1676.31	-9.00	-4.26
261.00	1681.16	-9.15	-4.46	265.60	1676.30	-9.07	-4.32
261.10	1681.02	-9.00	-4.46	265.70	1676.29	-8.95	-4.49
261.20	1680.88	-9.26	-4.36	265.80	1676.10	-9.14	-4.29
261.30	1680.72	-9.29	-4.45	265.90	1675.90	-9.24	-4.47
261.40	1680.54	-9.71	-4.74	266.00	1675.70	-9.36	-4.61
261.50	1680.29	-9.36	-4.39	266.10	1675.54	-9.40	-4.48
261.60	1680.14	-9.34	-4.31	266.20	1675.42	-9.15	-4.60
261.70	1680.00	-9.62	-4.23	266.30	1675.29	-8.97	-4.41
261.80	1679.87	-9.61	-4.48	266.40	1675.17	-9.29	-4.37
261.90	1679.75	-9.59	-4.35	266.50	1675.04	-9.14	-3.90
262.00	1679.64	-9.41	-4.36	266.60	1674.91	-9.04	-4.09
262.10	1679.54	-9.86	-4.48	266.70	1674.79	-9.11	-4.48
262.20	1679.45	-9.43	-4.44	266.80	1674.66	-9.16	-4.15

Sample depth (mm)	Date (C.E.)	$\delta^{13}C$ (‰VPDB)	$\delta^{18}O$ (‰VPDB)	Sample depth (mm)	Date (C.E.)	$\delta^{13}C$ (‰VPDB)	$\delta^{18}O$ (‰VPDB)
266.90	1674.54	-9.33	-4.48	271.50	1670.13	-9.39	-4.81
267.00	1674.44	-9.34	-4.26	271.60	1669.98	-9.64	-4.27
267.10	1674.37	-9.23	-4.26	271.70	1669.85	-9.74	-4.08
267.20	1674.29	-8.93	-4.36	271.80	1669.73	-9.75	-4.50
267.30	1674.19	-9.06	-4.44	271.90	1669.63	-9.80	-4.56
267.40	1674.09	-8.97	-4.43	272.00	1669.54	-9.85	-4.60
267.50	1673.99	-9.09	-4.09	272.10	1669.48	-9.71	-4.74
267.60	1673.88	-9.38	-4.27	272.20	1669.44	-9.52	-4.31
267.70	1673.78	-9.01	-4.36	272.30	1669.40	-9.93	-4.72
267.80	1673.66	-9.11	-4.03	272.40	1669.36	-9.51	-4.78
267.90	1673.54	-9.42	-4.26	272.50	1669.29	-9.23	-4.31
268.00	1673.42	-9.09	-4.54	272.60	1669.19	-9.40	-4.54
268.10	1673.29	-8.89	-4.41	272.70	1669.07	-9.53	-4.56
268.20	1673.17	-9.11	-4.55	272.80	1668.94	-9.85	-4.59
268.30	1673.04	-8.90	-4.37	272.90	1668.80	-10.17	-4.89
268.40	1672.92	-9.16	-4.44	273.00	1668.66	-10.24	-4.69
268.50	1672.79	-9.63	-4.44	273.10	1668.54	-10.31	-4.96
268.60	1672.67	-9.77	-5.09	273.20	1668.45	-10.16	-4.79
268.70	1672.54	-9.90	-4.82	273.30	1668.42	-9.89	-4.16
268.80	1672.42	-9.56	-4.16	273.40	1668.42	-9.70	-4.78
268.90	1672.29	-9.40	-4.81	273.50	1668.42	-9.44	-4.64
269.00	1672.17	-9.39	-4.29	273.60	1668.41	-9.41	-5.02
269.10	1672.06	-9.77	-5.32	273.70	1668.37	-9.43	-4.34
269.20	1671.96	-9.72	-4.81	273.80	1668.29	-8.76	-4.85
269.30	1671.87	-9.70	-4.52	273.90	1667.54	-9.72	-4.11
269.40	1671.78	-9.65	-4.23	274.00	1667.51	-9.67	-5.15
269.50	1671.69	-9.95	-4.72	274.10	1667.48	-9.59	-4.23
269.60	1671.62	-10.06	-4.26	274.20	1667.45	-9.04	-4.71
269.70	1671.54	-10.09	-5.10	274.30	1667.42	-9.05	-4.68
269.80	1671.48	-9.77	-4.57	274.40	1667.39	-8.96	-3.88
269.90	1671.44	-9.61	-4.56	274.50	1667.29	-8.84	-5.03
270.00	1671.41	-9.64	-4.58	274.60	1667.14	-8.95	-4.57
270.10	1671.40	-9.67	-3.96	274.70	1666.97	-9.69	-4.80
270.20	1671.39	-9.64	-4.54	274.80	1666.81	-9.81	-4.79
270.30	1671.38	-9.61	-4.64	274.90	1666.66	-9.90	-4.51
270.40	1671.36	-8.97	-3.99	275.00	1666.54	-10.16	-4.79
270.50	1671.33	-8.99	-4.47	275.10	1666.47	-10.15	-4.25
270.60	1671.29	-8.71	-4.22	275.20	1666.41	-10.08	-4.75
270.70	1671.23	-9.25	-4.71	275.30	1666.36	-9.57	-4.38
270.80	1671.15	-9.16	-4.49	275.40	1666.29	-9.23	-4.37
270.90	1671.06	-9.37	-4.45	275.50	1666.18	-9.49	-4.68
271.00	1670.96	-9.42	-4.72	275.60	1666.05	-9.38	-4.47
271.10	1670.83	-9.34	-4.66	275.70	1665.92	-9.42	-4.47
271.20	1670.69	-9.49	-4.78	275.80	1665.78	-9.91	-4.82
271.30	1670.54	-9.53	-4.73	275.90	1665.65	-9.90	-4.84
271.40	1670.29	-9.26	-4.34	276.00	1665.54	-10.13	-4.72

Sample depth (mm)	Date (C.E.)	$\delta^{13}C$ (‰VPDB)	$\delta^{18}O$ (‰VPDB)	Sample depth (mm)	Date (C.E.)	$\delta^{13}C$ (‰VPDB)	$\delta^{18}O$ (‰VPDB)
276.10	1665.47	-10.00	-4.37	280.70	1660.54	-9.91	-4.36
276.20	1665.45	-9.48	-4.63	280.80	1660.47	-9.66	-4.42
276.30	1665.44	-9.34	-4.58	280.90	1660.41	-9.61	-4.52
276.40	1665.44	-9.16	-4.53	281.00	1660.36	-9.45	-4.50
276.50	1665.43	-9.06	-5.01	281.10	1660.29	-9.43	-4.04
276.60	1665.38	-9.41	-4.96	281.20	1660.22	-9.43	-4.07
276.70	1665.29	-8.89	-4.73	281.30	1660.14	-9.91	-4.74
276.80	1665.15	-9.43	-5.03	281.40	1660.07	-10.00	-4.77
276.90	1665.00	-9.74	-4.78	281.50	1659.99	-9.98	-4.88
277.00	1664.84	-9.64	-4.88	281.60	1659.92	-9.98	-4.93
277.10	1664.68	-9.68	-4.78	281.70	1659.84	-9.68	-4.56
277.20	1664.54	-9.91	-5.31	281.80	1659.76	-10.00	-4.85
277.30	1664.42	-9.39	-4.40	281.90	1659.69	-10.14	-4.79
277.40	1664.29	-9.25	-4.65	282.00	1659.61	-10.20	-4.97
277.50	1664.15	-9.29	-4.35	282.10	1659.54	-10.40	-4.87
277.60	1663.99	-9.45	-4.85	282.20	1659.48	-10.42	-4.85
277.70	1663.83	-9.72	-5.14	282.30	1659.43	-10.31	-4.92
277.80	1663.68	-9.88	-5.24	282.40	1659.40	-10.16	-4.71
277.90	1663.54	-10.06	-4.78	282.50	1659.35	-10.26	-4.99
278.00	1663.45	-10.05	-5.03	282.60	1659.29	-9.95	-4.93
278.10	1663.40	-9.67	-4.87	282.70	1659.10	-9.98	-4.55
278.20	1663.36	-9.47	-4.74	282.80	1658.79	-10.04	-4.61
278.30	1663.29	-9.41	-4.74	282.90	1658.54	-10.25	-4.95
278.40	1663.18	-9.43	-4.57	283.00	1658.44	-10.19	-5.32
278.50	1663.06	-9.60	-4.81	283.10	1658.41	-9.97	-4.24
278.60	1662.92	-9.99	-5.24	283.20	1658.39	-9.94	-4.21
278.70	1662.78	-9.91	-5.51	283.30	1658.29	-9.73	-4.19
278.80	1662.65	-10.12	-5.12	283.40	1658.06	-9.85	-4.19
278.90	1662.54	-10.59	-5.10	283.50	1657.76	-10.02	-4.27
279.00	1662.47	-10.36	-4.51	283.60	1657.54	-10.22	-4.26
279.10	1662.43	-10.05	-4.79	283.70	1657.45	-10.16	-4.27
279.20	1662.42	-9.90	-5.03	283.80	1657.41	-10.25	-4.34
279.30	1662.40	-9.73	-4.44	283.90	1657.41	-10.23	-4.27
279.40	1662.36	-9.64	-4.61	284.00	1657.41	-10.15	-4.37
279.50	1662.29	-9.60	-5.07	284.10	1657.38	-10.04	-4.37
279.60	1662.14	-9.69	-4.53	284.20	1657.29	-9.90	-4.14
279.70	1661.93	-9.98	-5.26	284.30	1657.12	-10.19	-4.39
279.80	1661.71	-10.08	-5.07	284.40	1656.90	-10.13	-4.36
279.90	1661.54	-10.08	-4.82	284.50	1656.69	-10.08	-4.34
280.00	1661.46	-10.11	-5.49	284.60	1656.54	-10.24	-4.32
280.10	1661.42	-9.85	-4.79	284.70	1656.46	-9.77	-4.35
280.20	1661.38	-9.61	-5.33	284.80	1656.46	-9.84	-4.31
280.30	1661.29	-9.52	-4.87	284.90	1656.45	-10.04	-4.39
280.40	1661.12	-9.54	-5.11	285.00	1656.44	-9.81	-4.34
280.50	1660.89	-9.71	-4.80	285.10	1656.44	-9.78	-4.39
280.60	1660.68	-9.84	-4.69	285.20	1656.43	-9.89	-4.34

Sample depth (mm)	Date (C.E.)	$\delta^{13}C$ (‰VPDB)	$\delta^{18}O$ (‰VPDB)	Sample depth (mm)	Date (C.E.)	$\delta^{13}C$ (‰VPDB)	$\delta^{18}O$ (‰VPDB)
285.30	1656.42	-9.64	-4.25	289.90	1649.54	-9.07	-4.69
285.40	1656.37	-9.97	-4.42	290.00	1649.45	-9.05	-5.72
285.50	1656.29	-9.65	-4.47	290.10	1649.39	-8.93	-6.04
285.60	1656.16	-9.92	-4.46	290.20	1649.29	-8.78	-5.10
285.70	1656.01	-10.01	-4.41	290.30	1649.11	-8.83	-5.38
285.80	1655.84	-9.86	-4.49	290.40	1648.92	-8.94	-4.49
285.90	1655.68	-9.88	-4.47	290.50	1648.72	-9.08	-5.38
286.00	1655.54	-10.07	-4.66	290.60	1648.54	-9.11	-4.65
286.10	1655.46	-9.86	-4.60	290.70	1648.41	-8.92	-4.95
286.20	1655.42	-10.00	-4.56	290.80	1648.29	-8.78	-4.98
286.30	1655.39			290.90	1648.06	-8.82	-4.90
286.40	1655.29	-9.85	-4.49	291.00	1647.77	-8.94	-5.07
286.50	1654.93	-9.92	-4.47	291.10	1647.54	-9.33	-5.30
286.60	1654.54	-10.09	-4.60	291.20	1647.44	-9.14	-5.04
286.70	1654.41	-10.07	-4.60	291.30	1647.41	-9.13	-4.98
286.80	1654.29	-9.68	-4.44	291.40	1647.38	-9.11	-4.46
286.90	1654.04	-9.83	-4.47	291.50	1647.29	-9.07	-6.00
287.00	1653.76	-9.68	-4.43	291.60	1647.12	-9.21	-4.72
287.10	1653.54	-9.90	-4.50	291.70	1646.91	-9.19	-5.24
287.20	1653.51	-9.67	-4.41	291.80	1646.70	-9.04	-5.37
287.30	1653.48	-9.40	-4.19	291.90	1646.54	-9.26	-5.42
287.40	1653.44	-9.39	-4.23	292.00	1646.45	-9.15	-5.82
287.50	1653.41	-9.24	-4.00	292.10	1646.38	-9.17	-5.45
287.60	1653.38	-9.35	-4.31	292.20	1646.29	-9.00	-5.01
287.70	1653.29	-9.14	-4.25	292.30	1646.13	-9.26	-4.59
287.80	1653.12	-9.39	-4.29	292.40	1645.92	-9.38	-5.29
287.90	1652.91	-9.47	-4.43	292.50	1645.71	-9.27	-5.12
288.00	1652.70	-9.70	-4.42	292.60	1645.54	-9.49	-5.26
288.10	1652.54	-9.82	-4.45	292.70	1645.45	-9.50	-4.62
288.20	1652.45	-9.45	-4.43	292.80	1645.41	-9.33	-4.65
288.30	1652.39	-9.23	-4.30	292.90	1645.38	-9.29	-4.79
288.40	1652.29	-9.00	-4.08	293.00	1645.29	-9.25	-4.40
288.50	1652.14	-9.14	-4.50	293.10	1645.07	-9.33	-4.53
288.60	1651.97	-9.07	-4.24	293.20	1644.76	-9.35	-4.64
288.70	1651.77	-9.15	-4.49	293.30	1644.54	-9.56	-4.62
288.80	1651.54	-9.34	-4.53	293.40	1644.45	-9.52	-4.61
288.90	1651.29	-9.02	-5.49	293.50	1644.42	-9.35	-5.20
289.00	1651.04	-9.11	-5.49	293.60	1644.41	-9.17	-5.49
289.10	1650.79	-9.18	-5.78	293.70	1644.38	-8.75	-4.32
289.20	1650.54	-9.51	-5.47	293.80	1644.29	-8.72	-5.50
289.30	1650.39	-9.33	-5.29	293.90	1644.12	-9.19	-5.92
289.40	1650.38	-9.23	-5.31	294.00	1643.90	-9.46	-5.09
289.50	1650.37	-8.93	-5.27	294.10	1643.70	-9.56	-6.06
289.60	1650.29	-8.66	-5.55	294.20	1643.54	-9.75	-5.62
289.70	1650.06	-8.65	-5.01	294.30	1643.45	-9.48	-5.54
289.80	1649.76	-8.82	-4.98	294.40	1643.39	-9.13	-5.91

Sample depth (mm)	Date (C.E.)	$\delta^{13}C$ (‰VPDB)	$\delta^{18}O$ (‰VPDB)	Sample depth (mm)	Date (C.E.)	$\delta^{13}C$ (‰VPDB)	$\delta^{18}O$ (‰VPDB)
294.50	1643.29	-8.91	-4.69	299.10	1637.36	-9.04	-3.99
294.60	1643.15	-9.05	-5.45	299.20	1637.29	-8.93	-4.06
294.70	1643.00	-9.45	-5.33	299.30	1637.16	-9.25	-3.82
294.80	1642.84	-9.73	-5.07	299.40	1637.00	-9.27	-3.94
294.90	1642.69	-9.64	-4.94	299.50	1636.83	-9.38	-4.19
295.00	1642.54	-9.81	-5.05	299.60	1636.67	-9.55	-4.17
295.10	1642.41	-9.39	-5.33	299.70	1636.54	-10.21	-3.89
295.20	1642.29	-8.89	-4.57	299.80	1636.47	-9.70	-3.99
295.30	1642.07	-8.95	-5.28	299.90	1636.42	-9.46	-4.14
295.40	1641.78	-9.29	-5.41	300.00	1636.37	-9.20	-4.01
295.50	1641.54	-9.27	-4.00	300.10	1636.29	-9.02	-4.11
295.60	1641.51			300.20	1636.16	-9.34	-3.91
295.70	1641.48			300.30	1636.00	-9.51	-4.22
295.80	1641.45			300.40	1635.83	-9.77	-4.33
295.90	1641.42			300.50	1635.67		
296.00	1641.39			300.60	1635.54	-10.23	-4.67
296.10	1641.29	-9.15	-4.51	300.70	1635.45	-10.21	-5.51
296.20	1641.06	-9.47	-4.23	300.80	1635.38	-9.91	-4.94
296.30	1640.77	-9.55	-4.31	300.90	1635.29	-9.60	-5.11
296.40	1640.54	-9.77	-5.08	301.00	1635.17	-9.69	-4.76
296.50	1640.44	-9.57	-4.21	301.10	1635.05	-9.84	-5.14
296.60	1640.39			301.20	1634.91	-9.88	-5.07
296.70	1640.29	-8.92	-3.93	301.30	1634.78	-9.96	-5.05
296.80	1640.05			301.40	1634.65	-10.11	-5.14
296.90	1639.76	-9.25	-3.96	301.50	1634.54	-10.21	-5.43
297.00	1639.54	-9.51	-4.02	301.60	1634.46	-9.97	-5.33
297.10	1639.45	-9.24	-4.03	301.70	1634.39	-9.53	-5.47
297.20	1639.39			301.80	1634.29	-9.47	-5.14
297.30	1639.29	-8.93	-3.87	301.90	1634.17	-9.61	-4.50
297.40	1639.14	-9.03	-3.91	302.00	1634.04	-9.48	-4.79
297.50	1638.99			302.10	1633.92	-9.59	-5.02
297.60	1638.83			302.20	1633.79	-9.78	-4.82
297.70	1638.68	-9.14	-4.29	302.30	1633.66	-9.82	-4.78
297.80	1638.54	-9.21	-3.98	302.40	1633.54	-9.86	-5.11
297.90	1638.41	-9.10	-3.94	302.50	1633.42	-9.50	-4.31
298.00	1638.29	-8.89	-4.10	302.60	1633.29	-9.40	-4.71
298.10	1638.15	-9.07	-4.35	302.70	1633.15	-9.41	-4.71
298.20	1638.00			302.80	1633.00	-9.49	-3.90
298.30	1637.84	-8.98	-4.26	302.90	1632.84	-9.60	-4.83
298.40	1637.68			303.00	1632.68	-9.83	-4.85
298.50	1637.54	-9.32	-3.93	303.10	1632.54	-9.91	-5.17
298.60	1637.44	-9.01	-4.33	303.20	1632.44	-9.90	-4.99
298.70	1637.40	-9.15	-4.10	303.30	1632.41	-9.56	-4.66
298.80	1637.40	-9.18	-3.89	303.40	1632.39	-9.29	-4.60
298.90	1637.39	-9.10	-4.08	303.50	1632.36	-9.16	-4.34
299.00	1637.39	-9.25	-4.12	303.60	1632.29	-9.07	-4.62

Sample depth (mm)	Date (C.E.)	$\delta^{13}C$ (‰VPDB)	$\delta^{18}O$ (‰VPDB)	Sample depth (mm)	Date (C.E.)	$\delta^{13}C$ (‰VPDB)	$\delta^{18}O$ (‰VPDB)
303.70	1632.14	-9.35	-4.26	308.30	1627.46	-9.48	-4.29
303.80	1631.93	-9.61	-4.66	308.40	1627.41	-9.53	-4.20
303.90	1631.71	-9.97	-4.82	308.50	1627.36	-9.31	-4.27
304.00	1631.54	-10.02	-4.84	308.60	1627.29	-9.04	-4.14
304.10	1631.45	-9.81	-4.32	308.70	1627.18	-9.26	-4.48
304.20	1631.44	-10.01	-4.68	308.80	1627.05	-9.31	-4.45
304.30	1631.43	-9.88	-4.50	308.90	1626.91	-9.49	-4.09
304.40	1631.42	-9.37	-4.55	309.00	1626.77	-9.63	-4.65
304.50	1631.42	-9.38	-4.96	309.10	1626.64	-9.59	-4.40
304.60	1631.39	-9.53	-5.02	309.20	1626.54	-9.66	-4.62
304.70	1631.29	-9.35	-4.91	309.30	1626.47	-9.62	-4.54
304.80	1631.06	-9.47	-4.69	309.40	1626.42	-9.53	-4.18
304.90	1630.76	-9.69	-4.58	309.50	1626.36	-9.40	-4.36
305.00	1630.54	-9.83	-4.72	309.60	1626.29	-9.05	-4.47
305.10	1630.46	-9.82	-4.43	309.70	1626.20	-9.22	-4.39
305.20	1630.42	-9.72	-4.87	309.80	1626.11	-9.34	-4.48
305.30	1630.37	-9.32	-4.86	309.90	1626.01	-9.43	-4.39
305.40	1630.29	-9.23	-4.77	310.00	1625.91	-9.45	-4.50
305.50	1630.15	-9.70	-4.60	310.10	1625.82	-9.61	-4.76
305.60	1629.98	-9.39	-4.36	310.20	1625.72	-9.55	-4.69
305.70	1629.81	-9.66	-4.58	310.30	1625.63	-9.63	-4.61
305.80	1629.65	-9.66	-4.50	310.40	1625.54	-9.77	-4.04
305.90	1629.54	-9.77	-4.70	310.50	1625.46	-9.44	-4.70
306.00	1629.48	-9.70	-4.62	310.60	1625.38	-9.29	-4.67
306.10	1629.44	-9.59	-4.51	310.70	1625.29	-9.03	-4.69
306.20	1629.42	-9.75	-4.64	310.80	1625.19	-9.17	-4.43
306.30	1629.40	-9.69	-4.41	310.90	1625.09	-9.14	-4.38
306.40	1629.36	-9.60	-4.34	311.00	1624.99	-9.08	-4.48
306.50	1629.29	-9.28	-4.37	311.10	1624.88	-9.16	-4.74
306.60	1629.20	-9.36	-4.39	311.20	1624.77	-9.28	-4.39
306.70	1629.11	-9.33	-4.59	311.30	1624.65	-9.52	-4.92
306.80	1629.01	-9.34	-4.32	311.40	1624.54	-9.56	-4.78
306.90	1628.91	-9.38	-4.43	311.50	1624.41	-9.19	-4.58
307.00	1628.82	-9.39	-4.53	311.60	1624.29	-8.81	-4.60
307.10	1628.72	-9.39	-4.30	311.70	1624.19	-8.85	-4.47
307.20	1628.63	-9.60	-4.19	311.80	1624.09	-8.89	-4.56
307.30	1628.54	-9.66	-4.95	311.90	1623.99	-9.00	-4.31
307.40	1628.46	-9.52	-4.09	312.00	1623.90	-8.98	-4.51
307.50	1628.38	-9.46	-4.75	312.10	1623.80	-9.03	-4.40
307.60	1628.29	-9.20	-4.75	312.20	1623.71	-9.03	-4.69
307.70	1628.19	-9.22	-4.52	312.30	1623.63	-9.12	-4.23
307.80	1628.06	-9.27	-4.24	312.40	1623.54	-9.45	-4.92
307.90	1627.92	-9.45	-4.52	312.50	1623.46	-9.08	-4.71
308.00	1627.78	-9.39	-4.59	312.60	1623.38	-9.01	-4.61
308.10	1627.65	-9.57	-4.65	312.70	1623.29	-8.90	-4.54
308.20	1627.54	-9.61	-4.41	312.80	1623.20	-9.08	-4.22

Sample depth (mm)	Date (C.E.)	$\delta^{13}C$ (‰VPDB)	$\delta^{18}O$ (‰VPDB)	Sample depth (mm)	Date (C.E.)	$\delta^{13}C$ (‰VPDB)	$\delta^{18}O$ (‰VPDB)
312.90	1623.11	-9.16	-4.41	317.50	1617.68	-9.50	-5.51
313.00	1623.01	-9.23	-4.37	317.60	1617.54	-9.80	-5.55
313.10	1622.92	-9.21	-4.40	317.70	1617.45	-9.52	-5.27
313.20	1622.82	-9.08	-4.18	317.80	1617.38	-9.62	-4.99
313.30	1622.73	-9.27	-4.28	317.90	1617.29	-9.38	-3.77
313.40	1622.63	-9.43	-4.34	318.00	1617.13	-9.71	-4.97
313.50	1622.54	-9.51	-4.37	318.10	1616.93	-9.56	-5.19
313.60	1622.45	-9.36	-4.32	318.20	1616.72	-10.00	-4.57
313.70	1622.37	-9.16	-4.28	318.30	1616.54	-10.07	-4.94
313.80	1622.29	-8.87	-4.40	318.40	1616.45	-9.87	-5.02
313.90	1622.20	-9.04	-4.14	318.50	1616.41	-9.70	-5.00
314.00	1622.09	-9.01	-4.28	318.60	1616.38	-9.48	-4.44
314.10	1621.98	-9.03	-4.31	318.70	1616.29	-9.40	-4.84
314.20	1621.87	-9.21	-4.28	318.80	1616.07	-9.52	-4.38
314.30	1621.76	-9.21	-4.40	318.90	1615.77	-9.57	-5.05
314.40	1621.65	-9.15	-4.33	319.00	1615.54	-9.80	-5.31
314.50	1621.54	-9.26	-4.32	319.10	1615.44	-9.82	-4.52
314.60	1621.47	-8.93	-4.28	319.20	1615.42	-9.56	-5.24
314.70	1621.43	-8.75	-4.24	319.30	1615.41	-9.52	-4.76
314.80	1621.41	-8.73	-4.24	319.40	1615.39	-9.57	-4.99
314.90	1621.37	-8.71	-4.34	319.50	1615.29	-9.30	-4.97
315.00	1621.29	-8.61	-4.31	319.60	1615.06	-9.77	-5.02
315.10	1621.07	-8.87	-4.43	319.70	1614.76	-9.71	-4.62
315.20	1620.76	-9.35	-4.56	319.80	1614.54	-9.80	-4.81
315.30	1620.54	-9.53	-5.05	319.90	1614.45	-9.70	-4.98
315.40	1620.42	-9.34	-4.54	320.00	1614.42	-9.51	-4.43
315.50	1620.29	-8.90	-4.71	320.10	1614.38	-9.40	-5.46
315.60	1620.17	-9.00	-4.71	320.20	1614.29	-9.24	-4.82
315.70	1620.04	-9.24	-4.41	320.30	1614.12	-9.41	-5.54
315.80	1619.92	-9.58	-5.00	320.40	1613.92	-9.50	-5.21
315.90	1619.79	-9.50	-4.93	320.50	1613.71	-9.51	-4.75
316.00	1619.67	-9.64	-5.05	320.60	1613.54	-9.61	-5.19
316.10	1619.54	-9.71	-5.37	320.70	1613.44	-9.39	-4.33
316.20	1619.42	-9.61	-5.14	320.80	1613.39	-9.35	-4.97
316.30	1619.29	-9.35	-5.04	320.90	1613.29	-9.17	-4.06
316.40	1619.13	-9.41	-5.48	321.00	1613.07	-9.67	-5.14
316.50	1618.92	-9.43	-5.34	321.10	1612.77	-9.59	-4.83
316.60	1618.71	-9.59	-5.07	321.20	1612.54	-9.64	-5.23
316.70	1618.54	-9.70	-4.40	321.30	1612.44	-9.60	-6.02
316.80	1618.45	-9.65	-5.17	321.40	1612.41	-9.42	-5.44
316.90	1618.41	-9.67	-5.25	321.50	1612.39	-9.29	-5.02
317.00	1618.37	-9.58	-5.55	321.60	1612.29	-9.26	-5.25
317.10	1618.29	-9.34	-5.20	321.70	1612.07	-9.31	-4.22
317.20	1618.15	-9.35	-5.28	321.80	1611.78	-9.23	-3.94
317.30	1618.00	-9.53	-5.30	321.90	1611.54	-9.51	-5.64
317.40	1617.83	-9.53	-4.70	322.00	1611.43	-9.27	-5.32

Sample depth (mm)	Date (C.E.)	$\delta^{13}C$ (‰VPDB)	$\delta^{18}O$ (‰VPDB)	Sample depth (mm)	Date (C.E.)	$\delta^{13}C$ (‰VPDB)	$\delta^{18}O$ (‰VPDB)
322.10	1611.42	-9.13	-5.54	326.70	1604.14	-8.64	-3.79
322.20	1611.40	-9.15	-5.36	326.80	1603.99	-8.95	-3.82
322.30	1611.29	-9.10	-5.21	326.90	1603.83	-9.23	-3.97
322.40	1610.92	-9.23	-5.38	327.00	1603.68	-9.26	-4.00
322.50	1610.54	-9.28	-4.01	327.10	1603.54	-9.38	-4.22
322.60	1610.43	-9.30	-3.88	327.20	1603.45	-9.29	-4.04
322.70	1610.40	-9.06	-3.89	327.30	1603.39	-9.10	-4.15
322.80	1610.29	-9.03	-4.01	327.40	1603.29	-8.86	-4.02
322.90	1609.91	-9.15	-4.05	327.50	1603.13	-9.02	-3.92
323.00	1609.54	-9.35	-3.92	327.60	1602.93	-9.06	-3.84
323.10	1609.43	-9.31	-4.00	327.70	1602.72	-9.38	-4.01
323.20	1609.41	-9.23	-4.03	327.80	1602.54	-9.46	-4.09
323.30	1609.40	-9.17	-3.92	327.90	1602.41	-9.38	-4.04
323.40	1609.29	-9.10	-3.91	328.00	1602.29	-9.10	-3.94
323.50	1609.05	-9.18	-4.03	328.10	1602.06	-9.18	-4.03
323.60	1608.76	-9.23	-4.03	328.20	1601.76	-9.16	-3.91
323.70	1608.54	-9.50	-4.01	328.30	1601.54	-9.44	-3.98
323.80	1608.44	-9.34	-3.93	328.40	1601.45	-9.24	-3.91
323.90	1608.42	-9.11	-3.85	328.50	1601.41	-9.42	-3.99
324.00	1608.39	-9.14	-3.95	328.60	1601.40	-9.22	-3.93
324.10	1608.29	-8.98	-3.92	328.70	1601.37	-9.04	-3.98
324.20	1608.06	-9.12	-3.96	328.80	1601.29	-8.91	-3.93
324.30	1607.77	-9.06	-3.91	328.90	1601.15	-8.91	-4.02
324.40	1607.54	-9.22	-4.02	329.00	1600.99	-8.99	-3.92
324.50	1607.44	-9.13	-3.84	329.10	1600.82	-9.15	-3.91
324.60	1607.39	-8.91	-3.88	329.20	1600.67	-9.40	-4.03
324.70	1607.29	-8.82	-3.97	329.30	1600.54	-9.47	-4.08
324.80	1607.05	-9.02	-3.95	329.40	1600.45	-9.37	-4.12
324.90	1606.76	-9.06	-3.93	329.50	1600.38	-9.00	-4.04
325.00	1606.54	-9.11	-4.02	329.60	1600.29	-8.96	-4.04
325.10	1606.44	-9.15	-3.99	329.70	1600.16	-9.16	-4.03
325.20	1606.39	-8.79	-3.96	329.80	1600.01	-9.41	-4.14
325.30	1606.29	-8.82	-3.93	329.90	1599.84	-9.49	-4.15
325.40	1606.12	-8.98	-3.96	330.00	1599.68	-9.58	-4.33
325.50	1605.92	-8.99	-3.90	330.10	1599.54	-9.80	-4.30
325.60	1605.72	-8.76	-4.17	330.20	1599.45	-9.49	-4.21
325.70	1605.54	-9.12	-3.91	330.30	1599.41	-9.44	-4.31
325.80	1605.44	-8.99	-3.99	330.40	1599.37	-8.87	-4.01
325.90	1605.42	-9.02	-4.16	330.50	1599.29	-8.81	-3.91
326.00	1605.39	-9.05	-3.94	330.60	1599.08	-9.08	-4.01
326.10	1605.29	-8.99	-3.97	330.70	1598.79	-9.21	-3.93
326.20	1604.91	-8.98	-4.04	330.80	1598.54	-9.75	-4.16
326.30	1604.54	-9.07	-3.97	330.90	1598.51	-9.78	-4.13
326.40	1604.45	-9.07	-3.99	331.00	1598.49	-9.59	-3.99
326.50	1604.39	-8.87	-4.01	331.10	1598.46	-9.41	-3.96
326.60	1604.29	-8.65	-3.83	331.20	1598.43	-9.05	-3.97

Sample depth (mm)	Date (C.E.)	$\delta^{13}C$ (‰VPDB)	$\delta^{18}O$ (‰VPDB)	Sample depth (mm)	Date (C.E.)	$\delta^{13}C$ (‰VPDB)	$\delta^{18}O$ (‰VPDB)
331.30	1598.41	-8.87	-3.89	335.90	1591.41	-9.45	-4.95
331.40	1598.29	-8.67	-3.76	336.00	1591.37	-9.37	-3.86
331.50	1597.90	-9.27	-3.81	336.10	1591.29	-8.86	-4.33
331.60	1597.54	-9.45	-3.94	336.20	1591.19	-8.90	-4.65
331.70	1597.45	-9.41	-3.82	336.30	1591.08	-8.95	-4.82
331.80	1597.42	-9.11	-3.68	336.40	1590.97	-9.27	-4.55
331.90	1597.38	-8.88	-3.83	336.50	1590.86	-9.29	-4.54
332.00	1597.29	-8.53	-3.76	336.60	1590.75	-9.39	-4.27
332.10	1597.15	-8.77	-3.69	336.70	1590.64	-9.50	-5.15
332.20	1596.99	-8.98	-3.80	336.80	1590.54	-9.76	-4.43
332.30	1596.83	-9.30	-3.77	336.90	1590.45	-9.31	-4.48
332.40	1596.68	-9.62	-3.81	337.00	1590.38	-8.87	-4.55
332.50	1596.54	-9.79	-3.95	337.10	1590.29	-8.81	-4.30
332.60	1596.45	-9.82	-3.86	337.20	1590.08	-9.12	-3.88
332.70	1596.38	-9.22	-3.73	337.30	1589.77	-9.30	-4.25
332.80	1596.29	-9.02	-3.75	337.40	1589.54	-9.39	-4.38
332.90	1596.07	-9.39	-3.86	337.50	1589.45	-9.35	-4.03
333.00	1595.76	-9.52	-3.88	337.60	1589.38	-9.13	-4.75
333.10	1595.54	-9.62	-4.36	337.70	1589.29	-8.79	-4.28
333.20	1595.45	-9.39	-4.59	337.80	1589.15	-9.08	-4.67
333.30	1595.39	-8.80	-4.32	337.90	1588.99	-9.33	-4.49
333.40	1595.29	-8.71	-4.02	338.00	1588.83	-9.65	-4.66
333.50	1595.14	-9.04	-4.65	338.10	1588.68	-9.61	-4.39
333.60	1594.99	-9.43	-4.56	338.20	1588.54	-9.76	-4.41
333.70	1594.84	-9.49	-4.61	338.30	1588.45	-9.60	-4.35
333.80	1594.69	-9.43	-4.45	338.40	1588.38	-9.36	-4.66
333.90	1594.54	-9.56	-3.89	338.50	1588.29	-9.17	-4.10
334.00	1594.42	-9.20	-5.20	338.60	1588.14	-9.39	-4.64
334.10	1594.29	-9.16	-5.07	338.70	1587.93	-9.50	-5.23
334.20	1594.06	-9.35	-4.71	338.80	1587.72	-9.41	-4.76
334.30	1593.77	-9.64	-5.16	338.90	1587.54	-9.78	-3.59
334.40	1593.54	-9.72	-4.93	339.00	1587.51	-9.73	-4.49
334.50	1593.44	-9.62	-5.01	339.10	1587.48	-9.71	-4.15
334.60	1593.39	-9.30	-5.09	339.20	1587.45	-9.38	-4.37
334.70	1593.29	-8.85	-4.65	339.30	1587.42	-9.39	-4.90
334.80	1593.14	-9.26	-4.95	339.40	1587.39	-9.59	-5.51
334.90	1592.99	-9.46	-4.93	339.50	1587.29	-9.29	-5.15
335.00	1592.84	-9.69	-4.64	339.60	1586.91	-9.81	-4.97
335.10	1592.69	-9.63	-4.98	339.70	1586.54	-10.01	-5.03
335.20	1592.54	-9.71	-4.36	339.80	1586.45	-9.89	-5.72
335.30	1592.41	-8.89	-4.75	339.90	1586.42	-9.87	-5.38
335.40	1592.29	-8.75	-4.32	340.00	1586.38	-9.76	-4.53
335.50	1592.06	-9.02	-4.55	340.10	1586.29	-9.05	-4.14
335.60	1591.75	-9.46	-5.11	340.20	1586.16	-9.11	-4.60
335.70	1591.54	-9.49	-4.37	340.30	1586.03	-9.27	-4.75
335.80	1591.46	-9.51	-4.36	340.40	1585.89	-9.60	-4.23

Sample depth (mm)	Date (C.E.)	$\delta^{13}C$ (‰VPDB)	$\delta^{18}O$ (‰VPDB)	Sample depth (mm)	Date (C.E.)	$\delta^{13}C$ (‰VPDB)	$\delta^{18}O$ (‰VPDB)
340.50	1585.73	-9.66	-4.84	345.10	1579.29	-9.31	-4.15
340.60	1585.54	-9.70	-4.33	345.20	1579.12	-9.39	-3.98
340.70	1585.29	-9.22	-4.68	345.30	1578.91	-9.57	-4.43
340.80	1585.08	-9.32	-4.62	345.40	1578.70	-9.55	-3.88
340.90	1584.88	-9.30	-4.37	345.50	1578.54	-9.74	-4.27
341.00	1584.70	-9.32	-4.42	345.60	1578.42	-9.75	-3.96
341.10	1584.54	-9.38	-4.41	345.70	1578.29	-9.43	-4.46
341.20	1584.44	-9.32	-4.25	345.80	1578.17	-9.46	-4.00
341.30	1584.42	-9.09	-4.45	345.90	1578.04	-9.62	-4.17
341.40	1584.39	-9.03	-4.14	346.00	1577.92	-9.67	-4.27
341.50	1584.29	-8.82	-4.39	346.10	1577.79	-9.59	-3.92
341.60	1584.06	-9.04	-4.20	346.20	1577.66	-9.76	-3.96
341.70	1583.77	-9.06	-4.24	346.30	1577.54	-10.09	-4.13
341.80	1583.54	-9.27	-4.57	346.40	1577.44	-9.86	-4.78
341.90	1583.42	-9.29	-4.22	346.50	1577.38	-9.74	-3.86
342.00	1583.29	-9.04	-4.51	346.60	1577.38	-9.86	-4.25
342.10	1583.12	-9.14	-4.21	346.70	1577.38	-9.86	-4.56
342.20	1582.92	-9.06	-4.34	346.80	1577.38	-9.60	-3.85
342.30	1582.72	-9.26	-4.42	346.90	1577.38	-9.65	-4.18
342.40	1582.54	-9.39	-4.53	347.00	1577.38	-9.55	-4.02
342.50	1582.44	-9.38	-4.13	347.10	1577.37	-9.46	-3.92
342.60	1582.41	-9.33	-4.35	347.20	1577.37	-9.40	-3.95
342.70	1582.39	-9.24	-4.04	347.30	1577.37	-9.47	-4.08
342.80	1582.29	-9.14	-3.87	347.40	1577.29	-9.27	-3.88
342.90	1581.90	-9.29	-3.83	347.50	1577.14	-9.67	-3.86
343.00	1581.54	-9.45	-4.04	347.60	1576.93	-9.57	-4.84
343.10	1581.45	-9.31	-3.88	347.70	1576.71	-9.75	-4.25
343.20	1581.38	-9.40	-4.23	347.80	1576.54	-9.91	-4.27
343.30	1581.29	-9.31	-3.70	347.90	1576.45	-9.72	-4.18
343.40	1581.19	-9.41	-4.12	348.00	1576.39		
343.50	1581.08	-9.33	-3.85	348.10	1576.29	-9.44	-4.40
343.60	1580.98	-9.40	-3.90	348.20	1576.05	-9.44	-4.25
343.70	1580.87	-9.51	-3.74	348.30	1575.75	-9.63	-4.40
343.80	1580.76	-9.45	-3.73	348.40	1575.54	-9.77	-4.43
343.90	1580.65	-9.50	-4.28	348.50	1575.45	-9.76	-4.33
344.00	1580.54	-9.62	-3.86	348.60	1575.38	-9.68	-4.24
344.10	1580.42	-9.54	-4.15	348.70	1575.29	-9.59	-4.25
344.20	1580.29	-9.33	-3.88	348.80	1575.19	-9.64	-4.58
344.30	1580.15	-9.42	-3.79	348.90	1575.08	-9.78	-4.19
344.40	1580.00	-9.52	-3.94	349.00	1574.97	-9.97	-4.62
344.50	1579.84	-9.53	-4.19	349.10	1574.86	-9.80	-4.14
344.60	1579.68	-9.62	-4.03	349.20	1574.75	-10.24	-4.40
344.70	1579.54	-9.86	-4.06	349.30	1574.65	-10.09	-4.60
344.80	1579.45	-9.66	-4.57	349.40	1574.54	-10.27	-4.44
344.90	1579.42	-9.64	-3.83	349.50	1574.46	-9.95	-4.22
345.00	1579.38	-9.46	-4.01	349.60	1574.41	-9.78	-4.35

Sample depth (mm)	Date (C.E.)	$\delta^{13}C$ (‰VPDB)	$\delta^{18}O$ (‰VPDB)	Sample depth (mm)	Date (C.E.)	$\delta^{13}C$ (‰VPDB)	$\delta^{18}O$ (‰VPDB)
349.70	1574.37	-9.72	-4.18	354.30	1566.92	-9.58	-4.34
349.80	1574.29	-9.63	-4.21	354.40	1566.72	-9.58	-4.16
349.90	1573.92	-9.67	-4.67	354.50	1566.54	-9.61	-3.99
350.00	1573.54	-10.01	-4.39	354.60	1566.44	-9.29	-3.99
350.10	1573.47	-9.74	-4.62	354.70	1566.39	-9.18	-4.00
350.20	1573.43	-9.94	-4.46	354.80	1566.29	-9.06	-4.33
350.30	1573.40	-9.97	-4.19	354.90	1566.13	-9.56	-4.06
350.40	1573.36	-9.93	-4.25	355.00	1565.95	-9.22	-4.27
350.50	1573.29	-8.91	-3.92	355.10	1565.76	-9.15	-4.10
350.60	1573.19	-9.18	-4.12	355.20	1565.54	-9.37	-3.98
350.70	1573.08	-9.04	-4.29	355.30	1565.29	-9.03	-4.03
350.80	1572.97	-9.11	-3.93	355.40	1565.07	-9.21	-3.66
350.90	1572.86	-9.52	-3.94	355.50	1564.87	-9.20	-3.83
351.00	1572.75	-9.68	-4.05	355.60	1564.69	-9.61	-3.82
351.10	1572.65	-9.54	-3.99	355.70	1564.54	-9.62	-3.68
351.20	1572.54	-9.89	-4.17	355.80	1564.44	-9.49	-3.18
351.30	1572.46	-9.31	-4.17	355.90	1564.38	-9.68	-3.72
351.40	1572.42	-9.29	-3.99	356.00	1564.29	-9.26	-3.84
351.50	1572.37	-9.59	-3.96	356.10	1564.18	-9.68	-3.87
351.60	1572.29	-9.13	-3.92	356.20	1564.06	-9.36	-3.60
351.70	1571.54	-9.52	-4.10	356.30	1563.93	-9.25	-3.65
351.80	1571.42	-9.44	-4.12	356.40	1563.76	-9.42	-3.86
351.90	1571.29	-9.30	-4.14	356.50	1563.54	-9.76	-3.86
352.00	1571.04	-9.53	-4.04	356.60	1563.29	-9.60	-3.64
352.10	1570.79	-9.58	-4.13	356.70	1563.04	-9.78	-4.00
352.20	1570.54	-9.72	-4.15	356.80	1562.79	-9.79	-3.88
352.30	1570.29	-9.13	-4.27	356.90	1562.54	-10.03	-3.93
352.40	1570.08	-9.28	-3.98	357.00	1562.40	-9.92	-3.92
352.50	1569.92	-9.42	-4.04	357.10	1562.38	-9.53	-4.07
352.60	1569.75	-9.61	-4.09	357.20	1562.29	-9.41	-3.82
352.70	1569.54	-9.88	-4.15	357.30	1562.05	-9.66	-3.98
352.80	1569.29	-9.33	-4.13	357.40	1561.77	-9.78	-4.00
352.90	1569.04	-9.74	-4.13	357.50	1561.54	-10.08	-3.76
353.00	1568.79	-10.12	-4.15	357.60	1561.42	-9.76	-3.77
353.10	1568.54	-10.14	-4.34	357.70	1561.29	-9.31	-3.86
353.20	1568.40	-10.05	-4.35	357.80	1561.11	-9.33	-3.91
353.30	1568.36	-9.86	-4.09	357.90	1560.92	-9.60	-3.84
353.40	1568.29	-9.18	-4.09	358.00	1560.72	-9.62	-3.85
353.50	1568.14	-9.50	-5.18	358.10	1560.54	-9.77	-3.71
353.60	1567.99	-9.48	-4.04	358.20	1560.44	-9.72	-3.82
353.70	1567.83	-9.46	-4.13	358.30	1560.39	-9.57	-3.97
353.80	1567.68	-9.77	-4.14	358.40	1560.29	-9.42	-3.96
353.90	1567.54	-9.94	-4.29	358.50	1560.07	-9.80	-3.54
354.00	1567.42	-9.47	-4.17	358.60	1559.78	-9.76	-3.62
354.10	1567.29	-9.31	-3.97	358.70	1559.54	-10.04	-3.65
354.20	1567.12	-9.40	-4.25	358.80	1559.44	-9.77	-3.83

Sample depth (mm)	Date (C.E.)	$\delta^{13}C$ (‰VPDB)	$\delta^{18}O$ (‰VPDB)
358.90	1559.40	-9.89	-3.66
359.00	1559.29	-9.40	-3.80
359.10	1559.06	-9.62	-3.87
359.20	1558.78	-9.51	-3.60
359.30	1558.54	-9.83	-3.57
359.40	1558.41	-9.46	-3.55
359.50	1558.29	-9.32	-3.59
359.60	1557.92	-9.40	-3.52
359.70	1557.54	-9.71	-3.36
359.80	1557.49	-9.64	-3.46
359.90	1557.44	-9.46	-3.56
360.00	1557.43	-9.78	-3.41
360.10	1557.29	-9.42	-3.49
360.20	1557.04	-9.51	-3.62
360.30	1556.79	-9.62	-3.37
360.40	1556.54	-9.70	-3.39
360.50	1556.29	-8.90	-3.23
360.60	1555.93	-8.92	-3.29
360.70	1555.54	-9.19	-3.37
360.80	1555.40	-9.14	-3.49
360.90	1555.29	-9.06	-3.54
361.00	1554.89	-9.08	-3.39
361.10	1554.54	-9.26	-3.54
361.20	1554.44	-9.01	-3.52
361.30	1554.38	-8.90	-3.82
361.40	1554.29	-8.87	-3.55
361.50	1554.15	-9.31	-3.48
361.60	1553.99	-9.46	-3.57
361.70	1553.83	-9.61	-3.62
361.80	1553.68	-9.58	-3.57
361.90	1553.54	-9.74	-3.52
362.00	1553.44	-9.35	-3.66
362.10	1553.38	-9.05	-3.52
362.20	1553.29	-8.68	-3.57
362.30	1553.07	-9.10	-3.42
362.40	1552.76	-9.58	-3.49
362.50	1552.54	-10.06	-3.62
362.60	1552.46	-9.82	-3.78
362.70	1552.42	-10.01	-3.80
362.80	1552.41	-9.96	-3.71
362.90	1552.40	-9.64	-3.56
363.00	1552.37	-9.32	-3.62
363.10	1552.29	-9.29	-3.73
363.20	1552.17	-9.50	-3.81
363.30	1552.04	-9.86	-3.72
363.40	1551.90	-10.01	-3.76
363.50	1551.76	-10.06	-3.83
363.60	1551.64	-10.11	-3.76
363.70	1551.54	-10.26	-3.83
363.80	1551.47	-10.18	-3.77
363.90	1551.42	-10.14	-3.88
364.00	1551.36	-9.64	-3.70
364.10	1551.29	-8.95	-3.58
364.20	1551.20	-9.23	-3.73
364.30	1551.10	-9.19	-3.66
364.40	1551.00	-9.24	-3.61
364.50	1550.90	-9.35	-3.67
364.60	1550.78	-9.68	-3.68
364.70	1550.67	-9.52	-3.82
364.80	1550.54	-9.72	-3.66